UNIVERSIDAD COMPLUTENSE DE MADRID

FACULTAD DE CIENCIAS FÍSICAS
Departamento de Física de la Tierra, Astronomía y Astrofísica I
(Geofísica y Meteorología) (Astronomía y Geodesia)

TESIS DOCTORAL

Explosive cyclogenesis in the Euro-Atlantic sector: study of associated large-scale dynamics and variability

(Ciclogénesis explosivas en el sector Euro-Atlántico: estudio de su dinámica a gran escala y variabilidad)

MEMORIA PARA OPTAR AL GRADO DE DOCTOR

PRESENTADA POR

Íñigo Gómara Cardalliaguet

Directores

María Belén Rodríguez de Fonseca
Pablo Zurita Gotor
Joaquim G. Pinto

Madrid, 2016

Departamento de Física de la Tierra, Astronomía y Astrofísica I

Facultad de Ciencias Físicas
Universidad Complutense de Madrid

Explosive Cyclogenesis in the Euro-Atlantic sector: study of associated large-scale dynamics and variability

(Ciclogénesis Explosivas en el sector Euro-Atlántico: estudio de su dinámica a gran escala y variabilidad)

Iñigo Gómara Cardalliaguet

Memoria de Tesis presentada para optar al grado de Doctor

Dirigida por:

Dra. María Belén Rodríguez de Fonseca (UCM)
Dr. Pablo Zurita Gotor (UCM)
Dr. Joaquim G. Pinto (Univ. Reading)

Madrid, 2015

Iñigo Gómara Cardalliaguet: *Explosive Cyclogenesis in the Euro-Atlantic sector: study of associated large-scale dynamics and variability*, PhD thesis, @September 25, 2015. Madrid (Spain).

Special thanks are given to Michael Paperin and Brockmann Consult (http://www.brockmann-consult.de) for providing the extra-tropical cyclone images used on the cover pages of this thesis. The original pre-processed data was received from the MERIS - a programmable, medium-spectral resolution, imaging spectrometer installed on the ESA's satellite ENVISAT.

A la memoria de José y Ana María Gómara

Academic Acknowledgements

First and foremost I would like to thank my PhD supervisors, Belén Rodríguez-Fonseca, Pablo Zurita-Gotor and Joaquim G. Pinto their encouragement, advice, inspiration and support during the conduct of this work.

Many thanks also to the Department of Geophysics and Meteorology of Universidad Complutense de Madrid (UCM) for the support received during the PhD period. I am indebted to the Head of the Department and administrative assistants for their help on UCM bureaucracy. Thanks also to our technical assistant, for his priceless help on computer issues typically occurring days before important deadlines.

I am also grateful to the University of Cologne and the University of Reading for hosting my research stays. Thanks to the members of the Institute for Geophysics and Meteorology for their hospitality and help during my stay in Cologne.

Thanks also to the collaborators involved in the publications of this thesis. It has been a real pleasure working with Giacomo Masato, Tim Woollings, Helen Dacre, Rodrigo Caballero and Sven Ulbrich.

I want to express my gratitude to the members of the Tropical Atlantic Variability (TROPA) research group for the long and always enriching discussions on climate variability. Thanks also to the members of the research groups GICA (University of Salamanca), MAR (UCM), Micrometeorology (UCM), PALMA (UCM) and EOLO (UPV/EHU).

Finally, I want to thank the two external reviewers of this thesis, João Santos and Christoph Raible, for their pertinent comments and suggestions, which have contributed to improve this manuscript.

Funding Information

This thesis has been supported by Spanish and European funds through the research projects:

- TRACS: Tropical Atlantic Variability and the Climate Shift (CGL2009-10285; Spanish Ministry of Economy and Competitiveness).
- DEVIAJE: Dinámica del equilibrio y variabilidad interna anular del jet extra-tropical (CGL2009-06944; Spanish Ministry of Economy and Competitiveness).
- MULCLIVAR: Multiscale Climate Variability: Agronomical and Economic Impacts (CGL2012-38923-C02-01; Spanish Ministry of Economy and Competitiveness).
- PREFACE: Enhancing prediction of Tropical Atlantic climate and its impacts (European Commission's FP7/2007-2013; grant agreement 603521).

A short term stay at the University of Cologne (Germany) was funded by VALUE: COST Action ES1102. A short term stay at the University of Reading (UK) was funded by the host University. The Master's studies in Geophysics and Meteorology (UCM) that led to the realization of this PhD were financed by 'la Caixa' Welfare Projects (scholarships in Spain).

Gracias a

Belén, por apostar por mí y permitirme trabajar en un tema de tesis que me motivase lo suficiente. Gracias por tu atención, tenacidad y positivismo durante todo este periodo. Gracias por enseñarme que también existe el océano y juega un papel importante. Gracias por tu esfuerzo en mantener económicamente a flote a un nutrido grupo de jóvenes investigadores en tiempos tan oscuros para esta profesión en España.

Pablo, por tu confianza en mi trabajo cuando apenas comenzaba mi etapa de doctorado. Gracias por las numerosas discusiones científicas en tu despacho. Gracias por enseñarme que debemos ser críticos con todo resultado científico, especialmente con los de uno mismo. Gracias por tu paciencia corrigiendo textos en inglés.

Joaquim, por haberme dado la oportunidad de trabajar contigo durante mi primera estancia investigadora. Gracias por el alojamiento, y por el tiempo que invertiste durante mi aprendizaje. Gracias por permitirme trabajar con vuestro *tracking* automático de ciclones. Gracias por haberme introducido en la comunidad científica de esta disciplina, y por todos los conocimientos que me has transmitido.

Todos mis compañeros del Departamento de Geofísica y Meteorología de la UCM. Desde aquellos que recuerdan la tesis como aquella 'cosa' sin importancia que hicieron hace mucho, hasta los que todavía no son conscientes de lo que se les viene encima, pasando por ese numeroso grupo actual de 'ansiosos' por terminar. Sois muchos, y la elaboración de la tradicional lista kilométrica de nombres con agradecimientos individualizados no es nada trivial. Espero que podáis perdonarme la ausencia de 'folclore' en este apartado. Muchísimas gracias por vuestra compañía. Gracias de igual modo a los profesores de este Departamento, por vuestra asistencia y apoyo durante este periodo.

Concha, Carlos y Jon, por vuestra ayuda durante mi etapa pre-pre-doctoral (Licenciatura y Máster). Gracias por el tiempo dedicado a la búsqueda de todo tipo de becas de investigación.

EMOTAMZOR, por todos los encuentros de ensueño, fantasía y gran bizarría. Gracias a Édgar Roldán por ser tan *ALTINTOP*.

Mi 'cuadrilla' de amigos de Tudela, porque lo somos desde hace décadas.

Mis amigos y compañeros del Colegio Mayor Fray Luis de León y de la Licenciatura en Física de Salamanca, por vuestro esfuerzo en seguir viéndonos regularmente a pesar de nuestras actuales vidas 'más adultas'.

Los 'Riosecanos', familia Rodríguez-Santo Tomás, Sioux y postizos, por haberme acogido tan calurosamente durante estos años.

Mi familia cercana, por vuestro apoyo incondicional durante todo este tiempo.

Gracias a mis padres, Javier y Amelia, por la educación que me habéis dado y todo vuestro esfuerzo para que pudiese llegar hasta aquí.

Gracias a mi hermana, Sonsoles, por tu paciencia en los más de cien visionados de la película *Twister* durante nuestra infancia. Perdóname por ser el culpable de tus pesadillas recurrentes con tornados.

Gracias a mis abuelos, Constantino, Amelia y Pilar, por dar siempre una visión completamente objetiva y poco sesgada de mis cualidades positivas. Gracias por vuestro cariño.

Gracias a los que ya no están, mi abuelo José y mi tía Ana María, por sus lecciones de vida y todo su amor. Esta tesis va dedicada en solitario a la memoria de ambos.

Gracias a mis tíos y primos, por vuestra compañía y apoyo durante todo este tiempo.

Gracias a mi padrino, Chucho, por todo tu afecto.

Gracias a Marga, por tu infinita paciencia y siempre dulce compañía. Gracias por el camino que hemos recorrido juntos, y por el que nos queda por recorrer.

Todos los olvidados, porque sin vosotros estas últimas líneas carecerían de sentido.

Outline

Resumen

1. Introducción

Las ciclogénesis explosivas son sistemas de bajas presiones extra-tropicales que sufren un proceso súbito de intensificación [*Sanders y Gyakum*, 1980; Fig. RIa]. En Europa se encuentran entre los desastres naturales más significativos, debido a sus fuertes rachas de viento, precipitaciones intensas y mareas ciclónicas asociadas [e.g., *Fink et al.*, 2009; Fig. RIb]. Generalmente ocurren de manera individual, aunque en ocasiones aparecen en rápida sucesión [*Mailier et al.*, 2006]. Debido a los numerosos procesos físicos involucrados en su desarrollo [*Pinto et al.*, 2009] estos fenómenos son muy complejos de predecir y su relación con el flujo medio atmosférico es todavía incierta. Por tanto, esta tesis estudia en profundidad la dinámica de gran escala y variabilidad de las ciclogénesis explosivas en el Atlántico Norte.

(a) Densidad de ciclones (b) Ciclón Klaus

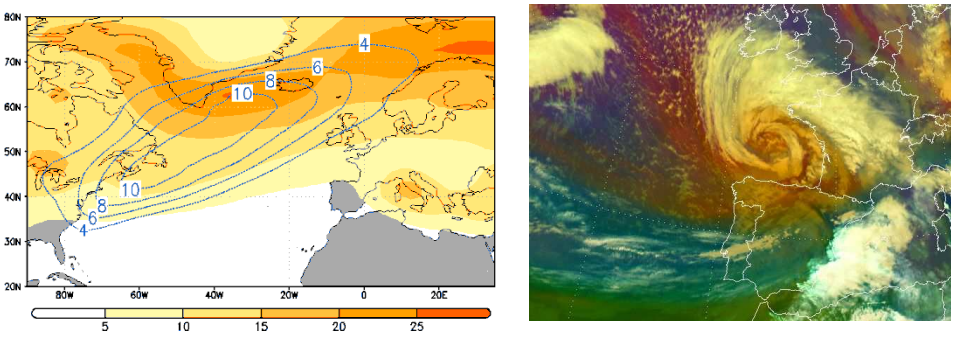

Fig. RI: (a) Densidad de ciclogénesis explosivas (contornos) vs. ciclones no explosivos (colores) en número de eventos por invierno por círculo de radio 7.5° (ERA-Interim). (b) Imagen satelital (RGB airmass) del ciclón Klaus (00 UTC 24/01/2009; EUMETSAT).

2. Objetivos

Los objetivos principales de esta tesis son:

- Analizar la relación bi-direccional entre el flujo medio atmosférico (caracterizado por la Oscilación del Atlántico Norte; NAO) y los ciclones explosivos[1] y no explosivos que afectan Europa.

- Describir la relación entre el flujo medio y los ciclones extra-tropicales en el Atlántico Norte mediante el análisis de procesos de ruptura de ondas de Rossby (RWB).

- Realizar el primer análisis dinámico sobre la ocurrencia secuencial de ciclones intensos sobre el oeste de Europa y su relación con procesos de RWB y ciclogénesis secundaria.

- Caracterizar la variabilidad climática (1-11 años) de las ciclogénesis explosivas en el Atlántico Norte y estudiar su posible relación con la variabilidad climática multi-decadal.

[1] Análogo al término ciclogénesis explosiva. Ambos términos se citan indistintamente a lo largo de la memoria de tesis.

3. Datos y Metodología

Esta tesis se sustenta en datos de reanálisis [ERA-Interim - *Dee et al.*, 2011; ERA-40 - *Uppala et al.*, 2005; NCEP - *Kalnay et al.*, 1996; SODA - *Carton and Giese*, 2008]; (ii) observaciones [HadISST - *Rayner et al.*, 2003; cartas meteorológicas del UK Met-Office]; y en una simulación del modelo ECHAM5/MPIOM1[2] [*Roeckner et al.*, 2003].

La identificación y caracterización de ciclones se ha realizado a través de un método de seguimiento automático [*Pinto et al.*, 2005]. Los ciclones se han clasificado en explosivos y no explosivos según su índice de profundización normalizado (NDR). Los eventos de RWB se han identificado y caracterizado (e.g. ciclónico/anticiclónico) mediante un índice bidimensional [*Masato et al.*, 2013a].

Numerosas herramientas matemáticas y estadísticas se han aplicado en esta tesis [*Wilks*, 2006]: filtrado espectral, significación estadística, Funciones Empíricas Ortogonales (EOFs), etc.

[2] Simulación acoplada océano-atmósfera de control (505 años, condiciones pre-industriales).

4. Resultados

Los resultados se encuentran divididos en cuatro publicaciones científicas diferentes:

1. **Sobre la relación entre las ciclogénesis explosivas que afectan Europa y la Oscilación del Atlántico Norte [*Gómara et al.*, 2014b]:** Los ciclones explosivos (EC) y no-explosivos (NoEC) que afectan Europa tienden a desarrollarse bajo condiciones de circulación a gran escala diferentes (NCEP). Mientras NoEC tienden a desarrollarse bajo NAO negativa y neutra, EC lo hacen bajo una NAO positiva, caracterizada por un *jet*[3] muy intenso al oeste de Europa. Durante su decaimiento, EC producen fuertes variaciones en el índice diario de la NAO, tanto positivas como negativas, aunque por razones dinámicas diferentes.

2. **Análisis de ruptura de ondas de Rossby y ciclogénesis explosivas en el sector Euro-Atlántico [*Gómara et al.*, 2014a]:** Los ciclones más intensos al oeste del Atlántico Norte están precedidos por mayor actividad de RWB ciclónica al oeste de Groenlandia (ERA-40). Los ciclones más intensos al este de la cuenca están precedidos por un patrón de RWB norte/ciclónico - sur/anticiclónico. En ambos casos los eventos de RWB comprimen e intensifican el *jet* sobre cada área del Atlántico Norte, creando unas condiciones óptimas para el desarrollo de los ciclones. El declive de los ciclones más intensos al oeste de la cuenca parece preceder la ocurrencia de un patrón de bloqueo atmosférico sobre Escandinavia. Los ciclones no explosivos no se encuentran asociados a ningún patrón coherente de RWB.

3. **Dinámica de gran escala asociada al paso secuencial de ciclones intensos sobre el oeste de Europa [*Pinto et al.*, 2014]:** Estos episodios están caracterizados por la existencia de un *jet* muy intenso al oeste de Europa (~1 semana), con múltiples eventos de RWB (norte-ciclónico/sur-anticiclónico) induciendo esta dinámica

[3] Del inglés, corriente en chorro.

(ERA-Interim). La ocurrencia de ciclogénesis secundaria también juega un papel importante, mediante el cual una baja incipiente se desarrolla en el frente frío asociado a un ciclón primario situado aguas abajo.

4. **Transiciones abruptas en la variabilidad climática principal de densidad de ciclones explosivos en el Atlántico Norte [*Gómara et al.*, 2015]:** Los modos de variabilidad principales de EC y NoEC son diferentes. La EOF1 de EC (1-11 años) representa una intensificación/debilitamiento de su actividad entre Terranova e Islandia. Para la mayoría de los periodos estudiados en NCEP, ERA-40 y ECHAM5/MPIOM1 la relación entre la NAO y EC EOF1 es robusta. Sin embargo, durante periodos específicos de NCEP y ECHAM5/MPIOM1 la correlación positiva entre ambas se reduce drásticamente. Estos periodos multi-decadales se caracterizan por una menor baroclinidad sobre el Atlántico Norte sub-polar. Como consecuencia, las ciclogénesis explosivas se ven forzadas a tomar trayectorias anómalas y nuevos modos de variabilidad (menos influenciados por NAO+) emergen.

5. Conclusiones

Las conclusiones principales de esta tesis son:

1. Las ciclogénesis explosivas (no-explosivas) que afectan Europa se desarrollan predominantemente bajo NAO+ (NAO-). Sólo los ciclones más intensos son capaces de alterar significativamente el estado de la NAO durante su decaimiento.

2. La relación bidireccional entre RWB y ciclones extra-tropicales en el sector Euro-Atlántico es susceptible a la intensidad, localización y evolución de los ciclones.

3. Los procesos de RWB y ciclogénesis secundaria aguas arriba juegan un papel importante en el paso continuado de ciclones intensos sobre el oeste de Europa.

4. Los modos de variabilidad climática principales de ciclogénesis explosivas y no explosivas son diferentes. La relación entre el modo dominante de las primeras y la NAO es no estacionaria, y parece modulada por variabilidad multi-decadal del sistema acoplado océano-atmósfera.

Summary

1. Introduction

Explosive cyclones are rapidly intensifying extra-tropical low pressure systems [*Sanders and Gyakum*, 1980; Fig RIa]. In Europe, they are among the most damaging natural hazards, due to their associated strong wind gusts, heavy precipitation and storm surge events [e.g., *Fink et al.*, 2009; Fig. RIb]. They generally occur individually or in quick succession [*Mailier et al.*, 2006], and constitute a great challenge to forecast. Their relation with the large-scale circulation is yet uncertain in the literature, as several physical mechanisms are typically involved in their development [*Pinto et al.*, 2009]. Therefore, this thesis aims to deeply analyze the large-scale dynamics and variability of explosive cyclogenesis over the North Atlantic.

(a) Cyclone density (b) Cyclone Klaus

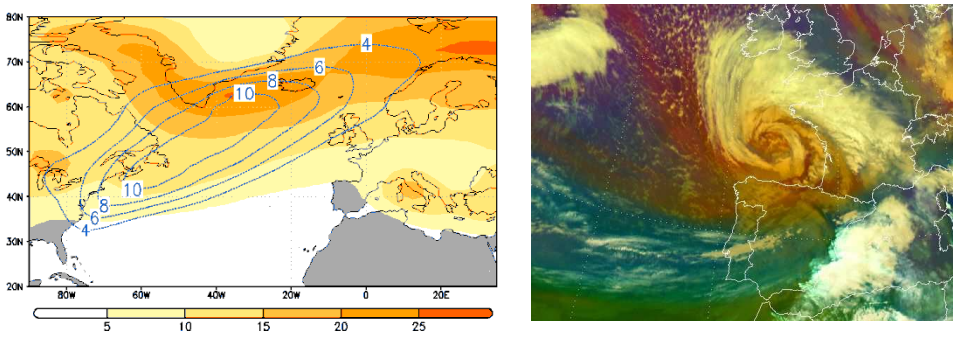

Fig. RI: (a) Density of explosive (contours) vs. non-explosive (shadings) cyclones in counts per 7.5° radius circle per winter on ERA-Interim. (b) RGB air mass satellite image of cyclone Klaus (00 UTC 24/01/2009) from EUMETSAT.

2. Objectives

The main objectives of this thesis are:

- To analyze the bi-directional relation between the large-scale mean flow (largely explained by the North Atlantic Oscillation; NAO) and explosive and non-explosive cyclones affecting Europe.

- To describe the two-way relationship between cyclones and the large-scale circulation in the North Atlantic through the analysis of Rossby Wave-Breaking (RWB) processes.

- To provide the first dynamical analysis of the occurrence of cyclone families over Western Europe, focusing on the role of RWB, jet dynamics and secondary cyclogenesis.

- To characterize the climate variability (1-11 yr.) of Explosive cyclogenesis in the North Atlantic and analyze the potential modulating role of multi-decadal atmospheric/oceanic variability.

3. Data and Methods

This thesis is based on: (i) reanalyses [ERA-Interim - *Dee et al.*, 2011; ERA-40 - *Uppala et al.*, 2005; NCEP - *Kalnay et al.*, 1996; SODA - *Carton and Giese*, 2008]; (ii) observations [HadISST - *Rayner et al.*, 2003; UK Met-Office weather charts]; and (iii) a 505 year simulation of ECHAM5/MPIOM1[4] [*Roeckner et al.*, 2003].

An automatic tracking scheme is applied to obtain complete cyclone life-cycles and characteristics [*Pinto et al.*, 2005]. Next, cyclones are separated into explosive and non-explosive depending on their Normalized Deepening Rate (NDR). A two-dimensional index [*Masato et al.*, 2013a] is used to identify and characterize (e.g., cyclonic or anticyclonic) RWB events.

Several mathematical tools for climate research are also applied [*Wilks*, 2006]: spectral filtering, hypothesis testing, Empirical Orthogonal Functions (EOF), etc.

[4] Coupled ocean-atmosphere control simulation (505-yr., pre-industrial conditions).

4. Results

Results are divided into four different scientific publications:

1. **<u>On the relation between explosive cyclones affecting Europe and the North Atlantic Oscillation [*Gómara et al.*, 2014b]</u>:** Explosive (EC) and non-explosive (NoEC) cyclones affecting Europe predominantly develop under different large-scale circulation conditions (NCEP). Whereas NoEC evolve more frequently under negative and neutral NAO phases, the number of EC is larger under a positive NAO phase, typically characterized by an intensified jet over Western Europe. During cyclone's decay, EC produce strong variations in the daily NAO index, both positive and negative, although for different dynamical reasons.

2. **<u>Rossby wave-breaking analysis of explosive cyclones over the Euro-Atlantic sector [*Gómara et al.*, 2014a]:</u>** The most intense cyclones in the eastern and western North Atlantic are preceded by two different RWB patterns (ERA-40). Western cyclones are preceded by enhanced cyclonic RWB over western Greenland. Eastern cyclones are preceded by a north-cyclonic and south-anticyclonic RWB pattern. In both cases, the RWB events squash and intensify the jet over each area. These RWB events thus create favorable upper-level conditions for cyclone amplification. The decline of the strongest western cyclones is potentially associated with the onset of Scandinavian Blocking. Non-explosive cyclones depict no sign of enhanced RWB over the whole North Atlantic.

3. **<u>Large-scale dynamics associated with clustering of extra-tropical cyclones affecting Western Europe [*Pinto et al.*, 2014]</u>:** Optimal conditions for the occurrence of cyclone clusters are provided by a recurrent extension of an intensified eddy-driven jet over Western Europe lasting at least 1 week, with multiple RWB occurrences on both the poleward and equatorward flanks of the jet (ERA-Interim). Secondary upstream cyclogenesis also plays an important role. A recurring pattern is identified, in which a secondary cyclone

develops in the cold front associated with a primary cyclone situated downstream.

4. **Abrupt transitions in the variability of explosive cyclones over the North Atlantic [*Gómara et al.*, 2015]:** The leading climate variability modes (EOFs) of explosive and non-explosive cyclones are different. EC EOF1 (1-11 yr.) represents a strengthening/weakening of EC activity between Newfoundland and Iceland. For most of the periods studied of NCEP, ERA-40 and ECHAM5/MPIOM1 there is a robust positive correlation between the NAO and EC EOF1. However, during specific periods of NCEP and ECHAM5/MPIOM1 the positive correlation with the NAO abruptly decreases. These periods agree with those associated with reduced baroclinicity over the sub-polar North Atlantic. As a consequence, explosive cyclones are forced to bend their trajectories and different modes of variability (less influenced by NAO+) emerge.

5. Conclusions

The main conclusions of this thesis are:

1. Explosive (non-explosive) cyclones affecting Europe predominantly develop under NAO+ (NAO-). Only explosive cyclones are able to influence the NAO short-term variability during their decay.

2. The links between RWB and cyclogenesis over the Euro-Atlantic sector are sensitive to cyclone's maximum intensity, deepening rate, timing and location.

3. Both RWB and secondary upstream cyclogenesis play a decisive role in the occurrence of cyclone clustering over Western Europe.

4. The leading climate variability modes of EC and NoEC are different. The connection of EC EOF1 with the NAO is non-stationary in time, and appears to be modulated by multi-decadal variability of the atmospheric/oceanic coupled system.

PREFACE

'Among famous traitors of history one might mention the weather'

Ilka Chase (actress and novelist; 1900-1978)

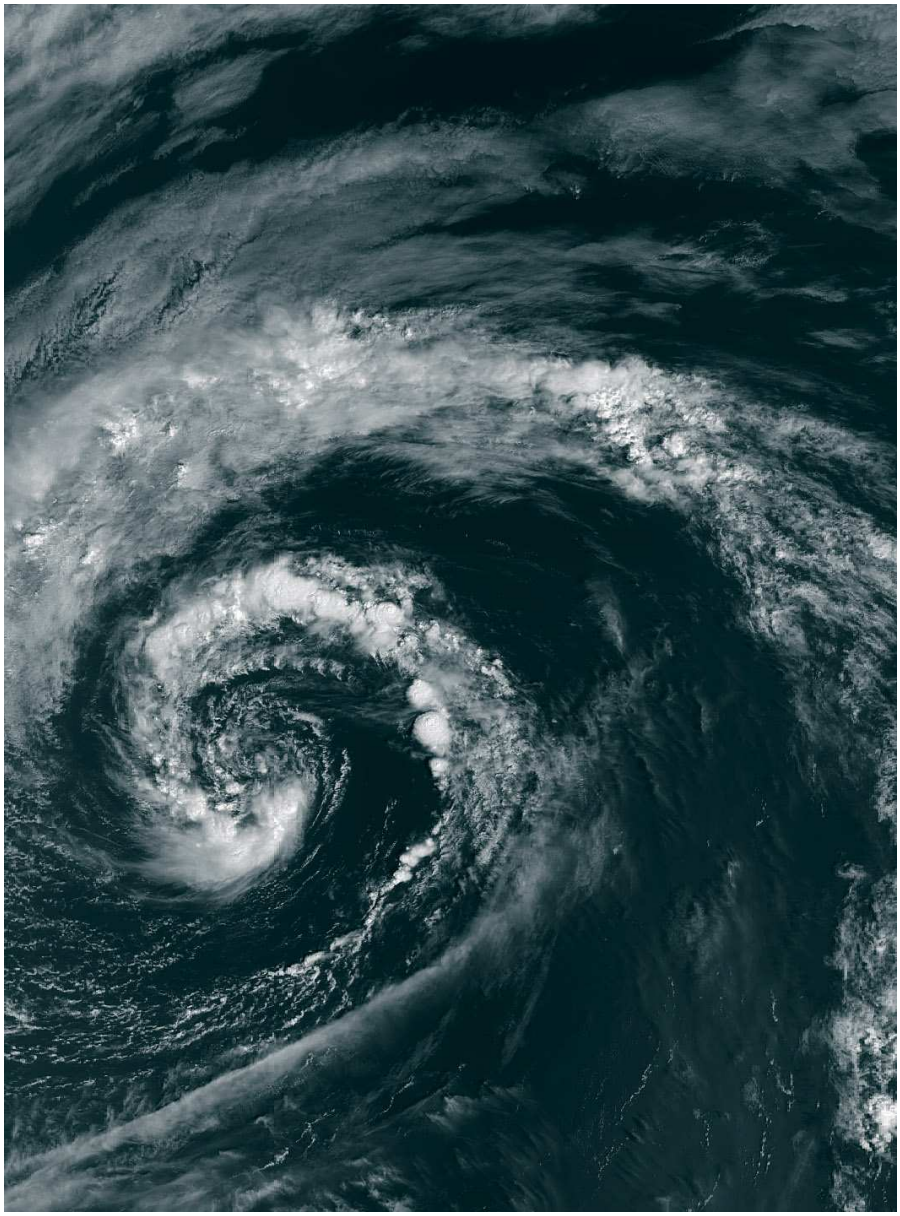

Preface

Intense extra-tropical cyclones with large deepening rates are often referred as 'explosive cyclones' or 'bombs'. By definition, the pressure fall evolution in their surface centre must be equal or greater than 24 hPa in 24 hours, at a reference latitude of 60˚N [*Sanders and Gyakum*, 1980]. In the North Atlantic, extra-tropical cyclones typically grow at the expense of baroclinic instability in the vicinity of Newfoundland, propagate from the south-west to the north-east across the oceanic basin, and affect Europe during their mature or occluding stages [Fig. Ia; *Dacre and Gray, 2009*; *Pinto et al.*, 2009]. Extra-tropical cyclone activity is greatest during the winter season, due to the enhanced meridional gradients of temperature and humidity [*Hoskins and Valdes*, 1990].

(a) Cyclone trajectories (b) Cyclone Klaus

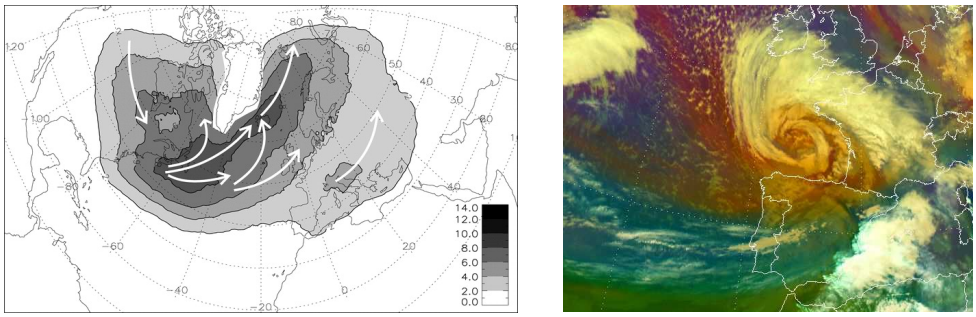

Fig. I: (a) Schematic of cyclone track paths plotted over track density. Contours every 2 cyclones (106 km^2)$^{-1}$ $month^{-1}$ from *Dacre and Gray* [2009]. (b) RGB air-mass satellite image of extra-tropical cyclone Klaus (00 UTC 24 January 2009) from EUMETSAT.

In Europe, explosive cyclones are considered as the most important natural hazard due to their associated hurricane-like strong wind gusts, precipitation and storm surge events [*Lamb*, 1991; *Della-Marta et al.*, 2010]. Well-known examples of explosive cyclones impacting Europe include Lothar and Martin in 1999, Kyrill in 2007, Klaus in 2009 (Fig. Ib), and Xynthia in 2010 [*Ulbrich et al.*, 2001; *Fink et al.*, 2009; 2012; *Liberato et al.*, 2011]. In some years, storms tend to develop and propagate in quick succession [Fig. II; *Mailier et al.*, 2006; *Vitolo et al.*, 2009]. These events are characterized by the passage of multiple strong cyclones over the same area in a short period of time (~2 weeks), and constitute a threat for human life and a concern for the insurance industry, as the accumulated losses during these periods remarkably increase. Clear examples of storm clustering

episodes over Europe took place during the winters of 1990, 1993, 1999 and 2007. In particular, the insured losses of the years 1990, 1999, and 2007 were quantified at $10, $18 and $10 billion [*MunichRe*, 2010].

Cyclone clustering over Western Europe

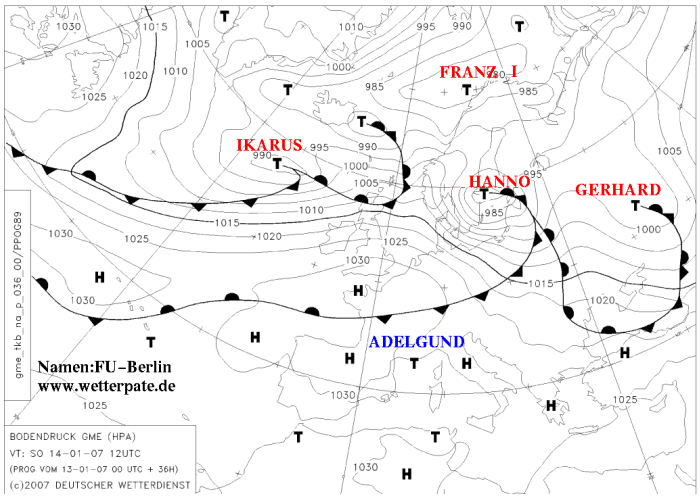

Fig. II: Cyclone clustering example: *Deutscher Wetterdienst* analysis weather chart (+36h) for 14 January 2007 (12 UTC). Mean sea level pressure (in hPa) in thin contours. Location of fronts in thick contours. Highs and Lows positions marked with H and T, respectively. Storm names taken from the *Freie Universität Berlin.*

Additionally, the influence of non-explosive or 'common' cyclones over Western and Central Europe is also paramount. In these areas, extra-tropical cyclones are responsible of the 70-85% winter precipitation and determine the day-to-day local weather variability [*Hawcroft et al.*, 2012].

In order to improve their predictability, several studies have analyzed the physical mechanisms contributing to explosive cyclone growth over the North Atlantic [*Fink et al.*, 2012]. On one hand, the presence of strong upper level winds and mobile upper troughs prior to cyclone intensification appears to play an important role [*Bosart and Lin*, 1984; *Hoskins et al.*, 1985; *Reader and Moore*, 1995; *Gyakum and Danielson*, 2000]. The former is consistent with amplification of cyclones while they cross the extra-tropical jet from the right-entrance to the left-exit regions, where updraft motion of air enhances atmospheric instability [*Uccellini*, 1990; *Rivière and Joly*, 2006a; 2006b]. On the other hand, enhanced low level baroclinicity by sensible and latent heat release processes also contributes to explosive cyclone development [*Manobianco*, 1989; *Fosdick and Smith*, 1991].

In the North Atlantic, the most prominent pattern of climate variability (the North Atlantic Oscillation, hereafter NAO) [*Walker*, 1924] is known to deflect extra-tropical cyclone trajectories poleward (equatorward) under its positive (negative) phase [*Wanner et al.*, 2001; *Hurrell et al.*, 2003; *Pinto and Raible*, 2012]. In addition, the positive phase of the NAO is associated with higher degree of baroclinicity in the North Atlantic, thus providing enhanced conditions for the occurrence of extreme cyclones [Fig. III; *Pinto et al.*, 2009]. In this line, European Windstorms over Northern and Central Europe tend to occur under a moderately positive NAO phase [*Raible*, 2007; *Donat et al.*, 2010]. Conversely, strong cyclones themselves can also play a significant role in steering the NAO phase [*Rivière and Orlanski*, 2007; *Michel et al.*, 2012]. In particular, this relation has been reported for individual cases in the literature. However, the robustness of this two-way relation between cyclones of varying intensities and the NAO remains largely unexplored. This is one of the motivating factors of the present thesis.

Extreme cyclones and NAO phase

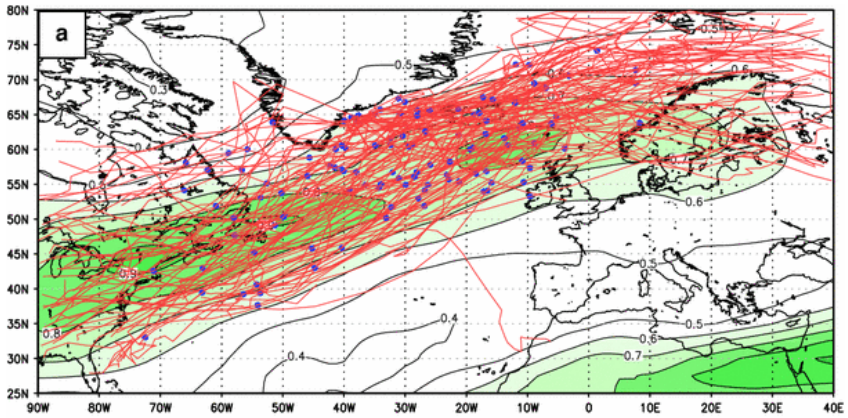

Fig. III: Composite of 3-day running mean of Eady growth rate 400 hPa (day^{-1}) in the extreme positive NAO phase. Cyclones tracks (10% strongest) displayed individually, maximum intensification phases marked with blue dots. From *Pinto et al.* [2009].

Regarding the underlying physics mediating into this two-way relation, some studies highlight the importance of Rossby Wave-Breaking processes [*Franzke et al.*, 2004; *Benedict et al.*, 2004]. On one hand, the North Atlantic Oscillation can be understood as a breaking wave, where a succession of RWB events of different signs (e.g. cyclonic or anti-cyclonic) appear to modulate its short-term variability [*Strong and Magnusdottir*, 2008b; *Woollings et al.*, 2008]. These RWB events may be associated in some cases with individual decaying

cyclones in the North Atlantic [*Thorncroft et al.*, 1993], but more generally arise from upper level Rossby waves of varying temporal and spatial scales not necessarily related with cyclonic development [*Randel and Held*, 1991; *Barnes and Hartmann*, 2011]. Regarding the occurrence of weather extremes, several studies also suggest the existence of a common RWB pattern prior to persistent blocking events [*Pelly and Hoskins*, 2003; *Santos et al.*, 2009; *Woollings et al.*, 2011]. In a similar way, *Hanley and Caballero* [2012] suggest the existence of a simultaneous north/cyclonic-south/anticyclonic pattern that appears to promote windstorm occurrence over Europe (Fig. IV). Their analysis is based on the 22 most destructive windstorms affecting Europe and they propose that the squeezing effect of RWB from both flanks accelerates the jet and shifts its core toward Western Europe. As a consequence, pre-existing cyclones encounter very favorable conditions for explosive amplification in the vicinity of Europe.

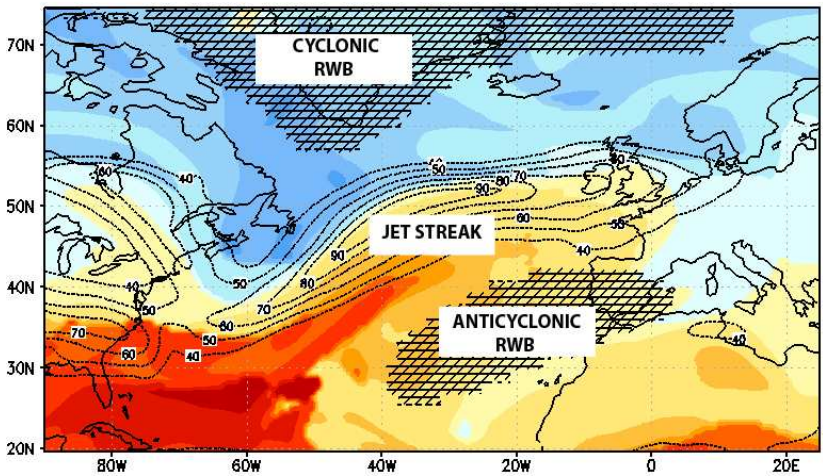

Fig. IV: Potential temperature on the 2PVU surface on 18 January 2007 (ERA-Interim). Cyclonic and anticyclonic RWB areas in hatched fields. Wind vector at 250 hPa in contours. Concept from *Hanley and Caballero* [2012].

However, this relation is not investigated yet through a lead-lag analysis using a comprehensive cyclone data set and a RWB index. For this purpose, the study of the two-way relation between RWB and extra-tropical cyclones is another motivating factor to be explored in this PhD. In particular, the existence of a common RWB pattern prior to and upstream of explosive cyclogenesis over the North Atlantic, together with the sensitivity of this relation to cyclone's intensity, trajectory and location (and vice-versa) are important questions to address.

Analogous to the study above, the large-scale dynamics associated with clustering of intense extra-tropical cyclones affecting Europe need to be explored, investigating whether the steering of the large-scale trough RWB processes is as well an important aspect in this process. In this context, the aim is to provide a more dynamical perspective of cyclone clustering over Western Europe. In the literature, several recent studies have analyzed the serial clustering of extratropical cyclones from a statistical perspective [e.g., *Mailier et al.*, 2006; *Vitolo et al.*, 2009], and demonstrated that this process occurs more frequently over the eastern North Atlantic and Western Europe than would be expected by chance (Poisson process).

Thus far, the motivational aspects leading to the study of variability and dynamics of explosive cyclogenesis in the synoptic scale are described. However, the picture of explosive cyclogenesis over the North Atlantic would remain incomplete (in the context of this thesis) without the study of its lower frequency variability, potential predictability and associated dynamics. In this context, other mechanisms apart from stochastic processes are suggested in the literature to influence the interannual to decadal variability of the North Atlantic storm track [*Hurrell et al.*, 2003]. For instance, the NAO decadal variability is known to have an important influence on North Atlantic storminess [*Luksch et al.*, 2005; *Matulla et al.*, 2007; *Lee et al.*, 2012; cf. Fig. V].

(a) (b)

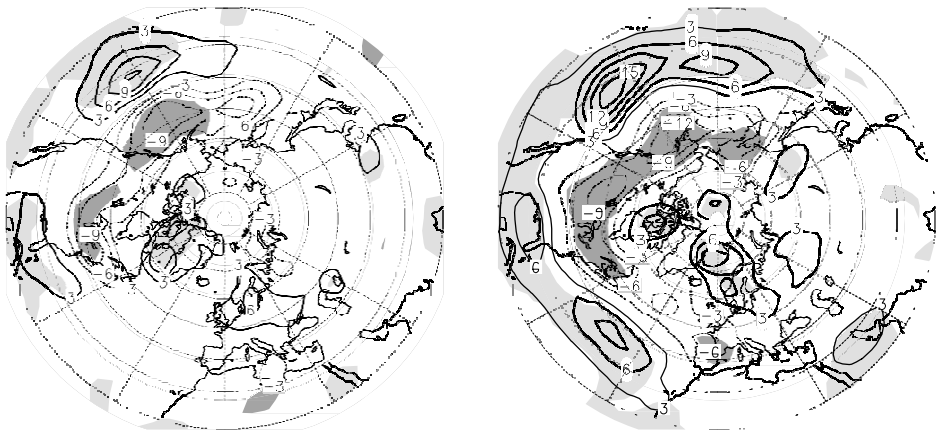

Fig. V: ENSO-Composite (warm El Niño - cold La Niña) for the sectoral (left; high decadal NAO) and hemispheric regime (right; low decadal NAO): (a,b) storm track or the 2.5-6 day bandpass-filtered standard deviation of the 500 hPa geopotential height (unit: gpm). From *Luksch et al.* [2005].

In this line, an eastward shift and intensification of the NAO centers of action has been reported during the last decades of the 20th century, thus leading to stronger cyclone activity over Northern and Central Europe [*Jung et al.*, 2003]. However, it is still unclear whether such changes in the NAO are due to natural decadal variability intrinsic to the climate system [*Wang et al.*, 2012; *Pinto and Raible*, 2012] or may be associated with anthropogenic climate change [*Ulbrich and Christoph*, 1999; *Osborn et al.*, 1999]. Another mechanism potentially leading to interannual to decadal changes of the North Atlantic storm track is the westerly flow advected from the North Pacific [*Honda et al.*, 2001; *Pinto et al.*, 2011]. In addition, the North Atlantic and tropical Pacific Ocean variability are also known to potentially influence the North Atlantic climate at interannual to decadal timescales [*Frankignoul and Kestenare, 2005; Losada et al., 2007; Brönnimann, 2007*].

However, the potential influence of these drivers onto explosive cyclogenesis climate variability still remains unclear. As a consequence, the high frequency climate variability (1-11 yr.) of explosive cyclogenesis needs to be analyzed. In particular, the potential decadal fluctuations in the relation between the NAO and explosive cyclones need to be addressed. This is motivated by the non-stationary teleconnections observed in the climate system, which in occasions, appear to be driven by multi-decadal variability [*Raible et al.*, 2004; *Vicente-Serrano and López-Moreno*, 2008; *López-Parages and Rodríguez-Fonseca*, 2012; cf. Fig. VI].

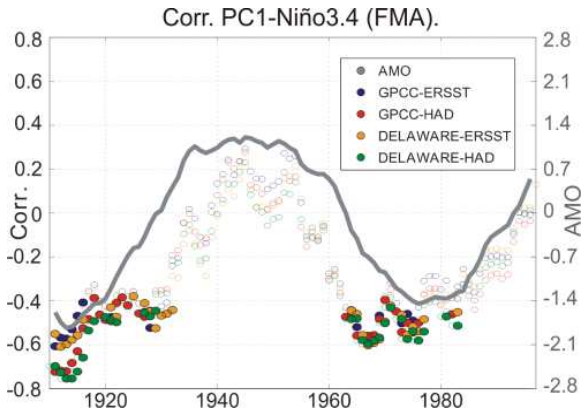

Fig. VI: Results for early spring (FMA): 21 year moving window correlations (left axis) between the EOF1 of interannual Euro-Mediterranean rainfall and Niño3.4 index for different precipitation and sea surface temperature datasets. In grey line, the standardized Atlantic Multidecadal Oscillation index. From *López-Parages and Rodríguez-Fonseca* [2012].

Thus, the influence of atmospheric/oceanic long term variability onto the potential time-evolving connection between the NAO and North Atlantic bombs is another motivating factor of this thesis.

The present work is structured as follows: the State of Knowledge is described in Chapter I, and the specific Objectives of the thesis are enumerated in Chapter II. Chapters III and IV describe the Data and Methodologies used throughout the PhD, respectively. The main Results are presented as a collection of scientific publications in Chapter V, and an integrative Discussion of the former follows in Chapter VI. Finally, the main Conclusions and Implications of the thesis are enumerated in Chapter VII, together with the potential paths for future research.

I. STATE OF KNOWLEDGE

'If you want to see the sunshine, you have to weather the storm'

Frank Lane (baseball executive; 1896-1981)

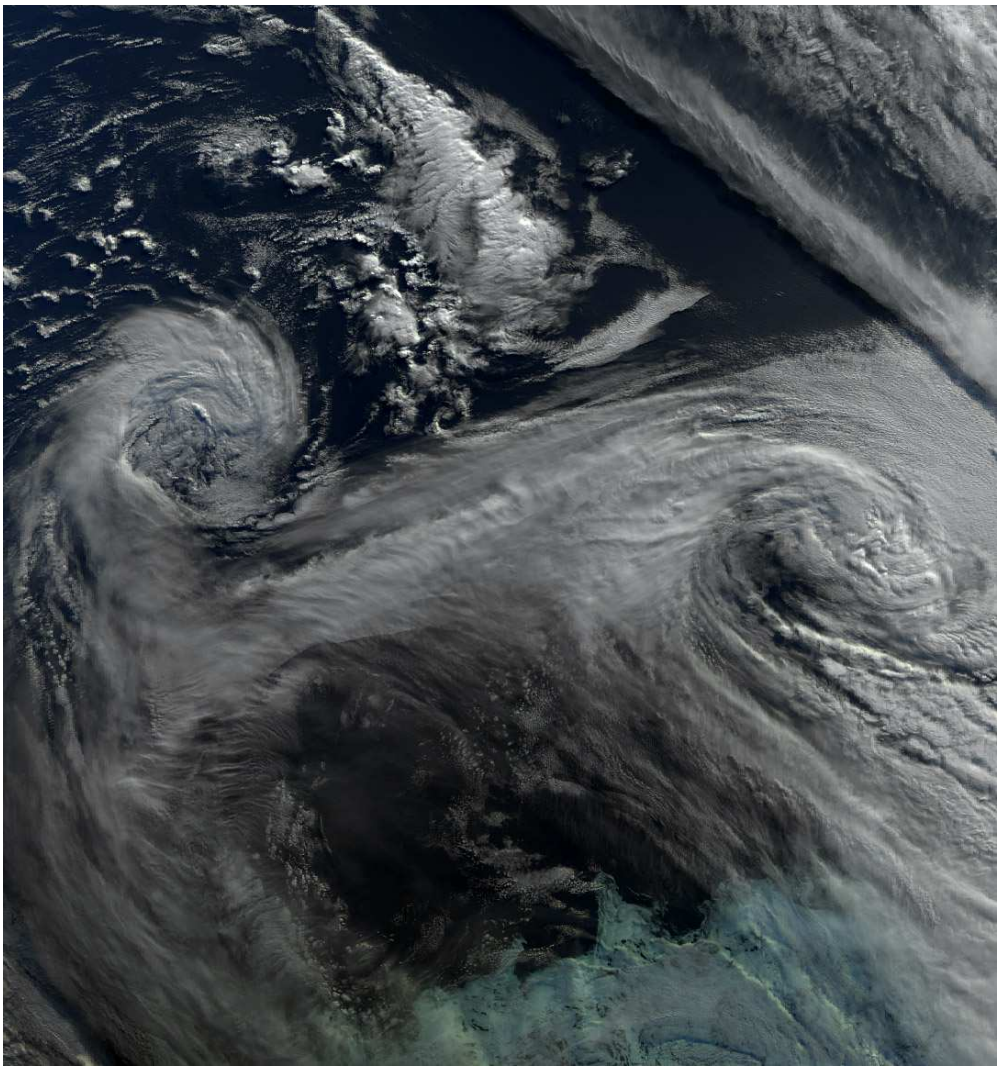

I. State of Knowledge

In this chapter a review of the current state of knowledge of the topics investigated in this thesis is provided. With this aim, the general circulation of the Earth's atmosphere and ocean is described in Section I.1. In Section I.2 the large-scale variability in the northern Hemisphere and the North Atlantic sector is introduced. A review of extra-tropical cyclones characteristics follows in Section I.3, and a description of eddy/mean flow interaction in the Euro-Atlantic sector concludes this chapter.

1. General circulation of the Atmosphere and the Ocean

a. General circulation of the Atmosphere

The main factors shaping the general circulation of the Earth's atmosphere are (i) the uneven incoming radiative forcing between the Equator and the Poles caused by the inclination of the Earth's ecliptic; and (ii) the Earth's rotation, which produces an acceleration of fluid parcels proportional to their travelling speed and latitude in a rotating frame of reference [*Vallis*, 2006]. The action of this 'apparent' force is measured through the Coriolis parameter (I.1):

$$f = 2\Omega sin\varphi, \tag{I.1}$$

where Ω is the rotation rate of the Earth (Ω = 7.2921 × 10^{-5} rad s^{-1}) and φ the latitude in radians. The unequal incoming radiation between the Poles and the Equator at the top of the atmosphere can be observed in Fig. 1.1a (solid line). The outgoing infrared radiation with latitude is plotted in the same figure (dashed line), and indicates net heating at low latitudes. Contrastingly, the heat balance over the Poles is negative. If the atmosphere was in equilibrium with this heating, that would imply a strong meridional gradient of temperature (Fig. 1.1b - solid line). However, the atmospheric and oceanic circulations act to mitigate this meridional gradient (Fig. 1.1b - dashed line) by transporting heat from the Equator toward the Poles.

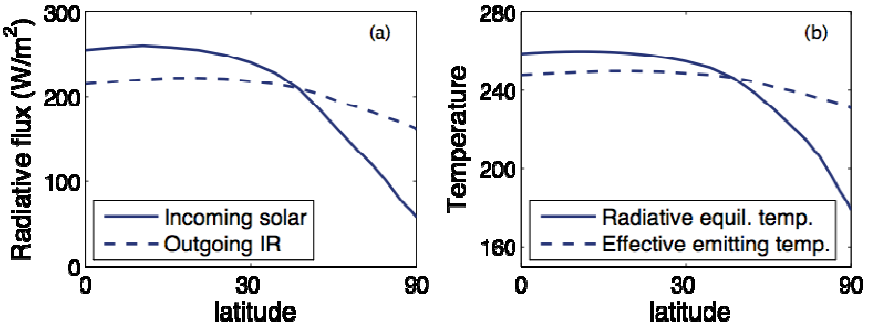

Fig. 1.1: (a) The (approximate) observed net average incoming solar radiation and outgoing infrared radiation at the top of the atmosphere, as a function of latitude (plotted on a sine scale). (b) The temperatures associated with these fluxes, calculated using a black body radiation approach. The solid line is an approximate radiative equilibrium temperature. From *Vallis* [2006].

If the Earth did not rotate, the meridional transport of heat would be organized in the troposphere in the form of a unique hemispheric cell, with ascent of air over the Equator and subsidence at high latitudes. However, in reality the Coriolis force deflects air parcels moving in the N-S direction and their trajectories are curved. This strong zonal acceleration produces an unstable jet and limits the poleward excursion of the air parcels rising at low latitudes. This leads to a meridional hemispheric circulation organized into three different cells: the Hadley, Ferrel and Polar cells [*Peixoto and Oort*, 1991]. Whereas the Hadley and Polar cells are thermally direct and transport heat polewards, the circulation over the mid-latitudes is indirect (Fig. 1.2). However, the net heat transport towards the Poles remains always positive when eddy transport is also included.

The circulation cells extend all over the troposphere's depth. In the Equator, the tropopause (defined as the transition layer between the troposphere and the stratosphere) is situated around 14 km above the surface. Over the Poles this height is significantly lower (~6 km) due to the colder and denser air. In general, the temperature decreases with height within the troposphere, whereas the contrary is observed over the stratosphere mainly due to shortwave heating (e.g., by ozone). A detailed description of the meridional circulation cells is given below:

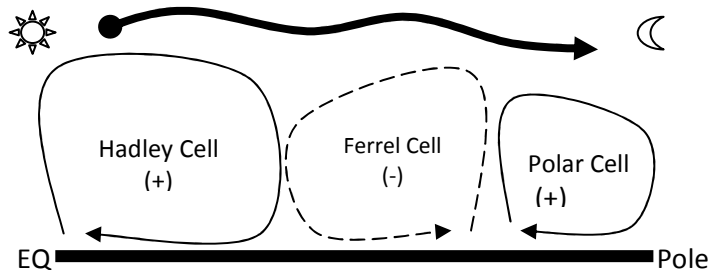

Fig. 1.2: Schematic of the meridional circulation of the Northern Hemisphere.

i Hadley Cell

The Hadley cell is associated with strong uplift of air in the summer hemisphere, meridional transport across the equator and subsidence over the sub-tropics. The region of maximum air ascent is known as the Inter-tropical Convergence Zone [ITCZ; *Peixoto and Oort*, 1991]. The subsidence creates a high-pressure belt over the subtropics (Fig. 1.3a). This latitudinal structure is responsible for the distribution of equatorial rainforests and sub-tropical deserts. The Hadley cell transports heat poleward due to the higher static energy values along its upper branch. Although the Coriolis parameter is very small near the Equator, at higher latitudes it forces the sub-tropical jet stream by deflecting eastward the air that moves poleward along the upper branch of the Hadley Cell (so as to conserve angular momentum). Likewise, the near-surface easterlies (Fig. 1.3b) are due to the westward deflection of the return flow in the lower branch.

(a) Mean Sea Level pressure (b) Zonal wind

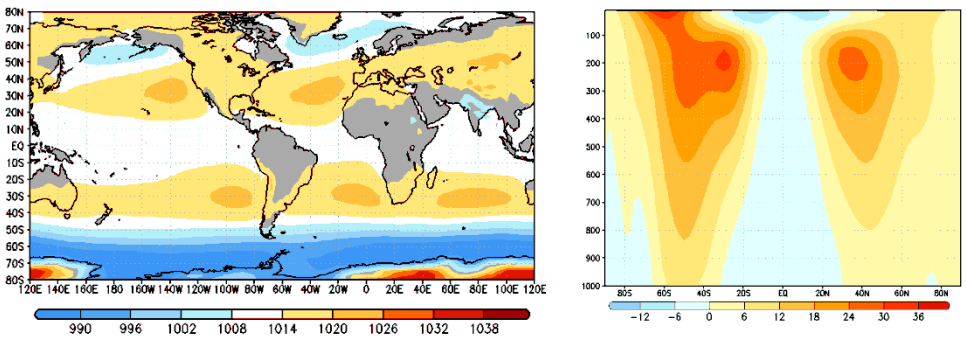

Fig. 1.3: (a) Mean sea level pressure in hPa. (b) Mean zonal wind in m s^{-1}. Jan to Dec 1949-2015, NCEP.

ii Ferrel Cell

Over the mid-latitudes the Coriolis parameter is greater and thus able to balance the pressure gradient between the sub-tropical and sub-polar areas (cf. Fig. 1.3a). As a result, the air moves parallel to the isobars and the circulation is nearly geostrophic. Geostrophic balance is an important constraint in the mid-latitudes: as thermal and mechanical forcing tend to disrupt this balance, ageostrophic circulations must be driven to restore it. In the zonal mean, this produces a thermally indirect meridional circulation known as the Ferrel cell. Although this cell transports heat equatorwards, the polewards transport by the transient eddies (Fig. 1.4b) dominates. These are sub-weekly disturbances that grow at the expense of the mean flow baroclinicity [e.g., the strong gradients of temperature and humidity; *Hoskins and Valdes*, 1990]. In the northern hemisphere baroclinic eddies typically grow near the planetary stationary troughs and propagate toward the regions of stationary ridges over the oceans [Fig. 1.4; *Lau*, 1988]. Stationary troughs and ridges arise due to the asymmetric continental arrangement and thus have greater amplitude in this hemisphere (cf. Fig. 1.4a). In addition, baroclinic eddy activity is maximum during wintertime, as the meridional gradient of temperature is largest in this season.

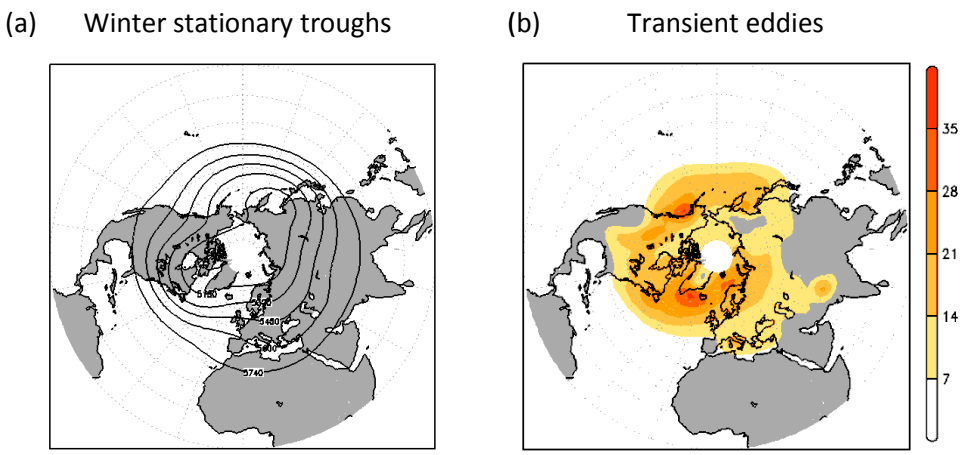

Fig. 1.4: (a) Mean geopotential height at 500 hPa in winter (gpm). DJF 1949-2015 NCEP (b) Cyclone track density (in counts per 7.5° radius circle area per DJF). 1957-2001 ERA-40.

Baroclinic eddies are also associated with extra-tropical cyclones. Besides transporting heat poleward in the mid-latitudes (Fig. 1.5a), they also accelerate the mean flow in this region [*Vallis*, 2006]. This is observed in Fig. 1.5b, in the form

of strong eddy momentum convergence at upper levels in the mid-latitudes. This convergence of eddy momentum fluxes is responsible for the existence of strong westerly winds in the mid-latitudes (i.e., the eddy-driven jet; Fig. 1.3b). In the upper branch of the Ferrel cell the Coriolis force balances the westerly acceleration induced by the eddy momentum convergence. In the lower branch, the Coriolis force acting on the return flow accelerates the westerly wind and frictional processes act to decelerate it. A schematic of the momentum balance in this circulation is provided in Fig. 1.5c. A more detailed description of mid-latitude eddies over the north Atlantic is provided in section I.3.

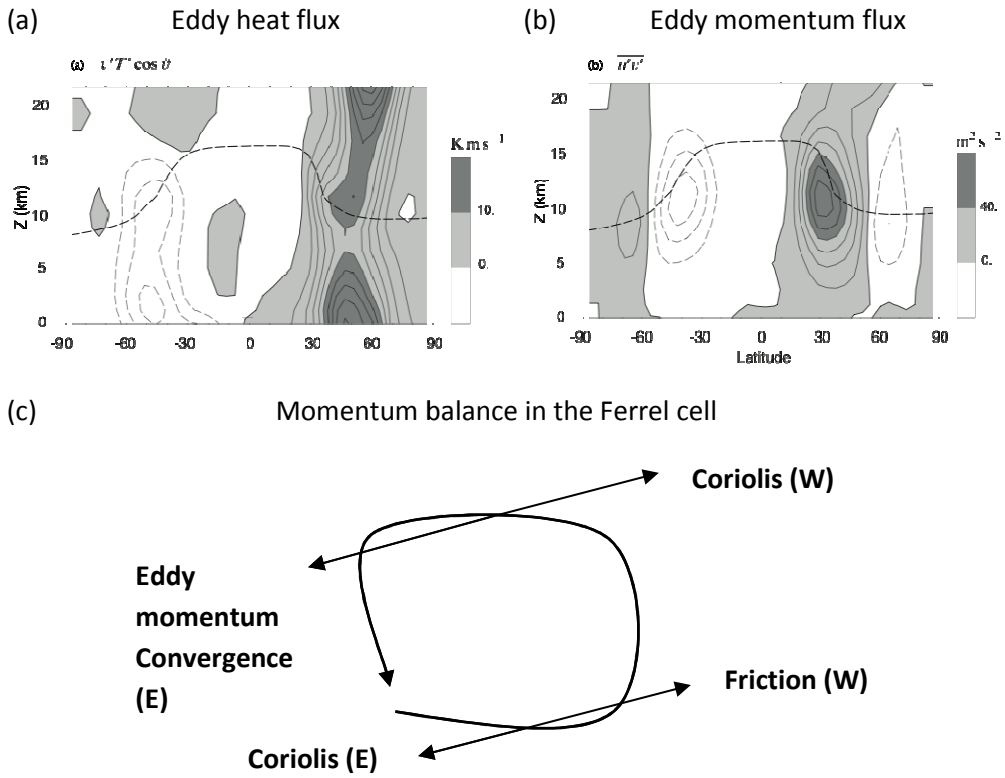

Fig. 1.5: (a) The average meridional eddy heat flux and (b) the eddy momentum flux in the northern hemisphere winter (DJF). The ordinate is log-pressure, with scale height H=7.5 km. Positive (northward) fluxes are shaded in both cases, and the dashed line marks the thermal tropopause. The eddy heat flux (contour interval 2 K m s^{-1}) is largely polewards, and down the temperature gradient, in both hemispheres. The eddy momentum flux (contour interval 10 m^2 s^{-2}) converges in mid-latitudes in the region of the mean jet, and must be upgradient there. (c) Schematic of the momentum balance in the Ferrel cell for the Northern Hemisphere. Figures taken and adapted from *Vallis* [2006].

iii Polar Cell

The polar cell extends from the mid-latitudes to the Poles (Fig. 1.2). In this direct circulation the air is pushed aloft along the polar front in the mid-latitudes (due to the effect of the baroclinic eddies) and moves at upper levels towards the Poles, where it sinks [*Peixoto and Oort*, 1991]. This leads to semi-permanent high pressures over the Arctic and Antarctica (Fig. 1.3a). The physical processes driving the Polar cell are similar to those of the Ferrel cell, though the sign of the circulation reverses because baroclinic eddies decelerate rather than accelerate the mean flow over this region. Although the circulation is thermally direct like the Hadley cell, its intensity is much weaker. Near the surface, the Coriolis force acting on the return flow deflects the wind westward, leading to an E-W-E surface wind pattern as we move from the Equator to the Poles in both hemispheres (cf. Fig. 1.3b).

b. General circulation of the Ocean

The oceans are a crucial component of the climate system. They cover 70% of the Earth's surface and their influence over the atmosphere is strong due to the great amount of solar energy they can store. The atmosphere and oceans are coupled through air-sea interactions, associated with sensible and latent heat exchanges between both fluids and the momentum flux given by the atmosphere to the ocean [*Vallis*, 2006]. Over the oceans there also exists a strong meridional gradient of temperature (especially over the mid-latitudes, Fig. 1.6a), that tends to be mitigated by the oceanic circulation [*Peixoto and Oort*, 1991]. These SST frontal zones appear to modulate the location and strength of the Eddy-driven atmospheric jets [*Minobe et al.*, 2008; *Nakamura et al.*, 2008]. In addition, there also exists a remarkable W-E temperature gradient over the oceans. This gradient is produced by the global atmospheric wind pattern and continental arrangement. Over the tropics, the surface easterly winds pile up warm waters over the westernmost areas of the oceanic basins. As a result, east in the basins strong upwelling of deep ocean waters occurs, thus leading to cold, nutrient-rich surface waters (e.g., Humboldt, Benguela, Canary currents). In the mid-latitudes, the continental arrangement leads to western boundary poleward warm currents produced by the geostrophic equilibrium associated with strong oceanic west-east pressure gradients (e.g. the Gulf and Kuroshio streams). In the North Atlantic, the Gulf Stream transports warm waters from the Caribbean Sea towards northern

Europe, and produces milder winter temperatures in this region than expected at these high latitudes. A schematic of the main oceanic surface currents is provided in Fig. 1.6b.

(a) Mean SST

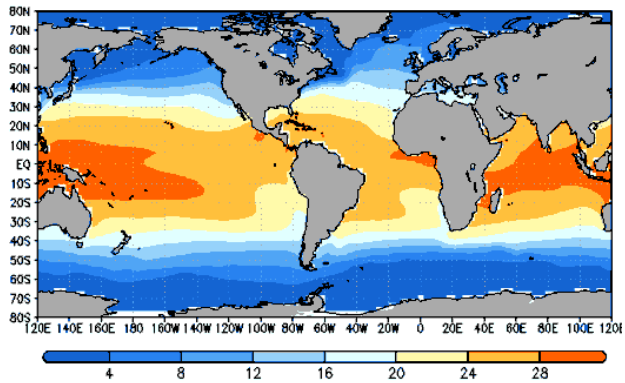

(b) Main oceanic currents

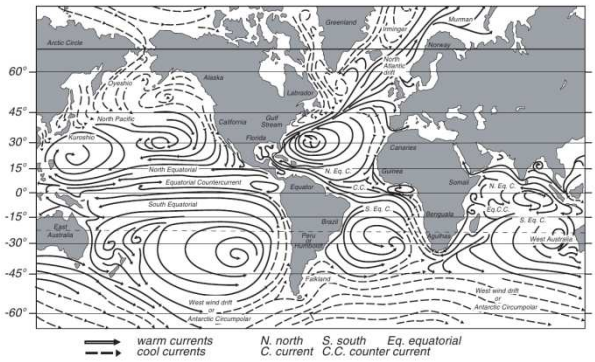

(c) Ocean's vertical structure

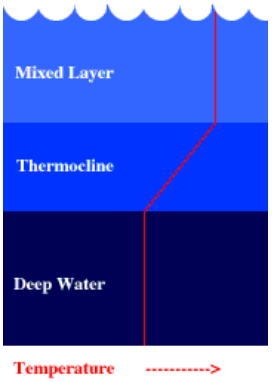

Fig. 1.6: (a) Mean Sea Surface temperature (Jan to Dec, 1949-2015 in deg. C; ERSST[1] data base); and (b) Main currents of the global ocean. From *Stewart* [2008]. (c) Schematic of the ocean's vertical layers. From the Department of Atmospheric Sciences (DAS) at the University of Illinois at Urbana-Champaign (http://ww2010.atmos.uiuc.edu).

Due to the vertical mixing induced by the atmospheric winds, in the uppermost part of the oceans a layer of almost constant vertical temperature exists. This is the so-called mixed layer and extends from the surface down to 500 m, although its depth is sensitive to location and season. The relatively warm and

[1] The Extended Reconstructed Sea Surface Temperature dataset: www.esrl.noaa.gov.

salty waters in this layer are separated from the colder and denser deep ocean waters by the thermocline region [Fig. 1.6c; *Peixoto and Oort*, 1991]. Additional to the wind-driven currents, the oceanic circulation is also highly influenced by thermal and saline mixing processes. These processes lead to the establishment of the Thermohaline Ocean Circulation [THC; *Rahmstorf*, 2006], which transports a large amount of heat between the deep ocean waters and the surface around the globe (Fig. 1.7). As the response of this circulation to external forcings appears to be non-linear, the THC is thought to play an important role for abrupt climate change. This current is associated with deepwater formation over the Greenland-Norwegian, Mediterranean, Labrador, Weddell and Ross Seas, due to the high density of the waters over these areas (very cold and saline). Reversibly, thermally-driven upwelling is observed over the Antarctic circumpolar region. This circulation leads to strong deep currents over the western boundaries of the oceans (e.g., the North Atlantic Deep Water current) and surface streams counteracting the outflow of the former (to some extent the Gulf and Kuroshio Streams, though they are mainly wind-driven ~80%).

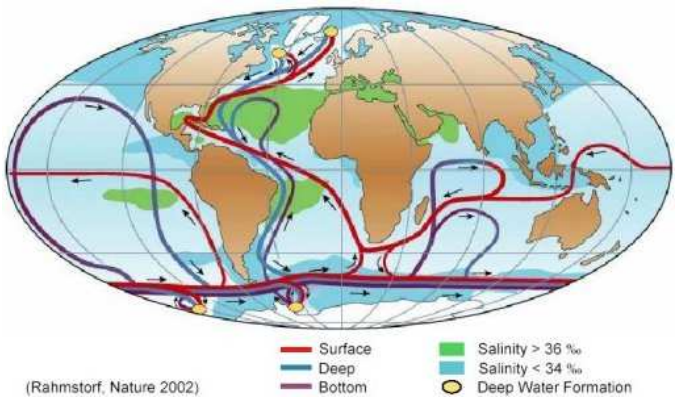

Fig. 1.7: Schematic representation of the global thermohaline circulation. Surface currents are shown in red, deep waters in light blue and bottom waters in dark blue. The main deep water formation sites are shown in orange. Adapted by S. Rahmstorf after *Broecker* [1991].

Although the THC and the Meridional Overturning Circulation (MOC) are often regarded as the same thing, the latter really only refers to the meridional transport, including wind-driven branches. In this thesis the potential influence of the MOC on the variability of intense extra-tropical cyclones over the North Atlantic is considered (cf. section V.4).

2. Large-scale climate variability and teleconnections

Climate variability is the science that studies the deviations of the atmospheric and oceanic states from their average or climatological conditions (cf. previous section). This is typically analyzed using temporal anomalies, which refer to the time-evolving differences of a physical variable relative to its climatological value. In the climate system anomalies can be triggered by multifarious physical processes with very different characteristic timescales. In addition, the spatial distribution of these temporal anomalies is often non-local and involves remote regions. The interrelated behavior of climate anomalies on distant regions is known as a teleconnection. Despite the high complexity of the climate system, there exists evidence of recurring anomaly patterns in the atmosphere and ocean [*Wallace and Gutzler*, 1981; *Barnston and Livezey*, 1987]. These cyclic patterns are able to explain a great fraction of the atmospheric and oceanic variability, and thus constitute a pivotal element of climate research. In the literature, several teleconnection patterns have been found to influence the North Atlantic sector [*Marshall et al.*, 2001]. In the following, the most prominent teleconnection patterns of the Northern Hemisphere known to impact the Euro-Atlantic sector are reviewed. We only introduce those patterns that are relevant for the results presented in this thesis.

a. Remote global teleconnection patterns with influence over the North Atlantic

i *El Niño-Southern Oscillation*

El Niño-Southern Oscillation (ENSO) phenomenon is the greatest source of variability in the global climate system at interannual timescales [Fig. 1.8; *Trenberth*, 1997]. Under its positive phase (El Niño), it is characterized by a warming of the sea surface temperatures of the central and eastern Equatorial Pacific (Fig. 1.8b). Due to air-sea interaction processes, this warming leads to low pressure anomalies aloft in the atmosphere, and a decrease of the zonal SLP gradient between the western and Eastern equatorial Pacific (i.e. the Southern Oscillation). These conditions are reversed under a negative phase of ENSO (La Niña; Fig. 1.8c). As a consequence, anomalous deep convection occurs over the Equatorial Pacific during El Niño years, whereas precipitation is enhanced over the western tropical Pacific during la Niña events. Locally, it also influences the zonal gradient of thermocline depth over the tropical Pacific. El Niño years are also

associated with weakened upwelling near Peru. Indeed, the name of El Niño (baby Jesus) was given by Peruvian sailors who noticed that during Christmas of the years of warmer waters their fishing captures strangely decreased.

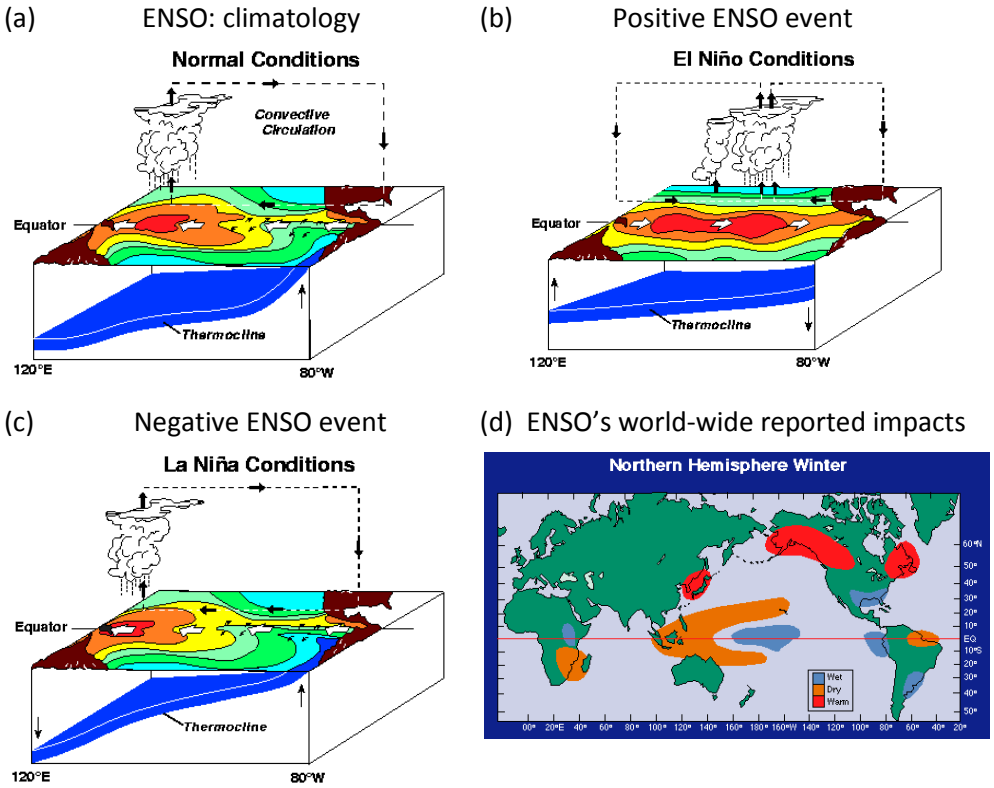

Fig. 1.8: (a)-(c) Schematic diagram of normal, El Niño, and La Niña conditions in the Pacific Ocean. (d) Precipitation anomalies during El Niño in winter. Source: NOAA (www.pmel.noaa.gov/tao/elnino/nino-home.html).

The persistence of El Niño/La Niña events is of about 15 months (depending on its strength) and its periodicity ranges from 3 to 7 years. El Niño and La Niña are very useful for predicting climatic anomalies over specific areas. This is due to the large amount of energy stored by the ocean, which is released into the atmosphere and leads to modifications in the global circulation and associated teleconnections. As a consequence, their impacts are strong and global and there is high forecasting skill several months in advance [Fig. 1.8d; *Jin et al.*, 2008]. The most commonly used index to analyze the ENSO variability is the Niño3-4 index [*Trenberth*, 1997]. This is calculated averaging the high-pass filtered (1-13 yr.) SST anomalies over the area [5°N-5°S; 170°W-120°W].

The influence of ENSO over the North Atlantic sector has been analyzed is many previous studies with differing conclusions [*Brönnimann*, 2007]. In particular, three main dynamical mechanisms are still under debate. The first is the so-called downstream effect [*Bjerknes*, 1966]. Under this mechanism ENSO disturbs the Hadley circulation over the North Pacific sector. This affects the climate anomalies not only in the Pacific but also downstream in the North Atlantic as they propagate embedded in the Westerly flow [*Cassou and Terray*, 2001; *Raible et al.*, 2004; *García-Serrano et al.*, 2011]. This mechanism involves the mediation of the mid-latitude eddies and it is suggested to be non-linear [*Pozo-Vazquez et al.*, 2001]. The second mechanism takes place in the tropical SSTs in the North Atlantic through a perturbation of the inter-basin Walker circulation that leads to a weakening of the Atlantic Hadley cell/Azores high [*Ruiz-Barradas et al.*, 2003; *Wang*, 2004]. The third mechanism occurs via downward propagation of stratospheric anomalies triggered by Rossby waves vertically travelling from the equatorial pacific toward the stratospheric polar vortex [*Baldwin and Dunkerton*, 2001; *Randel*, 2004]. Regardless of the mechanism involved, there exists some consensus on the ENSO impact over the North Atlantic circulation during autumn and late winter/early spring. In late winter, under El Niño conditions a weakened and equatorward displaced extra-tropical jet is observed over the North Atlantic. This leads to southwardly shifted extra-tropical cyclone trajectories. Under La Niña conditions these features are reversed [*Brönnimann*, 2007]. Nevertheless, the ENSO-Europe teleconnection is still unclear and recent studies suggest this relation may be non-stationary in time [*Mariotti et al.*, 2002; *Greatbach et al.*, 2004; *López-Parages et al.*, 2014]. In this thesis the possible role of ENSO variability onto intense extra-tropical cyclones in the North Atlantic is assessed.

i *The Arctic Oscillation*

The Arctic Oscillation (AO) is the leading pattern of atmospheric variability in the Northern Hemisphere from synoptic to seasonal timescales [*Wallace and Thompson*, 2002]. It characterizes the strength and location of the maximum westerly flow over the mid-latitudes. Under its positive phase it is associated with negative sea level pressure anomalies over the Arctic and positive anomalies over the Aleutians and Azores (Fig. 1.9a). These conditions thus lead to enhanced confinement of cold air at high latitudes. Under the negative phase the extra-tropical jet is less intense and curvier, hence leading to higher frequency of cold and warm air outbreaks over the mid-latitudes. The AO is defined as the leading

mode of Empirical Orthogonal Function analysis[2] (EOF) of geopotential height at 1000 hPa poleward of 20˚N (NOAA CPC definition).

The underlying physics of this pattern are still under debate. On one hand, some studies suggest that this is an annular mode that represents an oscillation (not necessarily longitudinally coherent) between sub-polar and sub-tropical latitudes in the North Atlantic and North Pacific [*Wallace and Thompson*, 2002]. On the other hand, other authors suggest that the AO is a non-annular mode, whose centers of action are part of a stationary wave of wave-number 5 embedded in the extra-tropical jet [*Branstator*, 2002; *Watanabe*, 2004]. In addition, it still unclear whether this oscillation arises by purely stochastic eddy/mean flow interactions or there is some intrinsic memory, and the possible forcing role by lower-frequency variability such as ENSO. The AO pattern is more prominent during winter due to the enhanced meridional temperature gradient during the boreal polar night.

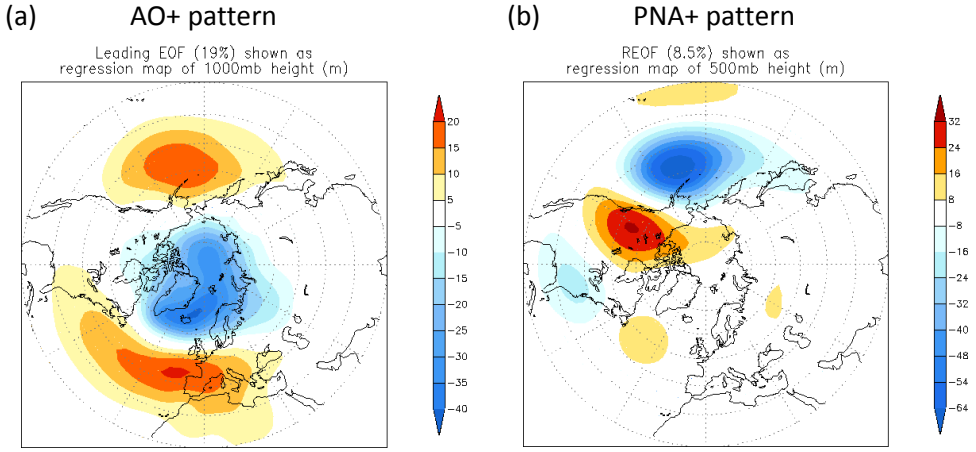

Fig. 1.9: (a) Loading AO pattern (in gpm std^{-1}). (b) Loading PNA pattern (in gpm std^{-1}). Source: NOAA CPC (www.cpc.ncep.noaa.gov).

ii *The Pacific North American pattern*

The Pacific North American pattern (PNA) is the second leading variability mode of the Northern Hemisphere from synoptic to seasonal timescales [*Wallace and Gutzler*, 1981]. Its structure consists of four centers of action that arch from the North Pacific onto the Western North Atlantic (Fig. 1.9b). This variability

[2] See section IV for further information on this analysis.

pattern is strongly connected with the extra-tropical jet stream over the Eastern Pacific. Under a positive phase, the jet is extended toward western North America. Under the negative phase, the jet is constrained over the western North Pacific and high-pressure anomalies are present over the Aleutians, thus disrupting the zonal Westerly flow. Although the PNA variability is known to be driven by internal variability of the climate system (e.g., eddy/mean flow interactions), the influence of ENSO on its behavior is important (cf. Tropical Northern Hemisphere pattern - TNH; *Mo and Livezey*, 1986; *Bladé et al.*, 2008]. As explained above, ENSO events act to modify the Hadley cell behavior in the North Pacific, and these anomalies influence the SLP over the Aleutians and downstream into the North Atlantic [*Cassou and Terray*, 2001; *Raible et al.*, 2004] via Rossby wave propagation at upper levels. The calculation of the PNA pattern is similar to the AO but considering the second leading EOF.

It has been suggested that the inter-basin connection between the North Pacific and the North Atlantic may occur via downstream propagation of synoptic anomalies [*Honda et al.*, 2001; *Riviére and Orlanski*, 2007; *Drouard et al.*, 2015]. In addition, other authors point to a non-stationary connection of the PNA influence over the eastern North Atlantic [*Pinto et al.*, 2011], which leads to changes in the storm track activity at both sides of North America. In this thesis this relation is also indirectly investigated through the use of cyclone track density data from the North Pacific and the North Atlantic.

b. Teleconnection patterns of the North Atlantic

i *The North Atlantic Oscillation*

In the North Atlantic, the most prominent pattern of climate variability at a wide range of frequencies (from days to several decades) is the North Atlantic Oscillation [NAO; *Walker*, 1924]. It characterizes a redistribution of mass between sub-tropical and sub-polar latitudes and controls the latitudinal position and strength of the maximum westerly flow in the Euro-Atlantic sector. It consists of a dipolar structure of SLP anomalies between the sub-tropical and sub-polar North Atlantic [Fig. 1.10 – top; *Rogers*, 1997; *Marshall et al.*, 2001; *Wanner et al.*, 2001]. Based on this structure, it is sometimes regarded as the regional signature of the AO pattern [*Wallace and Thompson*, 2002]. However this question is still under debate, as the physical processes involved in their variability appear to differ [*Hurrell et al.*, 2003].

Under a positive NAO phase (Fig. 1.10 - bottom/a), both the semi-permanent low over Iceland and the Azores high are reinforced, thus leading to a stronger SLP meridional gradient. The extra-tropical jet is accelerated and shifted to the northeast compared with its climatological location. This leads to a northward displacement of extra-tropical cyclone trajectories in the North Atlantic, and produces wetter and milder (drier and colder) atmospheric conditions over Northern Europe (Southern Europe) [*Pinto and Raible*, 2012].

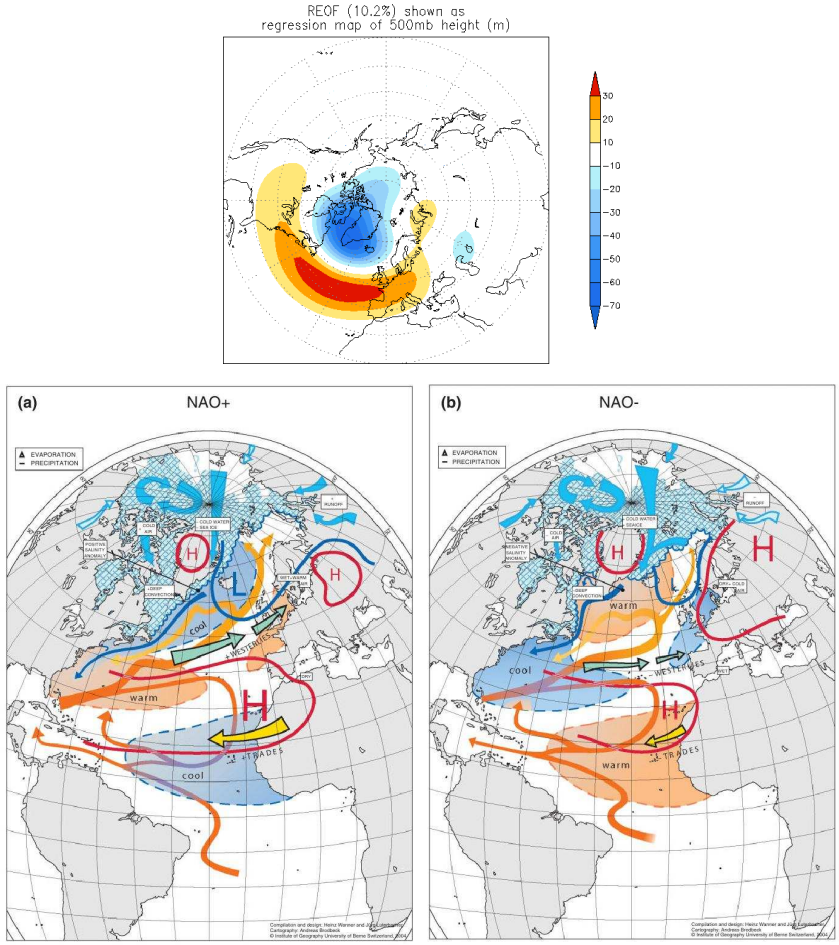

Fig. 1.10: *Top:* NAO pattern (in gpm std^{-1}) from NOAA CPC (www.cpc.ncep.noaa.gov). *Bottom:* A schematic overview of the two states of the NAO. Shading indicates SSTs (circled by dashed contours) and sea-ice extension; arrows show the flow in ocean, atmosphere and rivers; solid blue and red contours indicate sea level pressures; white rectangles describe either characteristic climate conditions or important processes: (a) The positive phase and (b) the negative phase of the NAO. Adapted from *Wanner et al.* [2001] by *Pinto and Raible* [2012].

Due to air-sea interactions processes, an imprint onto the ocean of the NAO+ configuration is observed [*Visbeck et al.*, 2003]. On one hand, the enhanced passage of low pressure systems over sub-polar latitudes induces a cold SST anomaly extending from Newfoundland to Iceland. As the strengthened Azores high leads to stronger trade winds over Northwestern Africa, a cold SST anomaly arises over this area (due to the stronger wind-driven upwelling). The NAO+ also leads to a warming in the ocean surface between Eastern North America and the central North Atlantic. In the literature this pattern is known as the Atlantic SST tripole [*Czaja and Frankignoul*, 1999], whose sub-tropical part is suggested to have predictive skill into the winter NAO [*Frankignoul and Kestenare*, 2005; *Losada et al.*, 2007; two way atmospheric-oceanic relation] and humidity advection over Europe [*Rodríguez-Fonseca et al.*, 2006]. Further information of the NAO+ impacts is provided in Fig. 1.10 [*Pinto and Raible*, 2012].

Under a negative NAO phase (Fig. 1.10 - bottom/b), the meridional SLP gradient between Azores and Iceland is weakened. As a consequence, the extra-tropical jet stream is decelerated, constrained upstream in the North Atlantic and shifted equatorward. This large-scale configuration leads to deflected cyclone trajectories towards the sub-tropical North Atlantic and southern Europe, where the atmospheric conditions are warm and wet [*Rodríguez-Puebla et al.*, 2001; *Fernández et al.*, 2003]. This configuration enhances the occurrence of atmospheric blocking in Northern Europe, thus leading to persistent episodes of 1-2 weeks of disrupted westerly flow over this area [*Barriopedro et al.*, 2006; *Woollings et al.*, 2008]. Regarding the NAO- imprint onto the ocean, the SST anomalies result in a similar shape but with opposite sign compared with NAO+. For further information of the NAO- phase see also Fig. 1.10.

Regarding the driving of the NAO variability, it is still unclear whether this variability primarily arises from pure stochastic processes [*Stephenson et al.,* 2000], or external low-frequency factors might also be important. These include: (i) the variability of the Tropical Atlantic [*Raible et al.*, 2001; *Visbeck et al.*, 2003; *Chen et al.*, 2015] and Tropical Pacific [*Toniazzo and Scaife*, 2006; *Brönnimann*, 2007]; (ii) the western flow from the North Pacific [*Honda et al.*, 2001; *Pinto et al.*, 2011; *Drouard et al.*, 2015]; (iii) downward propagation of stratospheric anomalies [*Baldwin and Dunkerton*, 2001; *Reichler et al.*, 2012]; (iv) solar variability [*Shindell et al.*, 2001]; and (v) the Indian Ocean [*Hoerling et al.*, 2001; 2004], among others. Given the wide range of frequencies in which the NAO variability dominates, it seems plausible that this variability might arise from a mix of disparate physical processes [*Hurrell et al.*, 2003].

On synoptic timescales, the variability of the NAO appears to be mainly driven by complex non-linear Eddy/mean flow interactions [*Feldstein*, 2003; *Franzke et al.*, 2004; *Woollings et al.*, 2008]. As explained in the previous section, the convergence of momentum from baroclinic eddies is maximum in the mid-latitudes, and this interaction leads to a modulation of the extra-tropical jet strength and location [*Vallis*, 2006]. Reversibly, the NAO also modulates the spatial structure (most importantly, their meridional tilt) and strength of baroclinic eddies over the North Atlantic [*Pinto et al.*, 2009]. In this regard, there exists evidence of a two-way relation between the large-scale circulation (represented by the NAO in the North Atlantic) and extra-tropical cyclone activity. In order to better introduce this relation (which is the main motivation for this thesis), in Sections 3 and 4 of this chapter the North Atlantic storm track and its interactions with the mean flow are extensively described.

At decadal to multi-decadal timescales there is some evidence of a strengthening and eastward displacement of the NAO dipole over the last decades of the 20th century [*Hurrell et al.*, 2003; *Jung et al.*, 2003]. Whereas some authors suggest this behavior could be caused by global warming [*Ulbrich and Christoph*, 1999; *Osborn et al.*, 1999; *Bader et al.*, 2011], others point to natural variability of the NAO [*Wang et al.*, 2012; *Pinto and Raible*, 2012; *Raible et al.*, 2014] or changes in the storm track activity [*Rogers*, 1997; *Lu and Greatbach*, 2002]. In this context, the analysis of the low-frequency changes associated with the NAO evolution has not received much attention in the literature in spite of their evident relevance for climate variability [e.g., in European precipitation; *Raible et al.*, 2004; *Vicente-Serrano and López-Moreno*, 2008]. Such low-frequency changes (either atmospheric or oceanic) often lead to non-stationary teleconnections between distant regions [*Pinto et al.*, 2011; *López-Parages and Rodríguez-Fonseca*, 2012], thus providing enhanced forecast skill of relevant phenomena during specific periods of time [*Rodríguez-Fonseca et al.*, 2009; *Losada et al.*, 2012]. As a consequence, one of the goals of this thesis is to analyze whether the relation between the NAO and extra-tropical cyclones (especially for the strongest events) is stationary in time.

ii The Atlantic Multi-decadal Oscillation

The Atlantic Multi-decadal Oscillation (AMO) is a long-term evolving pattern of SST anomalies (~ 1 K) extending over the North Atlantic (Fig. 1.11a). The characteristic period of this oscillation ranges from 30 to 60 years [Fig. 1.11b; *Knight et al.*, 2005]. The AMO is defined as the leading EOF of SST winter seasonal

low-pass filtered anomalies (>33 yr.; detrended) over the area [95˚W-30˚E, 0-70˚N; *Mohino et al.*, 2011].

The recent growing interest on the AMO behavior relies on the diverse, global climatic impacts this oscillation appears to trigger. For instance, the AMO phase has been suggested to influence tropical cyclone activity over the North Atlantic [*Trenberth and Shea*, 2006] and precipitation over Northeastern Brazil and the Sahel [*Knight et al.*, 2005; *Mohino et al.*, 2011]. The variability of the AMO appears to be associated with the intensification/slowdown of the Meridional Overturning Circulation (MOC). When the MOC is intensified, the Gulf Stream transports more heat northwards and the SSTs in the North Atlantic are warmer. If the MOC is decelerated, the reverse is observed [*Rahmstorf*, 2006].

(a) AMO pattern (b) AMO index

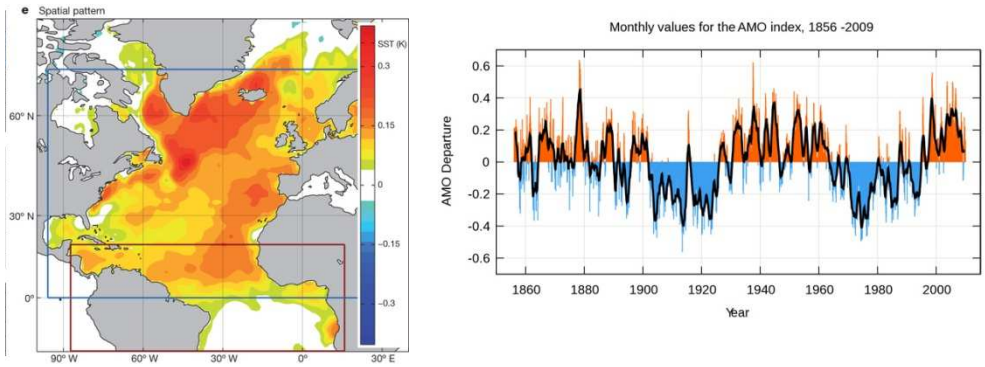

Fig. 1.11: (a) The spatial pattern of the Atlantic Multi-decadal Oscillation, defined as the normalized regression of north Atlantic SST (1870–2012) against the Atlantic Multi-decadal Oscillation index, exhibiting two warm centers, one south of Greenland and one in the tropics. From *Li et al.* [2013] (b) Variation in the Atlantic Multi-decadal Oscillation from 1856–2009. Data Source: NOAA.

Finally, the AMO and the MOC appear to exert some influence as well over the extra-tropics in the North Atlantic. In this context, a positive AMO phase and intensification of the MOC lead to a SLP response that resembles a negative phase of the NAO [*Gastineau and Frankignoul*, 2012]. In addition, these changes also appear to produce a response on the North Atlantic storm track [*Woollings et al.*, 2012]. Under a slowdown of the MOC potentially associated with increased greenhouse forcing, a strengthening and eastward propagation of the North Atlantic storm track is predicted. In this thesis the influence of the AMO onto explosive cyclones in the North Atlantic is analyzed (section V.4).

3. Extra-tropical cyclones over the North Atlantic

a. Geographical distribution

As explained in the previous sections, extra-tropical cyclones are baroclinic sub-weekly disturbances that mainly form over the oceanic basins of the mid-latitudes. Over the North Atlantic, the main region of cyclogenesis is situated over the eastern North American seaboard, where the presence of strong meridional gradients of temperature and moisture favor the growth of baroclinic waves [*Hoskins and Valdes*, 1990; *Nakamura et al.*, 2004]. In their evolution, extra-tropical cyclones typically propagate in the SW to NE direction along the North Atlantic storm track region, amplify over the ocean and reach the European continent during their mature or occluding stages [Fig. 1.12; *Dacre and Gray*, 2009; *Pinto et al.*, 2009]. Over the basin, the storm track maximum (shadings) is situated northeast of the eddy-driven jet stream core (contours). Such a configuration is consistent with baroclinic waves crossing the jet core from the right-entrance toward the left-exit regions, where intense uplift of air fosters amplification of weather systems [*Uccellini*, 1990; *Rivière and Joly*, 2006a; 2006b]. This mechanism is often referred to in the literature as the Fourth Quadrant Straight Jet Model [*Uccellini and Johnson*, 1979; *Uccellini and Kocin*, 1987].

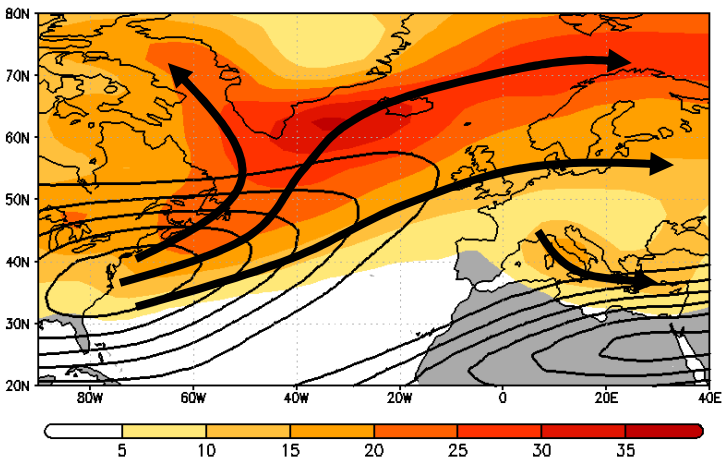

Fig. 1.12: Cyclone track density (shadings, in counts per 7.5° radius circle area per winter) and main extra-tropical cyclone trajectories in the North Atlantic (arrows). The extra-tropical jet is shown in contours (starting from 20 m s^{-1} in 5 m s^{-1} intervals). DJF 1957-2001 ERA-40.

b. Dynamical precursors and cyclone intensification

The factors contributing to cyclone formation and intensification in the North Atlantic are many and varied [*Fink et al.*, 2012]. The minimum MSLP of the cyclone surface center is often used as indicator of intensity [*Pinto et al.*, 2013]. Alternative intensity measures include the Laplacian of MSLP and the cyclone's maximum relative vorticity at 850 hPa [*Murray and Simmonds*, 1991]. Cyclone intensification is measured by the normalized deepening rate (NDR, in Bergeron) (I.2):

$$NDR = \frac{\Delta P}{24}\frac{\sin 60^\circ}{\sin \emptyset}, \qquad \text{(I.2)}$$

where ΔP is the pressure fall (hPa) and Φ the mean latitude of the cyclone's surface center over a period of 24 hours. The sine term accounts for the variation of geostrophic wind with latitude.

i Explosive and non-explosive cyclones

Depending on their maximum NDR, low pressure systems are classified as (i) explosive [EC, NDR ≥ 1 Bergeron; *Sanders and Gyakum*, 1980]; and (ii) non-explosive (NDR < 1 Bergeron) cyclones.

Whereas non-explosive cyclones predominantly intensify through moist baroclinic processes, explosive cyclones seem to be fostered by diverse dynamical mechanisms [*Reed et al.*, 1993]. These involve low and upper-level atmospheric precursors [*Hoskins et al.*, 1985], such as: (a) strong surface sensible and latent heat fluxes [*Davis and Emmanuel*, 1988; *Fosdick and Smith*, 1991]; (b) strong meridional SST gradients [*Sanders and Gyakum*, 1980]; (c) vertical low-level destabilization [*Manobianco*, 1989]; (d) upper-level mobile troughs and vertical intrusions of stratospheric air [*Bosart and Lin*, 1984; *Sanders*, 1986; *Gyakum and Danielson*, 2000]; and (e) strong upper-level winds [a jet streak; *Uccellini*, 1990].

The connection between low-level and upper-level precursors was conceptually established by *Hoskins et al.* [1985]: when an upper level Potential Vorticity anomaly (i.e. an upper level trough) crosses an area of enhanced baroclinicity at the surface, a coupling between both vertical precursors occurs and subsequent explosive cyclogenesis is triggered (Fig. 1.13a). Nevertheless, the existence of both precursors is not a necessary condition for the occurrence of

rapid cyclone intensification [*Pettersen and Smebye*, 1971]. For instance, over the Eastern north Atlantic the upper level forcing in explosive cyclogenesis dominates, whereas the contrary is observed west in the basin [*Dacre and Gray*, 2013].

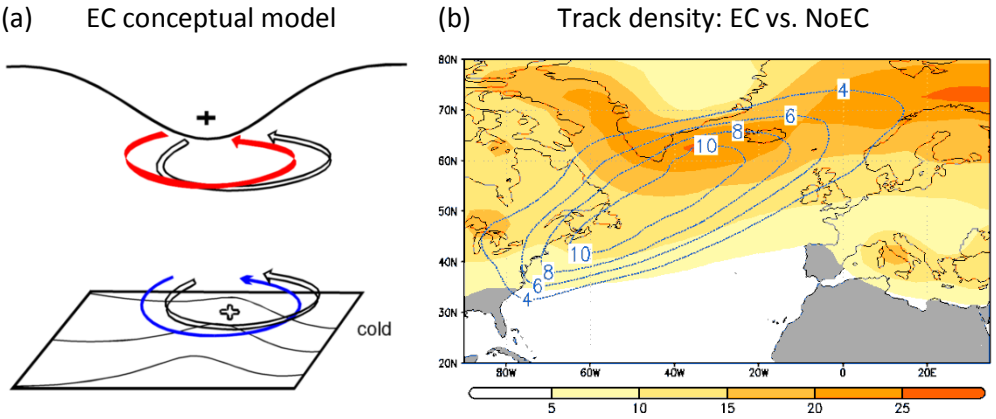

Fig. 1.13: (a) Conceptual model of explosive cyclogenesis in which a Potential Vorticity anomaly at the upper levels crosses a surface baroclinic region. From *Hoskins et al.* [1985]. (b) Explosive (contours) and non-explosive (shadings) cyclone track density (in counts per 7.5˚ radius circle area per winter). DJF 1957-2001 ERA-40. Adapted from *Gómara et al.* [2015].

For comparison, the track density of winter explosive and non-explosive cyclones over the North Atlantic is provided in Fig. 1.13b. Non-explosive cyclones (shadings) are more frequent between Greenland and Western Europe. Another maximum over the Mediterranean is found [*Pinto et al.*, 2009]. Explosive cyclones (contours) are maxima between Newfoundland and Iceland, over the left-exit region of the climatological jet [*Sanders and Gyakum*, 1980; *Uccellini*, 1990]. In this area explosive cyclones roughly represent one third of the total developing cyclones. Over the eastern US coast these systems are typically denominated Nor'easters, and are able to produce heavy snowfall and strong wind gusts [*Gyakum*, 1983; *Bosart and Lin*, 1984]. Over Europe they are linked with European Windstorms, and are the primary source of life-threatening weather due to their associated strong wind gusts, heavy precipitation and storm surge events [*Wernli et al.*, 2002; *Gómara et al.*, 2010; *Ludwig et al.*, 2014].

The frequency and variability of the dynamical precursors leading to explosive and non-explosive North Atlantic cyclones are tightly related with the large-scale circulation in the North Atlantic [*Pinto et al.*, 2009]. For instance, a positive NAO phase appears to enhance baroclinicity and extreme winter cyclone

activity in this sector [*Raible*, 2007; *Pinto et al.*, 2009]. Therefore, there exists a close connection between the large-scale flow, dynamical precursors and cyclonic activity in the North Atlantic. In Section I.4 the description of this relation is described in detail. Before that, some additional aspects of extra-tropical cyclones need to be introduced.

ii Clustering of intense extra-tropical cyclones

During specific winters explosive cyclones appear to develop and propagate in quick succession over Western Europe [Fig. 1.14; *Mailier et al.*, 2006; *Vitolo et al.*, 2009; *Pinto et al.*, 2013]. For instance, the winters of 1990, 1993, 1999, 2007, and 2014 have been characterized by the passage of multiple strong low pressure systems over the British Isles, leading to losses of human life and private property [*MunichRe*, 2010].

Cyclone clustering over Western Europe

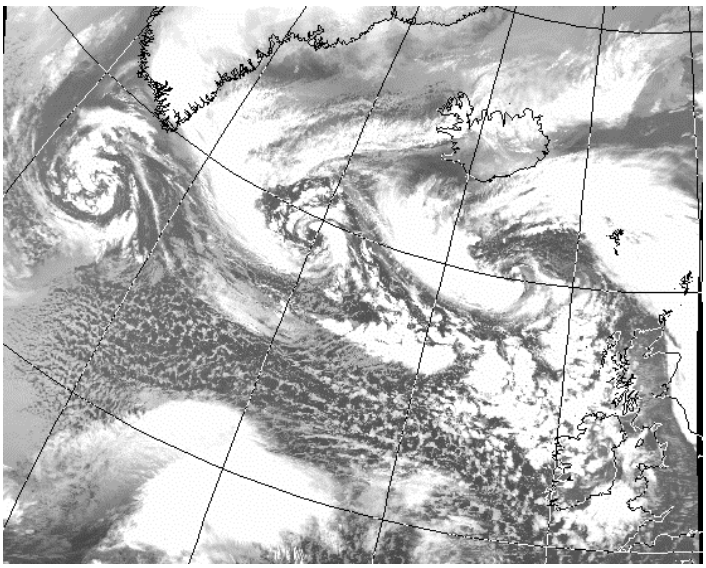

Figure 1.14: Satellite image depicting a family of low pressure centers approaching the British Isles on 11 February 2014. Courtesy: Dundee satellite receiving station (www.sat.dundee.ac.uk/) and Joaquim G. Pinto from 'The wet and stormy winter of 2013/14 over the British Isles' (http://blogs.reading.ac.uk/weather-and-climate-at-reading/2015/the-wet-and-stormy-winter-of-201314-over-the-british-isles/).

Over Western Europe, this process appears to occur more frequently than would be expected by chance (e.g., a Poisson process), thus indicating that specific dynamical factors may be favoring cyclone clustering. In the literature, several dynamical mechanisms have been proposed to explain this phenomenon: (i) the steering by strong upper level winds over Western Europe [*Mailier et al.*, 2006]; (ii) secondary upstream cyclogenesis occurring at the cold front of a previous primary cyclone [*Bjerknes and Solber*, 1922; *Parker*, 1998]; and (iii) secondary cyclogenesis forced by downstream propagation of Rossby waves [*Chang and Yu*, 1999]. However, no systematic investigation of the dynamical factors leading to storm clustering over Western Europe and their potential interrelation has been performed in previous studies. This provides the motivation for the analysis presented in section V.3, which investigates the relation between the large-scale flow, dynamical precursors and storm clustering events over Western Europe.

c. Life-cycle of extra-tropical cyclones

The life-cycle of extra-tropical cyclones is revisited in this section. A focus is laid on both the upper and lower tropospheric levels.

i *Surface evolution*

Nowadays two different conceptual models of cyclone surface evolution co-exist in the literature. These are the Norwegian [*Bjerknes and Solberg*, 1922] and the Shapiro-Keyser models [*Shapiro and Keyser*, 1990].

In the Norwegian model the incipient cyclone develops along a frontal zone of strong temperature and moisture gradients (Fig. 1.15a - I). As time evolves the wide low pressure along the front starts to bend and two different frontal zones start to organize. These are the cold and warm fronts (II). Due to the faster progression of the cold front, the area where warm and moist air is confined gets squeezed (III), until it finally occludes (IV). At this point of the process the cyclone reaches its maximum strength and starts to decay. In the Norwegian model the cold front is generally more intense than the warm front and most of the precipitation is concentrated over this area.

Cyclone formation in the Shapiro-Keyser model also starts from a long frontal area of different air-mass characteristics (Fig. 1.15b - I). However, as time evolves the cold front starts to propagate perpendicularly to the warm from (II). This process is denominated the frontal T-bone and both fronts never encounter

each other. In addition, an area of weakness arises near the surface low along the cold front (frontal fracture; III), and another front develops at the rear of the cyclone's centre (back-bent front; III). During their decaying stages, Shapiro-Keyser cyclones often feature a warm seclusion in the vicinity of the low centre (IV).

Whereas Norwegian cyclones tend to develop under a large-scale diffluent flow (exit regions of the jet core), Shapiro-Keyser cyclones are more frequent under confluent upper-level areas [*Schulz et al.*, 1998].

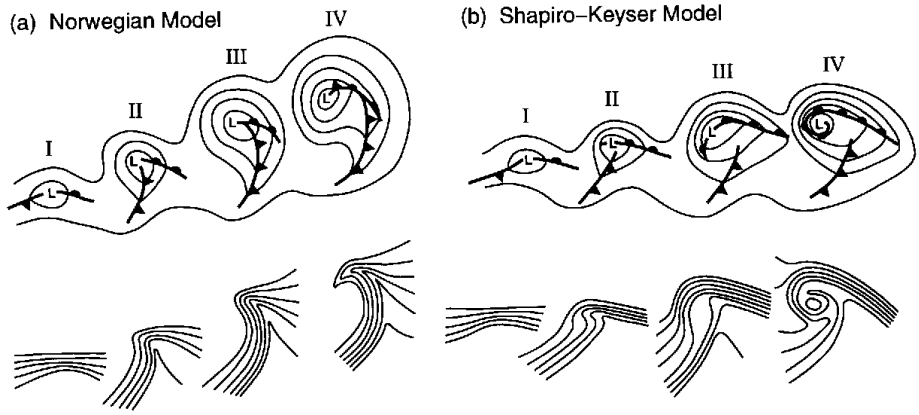

Figure 1.15: Conceptual models of cyclone evolution showing lower-tropospheric geopotential height and fronts (top), and lower-tropospheric potential temperature (bottom). (a) Norwegian cyclone model: (I) incipient frontal cyclone, (II) and (III) narrowing warm sector, (IV) occlusion; (b) Shapiro-Keyser cyclone model: (I) incipient frontal cyclone, (II) frontal fracture, (III) frontal T-bone and bent-back front, (IV) frontal T-bone and warm seclusion. Panel (b) is adapted from *Shapiro and Keyser* [1990, their Fig. 10.27]. Source: 'Determining Midlatitude Cyclone Structure and Evolution from the Upper-Level Flow' from http://www.cimms.ou.edu/~schultz/papers/marwealog.html

ii Upper-level evolution

In the upper levels, the non-linear evolution of baroclinic waves may also adopt different patterns. Two different life-cycle models (known as LC1 and LC2) have been proposed to describe the non-linear decay of the waves in case studies and model simulations [Fig. 1.16; *Thorncroft et al.*, 1993]. On one hand, LC1 lifecycles are characterized by anticyclonic deformation (SW-NE tilt) of potential vorticity contours on isentropic surfaces (or equivalently, potential temperature contours at the dynamical tropopause, Fig. 1.16a). In contrast, LC2 lifecycles are associated with a cyclonic tilt along the NW-SE axis (Fig. 1.16b). The spiraling of

the potential vorticity contours leads to the creation of small scale potential vorticity anomalies, and ultimately to dissipation, in a phenomenology known as Rossby Wave-Breaking [RWB; *McIntyre and Palmer*, 1983]. Both lifecycles differ pronouncedly on their impact on the mean flow. For LC1 there is equatorward propagation of eddies at upper levels and positive eddy momentum fluxes, while the reverse is true for LC2. For this reason, the type of lifecycle followed by the waves during their decay stage strongly affects the mean flow evolution.

The life-cycles of baroclinic waves are very sensitive to both their intrinsic characteristics and the large-scale flow in which they develop. In the next section, the two-way relation between extra-tropical cyclones and the large-scale flow in the North Atlantic is discussed. This is done in a separate section due to the high importance of this topic for the present thesis.

Non-linear decay of baroclinic eddies at upper levels

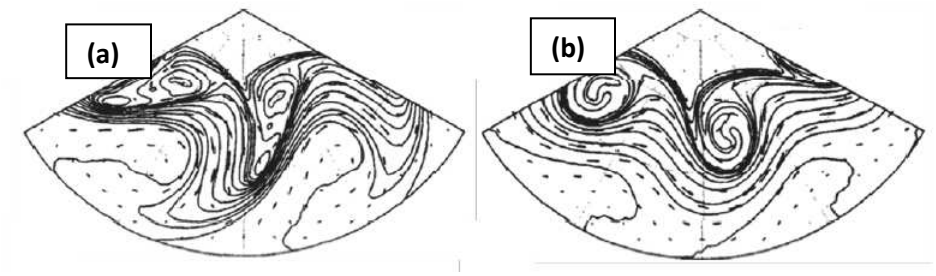

Fig. 1.16: The structure of two non-linear baroclinic waves as seen from a PV perspective. The two waves are from basic states on the sphere with the same baroclinic structure but differing barotropic structures and are referred to as LC1 and LC2 (Life-Cycles 1 and 2). (a) and (b) show contours of θ on the PV2 surface for LC1 and LC2, respectively, with contours every 5 K between 290 K and 350 K. The sector shown extends from the north pole to 20°N. Taken from *Thorncroft et al.* [1993].

4. Two-way relation between extra-tropical cyclones and the large-scale circulation in the North Atlantic

In this section the bi-directional relation between extra-tropical cyclones and the large-scale circulation in the North Atlantic is exhaustively described based on our current state of knowledge. Each branch of this connection is described separately.

a. Influence of the large-scale flow over extra-tropical cyclones

The storm track in the North Atlantic is shaped by the presence of strong low-level baroclinicity in the vicinity of Newfoundland [*Lau*, 1988; *Hoskins and Valdés*, 1990], together with strong upper-level winds typically situated over the eastern North American seaboard [*Chang and Orlanski*, 1993; *Woollings et al.*, 2010]. These large-scale factors are known to contribute to extra-tropical cyclone development in the North Atlantic and their behavior is found to be tightly connected with the North Atlantic Oscillation [*Hurrell et al.*, 2003; *Pinto et al.*, 2009]. Under a positive NAO phase the extra-tropical jet is accelerated and displaced northeastwardly in the North Atlantic. This produces two different impacts on extratropical cyclone characteristics in this sector. First, cyclone trajectories are deflected poleward steered by the extra-tropical jet [*Hurrell et al.*, 2003; *Trigo*, 2006]. Second, cyclone intensification rates and maximum intensity are enhanced by the stronger upper level flow [Fig. 1.17a; *Raible*, 2007; P*into et al.*, 2009]. If the vertical wind shear is increased associated with a stronger jet, a higher degree of baroclinicity is found below and cyclones encounter more favorable conditions for deep intensification [*Pinto et al.*, 2009]. Under a negative NAO phase these conditions are reversed. Hence, cyclones are weaker in average and propagate over the south-western North Atlantic. Consistent with these results, European Windstorms over Northern and Central Europe tend to be associated with a moderately positive NAO phase [Fig. 1.17b; *Raible*, 2007; *Donat et al.*, 2010]. However, the robustness of this relation for cyclones of varying intensities has not been studied yet in the literature. This aspect is analyzed in section V.1 of this thesis.

NAO as modulator of cyclone's intensity

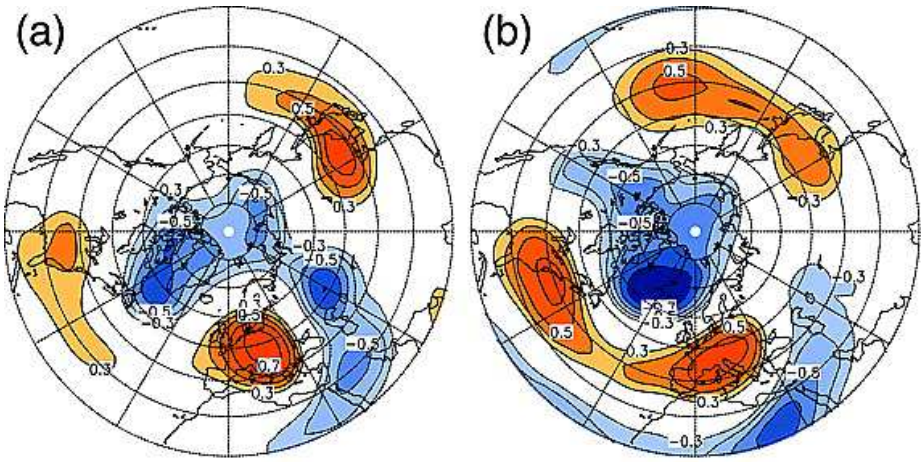

Fig. 1.17: Correlation pattern of the 500 hPa geopotential height with (a) North Atlantic, and (b) northern Europe Cyclone Intensity index (shading interval 0.1, contour labels 0.2, starting at ±0.3). From *Raible* [2007].

In recent studies, the relation between the NAO variability and the occurrence of RWB processes has been established [*Feldstein*, 2003; *Franzke et al.*, 2004; *Strong and Magnusdottir*, 2008b; *Woollings et al.*, 2008; *Drouard et al.*, 2013]. These RWB events may be associated with individual cyclone development in the North Atlantic [*Rivière and Orlanski*, 2007], but more generally arise from interactions between Rossby waves of varying temporal and spatial scales in the upper troposphere [*McIntyre and Palmer*, 1983; *Nakamura and Wallace*, 1993; *Tomikawa et al.*, 2006]. These waves are ultimately forced by baroclinic instability [*Edmon et al.*, 1980; *Thorncroft et al.*, 1993], however, their linear and non-linear upper-level behavior is complex and often modelled independently of the baroclinic source [*Randel and Held*, 1991; *Delsole*, 2001; *Barnes and Hartmann*, 2011]. As previously noted, the life-cycle of these baroclinic waves is highly sensitive to their intrinsic characteristics and the flow in which they are embedded. This results in two different evolution modes: LC1 and LC2 [*Thorncroft et al.*, 1993], which are mainly associated with anticyclonic and cyclonic RWB events.

The positive phase of the NAO appears to be initiated by anticyclonic RWB events along the west coast of North America and over the central sub-tropical North Atlantic (Fig. 1.18a). The negative NAO phase is triggered by cyclonic RWB on the poleward side of the extra-tropical North Atlantic jet (Fig. 1.18b).

Climatologically, the occurrence of RWB over the North Atlantic is primarily shaped by the jet structure (horizontal wind shear), with cyclonic RWB to the north and anticyclonic to the south, respectively [Fig. 1.18cd; *Gabriel and Peters*, 2008]. The life-cycles of the NAO anomalies associated with these RWB events have a typical persistence of about 12 days [*Feldstein*, 2003].

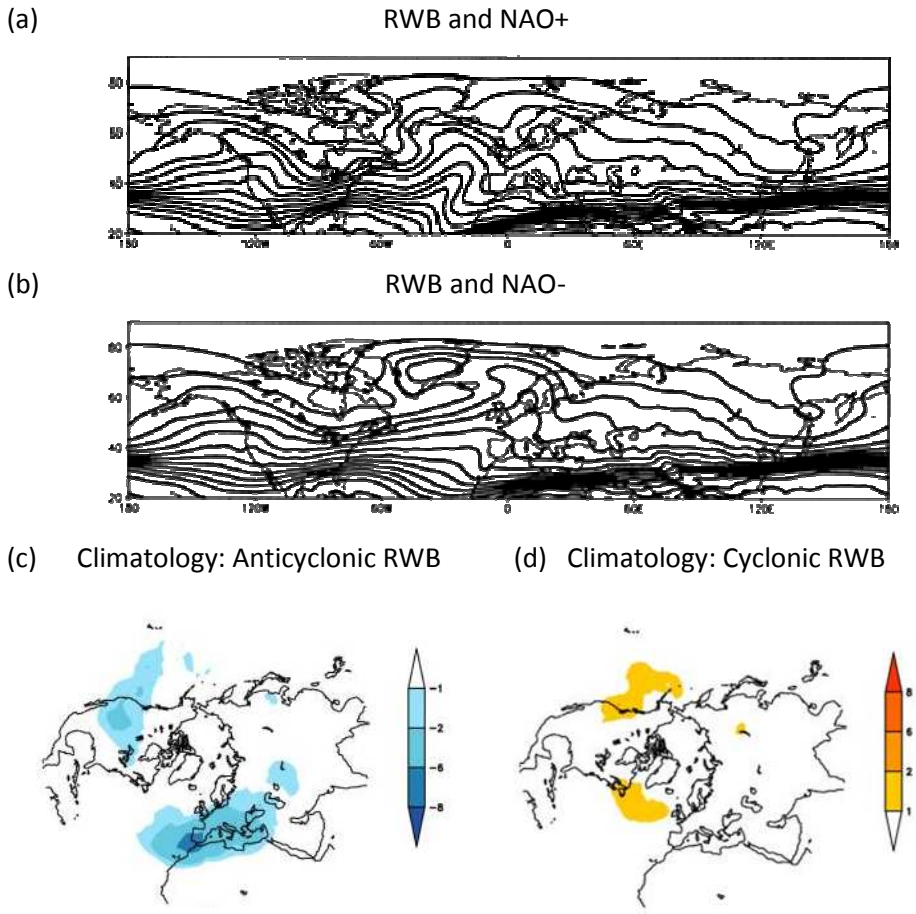

Fig. 1.18: Experiments with surface friction (damping time scale is 1 day): potential temperature on the 2-PVU surface for (a) NAO+ and (b) NAO-. Contour interval is 5.0 K. Adapted from *Franzke et al.* [2004]. (c)-(d) Climatological mean distribution of LC1 and LC2 RWB events (m^2 s^{-2}) for the decade 1990-1999. Anticyclonic events (c) are shown in blue, cyclonic RWB events (d) in yellow. Adapted from *Gabriel and Peters* [2008].

Due to the connection between RWB and the NAO phase, the occurrence of atmospheric blocking is also tightly connected with previous RWB activity in the North Atlantic. For instance, European blocking tends to be triggered by previous anticyclonic RWB events over the North Atlantic [*Pelly and Hoskins*, 2003; *Woollings et al.*, 2008; *Santos et al.*, 2009; *Woollings et al.*, 2011; *Masato et al.*, 2012; 2013a; 2013b]. Not surprisingly, the transitions between the most prominent weather regimes over the North Atlantic appear to be also modulated by the characteristics and evolution of RWB events [*Michel et al.*, 2011].

In relation with extra-tropical cyclone formation and intensification, a recent analysis from *Hanley and Caballero* [2012] suggests that simultaneous north-cyclonic and south-anticyclonic RWB events in the North Atlantic appear to promote windstorm activity over Europe. Under the mechanism they propose, the extra-tropical jet is squashed from both flanks by the RWB events and accelerated over the Western North Atlantic (Fig. 1.19). As a consequence, surface cyclones in the vicinity of Europe encounter very favorable upper-level conditions for rapid intensification. This relation was demonstrated for the 22 most destructive storms affecting Europe.

Hanley and Caballero's [2012] mechanism

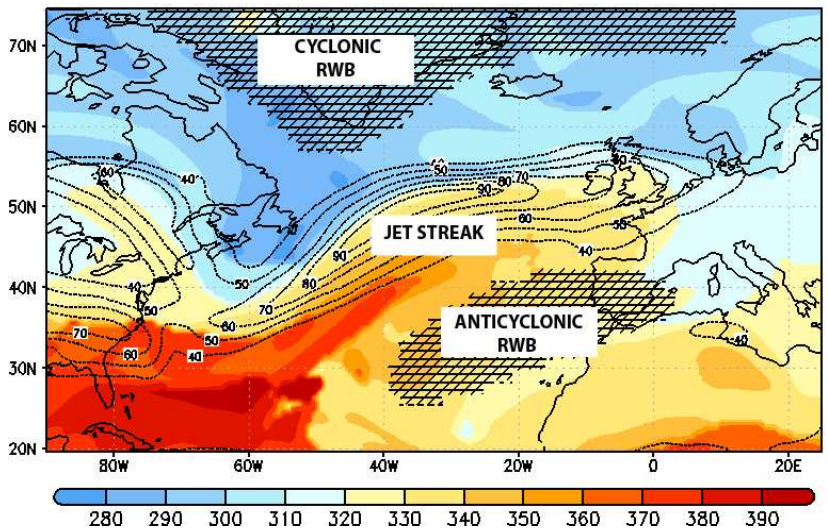

Fig. 1.19: Schematic based on the *Hanley and Caballero's* [2012] mechanism: Potential temperature on the 2PVU surface on 18 January 2007 (in K, ERA-Interim). Cyclonic and anticyclonic RWB areas are hatched. Wind vector at 250 hPa (in m s^{-1}) shown in contours.

However, this relation has not been investigated systematically for cyclones of varying intensities and on different North Atlantic regions (e.g., western and eastern North Atlantic) using a comprehensive cyclone dataset. In addition, it is unclear how often these RWB events trigger explosive cyclogenesis, and how often the cyclonic and anticyclonic RWB precursors occur simultaneously. These aspects are analyzed in section V.2 of this thesis. Additionally, the upper-level conditions described by *Hanley and Caballero* [2012] could also be responsible of the occurrence of storm clustering over Europe. As explained in the previous section, the steering of the large-scale is thought to be important for the occurrence of cyclone clustering over Western Europe [*Mailier et al.*, 2006; *Vitolo et al.*, 2009]. Motivated by this, the possible connection between RWB precursors and storm families is also analyzed in this thesis (cf. section V.3).

b. Influence of extra-tropical cyclones over the large-scale flow

As described in the previous section, the RWB events triggering large-scale anomalies over the North Atlantic are sometimes associated with previous cyclones in this sector. In the literature, the effect of cyclones over the mean flow is well established through the analysis of case studies [*Shutts*, 1983; *Colucci*, 1985; *Nakamura and Wallace*, 1993; *Rivière and Orlanski*, 2007; *Roebber*, 2009] and specific cyclone populations [*Michel and Rivière*, 2012].

For instance, *Rivière and Orlanski* [2007] analyze the influence of the March 1993 Superstorm on the mean flow. For the analysis, they calculate the eddy momentum fluxes (EMF, I.3) during the decay of this cyclone:

$$EMF = \overline{u' \cdot v'}, \tag{I.3}$$

where u’ and v’ are the high-pass filtered (2-6 days) anomalies of zonal and meridional upper-level winds (~300 hPa) with respect to their average (monthly/bars) values. The physical relation between EMF and the mean flow is given through the Eliassen-Palm vector (EP; I.4), as defined from *Hoskins et al.* [1983] in the zonal momentum equation for a non-divergent flow (I.5).

$$EP = \left(\overline{v'^2 - u'^2}, \overline{-u' \cdot v'}\right), \tag{I.4}$$

$$\frac{\partial}{\partial t}\bar{u} + \bar{u}\partial_x\bar{u} + \bar{v}\partial_y\bar{u} = f_0\bar{v}_a + \nabla \cdot EP, \qquad \text{(I.5)}$$

where f_0 is an approximate constant value of the Coriolis parameter and $\bar{v}_a$ the poleward ageostrophic motion in the jet entrance region. Further information on this relation can be found in *Trenberth* [1986] and *Riviére and Orlanski* [2007]. The use of upper-level wind fields is based on the enhanced momentum flux activity in the upper levels [cf. Fig. 1.5b; *Vallis*, 2006]. The focus on the cyclone's decay period is based on the characteristic life-cycles of baroclinic waves [*Thorncroft et al.*, 1993; and section I.3.c]. As discussed in that section, positive momentum fluxes are associated with anticyclonic RWB and tend to induce a positive NAO phase by pushing the jet poleward. Negative momentum fluxes are linked with cyclonic RWB and push the jet equatorward (NAO-).

Rivière and Orlanski [2007] conclude that the 1993 Superstorm was associated with strong positive momentum fluxes over the North Atlantic during its decay (Fig. 1.20a). As a consequence, the daily NAO index abruptly increased in a short period of time of 4-5 days (Fig 1.20b). Subsequently, the NAO phase remained in positive values until it reached equilibrium a couple of weeks later.

(a) Latitudinal jet motion, March 1993 (b) Daily NAO index, March 1993

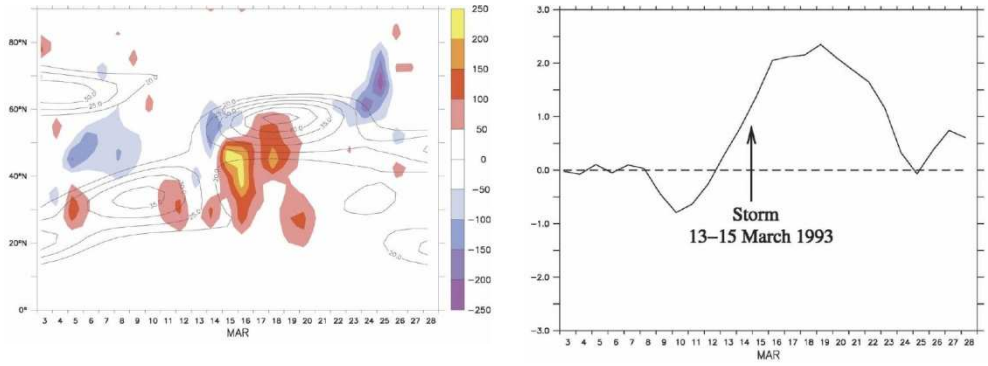

Fig. 1.20: Effect of a single storm (13–15 Mar 1993) on NAO. (a) Time-latitude plot of the low-frequency zonal wind (black contours, contour interval is 5 m s^{-1}, isotachs less than 20 m s^{-1} omitted) and of the high-frequency momentum fluxes (color shadings, in m^2 s^{-2}, data have been longitudinally averaged between 60° and 0°W) for March 1993, respectively. (b) Daily NAO index for March 1993. From *Rivière and Orlanski* [2007].

Based on this study, the influence that single cyclones may exert onto the mean flow appears to be sensitive to the cyclone's maximum intensity. This

suggests that there might be some predictability of the short-term NAO evolution based on the very different timescales of the processes involved in the short-term NAO growth and decay [*Rivière and Orlanski*, 2007]. Whereas eddy forcings (RWB, growth) can alter the large-scale circulation in a few days [*Riviére and Orlanski*, 2007; *Pinto et al.*, 2009], the frictional decay of the NAO anomalies back to their low-frequency equilibrium occurs in much longer, weekly timescales [e.g., *Lorenz and Hartmann*, 2001].

The onset of blocking over Scandinavia also appears to be associated with extra-tropical cyclone activity in the North Atlantic. In this way, the passage of strong cyclones south of Greenland is linked with enhanced cyclonic RWB activity over that area and anticyclonic RWB over Europe [Fig. 1.21; *Michel and Rivière*, 2012]. This leads to high pressure anomalies over Northern Europe and is consistent with previous studies on this topic [*Colucci*, 1985].

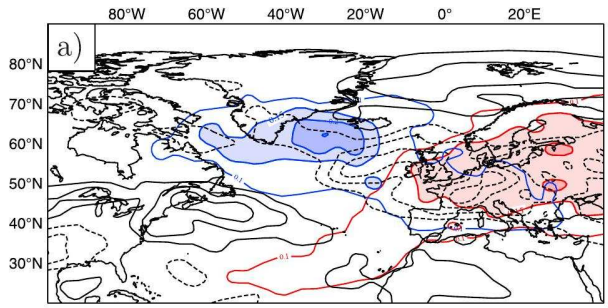

Fig. 1.21: Cyclonic Wave Breaking and Anticyclonic wave breaking frequencies, averaged over four isentropic levels (blue and red shading respectively, first contour is 0.1 day^{-1} and interval is 0.05 day^{-1}) and the zonal wind tendency due to the non-linear eddy vorticity fluxes at 300 hPa (black contours, interval is 2 10^{-5} m s^{-2}, the zero contour is omitted and solid (dashed) lines refer to positive (negative) values) for the Scandinavian Blocking onset. From *Michel and Rivière* [2012].

In sections V.1 and V.2 of this thesis the potential influence of extra-tropical cyclones on the North Atlantic mean flow is analyzed. A comprehensive cyclone data set is used to systematically investigate this connection. In particular, the sensitivity to cyclone's intensity, trajectory and location is analyzed. One of the main objectives of this thesis is to shed light into the two-way connection between extra-tropical cyclones and the large-scale circulation in the North Atlantic.

II. OBJECTIVES

'The most reliable way to forecast the future is to try to understand the present.'

John Naisbitt (economist; 1929-nowadays)

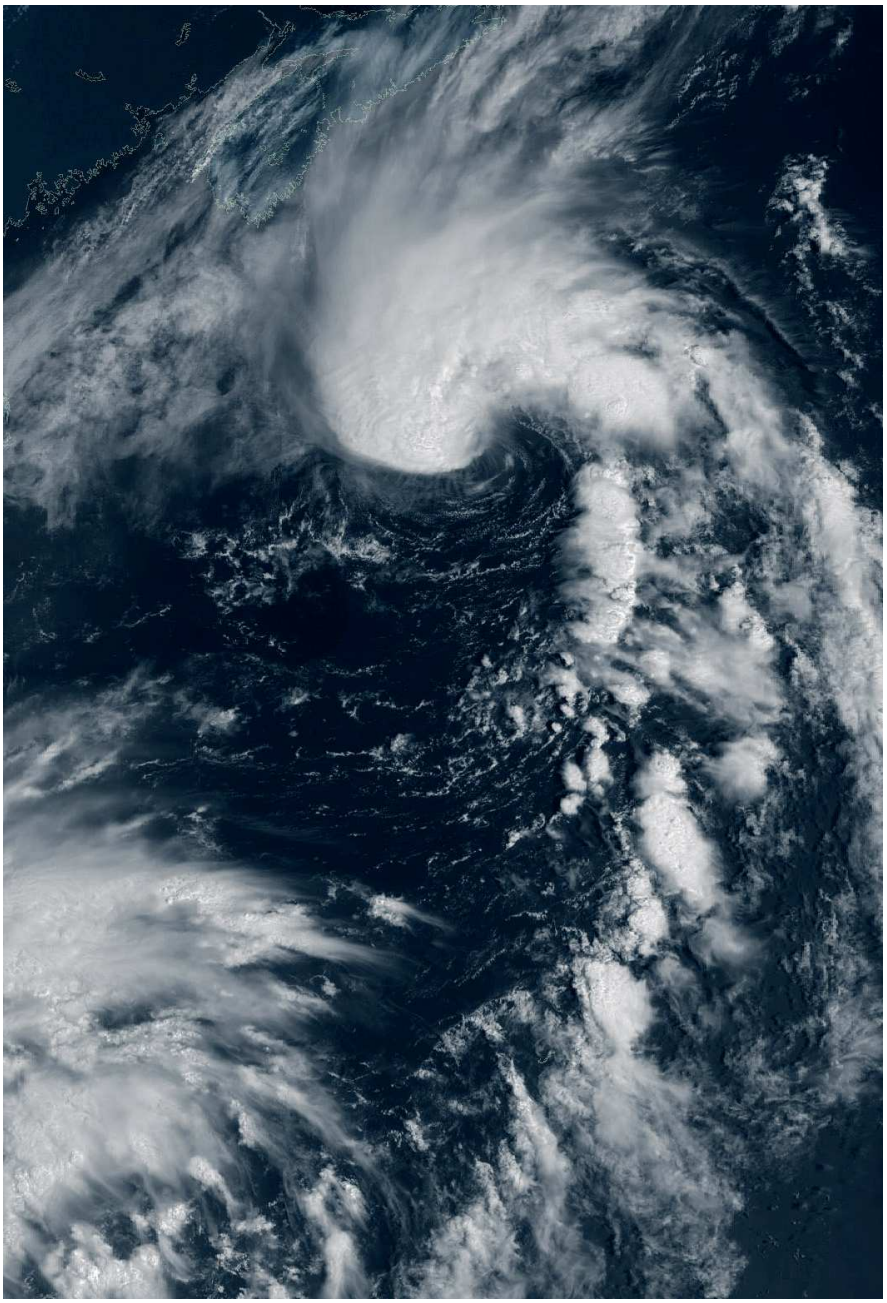

II. Objectives

In consideration of the Preface and State of Knowledge previous chapters, the main objective of this thesis is to analyze the large-scale dynamics and variability associated with explosive cyclogenesis in the Euro-Atlantic sector. In this frame, one important target is to acutely characterize the two-way relation between the large-scale circulation and explosive cyclones at synoptic timescales, with a special focus on storm families affecting Western Europe. Another fundamental goal is to analyze the climate variability of explosive cyclogenesis in the North Atlantic and its potential relation with lower frequency (e.g., multi-decadal) atmospheric/oceanic variability. These general objectives are divided into four different targets in this thesis, each one corresponding to a scientific publication enclosed in the Results chapter. The particular objectives and open questions of each study are the following:

1. To analyze the bi-directional relation between the large-scale mean flow (mostly explained by the North Atlantic Oscillation) and explosive and non-explosive cyclones affecting Western and Central Europe.

- *Which NAO phase is more favorable for the occurrence of explosive cyclones over Western and Central Europe?*
- *How is characterized the associated large-scale flow?*
- *What is the influence of explosive cyclones affecting Europe over the large-scale mean flow and the NAO?*
- *Are these relations sensitive to storm's intensity?*

The answers to these questions are available in section V.1: On the relation between explosive cyclones affecting Europe and the North Atlantic Oscillation [*Gómara et al.*, 2014b].

2. To provide a deeper and more general description of the two-way relationship between cyclones and the large-scale circulation in the North Atlantic through the analysis of Rossby Wave-Breaking processes.

- *Is there a common pattern of RWB upstream (downstream) and prior to (after) explosive cyclogenesis over the North Atlantic?*
- *Is RWB dependent on the cyclone's intensity?*
- *Is RWB sensitive to the cyclone's trajectory and location (and vice-versa)?*

These questions are resolved in section V.2: Rossby wave-breaking analysis of explosive cyclones over the Euro-Atlantic sector [*Gómara et al.*, 2014a].

3. To provide the first dynamical analysis of the occurrence of cyclone families over Western Europe, focusing on the role of Rossby Wave-Breaking, jet dynamics and secondary cyclogenesis.

- *Which are the potential physical mechanisms responsible for the occurrence of storm families over Western Europe?*
- *What is the role of the steering by the large-scale flow?*
- *Are upstream and downstream secondary cyclogenesis processes important?*
- *To what extent is the occurrence of these physical precursors sensitive to the intensity of the clustered cyclones involved (and vice-versa)?*

The questions above are addressed in section V.3: Large-scale dynamics associated with clustering of extra-tropical cyclones affecting Western Europe [*Pinto et al.*, 2014].

4. To characterize the high-frequency climate variability (1-11 yr.) of explosive cyclogenesis in the North Atlantic and analyze the potential modulating role of the coupled ocean-atmosphere multi-decadal variability.

- *Is the climate (1-11yr.) variability of explosive cyclogenesis over the North Atlantic similar to the observed for all cyclones?*

- *What is the role of the NAO and the extra-tropical jet stream in steering the climate variability of explosive cyclones?*
- *Is the connection with the NAO stationary in time?*
- *Does El Niño play an important role influencing explosive cyclogenesis?*
- *What is the potential role of the atmospheric/oceanic multi-decadal variability modulating the high-frequency climate behavior of explosive cyclogenesis?*

These questions are answered in section V.4: Abrupt transitions in the variability of explosive cyclones over the North Atlantic [*Gómara et al.*, 2015].

III. DATA

'Errors using inadequate data are much less than those using no data at all.'

Charles Babbage (mathematician; 1791-1871)

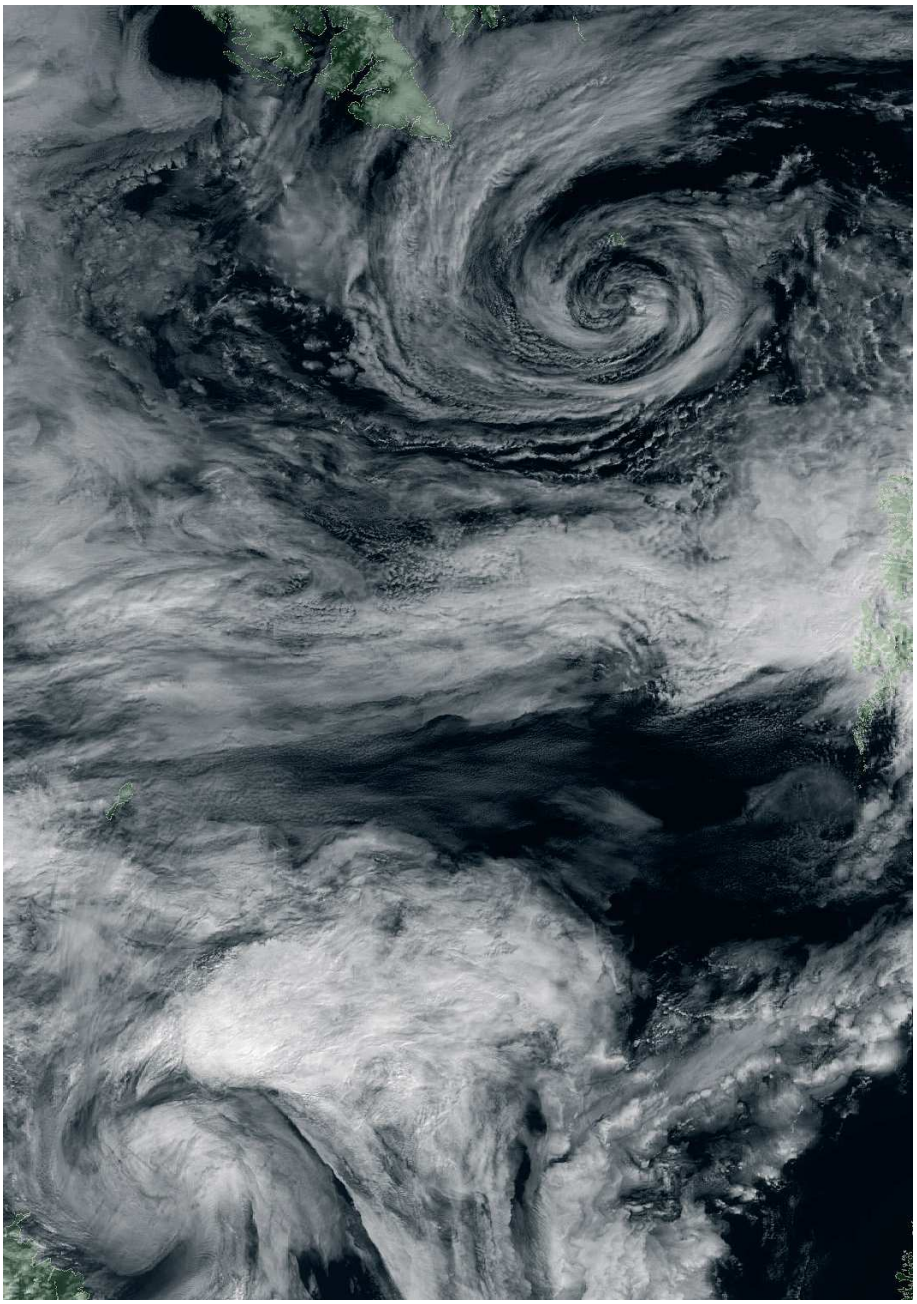

III. Data

The data sets used along this thesis are herein described and referenced. The description of the data sets is divided into two sections according to the characteristics of the data: (1) reanalysis and observations; and (2) model simulations.

1. Reanalysis and observations

In this section four different reanalysis products and three additional observational data sets are described.

a. Reanalysis data

Reanalysis products are a very powerful and useful tool in atmospheric research, as they provide information of the climate past over the entire globe. Their construction is simple: a single climate model (analysis) is forced to follow available observations at each location and time frame of the simulation. In order to produce homogeneous and consistent time series suitable for climate research, a constant configuration of the model is used along the whole simulation, together with an unvarying assimilating system of observations and measurements. Therefore, the level of freedom of the model run at each location and time frame is highly sensitive to the available measurements over that area and period. As a consequence, climate variability over regions with higher spatial-temporal density of observations (e.g., Europe, North America, Eastern Asia etc.; cf. Fig. 3.1) is better reproduced than in those where the background state has to be calculated by the model itself (e.g., the oceans). When available, observations are assimilated at each model time step, typically every 6 hours (00, 06, 12 and 18 UTC). The sources of instrumental data are many and varied, being radiosonde, ships, aircrafts, buoys and satellites the most commonly used[1].

Nowadays, different reanalysis products are available for the scientific community with different spatial-temporal resolutions and coverage: e.g., NASA[2] MERRA [*Rienecker et al.*, 2011]; NOAA[3] NCEP/NCAR reanalysis [*Kalnay et al.*,

[1] Reanalyses Home Page www.reanalyses.org
[2] National Aeronautics and Space Administration: www.nasa.gov
[3] National Oceanic and Atmospheric Administration: www.noaa.gov

1996]; NOAA 20th Century Reanalysis [20CR; *Compo et al.*, 2011]; ECMWF[4] ERA-40 [*Uppala et al.*, 2005]; ECMWF ERA-Interim [*Dee et al.*, 2011]; JMA[5] JRA-55 [*Kobayashi et al.*, 2015], etc. For computational optimization purposes, time coverage is generally increased at the cost of spatial resolution, and vice-versa. This is the case if 20CR and ERA-Interim, for instance, are compared against each other: whereas 20CR has a horizontal resolution of T62 and 28 vertical levels covering since 1871 to the present, ERA-Interim does after 1979 with T255 and 60 vertical levels. Additional to the problem of computational cost, the lack of observations before the mid-20th century and the introduction of information derived from satellites during the 1970s are other major issues in the quality and homogeneity of reanalysis products [*Harris and Kelly,* 2001*; Dee and Uppala,* 2009].

(a) Surface observations (b) Marine observations

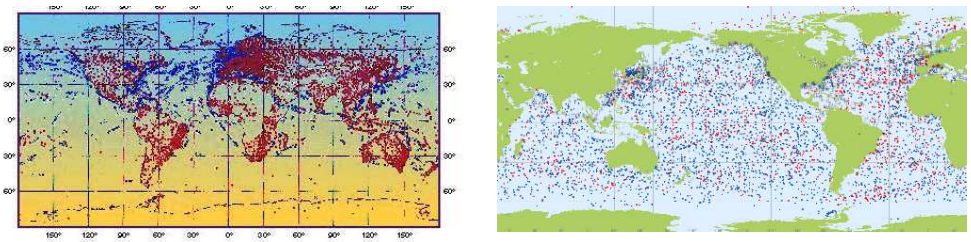

Fig. 3.1: Observational components of the *Global Observing System - World Meteorological Organization (WMO)*: (a) surface stations; and (b) marine observations. Source: WMO's home page: www.wmo.int

Within the scope of this thesis, reanalyses generally agree with respect to extra-tropical cyclone climatologies. However, higher resolution data sets typically exhibit more cyclones, deeper cores, and longer tracks [*Ulbrich et al.,* 2009]. This is partially due to the sensitivity of the identification and tracking methodologies to model data resolution [*Pinto et al.,* 2005*; Trigo,* 2006; cf. Section IV for further information]. In addition, the dependence of model dynamics, parametrizations, and assimilation schemes to resolution can also play an important role, especially for individual systems [cf. *Ulbrich et al.,* 2001*; Rivière et al.,* 2010; for the case of "Lothar" in 1999]. The reanalyses used in this thesis are the following:

[4] European Centre for Medium-Range Weather Forecasts: www.ecmwf.int
[5] Japan Meteorological Agency: www.jma.go.jp

i NCEP reanalysis

The *National Centers for Environmental Prediction/National Center for Atmospheric Research* (NCEP/NCAR) reanalysis data set covers the period 1948-2015. It has a horizontal spectral resolution of T62 (approximately 2.5°x2.5° in longitude/latitude), with 28 vertical levels from surface up to 3 hPa. Observations are incorporated every time step (00, 06, 12, 18 UTC) using a three-Dimensional Variational Data Assimilation Scheme (3D-Var). For additional technical information on this reanalysis see *Kalnay et al.* [1996].

NCEP reanalysis data have been retrieved from the web page http://www.esrl.noaa.gov/psd/data/gridded/data.ncep.reanalysis.html. Data are available in 4-times daily, daily and monthly time resolution in NetCDF[6] format. The NCEP/NCAR reanalysis problems list can be found in http://www.esrl.noaa.gov/psd/data/reanalysis/problems.shtml. In Table 3.1 and Section V the specific details (e.g., variable names, pressure levels etc.) of the data used from this reanalysis are provided.

ii ERA-40

ERA-40 is a second generation reanalysis from the *European Centre for Medium-Range Weather Forecasts* (ECMWF), an independent intergovernmental organisation supported by 34 states. It covers 45 years of data, from September 1957 to March 2002, with a spectral spatial resolution of T159 (1.125°x1.125° in longitude/latitude), and 60 vertical levels from the surface up to 0.1 hPa. The data assimilation scheme is 3D-Var as for NCEP (00, 06, 12 and 18 UTC). Additional details about this data set can be found in *Uppala et al.* [2005].

The data from the ERA-40 reanalysis have been retrieved from the main repository of meteorological data at ECMWF, the Meteorological Archival and Retrieval System (MARS, http://apps.ecmwf.int/datasets/). Data are available in 4 times daily, daily and monthly resolution in NetCDF or GRIB[7] format. In Table 3.1 and Section V.2 the specific details of the data used are given.

[6] Network Common Data Form
[7] GRIdded Binary or General Regularly-distributed Information in Binary form

iii ERA-Interim

ERA-Interim is a third generation reanalysis from the ECMWF, and was originally planned as an interim reanalysis in preparation for ERA-20C. It has a spectral horizontal resolution of T255 (~0.75°x0.75°), and 60 vertical levels from surface up to 0.1 hPa. It includes 36 years of data from 1979 to 2015. The data assimilation scheme is based on a 12-hourly (00, 12 UTC) four dimensional variational analysis (4D-Var). The main difference compared with 3D-Var schemes is that it interpolates observational data distributed around the target area to estimate the value at each location. ERA-Interim uses data prepared from ERA-40 until 2002, and afterwards from the ECMWF's operational repository. Further technical information about this data set is available in *Dee et al.* [2011].

The data from the ERA-Interim reanalysis have been retrieved from the ECMWF's MARS archive as for ERA-40. The data are available in 4 times daily, daily and monthly resolution in NetCDF or GRIB format. Further specifications of the characteristics of these data can be found in Table 3.1 and Section V.3.

iv Simple Ocean Data Assimilation

The Simple Ocean Data Assimilation (SODA; Maryland and Texas A&M Universities) covers the Earth's oceans since 1958 on monthly basis at a 0.5˚x0.5˚ horizontal resolution. It spans in the vertical from the ocean's surface down to 5375 m and uses 20crv2 winds. The SODA reanalysis is based on hydrographical profile data, surface stations, moors, and infrared satellite data, which are assimilated into the Modular Ocean Model (MOM) from the NOAA's Geophysical Fluid Dynamics Laboratory. Further information on this oceanic reanalysis can be found in *Carton et al.* [2005] and *Carton and Giese* [2008].

The SODA data have been retrieved from the Atmospheric and Oceanic Science's Data Storage and Retrieval System from the University of Maryland in NetCDF format (http://dsrs.atmos.umd.edu/?view=all).

b. Observations

Additional to the above reanalysis products, the following observational data sets were used:

i Sea Surface Temperature Data

The *Met Office Hadley Centre's* sea ice and sea surface temperature (SST) data set (HadISST) covers the Earth's surface oceans since 1870 to the present on monthly basis. It has a horizontal resolution of one degree in longitude and latitude. The SST data are obtained from the *Met Office Marine Data Bank* (MDB) and the *Global Telecommunications System* (GTS, only 1982 onwards). Additionally, monthly median SSTs from the *Comprehensive Ocean-Atmosphere Data Set* (COADS) are used where MDB presents gaps. Passive microwave retrievals and digitized charts are used among other measurements for the sea ice data. Regarding SST temperatures, these are reconstructed by interpolating gridded observations onto the reconstructions. A detailed description of the data set and its production method is available in *Rayner et al.* [2003].

The HadISST data have been retrieved from the web link http://www.metoffice.gov.uk/hadobs/hadisst/data/download.html in ASCII[8] format.

ii Weather Charts

Weather charts from the *UK Meteorological Office* provide the current state of the observed weather, along with the analysis fields for the forthcoming 5 days. Forecasts are typically updated twice a day (0730 and 1930 UTC). In the charts, the location of Highs (H), Lows (L) and associated warm and cold fronts appear overlaid over the surface pressure field (Fig. 3.2a). The frontal positions displayed in the analysis charts are made by forecasters using (i) model and observed parameters such as temperature, wind shifts, dew point, cloud cover, cloud types, visibility, and lines in precipitation patterns; and (ii) (post-2000 only) an automated frontal identification algorithm based on gradients of wet-bulb potential temperature [*Hewson,* 1997*;* 1998]. Thus, some subjectivity is present in the frontal analysis. To relate the frontal positions with reanalysis data, the frontal positions are re-projected onto a regular latitude/longitude grid in section V.3.

The weather charts are available from the UK Met Office (www.metoffice.gov.uk). In the context of this thesis, they provide a valuable and very illustrative view of the synoptic large-scale dynamics associated with low pressure systems.

[8] American Standard Code for Information Interchange

(a) UKMO - weather chart (b) FU - Storm Names

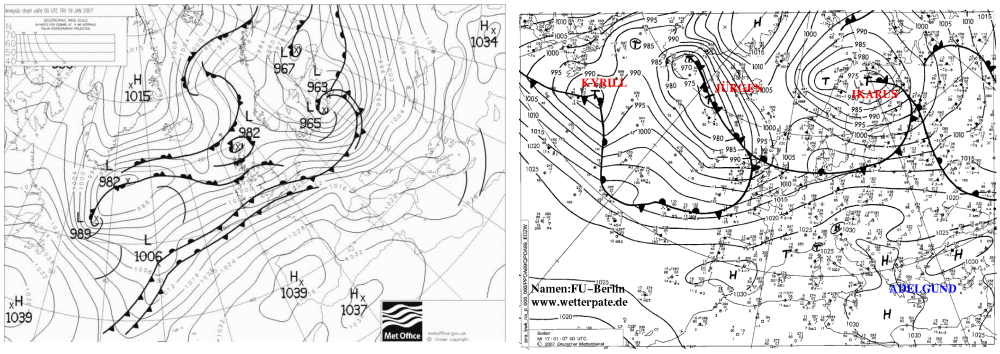

Fig. 3.2: (a) UK Met-Office weather chart from 00 UTC 19 Jan 2007. (b) Weather chart from FU with storm names overlaid (07 UTC 17 Jan 2007).

iii Storm Names from the Freie Universität Berlin

Storm names of extra-tropical cyclones (e.g., 'Lothar', 'Martin', 'Kyrill', 'Klaus' etc.; cf. Fig. 3.2b) are retrieved from the 'Adopt-a-Vortex' initiative from the *Freie Universität Berlin* (FU; www.met.fu-berlin.de/adopt-a-vortex). This initiative was established 50 years ago and provides the possibility of adopting high and low pressure systems to particulars. These names are available for use on the media (e.g., newspapers, radio, TV, internet etc.) and weather services, among other potential end users.

2. Model simulations

Climate model simulations are a very practical tool for atmospheric research. They provide a mathematical representation of the climate system, and typically incorporate the Earth's physics (e.g., atmosphere, ocean, solar variability, aerosols, etc.), as well as chemical processes (e.g., ozone, greenhouse gases, etc.). The great advantage of climate models in comparison with observations is that they provide long series of experimental data all over the climate system at reasonable horizontal and vertical resolutions. Such is particularly important over the regions where observations are coarse (cf. Fig. 3.1) and periods without instrumental data. The applications of climate models are many and varied: e.g., sensitivity experiments, global warming projections, paleoclimatology, etc.

In this thesis a long simulation of a coupled atmosphere/ocean model is used to analyze the variability of explosive cyclogenesis in the North Atlantic (cf.

Table 3.1 and Section V.4). The technical details of this simulation are described below.

a. ECHAM5/MPIOM1

A pre-industrial control simulation of the coupled atmosphere/ocean ECHAM5/MPIOM1 model from the *Max Planck Institute for Meteorology* (MPI-M) is used. The simulation was performed in the context of the IPCC[9] Fourth Assessment Report [*IPCC,* 2007]. The length of the simulation is 505-yr, with perpetual external forcing conditions from 1860 [*Roeckner et al.,* 2003*; Jungclaus et al.,* 2006]. ECHAM5 is the filth-generation atmospheric general circulation model from the MPI-M, which has evolved from the more primitive spectral prediction model of the ECMWF [*Simmons et al.,* 1989]. Its horizontal resolution is T63, with 31 vertical levels from surface up to 10 hPa. MPIOM1 is a primitive equation oceanic model with hydrostatic and Boussinesq assumptions. A dynamic/thermodynamic sea ice model is also embedded. It has a horizontal resolution of T31, with 40 levels from the ocean surface down to 5720 m. No flux adjustments are applied to the coupled atmospheric and oceanic models. In particular, tropical sea surface temperature [*Jungclaus et al.,* 2006], storm track and NAO variability [*Bengtsson et al.,* 2006*; Pinto et al.,* 2011] are found realistic in this simulation.

The data from ECHAM5/MPIOM1 have been retrieved from the *Deutsches Klimarechenzentrum* (DKRZ)/Center for Environmental Risk Assessment (CERA) database (http://cera-www.dkrz.de). These data are available in monthly resolution in NetCDF format. Further information on the variables used from this data set is provided in Table 3.1 and Section V.4.

[9] Intergovernmental Panel on Climate Change: www.ipcc.ch

Data set	Variable	Acronym	Resolution	Reference
NCEP	Mean Sea Level Pressure Zonal wind at 250 hPa Meridional wind at 250 hPa Geopotential Height at 500 hPa	MSLP u250 v250 z500	6-hourly/2.5°x2.5° Daily/2.5°x2.5° … …	*Kalnay et al.* [1996]
ERA-40	Mean Sea Level Pressure Zonal wind at 250 hPa Meridional wind at 250 hPa Potential temperature (2PVU)	MSLP u250 v250 θ	6-hourly/1.1°x1.1° … … …	*Uppala et al.* [2005]
ERA-Interim	Mean Sea Level Pressure Zonal wind (all levels) Meridional wind (all levels) Potential temperature (2PVU)	MSLP U V θ	6-hourly/0.7°x0.7° Daily/0.7°x0.7° … …	*Dee et al.* [2011]
SODA	Integrated temperature (0-300 m)	T300	Monthly/0.5°x0.5°	*Carton and Giese* [2008]
HadISST	Sea Surface Temperature	SST	Monthly/1°x1°	*Rayner et al.* [2003]
UK Met. Office	Weather charts	*	12-hourly/*	*Hewson* [1997]
FU Berlin	Adopt-a-Vortex Storm Names	*	*	*
ECHAM5	Mean Sea Level Pressure Zonal wind 850/700/500/250 hPa Meridional wind (same levels) Potential temperature (same) Geopotential Height at 500 hPa	MSLP U V θ z500	6-hourly/1.9°x1.9° Monthly/1.9°x1.9° … … …	*Roeckner et al.* [2003]
MPIOM1	Sea Surface Temperature Water temperature (0 to 123 m)	SST WT	Monthly/1.9°x1.9° …	*Jungclaus et al.* [2006]

Table 3.1: Summary of the atmospheric and oceanic variables used in this thesis. The resolution for the ECHAM5/MPIOM1 data is given after spatial interpolation. Asterisks denote not applicable fields.

IV. METHODOLOGY

'Essentially, all models are wrong, but some are useful.'

George E. P. Box (statistician; 1919-2013)

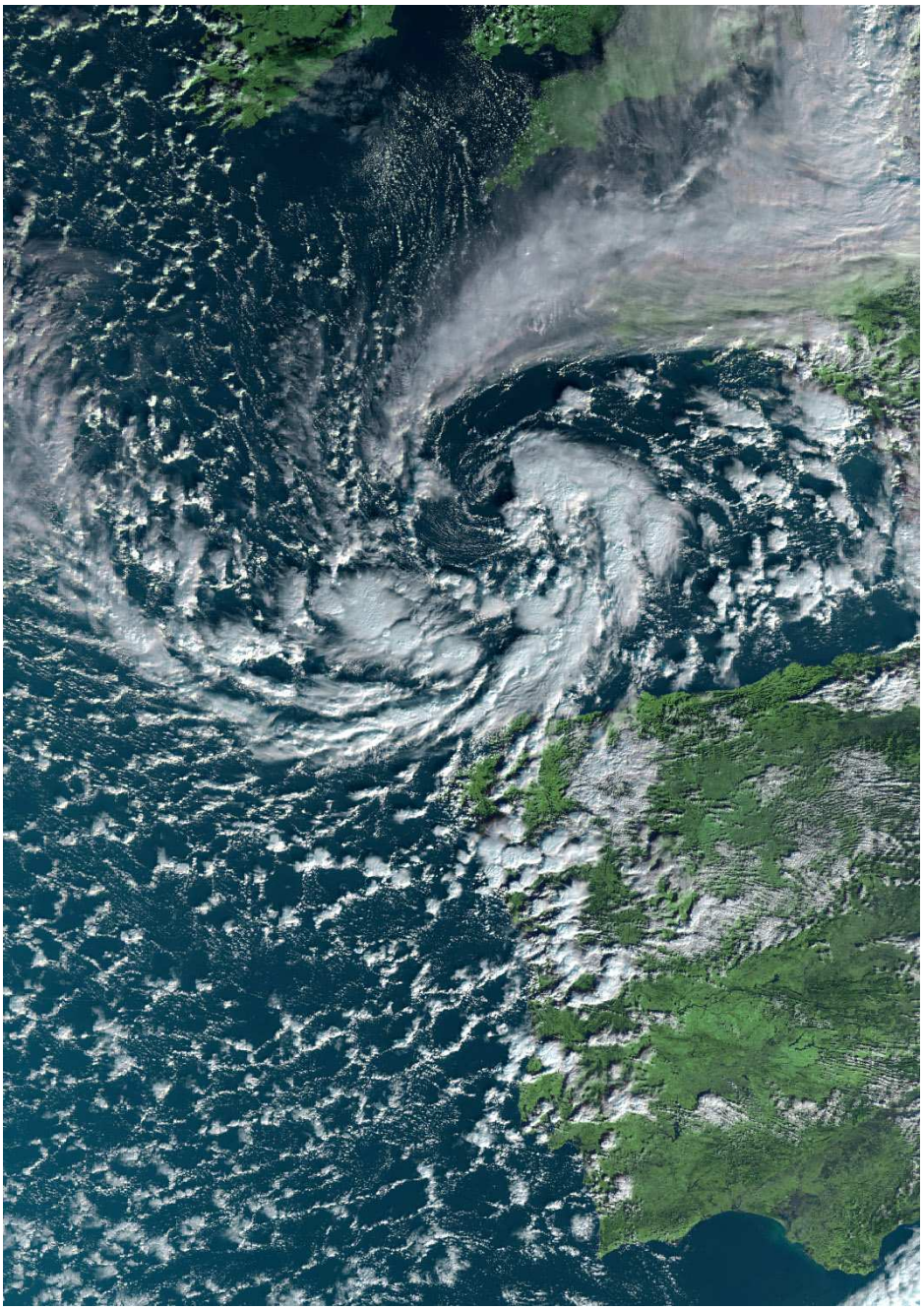

IV. Methodology

In this chapter the methodologies and techniques carried out in this thesis are described. These are divided into four different sections: (1) Data processing; (2) Hypothesis testing; (3) Dynamical diagnostics; and (4) Workflow diagram.

1. Data processing

The data processing techniques performed in this thesis are described below:

a. Spatial Interpolation

A triangulation-based linear interpolation of two-dimensional fields (typically longitude/latitude fields at a constant pressure level) is applied to climatic data to allow comparison between different resolution data sets (e.g., NCEP vs. ERA-40 reanalysis). This technique assumes linear behavior between neighboring lattice points (x_1,y_1) and (x_2,y_2), and calculates the value at an intermediate position y as a function of x (IV.1) [*Wilks*, 2006]:

$$y = y_1 + (y_2 - y_1)\frac{x - x_1}{x_2 - x_1} \qquad \text{(IV.1)}$$

b. Calculation of Standard deviation

The standard deviation of a finite set of numbers provides information of their dispersion (σ) with respect to their mean value (μ) (IV.2):

$$\sigma = \sqrt{\frac{1}{N}\sum_{i=1}^{N}(x_i - \mu)^2}; \qquad \mu = \frac{1}{N}\sum_{i=1}^{N} x_i, \qquad \text{(IV.2)}$$

where x_i are a set of N values having equal probability. As an example, the dispersion of a standard Gaussian distribution (in terms of σ values) is provided in Fig. 4.1.

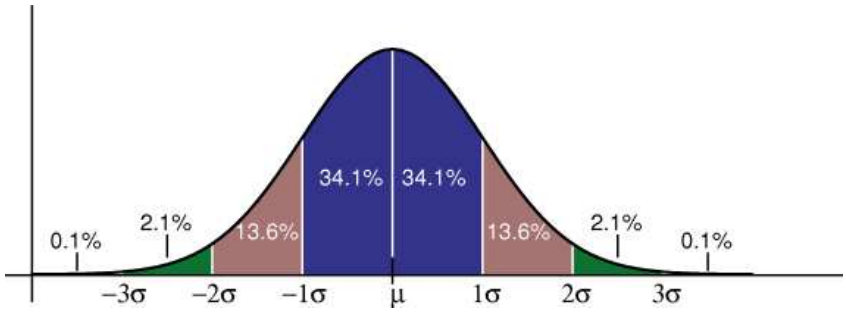

Fig. 4.1: Percentage of values (%) from a standard Gaussian distribution that lie within each standard deviation range. *Copyright © 2002–2012 Robert Sedgewick and Kevin Wayne.*

c. Calculation of anomalies

As explained in the Introduction section, the calculation and analysis of climatic anomalies is a pivotal aspect in climate variability. Generally, the anomaly of a given variable (A) is calculated with respect to its temporal ($\bar{A}$) or zonal average [A] (IV.3; IV.4):

$$A' = A - \bar{A}, \tag{IV.3}$$

$$A^* = A - [A], \tag{IV.4}$$

where the prime (asterisk) denotes the temporal (zonal) anomaly. In this thesis the temporal anomalies are mainly used. Typically, the behavior of variables such as geopotential height and wind speed during specific periods of time is compared against their climatological values. Next, anomalies are standardized by dividing each value of the timeseries by the standard deviation of the whole timeseries (IV.2, σ).

Another important aspect for the calculation of temporal anomalies is the period chosen as basis for climatology. For instance, the mean values of a variable during a given season or month are used as climatology. This is done in order to remove the signal of the seasonal cycle from the anomaly, which otherwise might influence the resulting field. In this thesis the temporal anomalies are generally calculated with regard to their corresponding month or season (e.g., winter: December to February; extended winter: October to March).

d. Spectral filtering

Spectral filtering is an important aspect in climate research, as different types of variability can be found in a wide spectrum of frequencies (e.g., synoptic, seasonal, inter-decadal, secular etc.).

i Lanczos filter

In this thesis a Lanczos filter is applied onto climatic time series either in high-pass, band-pass, or low-pass modes [*Duchon,* 1979]. This is done to retain, confine or detach different types of variability associated with diverse physical processes. The Lanczos filter transforms a time series x_t into y_t by performing its Fourier transform (IV.5):

$$y_t = \sum_{k=-\infty}^{\infty} w_k x_{t-k}, \qquad \text{(IV.5)}$$

where w_k are an optimized set of 'weights'. The relationship between *x* and *y* in the frequency domain is given by the response function *R(f)* (IV.6):

$$Y(f) = R(f) \cdot X(f), \qquad \text{(IV.6)}$$

where

$$R(f) = \sum_{k=-\infty}^{\infty} w_k \exp(i2\pi f_k \Delta), \qquad \text{(IV.7)}$$

and

$$w_k = \frac{1}{2f_N} \int_{-f_N}^{f_N} R(f) \exp(-i2\pi f_k \Delta) df, \qquad \text{for } k=\ldots,-1,0,1,\ldots, \qquad \text{(IV.8)}$$

being Δ the sampling interval, and f_N the Nyquist frequency (half cycle per data interval). For instance, a 31-point band-pass Lanczos filter (from 1 to 5 days) is used in Section V.1 as a synoptic filter [*Rivière and Orlanski*, 2007]. In Section V.4 a 33 yr. low-pass Lanczos filter is also used to extract the low-frequency variability and remove higher frequency oscillations [*Woollings et al*., 2015].

ii Running mean

A running mean is an auto-regressive moving average estimate that characterizes the time-evolving behavior of a physical system [*von Storch and Zwiers*, 1999]. For this purpose information from a finite set of m previous and subsequent members of a given value in the timeseries is retained, i.e., centered running means. The mathematical formulation of a running mean is as follows (IV.9):

$$X_t = \frac{\sum_{-i}^{i} Y_{t+i}}{m}, \qquad \text{(IV.9)}$$

where X_t are the t values of the running mean timeseries, Y_{t+m} the original data, and i the number of forward/backward members used to compute the mean; $m=2i+1$. Running means are commonly used in the literature as a smoothing low-pass filter. In this thesis this technique is applied in sections V.1 and V.4.

e. Principal Components Analysis

Principal Components Analysis (PCA) is a powerful discriminant statistical technique widely used in atmospheric sciences. It is also known as Empirical Orthogonal Function (EOF) analysis and was firstly introduced in this field by *Lorenz* [1956]. In this thesis PCA is applied onto temporal anomalies of time evolving two-dimensional fields of a given atmospheric variable (e.g., geopotential height, cyclone track density). The method acts to significantly reduce one of dimensions of the data by creating a new set of variables through a linear combination of the former. This is done by removing redundant information in the time-evolving fields, which typically present substantial correlations between different neighboring and remote grid-points in the data. The resultant variables represent the maximum possible fraction of the variability from the original data. The removal of one spatial dimension is also possible, although it is not performed in this thesis.

In Fig. 4.2, a schematic of a PCA analysis applied onto a two-dimensional time evolving field of spatial-temporal dimensions *Y[ns, nt]*, is provided. Once the temporal anomalies are calculated *Y'[ns,nt]*, each grid-point has an associated time series, and each time step has an associated two-dimensional map of anomalies.

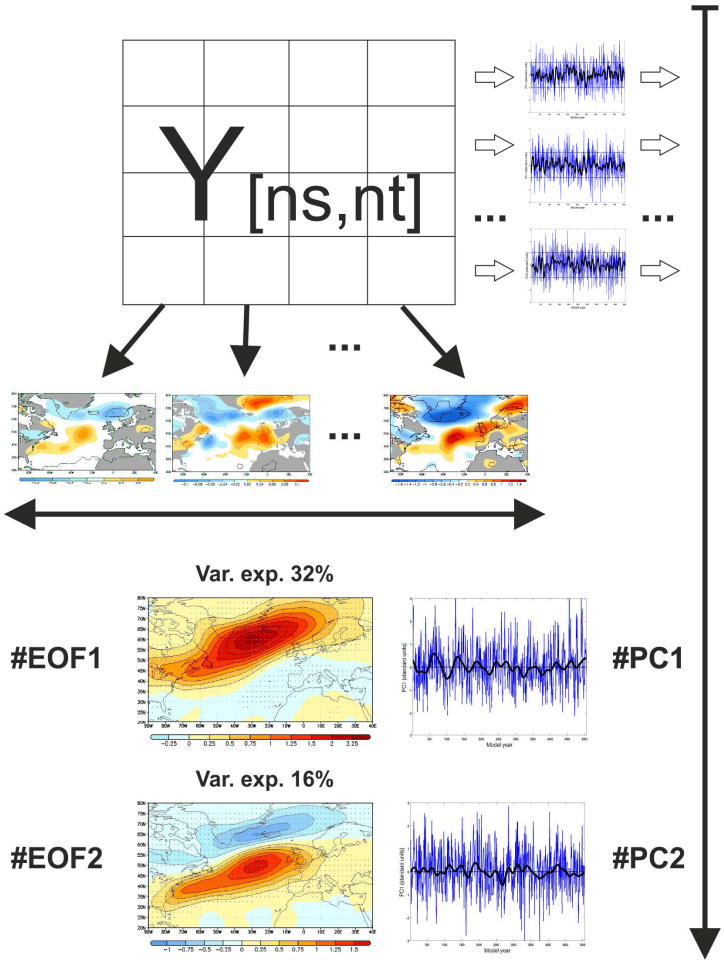

Fig. 4.2: Schematic of the Principal Components Analysis. *Y[ns,nt]* represents the original spatial-temporal field (matrix). On the right the time evolving anomalies for each grid-point are shown. The 2-D anomaly fields at a given time step appear below. The corresponding leading EOFs patterns and associated PCs are provided in the lower sub-panels together with the explained variance (in %). Figure adapted from *Rodríguez-Fonseca* [2001].

Next, the covariance matrix of the anomalies is calculated in the temporal dimension (IV.10) and diagonalized, with eigenvectors e_i and eigenvalues λi (IV. 11).

$$C = \frac{1}{nt}\, Y'[ns, nt] \cdot Y'^{T}[nt, ns] \qquad \text{(IV.10)}$$

$$(C - \lambda_i I)\overrightarrow{e_i} = 0 \qquad \text{(IV.11)}$$

Provided that C is a square, real and symmetric matrix, its eigenvectors fulfill the following characteristics:

- The eigenvectors are orthonormal: $\vec{e}_i^T \cdot \vec{e}_i = 1$; $\vec{e}_j^T \cdot \vec{e}_i = 0$ for i≠j.
- If E is a matrix containing the eigenvectors e_i, then: $E^{-1}CE = \Lambda$, where Λ is a diagonal definite positive matrix.

The principal components (PCs, α_i) are calculated as the projection of the anomalous field (*Y'*) onto the corresponding eigenvector (EOF; IV.12).

$$\overrightarrow{\alpha_i[nt,1]} = Y'^T[nt,ns] \cdot \overrightarrow{e_i[ns,1]} \qquad \text{(IV.12)}$$

Next, the PCs are standardized and re-projected onto the anomalous field (*Y'*), so that the units of the resultant EOF are the same as the field per standard deviation. At this point, an original anomalous field can be reconstructed as the linear combination of the total number of PCs multiplied by their corresponding EOF pattern (IV.13):

$$Y'[ns,nt] \approx \sum_{i=1}^{I} \cdot \overrightarrow{e_i[ns,1]} \cdot \overrightarrow{\alpha_i^T[1,nt]} \qquad \text{(IV.13)}$$

Such reconstruction of the anomalous field minimizes the mean square error (mse) in comparison with the original data (IV.14):

$$mse = (Y'[ns,nt] - \sum_{i=1}^{I} \cdot \overrightarrow{e_i[ns,1]} \cdot \overrightarrow{\alpha_i^T[1,nt]})^2 \qquad \text{(IV.14)}$$

Regarding the eigenvalues λ_i, it is useful to sort them out in descending order so that the corresponding eigenvector explaining the highest variance is first considered. Provided that the sum of all eigenvalues provides the total variance of the field *Y'*, then the fraction of variance (*fvar*, in %) of each EOF pattern can be calculated as (IV.15):

$$fvar_i = \left(\frac{\lambda_i}{\sum_I \lambda_i}\right) \cdot 100 \quad \text{(IV.15)}$$

In this thesis all EOF patterns and corresponding PCs are standardized by dividing each value by the standard deviation of that PC (IV.2). Finally, in order to determine the optimum number of modes representative of a spatial-temporal field of anomalies, the North criterion is applied [*North et al.*, 1982]. This criterion determines whether consecutive EOFs are well separated or, on the contrary, are degenerate and explain similar variability. In order to retain the maximum non-degenerate number of modes the sampling errors of the eigenvalues are considered. For the leading eigenvalue, its sampling error must not exceed the distance between its value and the second eigenvalue. This is successively applied over all eigenvalues (IV. 16).

$$\lambda_i - \lambda_{i+1} > \lambda_i \cdot \sqrt{2/nt} \quad \text{(IV.16)}$$

where *nt* is the temporal dimension.

f. Calculation of Composite, Regression and Correlation maps

Composites are calculated as the arithmetic mean of a given set of values or maps (IV.2, μ). In some cases, the composites are computed only for anomalies with values above/below a given threshold (e.g., σ > 1).

A regression map (R) is calculated as the projection between a timeseries T of dimensions [nt, 1] and a set of maps M of dimensions [ns,nt] (IV.17).

$$\overrightarrow{R[ns,1]} = M[ns,nt] \cdot \overrightarrow{T[nt,1]} \quad \text{(IV.17)}$$

where [ns,nt] are the [spatial,temporal] dimensions. In general, T is a standardized timeseries and the units of R are the same as M per standard deviation. Regression maps are also known in the literature as projection maps. Typically, a standardized timeseries is projected on a temporal succession of anomaly maps.

Correlation maps represent the spatial distribution of the Pearson's correlation coefficient (r) between a timeseries T[1,nt] and the time evolution of each grid-point from a time evolving map M[ns,nt] (IV.18).

$$r = \frac{nt\sum x_i y_i - \sum x_i \sum y_i}{\sqrt{nt\sum {x_i}^2 - (\sum x_i)^2}\sqrt{nt\sum {y_i}^2 - (\sum y_i)^2}} \quad \text{(IV.18)}$$

where [*xi,yi*] are the temporal components of each grid-point; *i=1,…,nt*. The correlation index provides information about the linear relation between two sets of variables, where 1 indicates perfect positive correlation, -1 perfect negative correlation and 0 no correlation. In addition, r^2 indicates the percentage of variance from the first variable that can be explained by the second. In climate research, linear correlation between two variables can indicate: (i) that variations in the first variable induce changes in the second; and (ii) that a third source of variability influences both of them. In the next section further information is provided on hypothesis testing for the r coefficient, etc.

2. Hypothesis testing

Hypothesis testing is a helpful statistical technique for decision making. First, an initial H_0 hypothesis, also known as the null hypothesis, is considered. What hypothesis testing provides is a set of statistical methods applied onto a sample of data, and the degree of confidence for the decision maker to accept or reject H_0. When H_0 is rejected, then the alternative hypothesis H_1 can be accepted with a high degree of certainty. This doesn't necessarily mean that H_1 is 100% correct, but there is strong evidence to assume it. The parameter α (1-α) is commonly used as the significance (confidence) interval (Fig. 4.3).

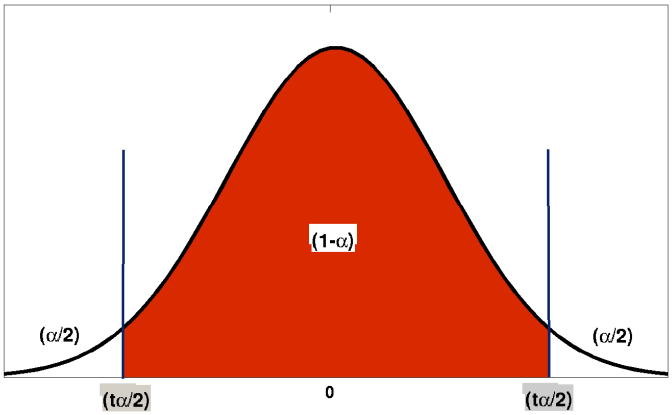

Fig. 4.3: Probability density function (black curve) of a statistic for a double-tailed test. The red area denotes the non-rejection region in which H_0 cannot be rejected with probability (1-α).

In climate research and other areas of expertise where the use of big data is common, this methodology tests the robustness of the findings and results, and filters out the outcomes potentially obtained by pure chance. Nevertheless, in the field of this thesis a physical and rational mechanism explaining the results obtained is equal or even more important than a result just based on pure statistics. In this thesis four different hypothesis testing methods are applied. These are divided into parametric and non-parametric tests, depending on the underlying statistical distribution used to infer the confidence levels. For further additional information on hypothesis testing see von *Storch and Zwiers* [1999] and *Wilks* [2006]. Both books have been used as reference in this section.

a. Parametric tests

Parametric tests assume that data follow a given statistical distribution (e.g., a normal distribution).

i Student's t test of correlation

The student's t test of correlation is applied onto two different samples of data and provides information about their linear dependence. This is a parametric test and assumes that the data follow the student distribution. The null hypothesis considers that both samples (s_1,s_2) are independent (r=0), whereas the alternative hypothesis assumes the contrary. The test statistic is calculated through (IV.19).

$$t = \frac{r\sqrt{n-2}}{\sqrt{1-r^2}} \quad \text{(IV.19)}$$

where (*n-2*) are the degrees of freedom of the timeseries and r the correlation coefficient. The null hypothesis will be rejected when $|t| > t_{\alpha/2,\, n-2}$. In this thesis the confidence levels adopted are generally 95, 98 and 99%. A common method for estimating effective degrees of freedom in auto-correlated data is also applied [*Bretherton et al.*, 1999].

ii Two-sample F test

The Two-sample F test applied onto two different populations analyzes whether their associated variances are equal (null hypothesis). The test statistic is conceived as the ratio of the two sample variances *(s_1,s_2)*. Under the null hypothesis the test statistic follows an F distribution with N_1*-1* degrees of freedom in the numerator and N_2*-1* in the denominator, being *(N_1, N_2)* the sample sizes of both populations (IV.20):

$$F = \frac{s_1^2}{s_2^2} \quad \text{(IV.20)}$$

In this thesis the Two-sample F test is usually applied onto different populations of time-evolving anomalies for specific periods of time. The aim is to

infer whether the variability of both specific periods is different or not (cf. Section V.4).

b. Non-parametric tests

Non-parametric tests do not assume parameterizations in the statistical distribution of data.

i *Monte Carlo test*

The Monte Carlo test recalculates a test statistic (T) for a large number (N) of realizations, each one performed by randomly resampling the data. Then T is compared against the corresponding value of the N realizations and its position in the probability density function is calculated. T will be statistically significant at 100(1-α) confidence level (in %) if $T>T_k$, where K=N(1-α). For instance, in this thesis the Monte Carlo test is used to infer the confidence level in the correlation between two timeseries. For this purpose, a large number of random permutations are applied into the timeseries (typically one thousand). For each realization, the correlation coefficient (r) is calculated between the newly created timeseries and stored. Finally, the correlation coefficient of the original timeseries is compared against its value for the 1000 random realizations. If this value is equal or above the 95^{th}, 98^{th} or 99^{th} percentiles then α is considered as 0.05, 0.02 or 0.01. Unlike parametric tests, the Monte Carlo method provides an accurate estimate of confidence levels even if applied onto much reduced data samples (e.g., a timeseries of 10 points or less). This method is used to calculate the statistical significance in sections V.1, V.2 and V.3.

ii *Mann–Whitney U test*

The Mann-Whitney U test is a non-parametric test that is applied onto two data samples and assumes as the null hypothesis that both samples have the same mean. Contrastingly, the alternative hypothesis states that both samples have different means and thus are part of different populations. In this case the test statistic U orders the members of both samples all together and gives a rank to each one. Then for each sample the sum of all ranks is performed and compared against the other. If the null hypothesis is true then the sum of ranges of both samples *(n1,n2)* might be equal regardless the way chosen for partitioning

the *n* data. In order to accept or reject the null hypothesis and avoid the calculation of the (n!)/(n1!)(n2!) possible combinations of data partitioning, the test statistic U is used (IV.21):

$$U_1 = R_1 - \frac{n_1}{2}(n_1 + 1) \quad \text{or} \quad U_2 = R_2 - \frac{n_2}{2}(n_2 + 1) \tag{IV.21}$$

where $U_1 + U_2 = n_1 n_2$, and (R_1, R_2) are the sum of ranks of each data sample. For moderately large samples ((n_1, n_2)>10)), the Mann-Whitney U statistic can be approximated as a Gaussian distribution, with mean (m_u) and median (σ_u, IV.22).

$$m_u = \frac{n_1 n_2}{2}, \quad \sigma_u = \sqrt{\frac{n_1 n_2 (n_1 + n_2 + 1)}{12}} \tag{IV.22}$$

In this thesis the Mann-Whitney U test is applied in Section V.4 onto time-evolving maps of different periods to infer whether their means are similar or no. As described, this non-parametric test performs well for much reduced data samples.

3. Dynamical Diagnostics

In order to analyze the variability and dynamics of extra-tropical cyclones and their relation with the large-scale circulation in the North Atlantic, different dynamical diagnostics are performed:

a. Cyclone identification and tracking algorithm

An automatic algorithm for the detection and tracking of extra-tropical cyclones is used. The algorithm was initially developed by *Murray and Simmonds* [1991], and subsequently adapted and validated for Northern Hemisphere characteristics by *Pinto et al.* [2005; 2007].

i Cyclone identification

The identification of cyclones is performed over 6-hourly Mean Sea Level Pressure (MSLP) fields, which are typically interpolated onto a regular higher horizontal resolution lattice (0.75˚ x 0.75˚). Despite this process doesn't give any additional information to the initial MSLP field, it provides a much finer resolution for subsequent cyclone identification and localization. This technique is particularly useful for small scale cyclones and occluding systems with weak MSLP gradients near their core [*Pinto et al.*, 2005]. Subsequently, the high-resolution MSLP field is examined by the automatic algorithm and the relative maxima of the Laplacian of MSLP ($\nabla^2 p$) are retained. This variable is used as proxy of the cyclone's quasi-geostrophic relative vorticity (ε; IV.23):

$$\varepsilon = \frac{1}{\rho 2 \Omega sin\emptyset} \nabla^2 p, \qquad \text{(IV.23)}$$

where ρ is the density of air, Ω the rotation rate of the Earth and ϕ the latitude. Next, a search of a corresponding MSLP minimum is performed in the vicinity (~1200 km) of each $\nabla^2 p$ maximum. This is done to classify the former into open or closed depressions. Whereas closed systems are located by the algorithm at the position of the MSLP minimum, open depressions are placed over the minimum pressure gradient point (i.e. inflection point).

ii Cyclone tracking

As a next step the tracking algorithm is applied to obtain cyclone trajectories and additional characteristics (e.g., intensification rate, travel speed, etc.). For this purpose an assignment algorithm is used to compile tracks considering the most probable cyclone trajectory between subsequent time frames. This is based on the information attained from the cyclone's previous path and speed, and the large-scale circulation conditions in which the cyclone is embedded (IV.24):

$$u_{pred} = (1 - w_{steer}) \cdot uM + w_{steer} \cdot (f_{steer} \cdot uS), \qquad \text{(IV.24)}$$

where *upred* is the 'prediction velocity', *uM* the cyclone's previous speed, *uS* the steering velocity at the surface level based on the average pressure gradient near the cyclone, and *fsteer* a factor that accounts for vertical wind shear. The weighting factor *wsteer* is set to 0.4, and therefore gives more importance to the first term of the equation. Once a minimum of MSLP is detected over the estimated area of subsequent cyclone location, the new position is added to its tracking information and identification number. This process is repeated until the cyclone eventually disappears (cf. Fig. 4.4).

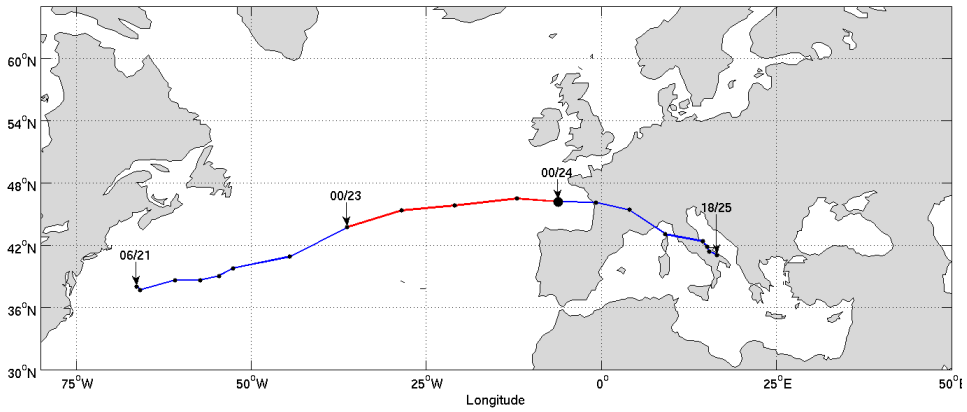

Fig. 4.4: Trajectory of extra-tropical cyclone Klaus (21-25 Jan 2009) on NCEP. Whole trajectory in blue, maximum intensification period of 24 h in red. Dots represent the location of the surface center at each time frame.

iii Cyclone selection

Thereafter, in order to keep only with physically coherent systems, some further filtering onto the tracking data is applied. This is done to remove systematic errors intrinsic to the tracking methodology or the MSLP data. A few examples are described below [*Pinto et al.*, 2005]:

- *High altitude issues:* MSLP data over mountainous areas are often inaccurate due to coarse model resolution (badly resolved topography). This is typically observed in reanalysis products (e.g., NCEP, ERA-40, ERA-Interim etc.). In addition, MSLP fields interpolated from vertical levels over high ground regions also tend to contain artificially created lows and vorticity maxima. For these reasons, the tracking data from areas higher than 1500 m above sea level are disregarded.

- *Vicinity issues:* Sometimes several vorticity maxima can be found over relatively small areas. This is generally observed near frontal zones of mature cyclones or orographic barriers. To avoid this issue the automatic algorithm only retains the strongest cyclone within a radius of 3 degrees latitude.

- *Minimum intensity issues:* In order to remove non-physical and artificial cyclones from the tracking data, a set of thresholds is applied to extra-tropical cyclone characteristics. These are mainly based on cyclone duration and intensity [*Pinto et al.*, 2009]: (i) cyclone lifetime ≥ 24 h; (ii) minimum MSLP (p) < 1000 hPa; (iii) Max. ($\nabla^2 p$) > 0.6 hPa deg.lat.$^{-2}$; and (iv) Max. $\frac{d}{dt}\nabla^2 p$ ≥ 0.3 hPa deg.lat.$^{-2}$ day^{-1}.

Further information of the automatic tracking method can be found in *Murray and Simmonds* [1991] and *Pinto et al.* [2005; 2007 and 2009]. In particular, this method has been tested against other tracking schemes and provides comparable and reliable results [*Raible et al.*, 2008; *Neu et al.*, 2013].

iv Cyclone classification

Next, cyclones are stratified in terms of their intensity. In this thesis two different indicators of cyclone's intensity are considered:

1. The first is the Normalized Deepening Rate (NDR, in Bergeron), which provides information of the intensification of the cyclone in time (IV.25):

$$NDR = \frac{\Delta p}{24} \cdot \frac{\sin 60^{\circ}}{\sin \varphi}, \qquad \text{(IV.25)}$$

   where Δp is the pressure fall in the cyclone's surface center over a period of 24 h (in hPa), and φ is the average latitude during the same time interval. A normalization factor that accounts for the variation of geostrophic wind with latitude is also introduced. Extra-tropical cyclones featuring intensification rates equal or above 1 Bergeron are denominated 'explosive cyclones' or 'bombs' [*Sanders and Gyakum*, 1980]. The acronym EC is typically used in this thesis to refer to such cyclones. Extra-tropical cyclones with maximum NDR lower than 1 Bergeron are denominated 'non-explosive' or 'common cyclones' (NoEC).

2. The second is the minimum MSLP of the cyclone's surface center. This variable is stratified in terms of percentiles (2nd and 5th lowest), and the corresponding cyclones are selected.

v Cyclone track-density data

Finally, cyclone track-density data are constructed by counting the number of cyclones of each class (e.g., explosive, non-explosive) intercepting a given detection area and time interval. The most simplistic approach of this methodology is performed in Section V.3. In that case, a unique circle centered over [55˚N, 5˚W] with a radius of 700 km is used to quantify cyclone clustering over Western Europe (Fig. 4.5a). In particular, the choice of radius for cyclone identification is an important issue in this methodology. If the radius is too small, then potential cyclones with direct influence over the area of interest (e.g., associated fronts etc.) might be disregarded. If the radius is too large, the fields might not capture regional features of the storm track. As a consequence, the

typical range of effective radius for extra-tropical cyclones is considered [600-1000km; *Rudeva and Gulev*, 2007] and r=700 km is chosen. As a generalization of this approach, the cyclone track-density data relies on a large number of detection circles distributed over a homogenous lattice (Fig. 4.5b). In section V.4 this technique is employed and track-density is provided in cyclone counts per winter per 7.5˚ radius circle area. This variable provides information of cyclone frequency and track lengths. Further details on this method can be found in *Murray and Simmonds* [1991], *Mumby et al.* [2011] and *Pinto et al.* [2013].

(a) Cyclone detection over the UK (b) Cyclone track-density

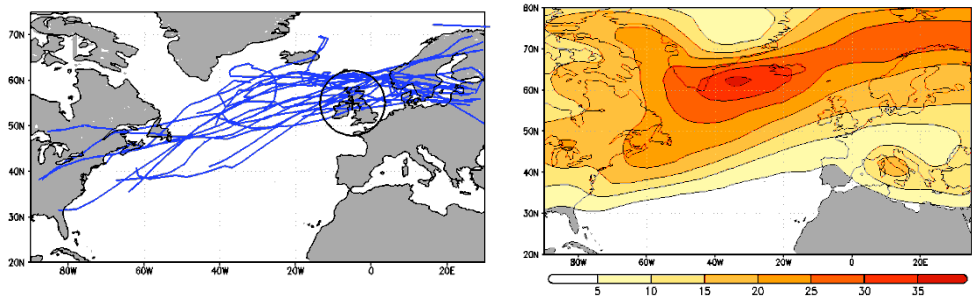

Fig. 4.5: (a) Trajectories of all cyclones (blue) crossing the circle detection area ([55°N, 5°W], r=700km) during January 2007 in ERA-Interim. Adapted from *Pinto et al.* [2014], their Fig. 1a (Section V.3). (b) Winter (DJF) cyclone track-density data on ERA-40 (1957-2001; in counts per 7.5° radius circle area).

b. Atmospheric mean flow characterization

Three different indices are used to characterize the upper and lower level large-scale circulation conditions in the Euro-Atlantic sector. These are the following:

i <u>*Two-dimensional Rossby Wave-Breaking index*</u>

A two-dimensional Rossby Wave-Breaking (RWB) index is used to detect and classify RWB events over the North Atlantic [*Masato et al.,* 2013a]. The index is based on the potential temperature (θ) of the dynamical tropopause (2 Potential Vorticity Units (PVU) = 2 x 10^{-6} K m^2 Kg^{-1} s^{-1} surface). The temporal resolution of the index is 6-hourly. However, sub-daily fields are averaged into daily means for simplicity. The horizontal resolution of the index is 4.5˚ x 1.125˚ in

longitude/latitude. The index provides information of large-scale instantaneous RWB occurrence (B index) and direction of breaking (DB index):

- The B index identifies regions where the mean meridional gradient of θ is reversed. This is performed through the calculation of the mean θ values to the north and south of each longitudinal grid-point *i* (IV.26; Fig. 4.6a):

$$\overline{\theta_i^n} = \frac{2}{\Delta\emptyset}\int_{\emptyset_0}^{\emptyset_0+\frac{\Delta\emptyset}{2}} \theta_i d\emptyset, \qquad \overline{\theta_i^s} = \frac{2}{\Delta\emptyset}\int_{\emptyset_0-\frac{\Delta\emptyset}{2}}^{\emptyset_0} \theta_i d\emptyset, \tag{IV.26}$$

  where Ø is latitude. Then the difference between the northern and southern terms is calculated (IV.27).

$$B_i = \overline{\theta_i^n} - \overline{\theta_i^s} \tag{IV.27}$$

  The B index provides 1s (RWB occurrence) and 0s (RWB absence) on daily basis with no duration condition imposed (cf. Fig. 4.6b). This is done to measure large-scale instantaneous RWB in general, rather than persistent blocking events. It is also important to note that thin θ streamers are disregarded by the index, which imposes a quite strict criterion on the scale of RWB (14.625 deg.lat. both to the north and south).

- A classification of different types of RWB events is provided by the DB index. The index calculates the difference of θ along longitude between points *i*-1 and *i*+1 of the same latitude (IV.28; Fig. 4.6a).

$$DB = \overline{\theta_{i-1}} - \overline{\theta_{i+1}}, \tag{IV.28}$$

  where

$$\overline{\theta_i} = \frac{\overline{\theta_i^n}+\overline{\theta_i^s}}{2}. \tag{IV.29}$$

The index is subsequently standardized (counting only cases with RWB occurrence: B>0). As a threshold for classification, the value of +0.2 (-0.2) is selected for anticyclonic (cyclonic) RWB events. Otherwise the events are defined as 'unclassified'. Despite these thresholds look somewhat arbitrary, it must be noted that distributions of RWB events change very little when the former are varied a few decimals.

(a) RWB schematic (b) RWB detection

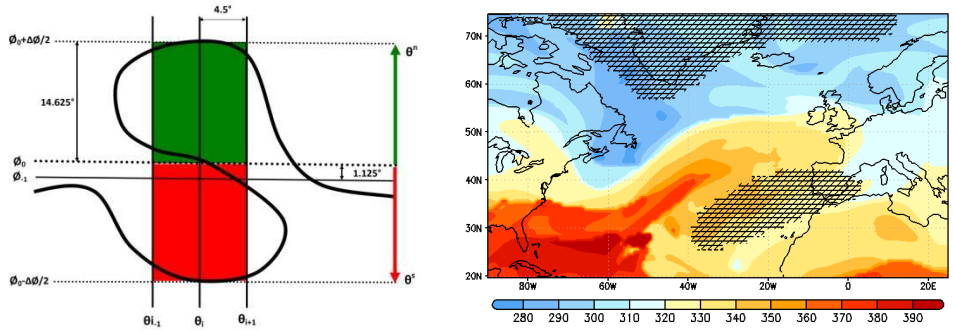

Fig. 4.6: (a) Schematic of B and DB indices based on θ (2PVU surface - cyclonic RWB). Adapted from *Gómara et al.* [2014a], their Fig. 1a. (b) θ on the 2PVU surface (shadings, in K) and identified areas of RWB occurrence (B>0) on 18 January 2007 (ERA-Interim). Adapted from *Pinto et al.* [2014], their Fig. 3.18.

For further details on the RWB index see *Pelly and Hoskins* [2003] and *Masato et al.* [2013a; 2013b].

ii Eddy-driven jet latitude index

An index indicating the latitudinal position of the eddy-driven jet in the North Atlantic is used [*Woollings et al.*, 2010]. The index is based on the zonal wind at 850 hPa, averaged in longitude between 40˚W-10˚E. The choice of longitudes is done to characterize the extra-tropical jet over Western Europe, an area where cyclones generally intensify rapidly before affecting the continent [*Hanley and Caballero*, 2012]. The choice of the vertical level is done to enable a clear separation for the diagnostics between the extra-tropical and sub-tropical jets. This is based on their vertical structure: whereas the extra-tropical jet

extends well throughout the whole troposphere, the sub-tropical jet is much more confined to the upper levels. Next, the resulting field is low-pass filtered using a Lanczos filter (10 day cut-off frequency) and the latitudinal position of the maximum westerly flow is retained. Further information of this index is available in *Woollings et al.* [2010].

iii *Baroclinicity index: Maximum Eady Growth Rate*

In this thesis the Maximum Eady Growth Rate index is considered as a measure of large-scale baroclinicity (*bi,* in days^{-1}). This variable quantifies the potential wave growth in the atmosphere and is sensitive to the vertical wind shear and the static stability between two given atmospheric levels (typically 300-500 and 700-850 hPa; IV.30).

$$bi = 0.31 \left(\frac{f}{N}\right) \left|\frac{\mathrm{dv}}{\mathrm{dz}}\right|, \qquad \text{(IV.30)}$$

where *f* is the Coriolis parameter, *N* is the static stability, *z* the vertical coordinate and *v* the horizontal wind vector. In general, the areas of enhanced baroclinicity in the North Atlantic tend to overlap the climatological position of the extra-tropical jet core. This effect is clearer for the upper level baroclinicity than for the lower level. Further information of this variable can be found in *Hoskins and Valdes* [1990] and *Hoskins and Hodges* [2002].

4. Workflow diagram

Based on the previous sections, a workflow diagram of the methods followed in this thesis is provided below (Fig. 4.7).

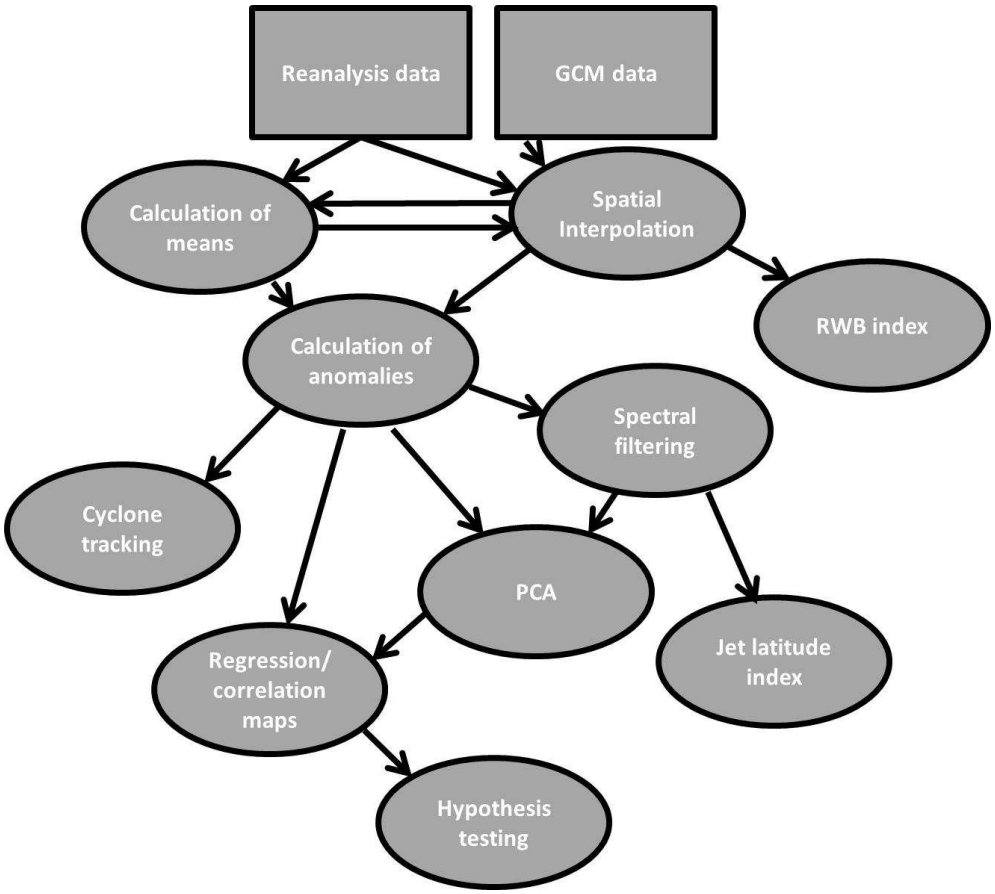

Fig. 4.7: Schematic flowchart of the methodologies carried out in this thesis.

V. RESULTS

'The great tragedy of science: the slaying of a beautiful hypothesis by an ugly fact.'

Thomas H. Huxley (biologist; 1825-1895)

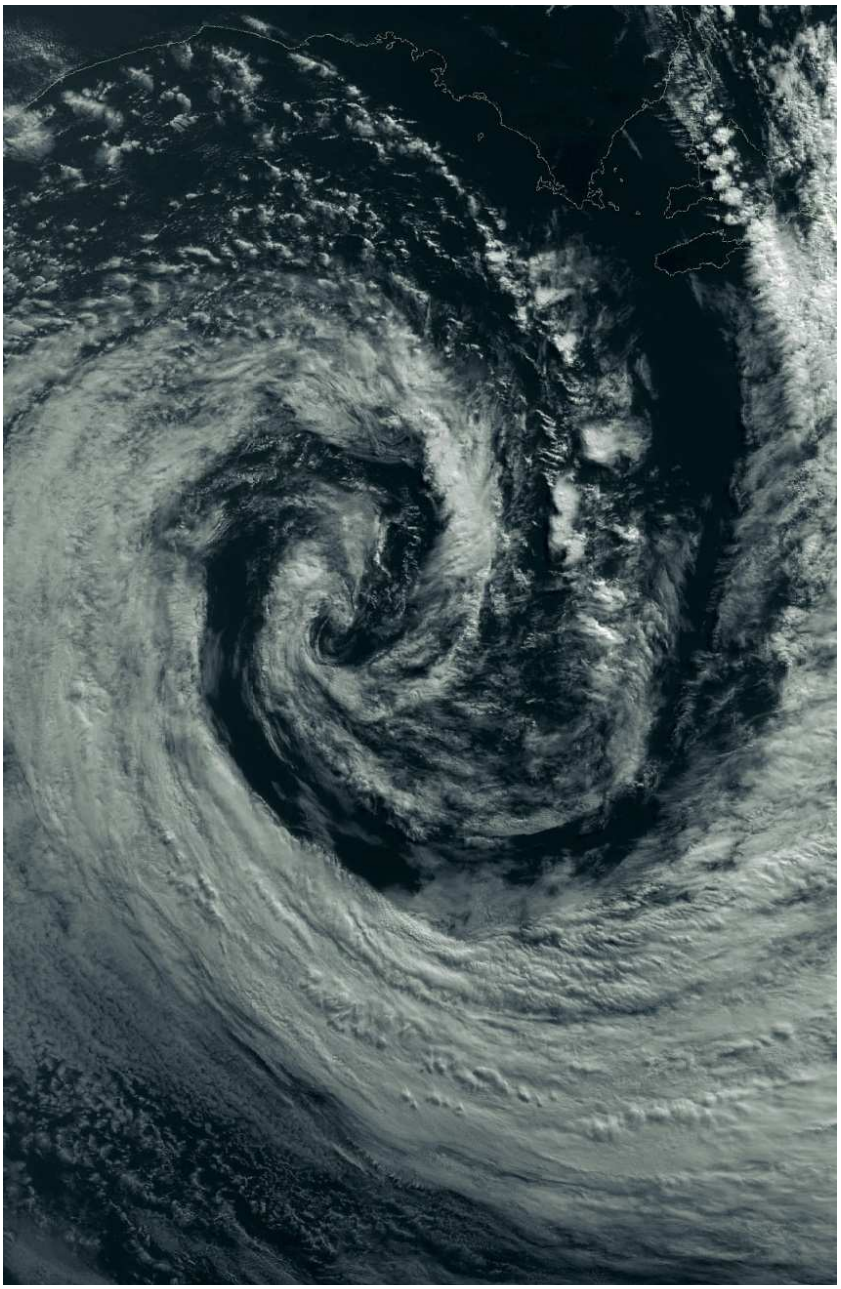

V. Results

The results of this thesis are divided into four different sections. Each section corresponds to an article published (or under review[1]) in journals from the Science Citation Index. Supplementary material files are provided after each article.

1. On the relation between explosive cyclones affecting Europe and the North Atlantic Oscillation

Abstract: Intense winter cyclones often lead to hazardous weather over Europe. Previous studies have pointed to a link between the North Atlantic Oscillation (NAO) and strong European windstorms. However, the robustness of this relation for cyclones of varying intensities remains largely unexplored. In this paper, the bi-directional relation between the NAO and cyclones impacting Europe is analyzed for the period 1950-2010 focusing on the sensitivity to storm intensity. Evidence is given that explosive (EC) and non-explosive cyclones (NoEC) predominantly develop under different large-scale circulation conditions over the North Atlantic. Whereas NoEC evolve more frequently under negative and neutral NAO phases, the number of EC is larger under a positive NAO phase, typically characterized by an intensified jet toward Western Europe. Important differences are also found on the dynamics of NAO evolution after peak intensity for both cyclone populations.

***Gómara** I, Rodríguez-Fonseca B, Zurita-Gotor P, and Pinto JG (2014b) On the relation between explosive cyclones affecting Europe and the North Atlantic Oscillation, Geophys. Res. Lett., 41, 218-2190, doi: 10.1002/2014GL059647*

[1] Article in Section V.4

AGU PUBLICATIONS

Geophysical Research Letters

RESEARCH LETTER
10.1002/2014GL059647

Key Points:
- The links between European cyclones and the NAO are systematically analyzed
- NAO conditions fostering explosive/non-explosive cyclones are different
- Eddy feedback on the daily NAO index is evident for the strongest cyclones

Supporting Information:
- Readme
- Figure S1
- Figure S2

Correspondence to:
I. Gómara,
i.gomara@ucm.es

Citation:
Gómara, I., B. Rodríguez-Fonseca, P. Zurita-Gotor, and J. G. Pinto (2014), On the relation between explosive cyclones affecting Europe and the North Atlantic Oscillation, *Geophys. Res. Lett.*, *41*, 2182–2190, doi:10.1002/2014GL059647.

Received 18 FEB 2014
Accepted 26 FEB 2014
Accepted article online 3 MAR 2014
Published online 19 MAR 2014

On the relation between explosive cyclones affecting Europe and the North Atlantic Oscillation

Iñigo Gómara[1,2], Belén Rodríguez-Fonseca[1,2], Pablo Zurita-Gotor[1,2], and Joaquim G. Pinto[3,4]

[1]Dpto. Geofísica y Meteorología, Universidad Complutense de Madrid, Spain, [2]Instituto de Geociencias (IGEO), UCM, CSIC, Spain, [3]Department of Meteorology, University of Reading, UK, [4]Institute for Geophysics and Meteorology, University of Cologne, Germany

Abstract Intense winter cyclones often lead to hazardous weather over Europe. Previous studies have pointed to a link between the North Atlantic Oscillation (NAO) and strong European windstorms. However, the robustness of this relation for cyclones of varying intensities remains largely unexplored. In this paper, the bi-directional relation between the NAO and cyclones impacting Europe is analyzed for the period 1950–2010 focusing on the sensitivity to storm intensity. Evidence is given that explosive (EC) and non-explosive cyclones (NoEC) predominantly develop under different large-scale circulation conditions over the North Atlantic. Whereas NoEC evolve more frequently under negative and neutral NAO phases, the number of EC is larger under a positive NAO phase, typically characterized by an intensified jet toward Western Europe. Important differences are also found on the dynamics of NAO evolution after peak intensity for both cyclone populations.

1. Introduction

Hazardous weather conditions over Europe are frequently associated with the passage of intense extra-tropical cyclones, especially during winter [*Lamb*, 1991]. Such storms typically induce intense wind gusts and sometimes heavy precipitation and storm surges, leading to disruption of normal socio-economic activity and large property damage [e.g., *Fink et al.*, 2009]. The explosive intensification of cyclones [*Sanders and Gyakum*, 1980; pressure fall greater than 24 hPa day^{-1} at 60ºN, or equivalent], often leading to storms with hurricane-like strong winds over the eastern North Atlantic (NA), is one of the several reported sources of uncertainty in weather forecasts [e.g., *Wernli et al.*, 2002].

The anomalous mean flow over the North Atlantic on days prior, during, and after the occurrence of European windstorms has been analyzed in previous studies [e.g., *Raible*, 2007; *Pinto et al.*, 2009; *Hanley and Caballero*, 2012; *Gómara et al.*, 2013]. The North Atlantic Oscillation (NAO), the most prominent pattern influencing the European weather variability [*Hurrell et al.*, 2003], has a clear link to storm activity: under a positive NAO phase, the jet is northeastwardly shifted and accelerated over the NA, with cyclone trajectories tilted north-eastward toward northern Europe. Conversely, the negative NAO phase is characterized by a more equatorward and less eastward extended jet, with more zonal orientated cyclone tracks typically directed toward southwestern Europe [cf. *Pinto and Raible*, 2012]. As a consequence, windstorms affecting Central Europe tend to occur under a moderately positive NAO phase [*Donat et al.*, 2010], and their development can be supported by Rossby wave-breaking (RWB) processes [cf. *Hanley and Caballero*, 2012; *Gómara et al.*, 2013]. Conversely, intense cyclones themselves can also play an important role modifying the large-scale flow and thus driving the short-term NAO variability on days following their maximum intensification period [*Rivière and Orlanski*, 2007; *Michel et al.*, 2012]. However, the sensitivity of this two-way relation to cyclone's intensity has received little attention.

In this study, the bi-directional relation between the large-scale mean flow (represented by the NAO) and explosive and non-explosive cyclones affecting Western and Central Europe is examined using a long reanalysis data set. A question of prime interest is whether this relation is sensitive to storm's intensity. A daily NAO index (DNI) and three different cyclone subsets, stratified in terms of cyclone intensity, are considered.

This letter is structured as follows. Cyclone and NAO considerations are detailed in section 2. Section 3 outlines the main results, and a short discussion concludes the study.

2. Data and Methodology

The National Centers for Environmental Prediction (NCEP) reanalysis data [*Kalnay et al.*, 1996] are used over 60 extended winter seasons (October–March 1950–2010) with a 6-hourly temporal resolution and a 2.5° horizontal grid. Mean sea level pressure data (6-hourly), daily averaged geopotential height at 500 hPa (z500), and zonal and meridional winds at 250 hPa (u250, v250) are used to analyze the anomalous mean flow associated with cyclone occurrences. For each day, the monthly mean associated with the corresponding year is removed in order to compute the anomalies (e.g., if 17 March 1985 is selected, then the monthly mean of March 1985 is subtracted). This is done to remove intra-seasonal/seasonal (e.g., a more intense jet in January than in October) and long-term decadal/multidecadal variability from the anomalous fields. Finally, a 5 day (centered) running mean smoothing is applied to minimize the influence of individual cyclones onto the large-scale mean flow [cf. *Pinto et al.*, 2009]. The methods and confidence intervals used for statistical hypothesis testing (e.g., Monte Carlo, *t* test) are detailed in figure captions.

2.1. Cyclone Considerations

An automatic tracking method [*Murray and Simmonds*, 1991] adapted and validated for Northern Hemisphere cyclone characteristics [*Pinto et al.*, 2005] is applied to mean sea level pressure data to obtain complete cyclone life cycles and additional properties. Cyclone normalized deepening rate (NDR, in Bergeron) is used as indicator of intensity:

$$NDR = \frac{\Delta P}{24}\frac{\sin 60^\circ}{\sin \phi}, \quad (1)$$

where ΔP accounts for the pressure drop and Φ is the average latitude of the cyclone's surface centre over a time interval of 24 h. To ensure that cyclones affect the European continent during their mature stage, we follow *Gómara et al.* [2013] and select cyclones located within the latitude-longitude box [35°N–65°N, 20°W–10°E] (dashed rectangle in Figure 1a) at the final time step of the 24 h of maximum NDR (red segments in the 6-hourly trajectories).

Finally, depending on their maximum NDR (intensity), the selected cyclones are divided into three different subsets (Figure 1c): (1) Non-explosive cyclones (NoEC = 1665 cases; $0 < NDR_{NoEC} < 1$ Bergeron); (2) Explosive cyclones (EC = 424 cases; $NDR_{EC} \geq 1$ Bergeron); and (3) "Extreme" cyclones, defined as explosive cyclones with NDR equal or above the 95th percentile (EC95 = 104 cases; $NDR_{EC95} \geq NDR_{95th}$). Note that these are also included in (2).

Figures 1a and 1b show the complete cyclone trajectories (blue) and the segment corresponding to the 24 h maximum intensification period (red) of NoEC and EC. As a general note, it can be observed that NoEC (Figure 1a) roughly span in latitude over the entire "European box area." In contrast, EC (Figure 1b) depict more coherent and latitudinal constrained tracks over higher latitudes [50°N–65°N], as they tend to develop along an intensified jet stream [cf. *Uccellini*, 1990; *Hanley and Caballero*, 2012; *Gómara et al.*, 2013].

For the lag composite analysis, lag 0 is defined as the day in which the period of maximum NDR (24 h) starts (e.g., if a cyclone features its maximum intensification between 12 UTC 10 January and 12 UTC 11 January, then 10 January is defined as lag 0).

2.2. NAO Definition and Classification

A daily NAO index (DNI) is constructed to analyze the NAO variability at synoptic timescales [cf. *Pinto et al.*, 2009]. First, the leading EOF (Empirical Orthogonal Function) of monthly mean z500 anomalies [25°N–80°N, 80°W–40°E] over the time period October–March 1950–2010 is calculated (explained variance of 33.89%). Next, a daily index is constructed projecting the z500 daily anomalies in the Euro-Atlantic sector onto this EOF1. The resulting time series has a correlation of 0.78 with the NOAA Climate Prediction Centre (CPC) daily NAO index (99% confidence interval, bilateral *t* test). We then subtract from this time series the monthly mean DNI of the corresponding year and apply a 5 day (centered) running mean smoothing. Finally, the index is standardized. The same methodology is applied to the anomalous mean flow fields, except for the standardization.

In Figure 1d, the pattern associated with EOF1 is provided: a NAO-like structure can be identified with two centers of action, one over southern Greenland and the other spanning over the sub-tropical NA and

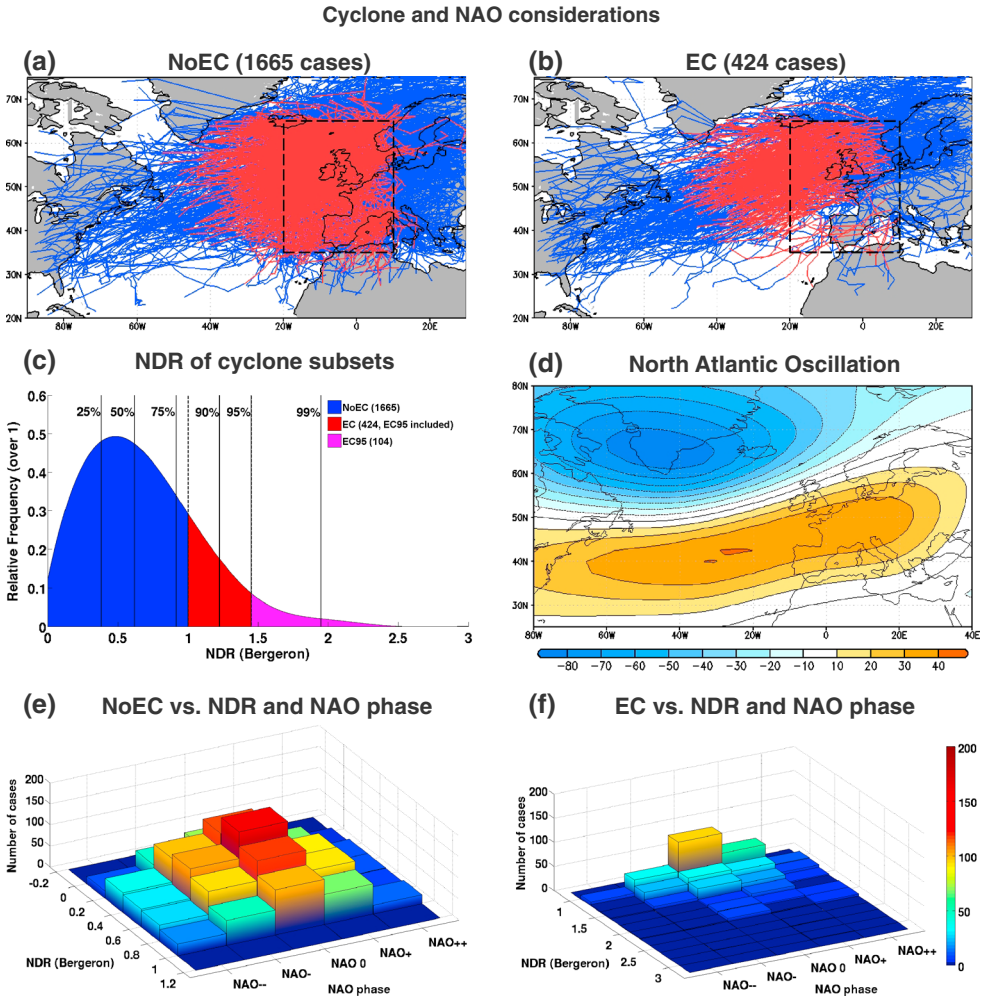

Figure 1. (a) Whole non-explosive cyclones (NoEC) trajectories (blue) and segments of maximum normalized deepening rate (NDR) (24 h, red). "European box area" for cyclone selection (dashed rectangle). (b) Same as Figure 1a but for explosive cyclones (EC). (c) Relative frequency (over 1) of cyclone NDR (curve, in Bergeron). NDR range of cyclone subsets (filled colored areas). NDR percentiles (vertical lines). (d) North Atlantic Oscillation (NAO) pattern (Empirical Orthogonal Function 1; regression map in gpm). (e) 3-D histogram of NoEC on lag 0: Number of cases vs. NDR vs. NAO phase. (f) Same as Figure 1e but for EC.

SW/central Europe. Subsequently, five different NAO phases (frequencies shown in Figure 3a, solid black line) are derived depending on the DNI value following *Pinto et al.* [2009]: NAO++ (DNI ≥ +1.5); NAO+ (+0.5 ≤ DNI < +1.5); NAO 0 (−0.5 < DNI < +0.5), NAO− (−1.5 < DNI ≤ −0.5); and NAO−− (DNI ≤ −1.5).

In Figures 1e and 1f, the 3-D histograms of cyclone counts, maximum NDR, and NAO phase (at lag 0) are provided for NoEC and EC, respectively. The total number of cyclones is highest under NAO 0 (also the most frequent phase, cf. Figure 3a). Comparing the non neutral phases, a negative NAO shift can be observed for NoEC and the reverse for EC. This asymmetry is analyzed in more detail in section 3.1.2.

3. Results

3.1. Influence of the Background Field Over the Cyclones

3.1.1. Structure of Mean Flow North Atlantic Anomalies

The anomalous mean flow over the NA on lagged cyclone days is shown in Figure 2. For EC95, a downstream propagating north-negative and south-positive pattern of z500 composite anomalies is observed (Figures 2a, 2d, and 2g). This structure resembles the positive NAO phase and is accompanied by an intensified jet stream

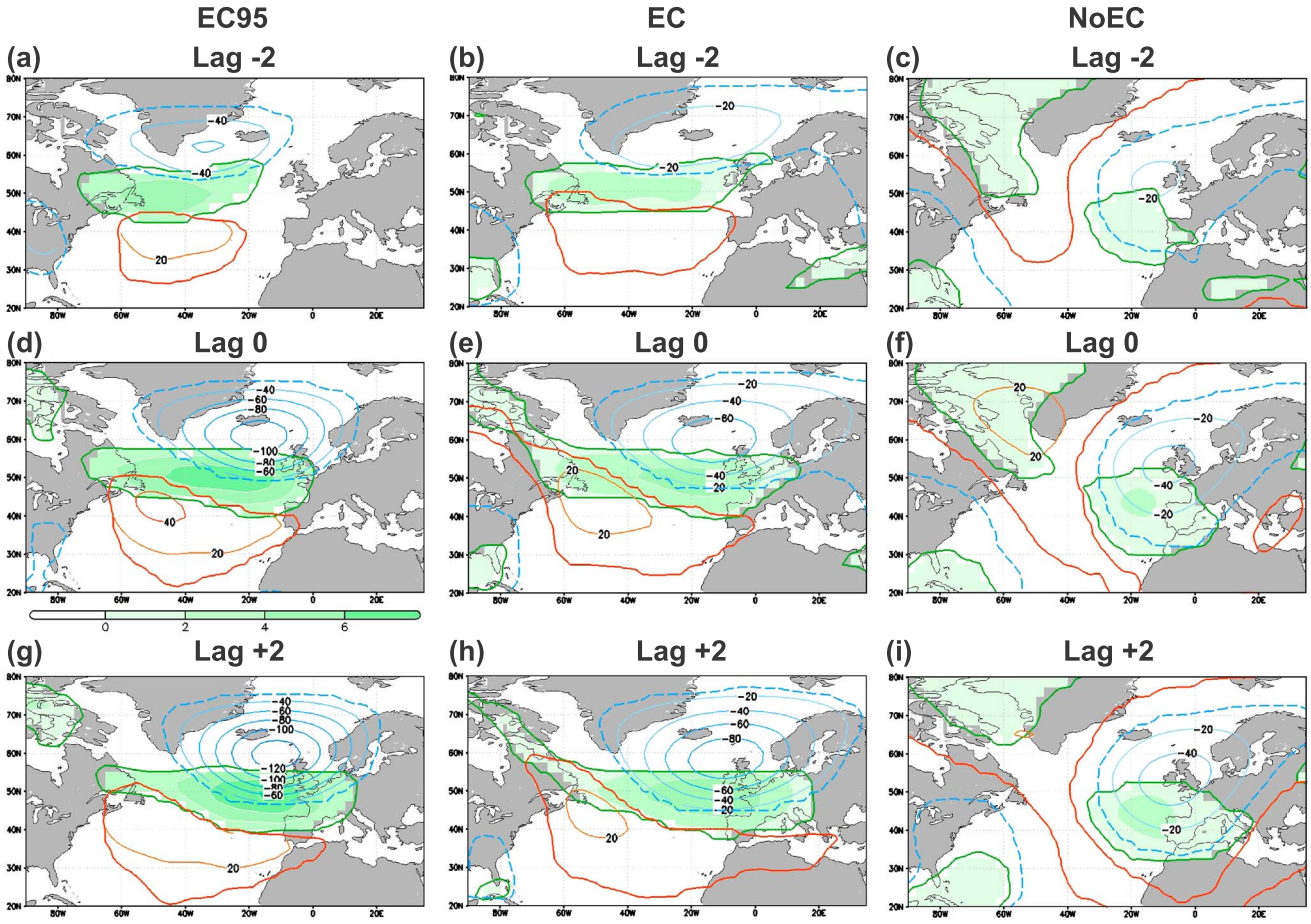

Figure 2. (a)–(i) Composites: significant positive/negative daily z500 anomalies (in gpm at lags −2, 0, and +2, red/blue contours) of (left column) EC95, (central column) EC, and (right column) NoEC. Significant positive 250 hPa jet intensity anomalies in green shadings ($m\,s^{-1}$). Confidence interval: 99%—Monte Carlo test. A 5 day running mean smoothing is applied to the daily anomalies of all variables.

over Western Europe at lag 0 (Figure 2d). This configuration may be forced by RWB at negative lags, which leads to the intensification of the jet stream [*Hanley and Caballero*, 2012; *Gómara et al.*, 2013]. As a consequence, cyclones encounter very favorable upper-level conditions for explosive growth [*Uccellini*, 1990].

Conversely, NoEC predominantly develop under a different mean flow pattern (Figures 2c, 2f, and 2i) which is less transient in time. It consists of three centers of action, with negative anomalies over eastern North America and north-western Europe and a positive anomaly over south-western Greenland. Even though the structure does not resemble the NAO pattern, it projects more onto the negative phase due to the high pressure anomalies over Greenland. In this case the mean flow anomalies do not appear to promote rapid intensification as for EC95 but to deflect the cyclone trajectories toward Europe due to the comparatively high pressures near Greenland (Figures 2c and 2f). As expected from their NDR, the anomalies associated with EC (Figures 2b, 2e, and 2h) are a blend of the previous two patterns.

Since the composite analysis includes cyclones spread over a wide area, the broad low in Figure 2 may be affected by the cyclone imprint at 500 hPa, an effect that we aimed to minimize with the 5 day running mean smoothing (compare to the unsmoothed Figure S1). However, the large-scale pattern shown in Figures 2 and S1 does not seem to be an artifact of the analysis: it extends hemispherically (not shown) and displays a similar structure at negative lags, when the cyclones are located far away and much more widespread (positions at lag −2 are shown in Figures S1g, S1h, and S1i).

The previous analysis shows that the background flow associated with explosive and non-explosive cyclones is different. In the following, these differences are quantified using the NAO index.

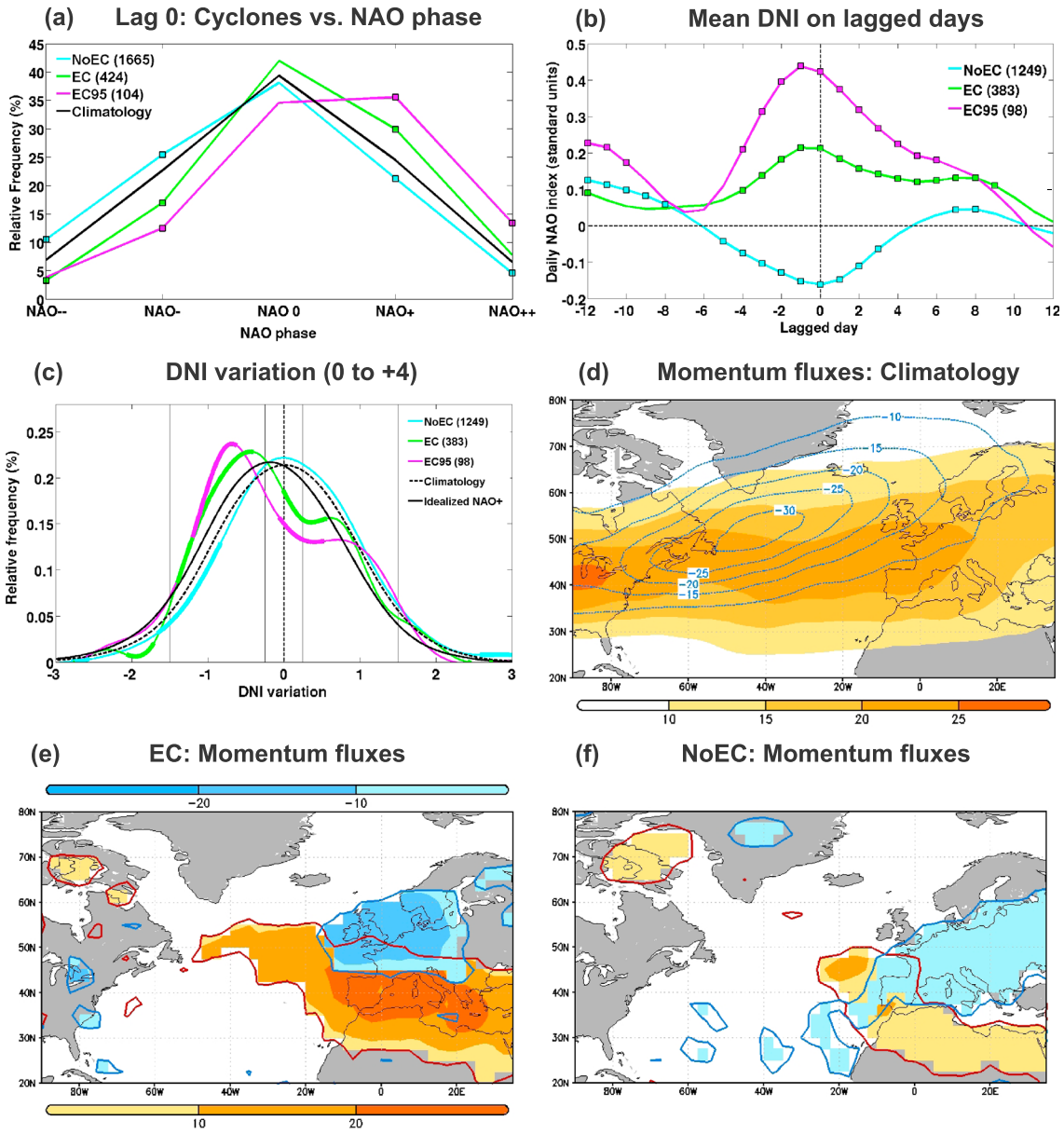

Figure 3. (a) Relative frequency (in % of days) of each NAO phase: climatology (October–March 1950–2010, solid black line); cyclone subsets at lag 0 (NoEC—blue, EC—green, and EC95—magenta). Significant anomalies: black squares. (b) Mean daily NAO index (DNI) (standard units, solid lines) from lags −12 to +12 for cyclone subsets (see legend). Significant anomalies: black squares. (c) Relative frequency (%) of DNI variations ($DNI_{lag+4} - DNI_{lag0}$). Curves: Climatology (dashed black), cyclone subsets (solid blue/green/magenta, see legend). The curves (histograms) are smoothed using a spline interpolation from 0.5 to 0.01 Standard Unit box lengths. Significant anomalies: thicker line. The solid black line is a composite of DNI variations constructed combining climatological distributions for each NAO phase and the frequency of occurrence of that phase for EC95. (d) Climatology of positive (shadings) and negative (contours) high-frequency (1–5 days) Lanczos filtered momentum fluxes over the NA ($m^2 s^{-2}$; daily basis). Positive and negative momentum fluxes are averaged separately (and set to zero when displaying the opposite sign) to avoid compensation. (e) Enhanced positive (red shadings) and negative (blue) momentum fluxes associated with EC (averaged over lags 0 to +4, $m^2 s^{-2}$). (f) Same as Figure 3e but for NoEC. All anomalies are calculated subtracting climatology. Confidence interval: 95%—Monte Carlo test.

3.1.2. Analysis of NAO Conditions

As expected, EC95/EC and NoEC predominantly evolve under different NAO conditions (Figure 3a): whereas a significant shift to negative NAO phases (especially NAO−−) is observed for NoEC compared with climatology, EC95/EC tend to develop under anomalous NAO+.

To provide a more comprehensive view of the NAO behavior, the composite DNI evolution on positive and negative lagged days is shown in Figure 3b. Because of the large lags considered, only cyclones with lag 0

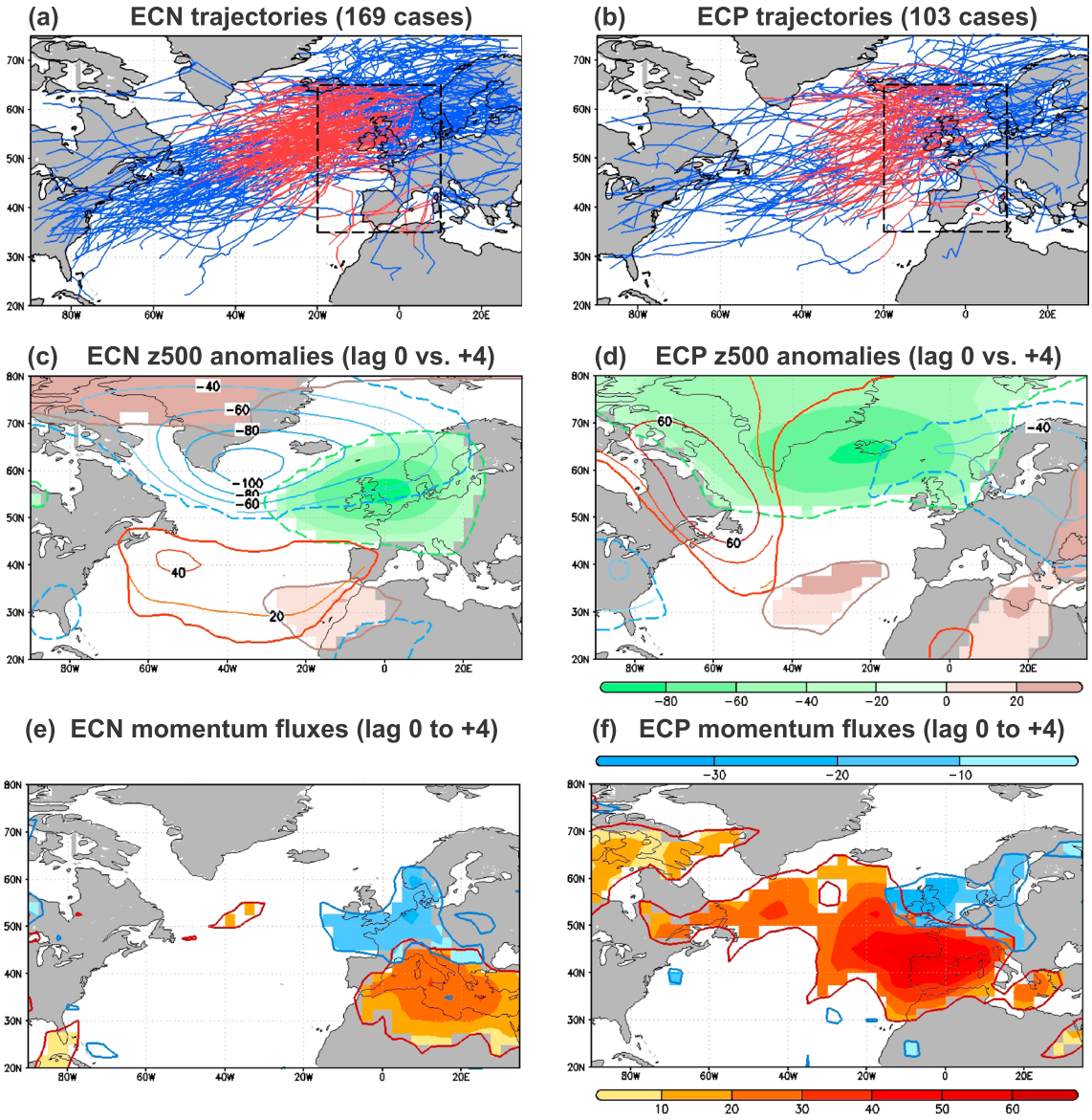

Figure 4. (a) Same as Figure 1a but for Explosive Cyclones followed by Negative NAO variations (ECN). (b) Same as Figure 1a but for Explosive Cyclones followed by Positive NAO variations (ECP). (c) Significant (99%—Monte Carlo test) positive/negative daily z500 anomalies (in gpm, 5 day running means removed) of ECN (red/blue contours—lag 0, grey/green shadings—lag +4). (d) Same as Figure 4c but for ECP. (e) Same as Figure 3e but for ECN. (f) Same as Figure 3e but for ECP.

from 21 October to 10 March are included in this figure. Results suggest that the predominant NAO conditions fostering EC (NoEC) are part of a growing and decaying positive (negative) NAO cycle of 8 to 12 days, peaking around lags −1 to 0 [*Feldstein*, 2003]. Of particular interest is the sharp growth of the DNI index toward positive values for EC95 from lags −6 to −1 (magenta solid line), followed by a decay after peak intensity.

Both the abrupt growth and decay of the DNI for EC95 are consistent with the downstream propagation (and thus higher/lower projection onto the canonical NAO pattern in Figure 1d) of the z500 anomalies. In addition, the growth of this pattern during negative lags might be forced by RWB processes [*Hanley and Caballero*, 2012; *Gómara et al.*, 2013—see their Figure 5] unrelated to the cyclonic development.

3.2. Influence of the Cyclones on the Background Field

In order to investigate the eddy feedback onto the NAO, we analyze the (unsmoothed) DNI variations following the maximum NDR period for the different cyclone samples. Figure 3c shows the relative frequency of DNI variations from lags 0 to +4 ($DNI_{lag+4} - DNI_{lag0}$) for all cyclones in each subset.

Comparison between EC (particularly EC95) and NoEC reveals qualitative differences in the observed distribution of DNI variations after cyclone's peak intensity. For NoEC, the distribution has a Gaussian structure and resembles climatology, except for a small shift to positive values. The latter is consistent with weak frictional damping of the NAO anomalies because this population is characterized by a negative NAO pattern. In contrast, the bimodal distribution of DNI variations for EC/EC95 cannot be explained by frictional effects alone: the idealized NAO+ curve (black solid line in Figure 3c), a composite of DNI variations constructed by combining climatological distributions for each NAO phase and the frequency of occurrence of that phase for EC95, is clearly unimodal. This suggests that other processes like eddy feedbacks [*Lorenz and Hartmann*, 2001] might also play a role in this case.

In order to understand the differences between EC and NoEC, we calculate the high-frequency eddy momentum fluxes (EMF) associated with both subsets (2).

$$EMF = u'v', \tag{2}$$

where u' and v' represent high-frequency (1–5 days) Lanczos filtered zonal and meridional winds at 250 hPa. Climatological values over the NA are shown in Figure 3d. Whereas positive momentum fluxes are more zonal and intense over sub-tropical latitudes, negative values tend to deflect poleward along the NA storm track.

Figures 3e and 3f show that while positive eddy momentum fluxes from lags 0 to +4 are enhanced for both EC and NoEC, they are significantly broader and stronger for the former. A more detailed analysis of the eddy momentum fluxes associated with EC95, EC, and NoEC at individual positive lags confirms the high sensitivity of the eddy forcing on cyclone's intensity (see Figure S2). This is consistent with previous case studies [*Rivière and Orlanski*, 2007] and may explain the positive peak in the distribution of DNI variations for EC/EC95 observed in Figure 3c. In contrast, the enhanced negative eddy momentum fluxes appear too far downstream to play a role for the negative DNI variations.

In order to elucidate the dynamics of the DNI variations for EC, two additional subsets are constructed representative of each of the modes in the distribution. For this purpose, explosive cyclones displaying DNI variations (lags 0 to +4) between −1.5/−0.25 and +0.25/+1.5 (thin vertical lines in Figure 3c) are selected. These are named, respectively, "Explosive Cyclones followed by Negative NAO variations" (ECN) and "Explosive Cyclones followed by Positive NAO variations" (ECP). In Figure 4 cyclone trajectories, z500 anomalies (at lags 0 and +4) and anomalous eddy momentum fluxes (integrated from lags 0 to +4) associated with ECN and ECP are provided. The first clear difference is that cyclone trajectories are tighter for the former, which may have dynamical implications as discussed below.

ECN z500 anomalies are characterized by a downstream propagating NAO+ structure (Figure 4c), similar to the composite pattern for EC95 (Figures 2a, 2d, and 2g). That pattern is also associated with a strong zonal jet, which may account for the explosive intensification. As lags progress, the whole pattern shifts southeastwardly (Figure 4c), and the projection onto the canonical NAO (Figure 1d) is reduced. Since the anomalous eddy momentum fluxes are weak and predominantly positive (Figure 4e), downstream propagation must be the dominant mechanism for the negative DNI variations in this subset.

On the other hand, the ECP z500 anomaly at lag 0 (Figure 4d) resembles the pattern found for NoEC (Figure 2f), which seems to deflect cyclones toward Europe. Since the jet stream is weaker in this case, the explosive intensification of ECP might be primarily influenced by low-level processes [e.g., moist adiabatic processes; *Fink et al.*, 2012; *Dacre and Gray*, 2013] instead of upper-level forcing. On positive lags, positive eddy momentum fluxes are strong and extensive (Figure 4f), which likely explains the positive DNI variations for this subset.

4. Concluding Remarks

In this study the two-way relationship between the North Atlantic Oscillation (NAO) and cyclones affecting Europe is systematically analyzed using reanalysis data. For this purpose, cyclones are classified into three different subsets depending on their intensity, and the NAO is divided into five different classes using a daily index (DNI). We have focused on contrasting explosive vs. non-explosive cyclones, an aspect not analyzed in previous studies.

Composite analysis shows that explosive (EC/EC95) and non-explosive cyclones (NoEC) tend to develop (lags −4 to 0) under different mean flow (and therefore NAO) conditions. On one hand, EC95 (5% most intense cyclones) evolve under a positive NAO-like pattern (Figures 2a, 2d, and 2g), associated with an intensified jet stream over Western Europe. This upper-level configuration is known to foster explosive growth of cyclones [*Uccellini*, 1990; *Hanley and Caballero*, 2012; *Gómara et al.*, 2013]. On the other hand, NoEC are linked to a tripole pattern (wave-like, arched in the NA) of z500 anomalies (Figures 2c, 2f, and 2i). Although this second pattern does not resemble the canonical NAO structure, it projects more onto NAO− due to a common center of action near Greenland (by construction of the index) and is similar to the Greenland Anticyclone pattern described by *Vautard* [1990]. Dynamically, it appears to deflect cyclone's trajectories toward Europe. The spatial extent and temporal evolution of the observed anomalies suggest that they reflect real large-scale circulation patterns and not just the cyclone's imprint (Figures 2 and S1).

After cyclone's peak intensity (lags 0 to +4), contrasting NAO behavior is observed for explosive and non-explosive cyclones. Not surprisingly, explosive cyclones tend to produce stronger DNI variations, both positive and negative, although for different reasons in each case. Negative DNI variations are due to the downstream (both eastward and equatorward) propagation of the z500/jet structure (NAO+ like) and are observed for a large number (169/424) of EC. This propagation results in a reduced projection onto the canonical NAO pattern as lags progress (compare Figures 1d and 4c). Positive DNI variations are due to enhanced positive eddy momentum fluxes, which appear to force a NAO+ on positive lags (compare z500 anomalies at lags 0 and +4 in Figure 4d). This is observed in a smaller subset (103/424) of EC and is typically associated with a weaker jet stream. The enhancement of eddy momentum fluxes with weak upper-level flow and its importance for NAO growth are consistent with previous studies [*Feldstein*, 2003; *Michel and Rivière*, 2011].

The findings from the lag composite analysis performed in this study may contribute to improve predictions (lags −4/−3) of cyclones impacting Europe and enhance the predictability on short-term NAO-like variability. Topics for future research include cyclone clustering during the reported NAO+ episodes and the impact of lower frequency variability (e.g., interannual, multidecadal etc.) over eastern North Atlantic cyclones.

Acknowledgments

We are indebted to the National Centers for Environmental Prediction (NCEP) and NOAA Climate prediction Center for the reanalysis and daily NAO index data. This work was supported by Spanish national funds: research projects MULCLIVAR (CGL2012-38923-C02-01) and DEVIAJE (CGL2009-06944). J. G. Pinto was partially supported by the German Federal Ministry of Education and Research (BMBF) under the project "Probabilistic Decadal Forecast for Central and western Europe" (MIKLIP-PRODEF, contract 01LP1120A). We thank Carlos Yagüe (UCM), Concepción Rodríguez-Puebla (USAL), Javier García-Serrano (LOCEAN/IPSL), and Jorge López-Parages (UCM) for fruitful discussions, and Sven Ulbrich (Univ. Cologne) for help with cyclone data. We also thank the two anonymous reviewers for their helpful comments and suggestions, which contributed to improve this manuscript.

The Editor thanks two anonymous reviewers for assistance in evaluating this manuscript.

References

Dacre, H. F., and S. L. Gray (2013), Quantifying the climatological relationship between extratropical cyclone intensity and atmospheric precursors, *Geophys. Res. Lett.*, *40*, 2322–2327, doi:10.1002/grl.50105.

Donat, M. G., G. C. Leckebusch, J. G. Pinto, and U. Ulbrich (2010), Examination of wind storms over Central Europe with respect to circulation weather types and NAO phases, *Int. J. Climatol.*, *30*, 1289–1300.

Feldstein, S. B. (2003), The dynamics of NAO teleconnection pattern growth and decay, *Q. J. R. Meteorol. Soc.*, *129*, 901–924.

Fink, A. H., T. Brücher, V. Ermert, A. Krüger, and J. G. Pinto (2009), The European storm Kyrill in January 2007: Synoptic evolution and considerations with respect to climate change, *Nat. Hazards Earth Syst. Sci.*, *9*, 405–423.

Fink, A. H., S. Pohle, J. G. Pinto, and P. Knippertz (2012), Diagnosing the influence of diabatic processes on the explosive deepening of extratropical cyclones, *Geophys. Res. Lett.*, *39*, L07803, doi:10.1029/2012GL051025.

Gómara, I., J. G. Pinto, T. Woollings, G. Masato, P. Zurita-Gotor, and B. Rodríguez-Fonseca (2013), Rossby wave-breaking analysis of explosive cyclones in the Euro-Atlantic sector, *Q. J. R. Meteorol. Soc.*, doi:10.1002/qj.2190.

Hanley, J., and R. Caballero (2012), The role of large-scale atmospheric flow and Rossby wave breaking in the evolution of extreme windstorms over Europe, *Geophys. Res. Lett.*, *39*, L21708, doi:10.1029/2012GL053408.

Hurrell, J. W., Y. Kushnir, G. Ottersen, and M. Visbeck (2003), An overview of the North Atlantic Oscillation, in *The North Atlantic Oscillation: Climate Significance and Environmental Impact*, *Geophys. Monogr. Ser.*, vol. 134, edited by J. W. Hurrell, pp. 279, AGU, Washington, D. C.

Kalnay, E., et al. (1996), The NCEP/NCAR 40-year reanalysis project, *Bull. Am. Meteorol. Soc.*, *77*, 437–471.

Lamb, H. H. (1991), *Historic Storms of the North Sea, British Isles, and Northwest Europe*, pp. 204, Cambridge Univ. Press, Cambridge, U. K., and New York.

Lorenz, D., and D. Hartmann (2001), Eddy-zonal flow feedback in the Southern Hemisphere, *J. Atmos. Sci.*, *58*, 3312–3327.

Michel, C., and G. Rivière (2011), The link between Rossby wave breakings and weather regime transitions, *J. Atmos. Sci.*, *68*, 1730–1748, doi:10.1175/2011JAS3635.1.

Michel, C., G. Rivière, L. Terray, and B. Joly (2012), The dynamical link between surface cyclones, upper-tropospheric Rossby wave breaking and the life cycle of the Scandinavian blocking, *Geophys. Res. Lett.*, *39*, L10806, doi:10.1029/2012GL051682.

Murray, R. J., and I. Simmonds (1991), A numerical scheme for tracking cyclone centers from digital data. Part I: Development and operation of the scheme, *Aust. Meteorol. Mag.*, *39*, 155–166.

Pinto, J. G., and C. C. Raible (2012), Past and recent changes in the North Atlantic oscillation, *WIREs Clim. Change*, *3*, 79–90, doi:10.1002/wcc.150.

Pinto, J. G., T. Spangehl, U. Ulbrich, and P. Speth (2005), Sensitivities of cyclone detection and tracking algorithm: Individual tracks and climatology, *Meteorol. Z.*, *14*, 823–838.

Pinto, J. G., S. Zacharias, A. H. Fink, G. C. Leckebusch, and U. Ulbrich (2009), Factors contributing to the development of extreme North Atlantic cyclones and their relationship with the NAO, *Clim. Dyn.*, *32*, 711–737.

Raible, C. C. (2007), On the relation between extremes of midlatitude cyclones and the atmospheric circulation using ERA40, *Geophys. Res. Lett.*, *34*, L07703, doi:10.1029/2006GL029084.

Rivière, G., and I. Orlanski (2007), Characteristics of the Atlantic storm-track eddy activity and its relation with the North Atlantic Oscillation, *J. Atmos. Sci.*, *64*, 241–266.

Sanders, F., and J. R. Gyakum (1980), Synoptic-dynamic climatology of the bomb, *Mon. Weather Rev.*, *108*, 1589–1606.

Uccellini, L. W. (1990), Processes contributing to the rapid development of extratropical cyclones, in *Extratropical Cyclones - The Erik Palmen Memorial Volume*, edited by C. Newton and E. O. Holopainen, pp. 81–105, Am. Meteorol. Soc, Boston, Mass.

Vautard, R. (1990), Multiple weather regimes over the North Atlantic: Analysis of precursors and successors, *Mon. Weather Rev.*, *118*, 2056–2081.

Wernli, H., S. Dirren, M. A. Liniger, and M. Zillig (2002), Dynamical aspects of the life-cycle of the winter storm "Lothar" (24–26 December 1999), *Q. J. R. Meteorol. Soc.*, *128*, 405–429.

Supplementary Material for

On the relation between Explosive cyclones affecting Europe and the North Atlantic Oscillation

Geophysical Research Letters

Introduction

The two figures provided supplement article Figures 2 and 3e-f, respectively.

Figure S1. Supplementary of Figure 2. Jet and z500 anomalies are provided on individual lagged days (-4 to +4) for the 3 cyclone subsets (NoEC, EC and EC95). The 5-day running mean smoothing is removed from the composite lags to show the higher frequency plots.

Figure S2. Supplementary of Figures 3e and 3f. Enhanced momentum fluxes are provided on individual lags (0 to +4) for the 3 cyclone subsets (NoEC, EC and EC95).

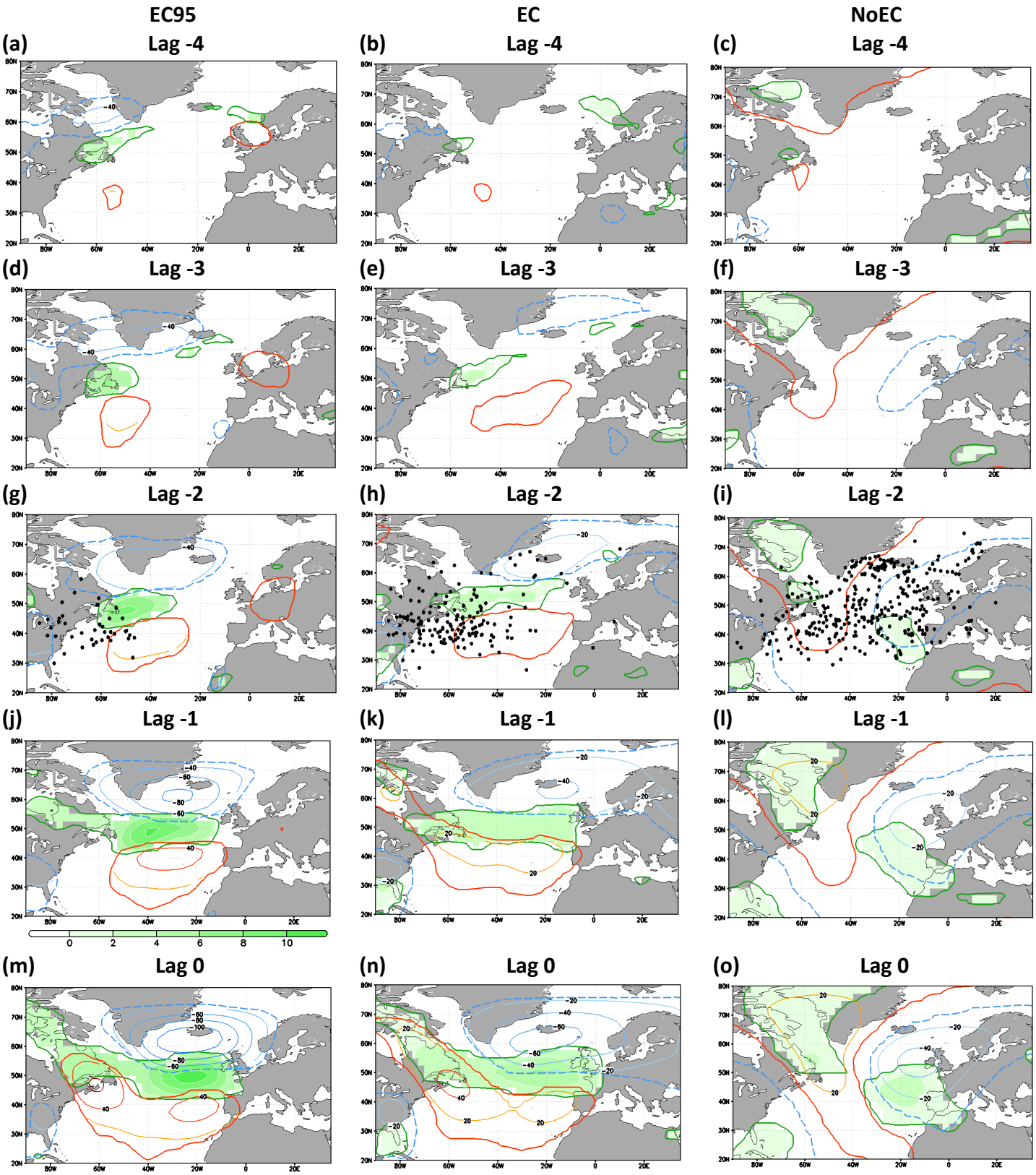
EC95
EC
NoEC
(a) Lag -4
(b) Lag -4
(c) Lag -4
(d) Lag -3
(e) Lag -3
(f) Lag -3
(g) Lag -2
(h) Lag -2
(i) Lag -2
(j) Lag -1
(k) Lag -1
(l) Lag -1
(m) Lag 0
(n) Lag 0
(o) Lag 0
0 2 4 6 8 10

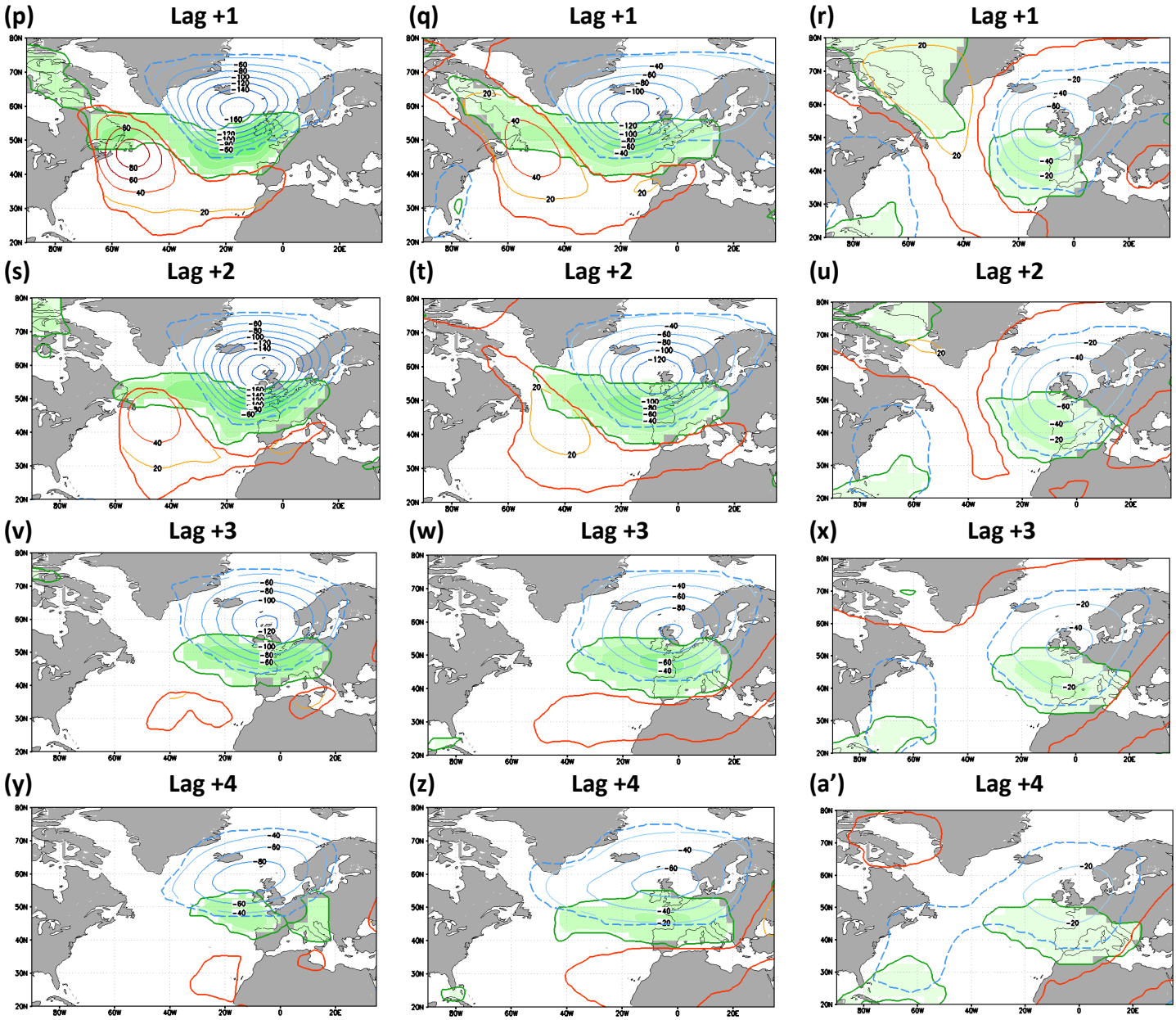

Figure S1: (a)-(a') Composites: Significant positive/negative daily z500 anomalies (in gpm, lags -3 to +4) of EC95 (red/blue contours, left-column), EC (central column) and NoEC (right-column). Significant positive jet intensity anomalies in green shadings (250 hPa, m s^{-1}). The cyclone positions at lag -2 are indicated with black dots. Confidence interval: 99% - Monte Carlo test. The 5-day running mean smoothing is removed from the daily anomalies of all variables.

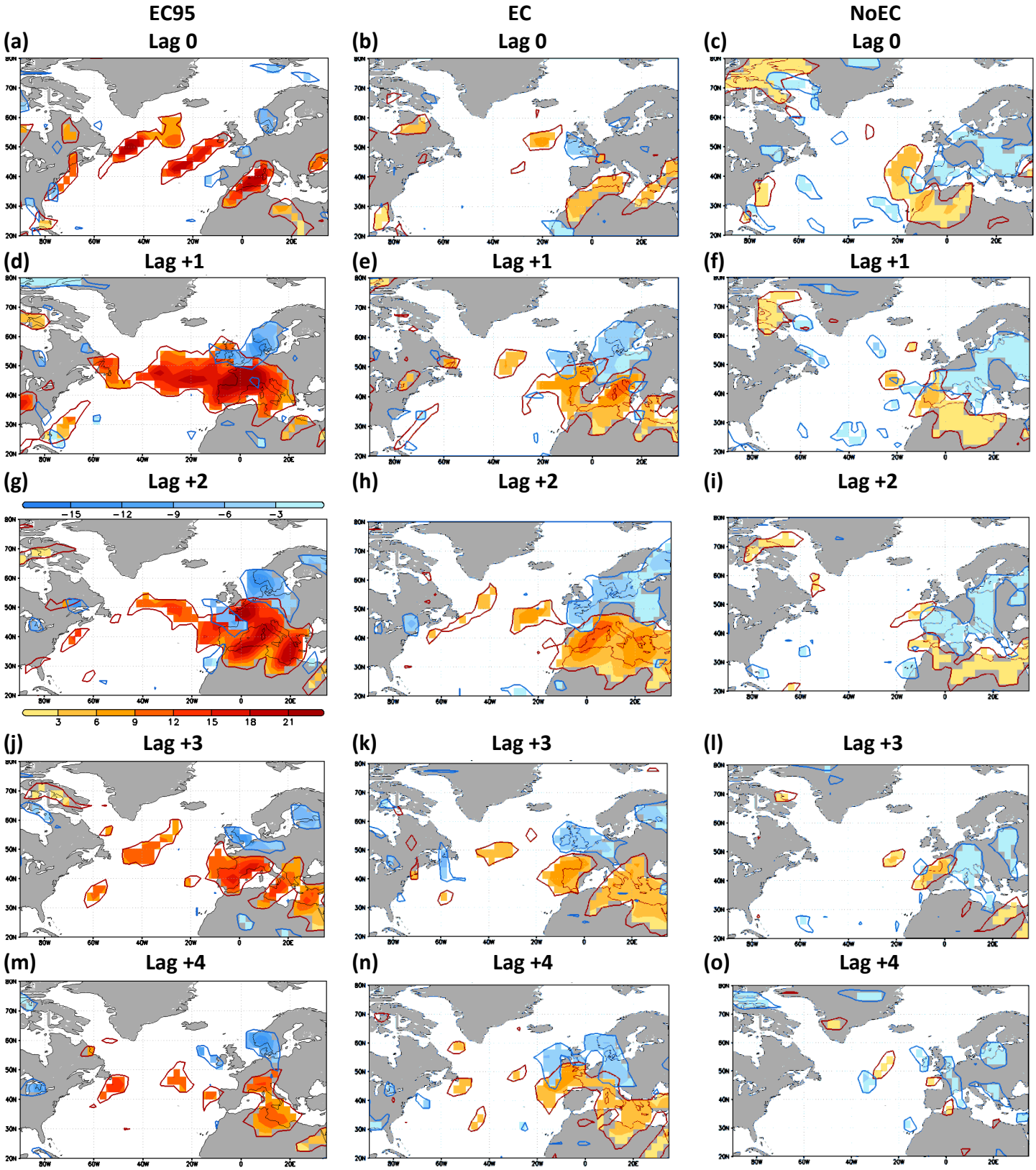

Figure S2: (a)-(o) Enhanced positive (red shadings) and negative (blue) momentum fluxes associated with EC95 (left), EC (central) and NoEC (right column) on lags 0 to +4 (daily basis, $m^2\ s^{-2}$). All anomalies are calculated subtracting climatological values from manuscript Figure 3d. Confidence interval: 95% - Monte Carlo test.

2. Rossby Wave-Breaking analysis of explosive cyclones in the Euro-Atlantic sector

Abstract: The two-way relationship between Rossby wave-breaking (RWB) and intensification of extratropical cyclones is analysed over the Euro-Atlantic sector. In particular, the timing, intensity and location of cyclone development are related to RWB occurrences. For this purpose, two indices based on potential temperature are used to detect and classify anticyclonic and cyclonic RWB episodes from ERA-40 reanalysis data. Results show that explosive cyclogenesis over the North Atlantic (NA) is fostered by enhanced occurrence of RWB on days prior to the cyclone's maximum intensification. Under such conditions, the eddy-driven jet stream is accelerated over the NA, thus enhancing conditions for cyclogenesis. For explosive cyclogenesis over the eastern NA, enhanced cyclonic RWB over eastern Greenland and anticyclonic RWB over the subtropical NA are observed. Typically only one of these is present in any given case, with the RWB over eastern Greenland being more frequent than its southern counterpart. This leads to an intensification of the jet over the eastern NA and enhanced probability of windstorms reaching Western Europe. Explosive cyclones evolving under simultaneous RWB on both sides of the jet feature a higher mean intensity and deepening rates than cyclones preceded by a single RWB event. Explosive developments over the western NA are typically linked to a single area of enhanced cyclonic RWB over western Greenland. Here, the eddy-driven jet is accelerated over the western NA. Enhanced occurrence of cyclonic RWB over southern Greenland and anticyclonic RWB over Europe is also observed after explosive cyclogenesis, potentially leading to the onset of Scandinavian blocking. However, only very intense developments have a considerable influence on the large-scale atmospheric flow. Non-explosive cyclones depict no sign of enhanced RWB over the whole NA area. We conclude that the links between RWB and cyclogenesis over the Euro-Atlantic sector are sensitive to the cyclone's maximum intensity, deepening rate and location.

***Gómara** I, Pinto JG, Woollings T, Masato G, Zurita-Gotor P, and Rodríguez-Fonseca B (2014a) Rossby wave-breaking analysis of explosive cyclones in the Euro-Atlantic sector, Q.J.R. Meteorol. Soc., 140, 738–753, doi: 10.1002/qj.2190*

 Q. J. R. Meteorol. Soc. 140: 738–753, April 2014 DOI:10.1002/qj.2190

RMetS
Royal Meteorological Society

Rossby wave-breaking analysis of explosive cyclones in the Euro-Atlantic sector

Iñigo Gómara,[a,b]* Joaquim G. Pinto,[c,d] Tim Woollings,[c] Giacomo Masato,[c] Pablo Zurita-Gotor[a,b] and Belén Rodríguez-Fonseca[a,b]

[a]*Departamento de Geofísica y Meteorología, Universidad Complutense de Madrid, Spain*
[b]*Instituto de Geociencias (IGEO), Universidad Complutense de Madrid, CSIC, Spain*
[c]*Department of Meteorology, University of Reading, United Kingdom*
[d]*Institute for Geophysics and Meteorology, University of Cologne, Germany*

*Correspondence to: I. Gómara, Departamento de Geofísica y Meteorología, Universidad Complutense de Madrid, Facultad de CC. Físicas, Ciudad Universitaria s/n. 28040 Madrid, Spain. E-mail: i.gomara@ucm.es

The two-way relationship between Rossby wave-breaking (RWB) and intensification of extratropical cyclones is analysed over the Euro-Atlantic sector. In particular, the timing, intensity and location of cyclone development are related to RWB occurrences. For this purpose, two indices based on potential temperature are used to detect and classify anticyclonic and cyclonic RWB episodes from ERA-40 reanalysis data. Results show that explosive cyclogenesis over the North Atlantic (NA) is fostered by enhanced occurrence of RWB on days prior to the cyclone's maximum intensification. Under such conditions, the eddy-driven jet stream is accelerated over the NA, thus enhancing conditions for cyclogenesis. For explosive cyclogenesis over the eastern NA, enhanced cyclonic RWB over eastern Greenland and anticyclonic RWB over the subtropical NA are observed. Typically only one of these is present in any given case, with the RWB over eastern Greenland being more frequent than its southern counterpart. This leads to an intensification of the jet over the eastern NA and enhanced probability of windstorms reaching western Europe. Explosive cyclones evolving under simultaneous RWB on both sides of the jet feature a higher mean intensity and deepening rates than cyclones preceded by a single RWB event. Explosive developments over the western NA are typically linked to a single area of enhanced cyclonic RWB over western Greenland. Here, the eddy-driven jet is accelerated over the western NA. Enhanced occurrence of cyclonic RWB over southern Greenland and anticyclonic RWB over Europe is also observed after explosive cyclogenesis, potentially leading to the onset of Scandinavian blocking. However, only very intense developments have a considerable influence on the large-scale atmospheric flow. Non-explosive cyclones depict no sign of enhanced RWB over the whole NA area. We conclude that the links between RWB and cyclogenesis over the Euro-Atlantic sector are sensitive to the cyclone's maximum intensity, deepening rate and location.

Key Words: extratropical cyclones; Rossby wave-breaking; explosive cyclogenesis; jet stream; dynamical precursors; Euro-Atlantic sector

Received 31 January 2013; Revised 27 April 2013; Accepted 10 May 2013; Published online in Wiley Online Library 31 July 2013

1. Introduction

Weather conditions in the mid-latitudes are strongly influenced by the passage of extratropical cyclones, especially during the winter season. Over the North Atlantic (NA) the main region of cyclogenesis is located near the east coast of North America, where the presence of strong meridional gradients of temperature and humidity favours the growth of baroclinic waves (Hoskins and Valdes, 1990; Nakamura *et al.*, 2004). During their evolution, extratropical cyclones typically move from southwest to northeast across the NA storm track region, where they intensify before reaching the European continent during their mature or occluding stages (Dacre and Gray, 2009; Pinto *et al.*, 2009). Such cyclones may lead to strong weather impacts, both in terms of strong wind gusts and heavy precipitation (e.g. Raible *et al.*, 2007; Fink *et al.*, 2009).

So-called 'explosive cyclones' are typically intense extratropical cyclones that undergo very rapid intensification (Sanders and Gyakum, 1980; Trigo, 2006; Allen *et al.*, 2010). In particular, they feature large deepening rates (pressure fall above 24 hPa in

24 h for 60°N or equivalent). The presence of a strong polar jet is one of several reported physical mechanisms contributing to rapid cyclone growth over the NA, other factors being strong upper level forcing, low atmospheric stability, strong lower level temperature and moisture gradients (e.g. Wang and Rogers, 2001; Pinto *et al.*, 2009; Fink *et al.*, 2012; Dacre and Gray, 2013). Examples of explosive cyclones affecting Europe include the well-known cases of Lothar and Martin in 1999, Kyrill in 2007, Klaus in 2009 and Xynthia in 2010, all of which led to very strong socio-economic impacts, and in some cases were considerable challenges to forecasting (Wernli *et al.*, 2002; Fink *et al.*, 2009, 2012; Rivière *et al.*, 2010, 2012; Liberato *et al.*, 2011). Hence, a better understanding of the factors contributing to the intensification of such cyclones, which may considerably depend on the area of development (e.g. Dacre and Gray, 2013), may help to improve predictions of these events and to quantify their potential impacts under current and future climate conditions (e.g. Schwierz *et al.*, 2010; Champion *et al.*, 2011; Pinto *et al.*, 2012).

Additional to the ongoing efforts in the refinement of numerical modelling of explosive cyclogenesis (Kuwano-Yoshida and Asuma, 2008; Roebber and Schumann, 2011), the analysis of case studies and their associated large-scale circulation conditions may help in understanding the involved physical mechanisms. The North Atlantic Oscillation (NAO) is the dominant variability pattern in the North Atlantic and is characterised by the redistribution of subpolar and subtropical air masses (Walker, 1924; Wanner *et al.*, 2001; Hurrell *et al.*, 2003; Pinto and Raible, 2012). Many previous studies have shown the influence of this oscillation on the storm track activity (van Loon and Rogers, 1978; Wallace and Gutzler, 1981; Barnston and Livezey, 1987; Chang, 2009). A positive NAO phase is related with wetter (drier) and warmer (colder) weather in northern (southern) Europe due to a poleward shift of cyclone trajectories (e.g. Hurrell *et al.*, 2003). These characteristics are reversed under a negative NAO phase. A strong positive NAO phase enhances the frequency of extreme cyclones over the NA (Raible, 2007; Pinto *et al.*, 2009). However, European windstorms typically occur during a moderately positive NAO phase (Donat *et al.*, 2010). Further work has suggested that cyclones themselves play an important role in steering the NAO phase through Rossby wave-breaking (RWB) processes (Feldstein, 2003; Franzke *et al.*, 2004; Benedict *et al.*, 2004; Strong and Magnusdottir, 2008a, 2008b), defined as the irreversible overturning of potential temperature contours on the tropopause (McIntyre and Palmer, 1983). This second relationship appears to be particularly important for extreme cyclones, which apparently have a strong effect on the NAO short-term variability (e.g. Blessing *et al.*, 2005). This is supported by several case studies reported in the literature (Shutts, 1983; Colucci, 1985; Nakamura and Wallace, 1993; Rivière and Orlanski, 2007; Roebber, 2009). Therefore, the dynamics of the bidirectional relationship between extratropical cyclones (including extremes) and the NAO is well documented in the literature.

Less attention has been given to the role of RWB in mediating this relationship between extratropical cyclones and the large-scale circulation. For weather and climate extremes, several studies have already shown the presence of a common RWB pattern in the NA during the onset and decaying stages of blocking events (Pelly and Hoskins, 2003; Woollings *et al.*, 2008; Woollings *et al.*, 2011; Masato *et al.*, 2012).

Hanley and Caballero (2012; hereafter HC12) have recently shown the existence of a simultaneous cyclonic–anticyclonic RWB pattern that seems to foster explosive development. Based on a sample of the top 22 most destructive windstorms affecting western Europe, they suggest that simultaneous north cyclonic and south anticyclonic RWB sharpens the jet stream, leading to more intense and zonally oriented upper-level winds in the eastern NA. The existence of such upper-level conditions might act as a dynamical precursor of explosive amplification of pre-existing storms (Uccellini, 1990; Rivière and Joly, 2006a, 2006b). On the other hand, the presence of enhanced RWB (after and downstream of the cyclone) appears to strongly influence the NA circulation conditions at synoptic time-scales (Rivière and Orlanski, 2007; Michel and Rivière, 2011; Michel *et al.*, 2012). However, the relationship between extratropical cyclones, RWB and anomalous mean flow has not been investigated through a lead-lag analysis using a comprehensive cyclone dataset.

In order to provide a deeper and more general description of the bidirectional relationship between cyclones and RWB in the NA, this study aims to address the following (and still unresolved) questions:

(1) Is there a common pattern of RWB prior to (after) and upstream (downstream) of explosive cyclogenesis over the NA?
(2) Is RWB dependent on the cyclone's intensity (and vice-versa)?
(3) Is RWB sensitive to the cyclone's trajectory and location of its maximum intensity (and vice-versa)?

The structure of the article is as follows. The main features of RWB and extratropical cyclone classification are described in Section 2. Section 3 describes the results, and a short discussion concludes the article.

2. Data and methodology

The 40-year European Centre for Medium-Range Weather Forecasts (ECMWF) reanalysis data (ERA-40; Uppala *et al.*, 2005) are used. The data investigated span over 44 extended winter seasons (from October 1957 to March 2001). The Gaussian horizontal resolution of the data is 1.125° for 60 vertical sigma-levels, with six-hourly data.

The two-dimensional RWB index (Masato *et al.*, 2013) used in this study is based on the potential temperature (θ) field on the dynamical tropopause (2 potential vorticity units (PVU) $= 2 \times 10^{-6}$ K m^{2}Kg^{-1}s^{-1} surface). The temporal resolution of the index is daily (six-hourly data of θ have been averaged into daily means) and the horizontal resolution is 4.5° in longitude and 1.125° in latitude. This index provides information of local-instantaneous RWB occurrence (B index) and direction of breaking (DB index). The B index (Eq. (2)) searches for regions where the mean meridional gradient of θ is reversed by calculating the difference of averaged θ to north and south ($\Delta\phi = 29.25$ deg.lat.) of each longitudinal grid point i:

$$\overline{\theta_i^n} = \frac{2}{\Delta\phi}\int_{\phi_o}^{\phi_o+\frac{\Delta\phi}{2}} \theta_i d\phi, \quad \overline{\theta_i^s} = \frac{2}{\Delta\phi}\int_{\phi_o-\frac{\Delta\phi}{2}}^{\phi_o} \theta_i d\phi, \qquad (1)$$

$$B_i = \overline{\theta_i^n} - \overline{\theta_i^s}, \qquad (2)$$

where ϕ is latitude. Hence, when B is positive at a grid point, local-instantaneous RWB is detected at that location. Note that no duration condition is imposed, because the focus here is on wave-breaking in general rather than persistent blocking events. The DB index (Eq. (3)) calculates the difference of $\bar{\theta}$ along longitude (at constant latitude) between points $i-1$ and $i+1$.

$$DB = \overline{\theta_{i-1}} - \overline{\theta_{i+1}}, \qquad (3)$$

where

$$\overline{\theta_i} = \frac{\overline{\theta_i^n} + \overline{\theta_i^s}}{2}. \qquad (4)$$

The DB index has been normalised by its standard deviation (counting only cases with $B > 0$). In this study, positive (negative) values of DB above (below) a threshold of +0.2 (−0.2) are identified as anticyclonic (cyclonic) RWB events. Otherwise

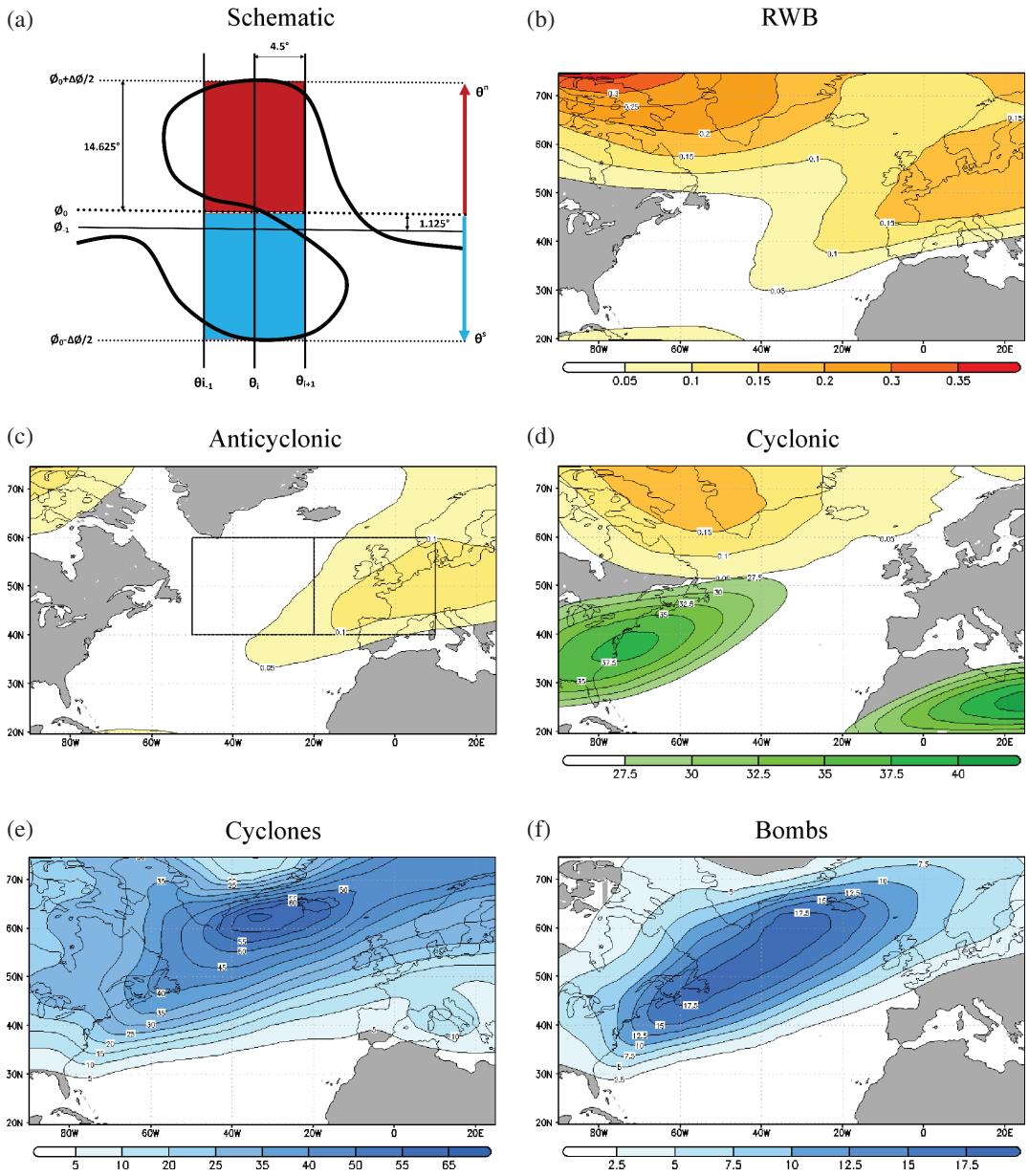

Figure 1. (a) Schematic of B and DB indices based on the θ field on the 2 PVU surface (example of cyclonic Rossby wave-breaking (RWB)). (b) Relative daily frequency (over 1) of local-instantaneous RWB ($B > 0$) in filled contours. (c) Relative daily frequency (over 1) of anticyclonic RWB ($B > 0$; $DB > 0.2$) in filled contours. Boxes considered for western (40–60°N, 50–20°W) and eastern (40–60°N, 20°W–10E) North Atlantic (NA) cyclone classification in thick contours. (d) Relative daily frequency (over 1) of cyclonic RWB ($B > 0$; $DB < -0.2$) in light-yellow to dark-red-filled contours. Mean wind intensity at 250 hPa in light to dark-green-filled contours (m s^{-1}). (e) Cyclone track density (full trajectory of cyclones meeting criteria 1 to 4 in Section 2 over a 7.5° radius for each grid point) for developing systems in cyclone days per extended winter per deg.lat.^{2} (filled contours). (f) Same as (e) but for bombs. Time period: October–March 1957–2001 ERA-40. Note for all figures: colour bars are applicable to all subfigures whenever an explicit one is not provided at the top/bottom.

events are defined as 'unclassified'. Despite the arbitrariness of this threshold, it should be noted that the final frequency distributions change little when varying this value by a few tenths. In Figure 1(a) a schematic of the B and DB indices is provided. The climatology of local-instantaneous RWB ($B > 0$) follows in Figure 1(b). Anticyclonic ($B > 0$; $DB > 0.2$) and cyclonic ($B > 0$; $DB < -0.2$) RWB climatologies are shown, respectively, in Figures 1(c) and 1(d) (filled contours). For further details on the RWB index see Masato *et al.* (2013). Note that this index imposes a quite strict criterion on the scale of the wave-breaking by integrating over two boxes of 14.625 deg.lat., so that an overturning which is too small to reverse the gradient on this scale will not be counted.

Complete life cycles of cyclones from ERA-40 reanalysis are described using an automatic tracking method. Based on an algorithm originally developed by Murray and Simmonds (1991), the tracking scheme has been adapted and evaluated for Northern Hemisphere cyclone properties (Pinto *et al.*, 2005, 2007). Cyclone identification considers the Laplacian of the mean sea level pressure (MSLP) as a proxy for their relative geostrophic vorticity (cf. Murray and Simmonds, 1991). Subsequently, taking into consideration the most likely trajectory of a cyclone under the given large-scale circulation conditions, previous path and speed, a tracking algorithm is applied. This method provides basic properties (e.g. core pressure, intensity and propagating velocity) at each stage of the systems' life cycle. Further details on this technique can be found in Murray and Simmonds (1991), Simmonds *et al.* (1999) and Pinto *et al.* (2005). The methodology provides comparable results with other tracking methods (cf. Neu *et al.*, 2013).

Following Pinto *et al.* (2009), the criteria for developing cyclones are:

(1) The lifetime of cyclones must be at least 24 h (five time steps).
(2) The cyclone's minimum pressure must be lower than 1000 hPa at least once during its lifetime.
(3) The cyclone's maximum Laplacian of MSLP ($\nabla^2 p$) must be greater than 0.6 hPa deg.lat.$^{-2}$.

099

Table 1. Cyclone populations. Characteristics of the seven subpopulations of cyclones used in this study. The Top100 and Top50 are the most intense cyclones (in terms of maximum $\nabla^2 p$) selected over each NA sector. The 50 random explosive cyclones (RE50) are selected from the identified non-top 50 explosive cyclones in the western (573 cases) and eastern (196 cases) NA. The 50 random non-explosive cyclones (RNE50) are selected from the identified non-explosive events (992 cases for western NA and 793 cases for eastern NA). The mean maximum $\nabla^2 p$ and *NDR* of cyclones in the Top50 subpopulations lie above the 95th percentile when considering separately all identified cyclones in the eastern and western NA (extremes, Figures S2 and S3 of online Supporting information). For the Top100 this condition is also fulfilled over the whole NA.

			Subpopulation	
			Western NA (40–60°N, 50–20°W)	Eastern NA (40–60°N, 20°W–10°E)
Explosive cyclones	*NDR* ≥ 1 Bergeron	Top 100($\nabla^2 p$)	Top100 (30–75°N, 80°W–40°E)	
		Top 50($\nabla^2 p$)	Top50W	Top50E
		Non-top 50($\nabla^2 p$)	RE50W	RE50E
Non-explosive cyclones	0 < *NDR* < 1 Bergeron		RNE50W	RNE50E

(4) The cyclone's deepening rate must be equal or greater than 0.3 hPa deg.lat.$^{-2}$day^{-1} within a time period of 24 h (in terms of d/d$t(\nabla^2 p)$).

The resulting climatology of developing cyclones is shown in Figure 1(e). Next, we define the normalised deepening rate (NDR, in Bergeron units) of a cyclone (5).

$$NDR = \frac{\Delta p}{24} \times \frac{\sin 60^\circ}{\sin \phi}, \quad (5)$$

where Δp is the pressure fall in hPa and ϕ is the average latitude of the cyclone's surface centre within a time period of 24 h. The sine term is a normalisation factor to account for the variation of geostrophic wind with latitude. Cyclones that verify *NDR* ≥ 1 Bergeron are considered as explosive (Sanders and Gyakum, 1980). The climatology of these bombs is shown in Figure 1(f). To study the sensitivity of our results to the location and intensity of cyclones, several subpopulations of cyclones are defined based on the cyclone's intensity (maximum of $\nabla^2 p$). First, the top 100 most intense cyclones over the whole NA are selected. Second, six different subpopulations of 50 cyclones have been selected based on the value and location of their maximum Laplacian of pressure ($\nabla^2 p$) and *NDR*. Further information on the characteristics of each subpopulation and the applied constraints is provided in Table 1 and Figures 1(c) and S1–S3 of the online Supporting information.

Additional to the RWB index and θ field on the 2 PVU surface, u and v winds at the 250 hPa pressure level have also been used in this study. The climatological jet stream considered for the time window of this study (October 1957 to March 2001) is provided in Figure 1(d) in green-filled contours. While the data of the RWB are daily means, θ, $u250$ and $v250$ have been considered at 0000 UTC of each day. To homogenise the timing of each cyclone's evolution, lag 0 has been defined as the day in which the 24 h of maximum intensification (maximum *NDR*) start (e.g. if the explosive development takes place between 21 January 1200 UTC and 22 January 1200 UTC, then 21 January is chosen as lag 0). Hence, lagged days −1 and +1 correspond to days prior to and following the start of the maximum intensification period of each cyclone. The consideration of different lags allows us to analyse the timing between the occurrence of RWB and the development of the cyclone.

3. Results

3.1. Top ranking explosive cyclones over the North Atlantic

In order to provide a general idea of the relationship between RWB occurrence and explosive cyclogenesis over the NA, the top 100 cyclones over the whole NA (30–75°N, 80°W–40°E) are analysed first. Composite values of enhanced and decreased RWB occurrence, together with the jet intensity and its positive anomalies compared with climatology are shown from lagged days −3 to +2 in Figure 2. Prior to the explosive development, three areas of anomalies arise over the NA: (i) enhanced RWB occurrence over western Greenland, which reaches its maximum intensity on lag 0 (light yellow to dark red shadings, Figure 2(d)); (ii) an accelerated jet, which zonally spans over the western NA and peaks also on lag 0 (light to dark green shadings); and (iii) some areas of decreased RWB activity overlapping the positive jet anomalies (thick, blue contours). The spatial coherence between the negative anomalies of RWB and the jet location is not surprising, given that a strong westerly flow tends to inhibit RWB activity, as shown in the climatology of RWB occurrence (Figure 1(b)). Additionally, the timing of explosive development is consistent with the favourable upper-level conditions observed on lagged days −1/0 over the western NA (Figure 2(g) and (h)). An accelerated polar jet is also associated with increased baroclinicity in the jet area (e.g. Pinto *et al.*, 2009; their figure 2). The cyclone trajectories occurring during this period are shown in Figure 2(g) and (h), with the lag −1/0 segments shown in red. The position of the tracks, particularly over the right-entrance and left-exit regions of the jet, are known to enhance cyclone development due to upward motion of air in these areas (Uccellini, 1990; Rivière and Joly, 2006a, 2006b).

Thus, we conclude that the presence of enhanced RWB over Greenland appears to be associated with an accelerated jet over the western NA. As a possible mechanism we hypothesise that the breaking events occurring over Greenland narrow and intensify the jet over the western NA, leading to more favourable conditions for explosive cyclone growth over that area. This is in line with the mechanism proposed by HC12 for windstorms affecting Europe. After the maximum intensification date, the area of enhanced RWB then extends over southern Greenland at lag +2 (Figure 2(f)). The presence of enhanced RWB at lag +2 over continental Europe is also evident and is thought to be related to the onset of Scandinavian blocking, as reported by Michel *et al.* (2012). A more detailed analysis of this will be provided later in this article. Regarding the jet anomalies, on positive lagged days the intensified upper-level winds extend from the western NA towards Iceland (Figure 2(e) and (f)). Such extension of the jet anomalies is consistent with the occurrence of RWB and with the displacement of the cyclones observed in Figure 2(h) (blue trajectories) and their associated strong winds at 250 hPa.

Nevertheless, further analysis is needed to elucidate whether the relationship between RWB and extratropical cyclones is sensitive to the cyclone's deepening rate, maximum intensity and location in the NA. In order to answer these questions, we focus in the next sections on six subpopulations of 50 cyclones of different intensities for the western (40–60°N, 50–20°W) and eastern (40–60°N, 20°W–10°E) NA.

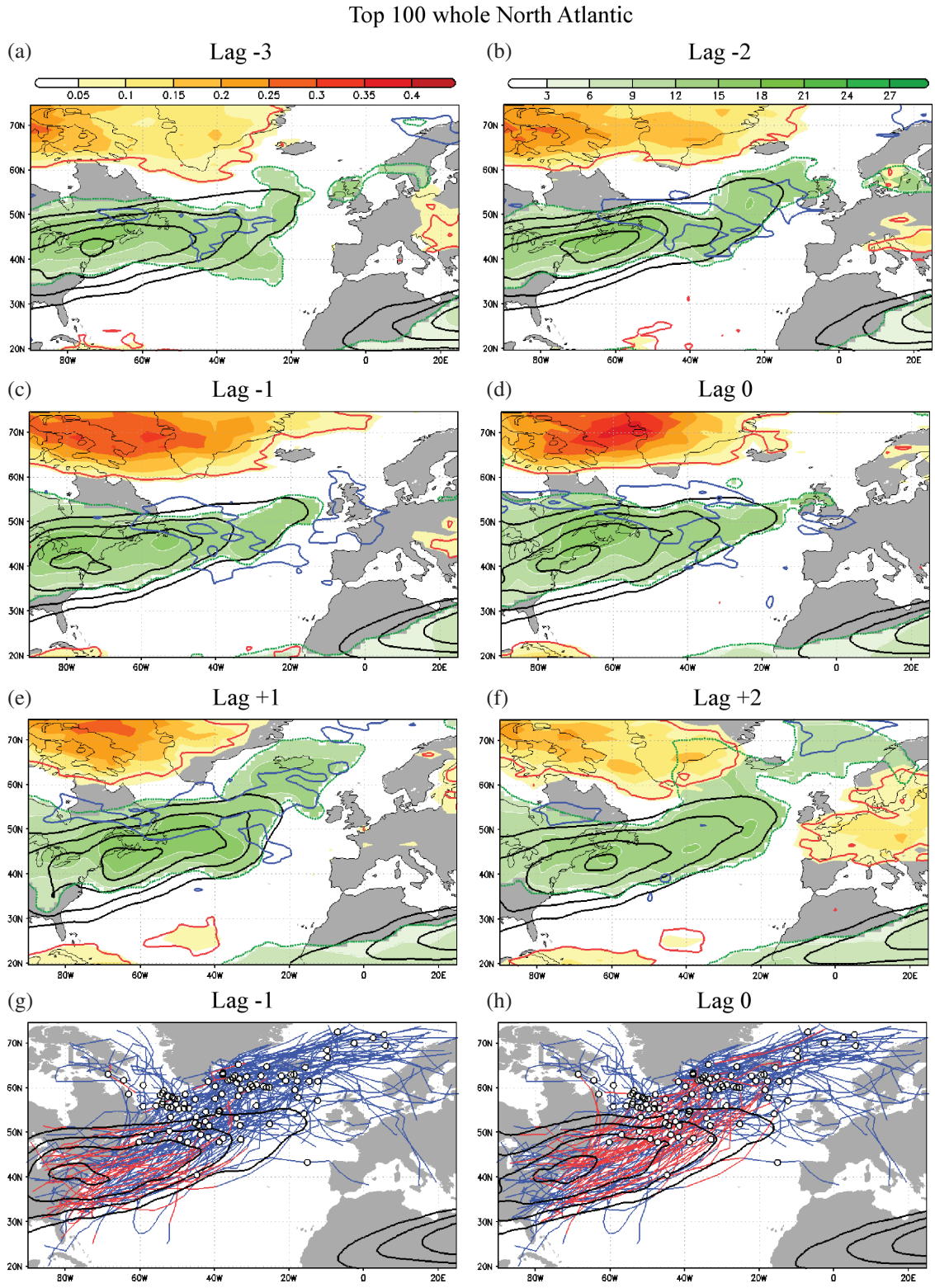

Figure 2. Top 100 cyclones. ((a)–(f)) Shadings: composite anomalies of enhanced RWB occurrence ($B > 0$) on lagged days of explosive development for the Top100 cyclones (light yellow to dark red); composite anomalies (positive) of the jet stream's intensity (light to dark green, m s^{-1}). Contours: positive anomalies (Monte Carlo 95% confidence level) of RWB occurrence (red) and jet stream's intensity (green); composite anomalies of decreased RWB occurrence (Monte Carlo 95% confidence level) in blue contours; composite jet stream's intensity in thick black contours (starting from 35 m s^{-1}, interval 5 m s^{-1}). ((g) and (h)) Composite jet stream's intensity (black contours, m s^{-1}), cyclone trajectories (full trajectory in blue, current lagged day in red) and position of cyclone's maximum Laplacian of pressure (white open circles).

3.2. *Cyclones over the western North Atlantic*

The top 50 western (Top50W) cyclones (Figure 3) depict very similar features compared to the Top100 (Figure 2) because most of the events are coincident in both subpopulations (34 of Top50W are included in the Top100). This is not simply fortuitous, because in climatological terms bombs are more frequent (Figure 1(f)) and more intense over the western NA. For clarity, the areas with decreased RWB occurrence are no longer displayed in Figures 3 to 7, because they typically overlap the positive anomalies of the jet intensity. Enhanced RWB activity over western Greenland is present again at lags −3 to 0 (Figure 3(a)–(d)), accompanied by an accelerated jet over the western NA. Figure 3(g) and (h) shows that the Top50W cyclones also develop under very favourable upper-level conditions, i.e. with cyclones crossing the core of a very strong jet from the right-entrance to the left-exit regions. After lag 0, the spot of enhanced RWB over western Greenland is then extended to

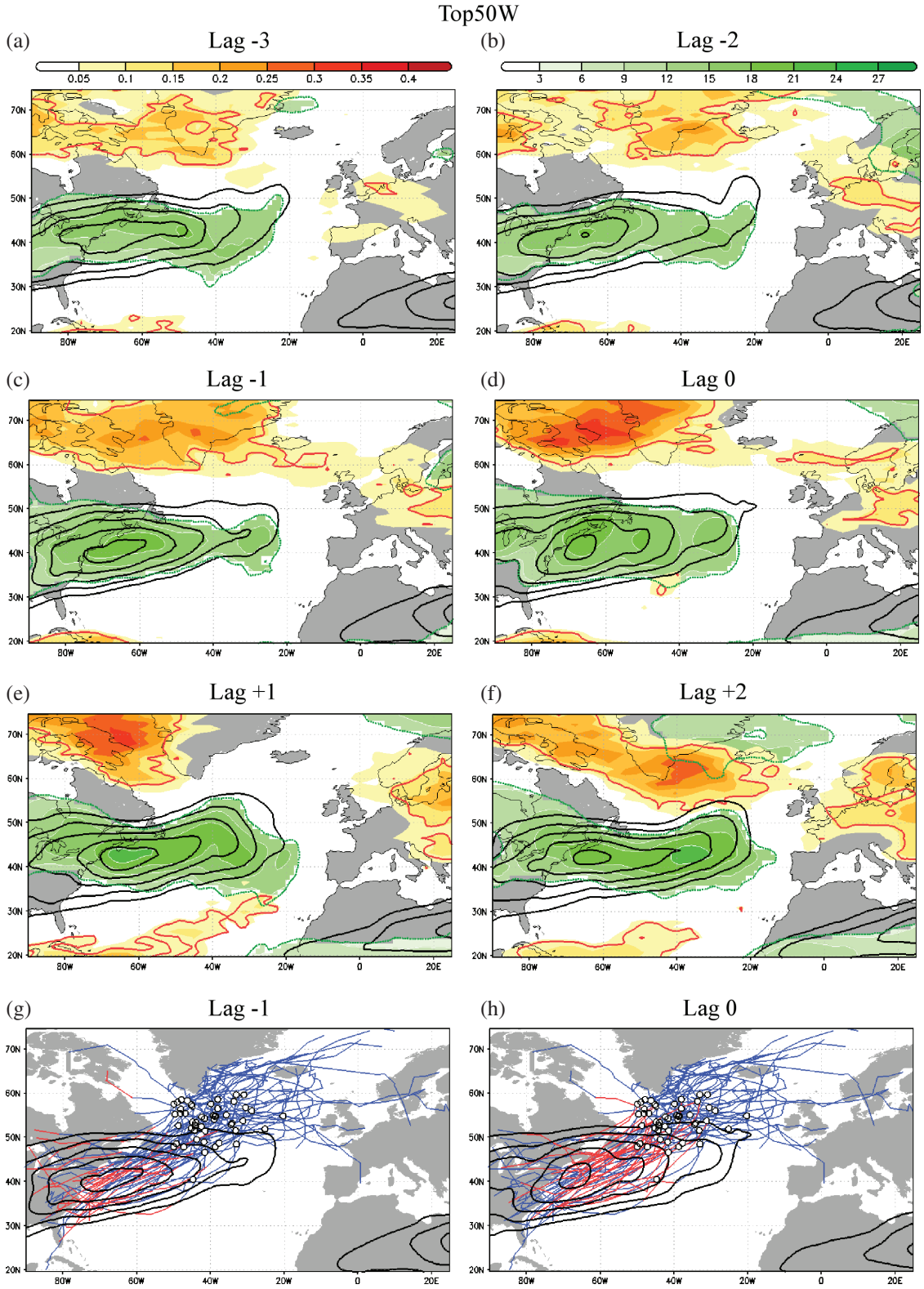

Figure 3. As Figure 2, but for the top 50 western (Top50W) cyclones. Negative anomalies of the jet stream's intensity are removed.

the southeast, as for the Top100, reaching its maximum value at lag +2 (Figure 3(f)). It is worth noting that as this Greenland RWB moves south it becomes more important, in that the circulation anomalies associated with it become larger (Woollings *et al.*, 2008). A second area of enhanced RWB over Europe is also observed at the same lagged day (lag +2). In this case, the pattern related to the onset of the Scandinavian blocking appears to be even clearer than for the Top100 cyclones (note that in the *B* index definition the anticyclone lies to the north of the location where breaking is identified). This is attributed to the location of the maximum intensity of cyclones, being for the Top50W more limited over southern Greenland (as imposed in the selection criteria) than for the Top100 (which are more spread over the whole NA). This agrees with Orlanski (2003), who suggested that the most intense cyclones are particularly able to dramatically change the large-scale circulation conditions.

Additional subpopulations of 50 randomly selected explosive cyclones (RE50W; excluding the Top50W) and non-explosive cyclones (RNE50W) in the western NA are analysed for comparison. Figure 4 presents the results for even time lags. At lag −2, the RE50W cyclones are associated both with increased RWB near southwest Greenland and an accelerated jet that extends along a large area of the western NA (Figure 4(a)). The shape and timing of this pattern (Figure 4(a), (c) and (e)) is

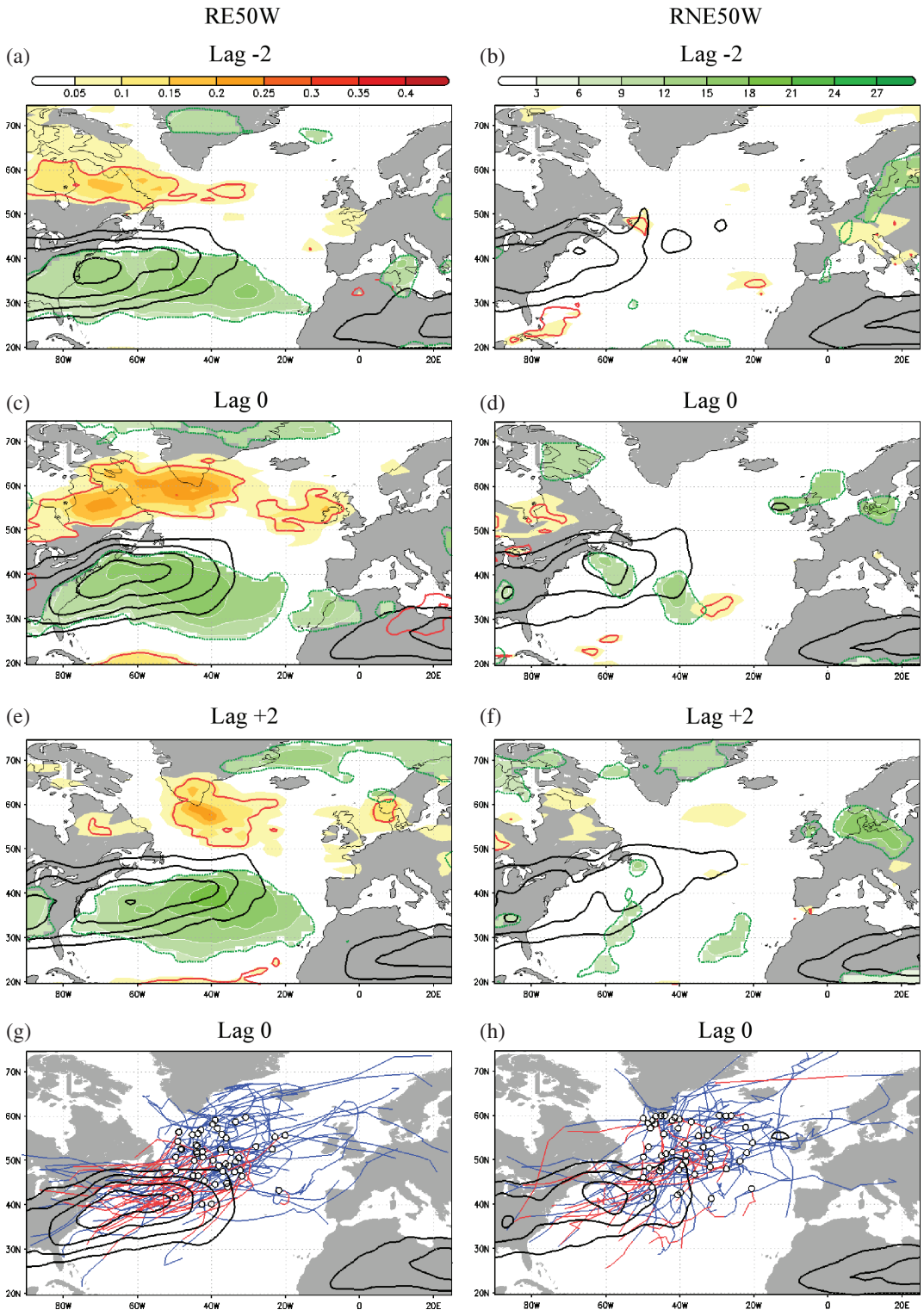

Figure 4. As Figure 3, but for RE50W and RNE50W cyclones on even lagged days.

indeed quite similar to that detected for the Top50W. However, the magnitude of the signal is weaker, the area is smaller and it is apparently shifted southwest. The positive anomalies of the jet intensity are also consistent with this shift and span the western NA at southern latitudes. Nevertheless, the mechanism proposed for explosive cyclogenesis over the western NA still holds. At lag +2 (Figure 4(e)), the area of increased RWB activity northward of the intensified jet is shifted to the east and RWB occurrence over continental Europe is not increased compared with climatology. On the other hand, the analysis for the RNE50W cyclones shows quite different results. There is not a significant signal in RWB activity or jet intensity over the western NA at any lags (Figure 4(b), (d) and (f)). The trajectories of these cyclones (Figure 4(h)) are quite random compared with the more coherent tracks of explosive cyclones (Figure 4(g)) and the jet stream is also considerably weaker.

In conclusion, two composite RWB patterns have been found associated with explosive cyclogenesis in the western NA. First, an area of increased RWB occurrence over western Greenland that squeezes and intensifies the jet over western NA has been found on negative lagged days. This mechanism leads to very favourable upper-level conditions for explosive development of cyclones (Top50W and RE50W) at lag 0. In this case the subsequent cyclone's intensity and location is sensitive to the observed RWB pattern. Second, a composite pattern of enhanced RWB over southern Greenland and Europe has been found at lag +2. However, this pattern is apparent only for the most intense cyclones and gradually vanishes when the cyclone's mean

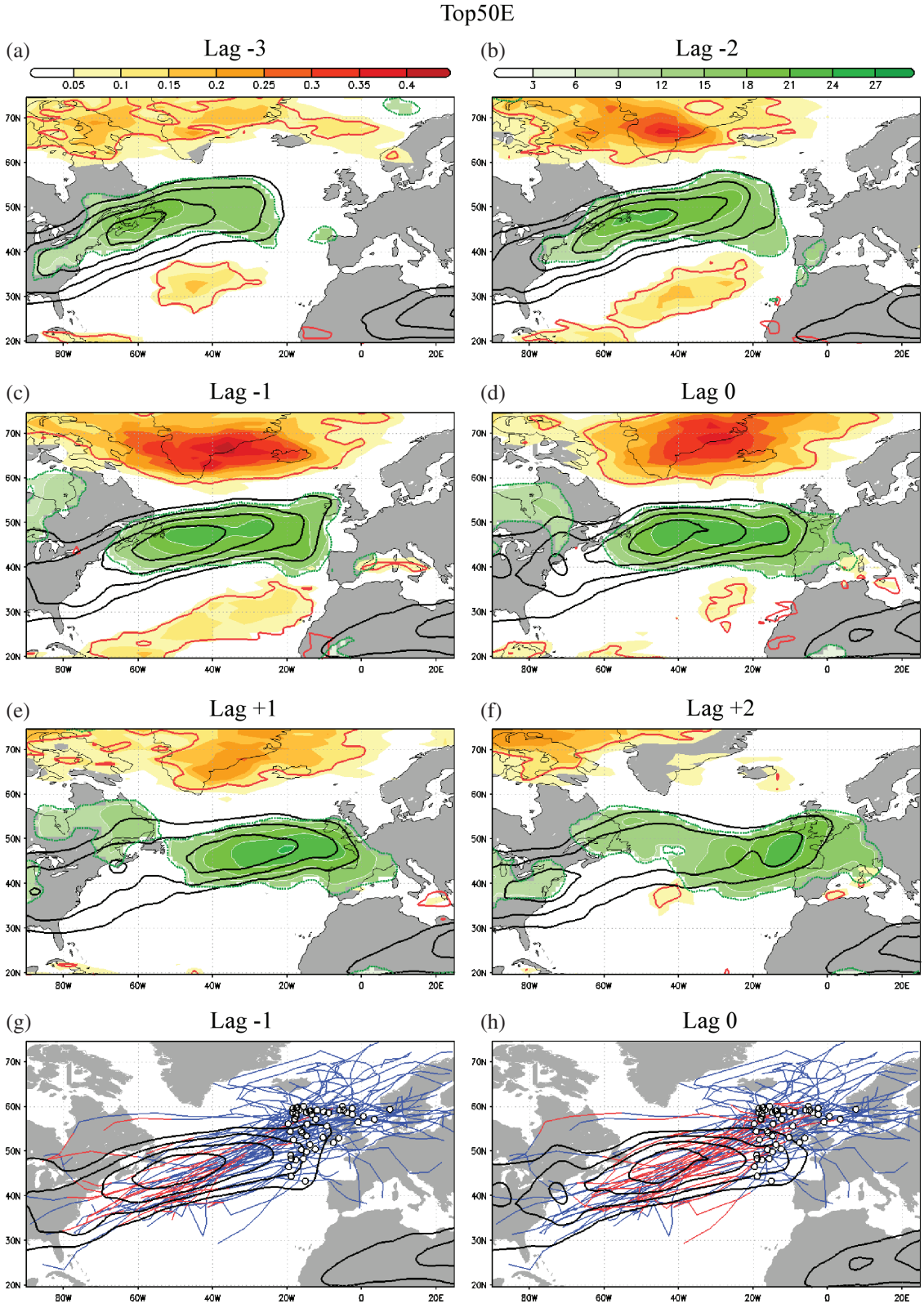

Figure 5. As Figure 3, but for the top 50 eastern (Top50E) cyclones.

intensity is reduced. Here it is the RWB pattern that is sensitive to the cyclone's characteristics.

3.3. *Cyclones over the eastern North Atlantic*

Figures 5 and 6 provide a similar analysis for cyclones developing in the eastern NA. On days prior to the explosive intensification date of the top 50 eastern (Top50E) cyclones, two areas of enhanced RWB occurrence arise over the NA (Figure 5(a)–(c)): (i) a strong positive anomaly of RWB activity over eastern Greenland which peaks at lag −1; and (ii) a region of enhanced breaking spanning the subtropical NA at lags −3 to −1. The composite anomalies of the jet intensity show an extension of the upper-level winds towards Europe and a shift of its core. Thus, for the Top50E cyclones, two areas of enhanced RWB appear to sharpen, accelerate and extend the jet stream towards the eastern NA prior to explosive development. Such large-scale conditions may foster the occurrence of windstorms over Europe (Figure 5(g) and (h)). At positive lagged days (Figure 5(e) and (f)) the RWB anomalies start to decay and the jet is extended over western Europe. Hence, these cyclones do not appear to considerably alter the large-scale conditions over the NA.

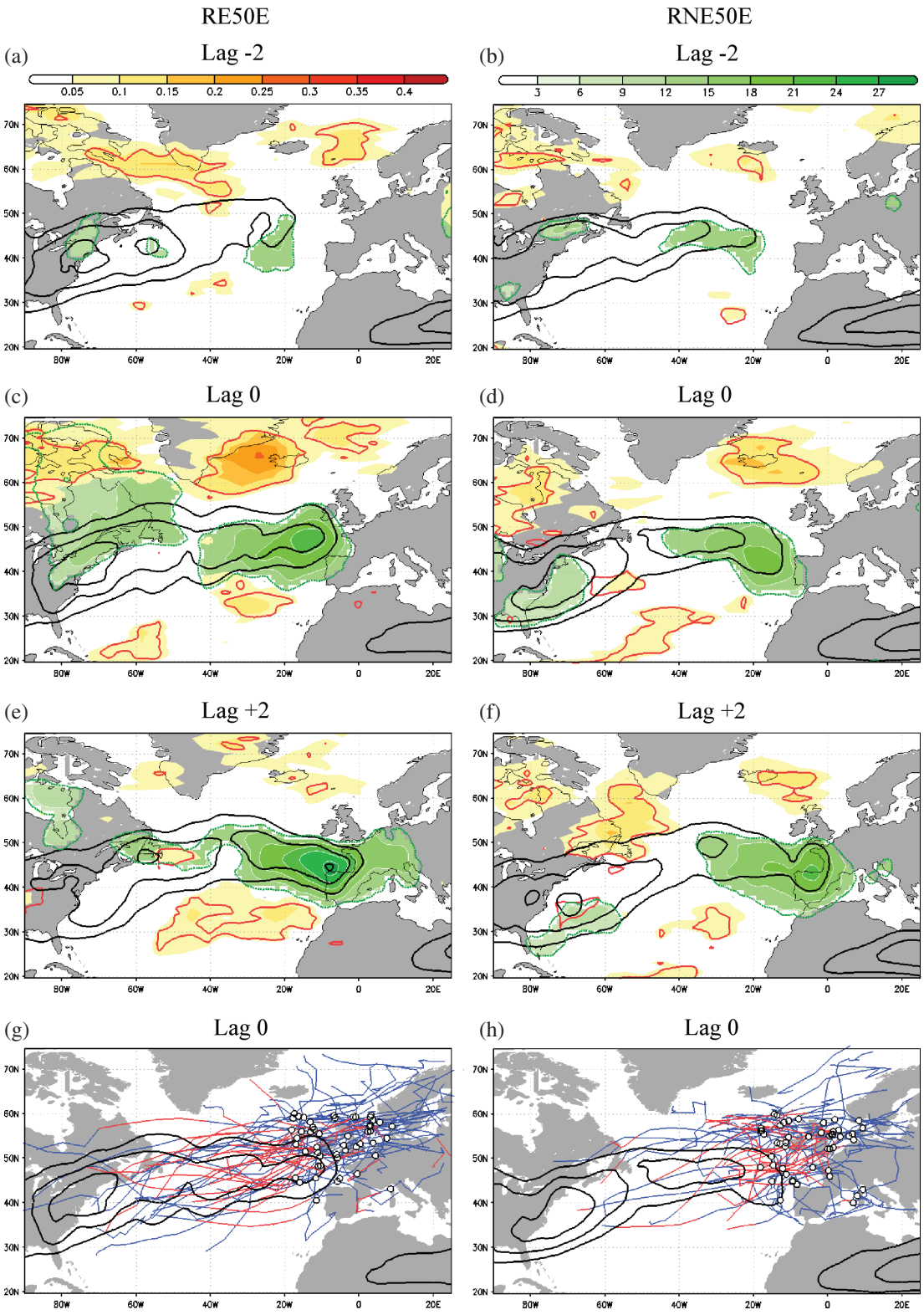

Figure 6. As Figure 3, but for RE50E and RNE50E cyclones on even lagged days.

In Figure 6, RWB occurrences associated with random explosive non-top (RE50E, excluding the Top50E) and random non-explosive (RNE50E) cyclones in the eastern NA are shown for even lagged days. Analysis of RE50E cyclones (Figure 6(a), (c) and (e)) reveals that a common pattern of enhanced RWB to the north and south of an accelerated jet is also present at negative lagged days. However, since the average cyclone intensity is lower, the area and strength of the anomalies are also smaller and weaker. For the RNE50E cyclones, although enhanced RWB is present in some areas, the anomalies are much weaker than for explosive cyclogenesis (Figure 6(b), (d) and (f)). Nevertheless, the jet is still enhanced over the eastern NA, consistent with downstream intensification of cyclones in the NA (Figure 6(g) and (h)). The anomalies over the subtropical NA have a different timing compared with the northern ones (peak at lag +2, Figure 6(e)).

3.4. *Characterisation of local-instantaneous RWB*

So far, evidence has been given that the bidirectional relationship between RWB and intensification of extratropical cyclones is sensitive to the timing, intensity and location of the cyclone's development. The three strongest patterns are:

(1) Enhanced RWB over western Greenland with an intensified jet over western NA at lag −1 (Figure 3(c), Top50W cyclones).

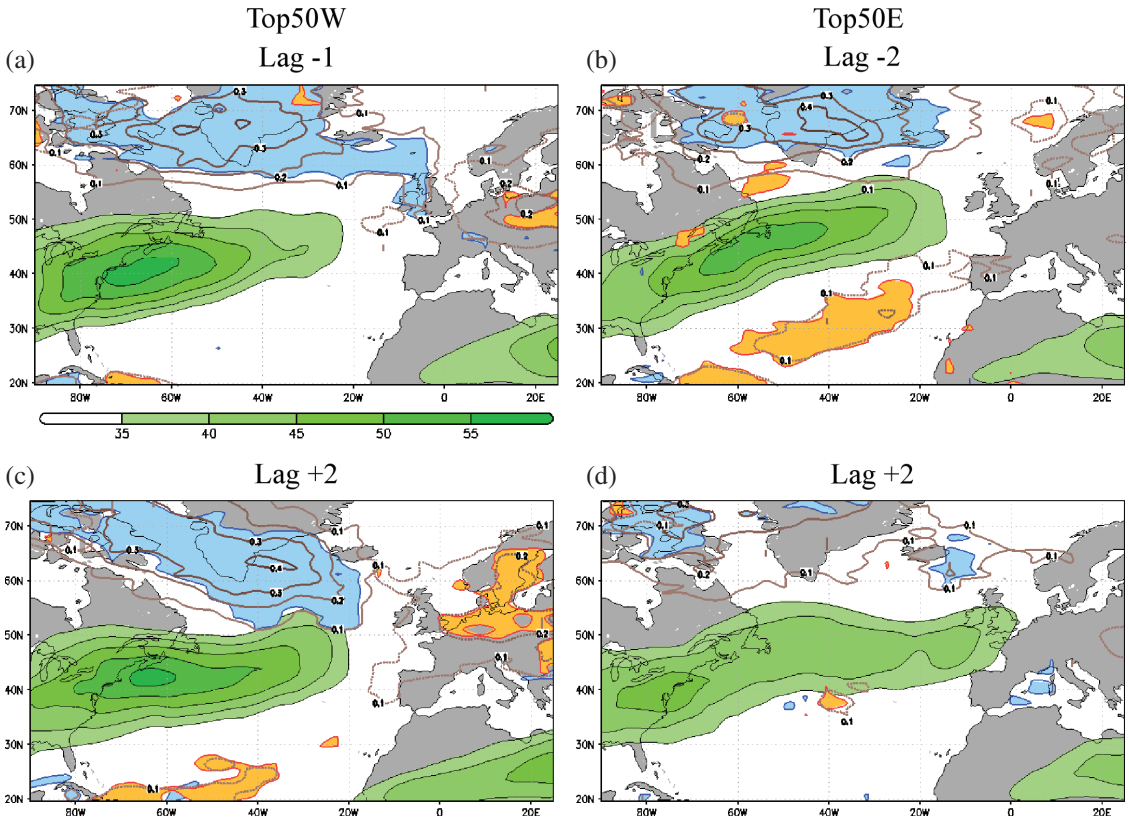

Figure 7. Shadings: enhanced occurrence (Monte Carlo 95% confidence level) of anticyclonic ($B > 0$; $DB > 0.2$ in orange) and cyclonic ($B > 0$; $DB < -0.2$ in blue) Rossby wave-breaking (RWB) on lagged days of explosive development; composite jet stream's intensity in light to dark green (starting from 35 m s^{-1}, interval 5 m s^{-1}). Contours: Monte Carlo 95% confidence level of enhanced RWB (anticyclonic – solid red; cyclonic – solid blue) and relative frequency (daily) of local-instantaneous RWB (anticyclonic – dotted; cyclonic – solid light to dark brown).

(2) Enhanced RWB over southern Greenland and continental Europe at lag +2 (Figure 3(f), Top50W cyclones).
(3) Enhanced RWB over eastern Greenland and subtropical NA accompanied by an intensified jet over western Europe at lag −2 (Figure 5(b), Top50E cyclones).

In Figure 7, the type of breaking and its frequency anomalies of occurrence are provided for these three cases. Regarding pattern 1, the breaking occurring over western Greenland at lag −1 is cyclonic and its frequency of occurrence is around 30–40% (Figure 7(a)). As for pattern 2 (lag +2, Figure 7(c)), the RWB occurrence over southern Greenland is also cyclonic (probably associated with the cyclone itself) and its relative frequency is around 40%. In contrast, the detected RWB over Europe is anticyclonic and its relative frequency of occurrence peaks at 20%. As described by Michel *et al.* (2012), the configuration of the RWB events at lag +2 for the Top50W cyclones may potentially lead to the onset of Scandinavian blocking. Regarding pattern 3, the analysis reveals that while the breaking over eastern Greenland is cyclonic, its southern counterpart over the subtropical NA is anticyclonic at lag −2 (Figure 7(b)). The relative frequency of breaking also depicts that the cyclonic breaking over Greenland is more frequent compared with its southern counterpart (for a more detailed analysis see Section 3.6). The types of breaking and relative frequency of occurrence are also provided at lag +2 for the Top50E cyclones (Figure 7(d)). As already described, no enhanced RWB activity is linked to explosive cyclones in the eastern NA on positive lagged days. As a general note, it is confirmed that the RWB occurring to the north of the jet is cyclonic, whereas that occurring over Europe, at the exit region of the jet, and that south of the jet is anticyclonic (cf. Masato *et al.*, 2013).

3.5. *Sensitivity to sample*

In the previous sections we have based our analysis on random samples of 50 cyclones. Here, we analyse whether the results are sensitive to the choice of sample. Ten different populations of cyclones with similar characteristics are randomly selected with the aim of determining how many of these populations show the same significant results as the original set. An analogous approach is used for the areas with an intensified jet. The total numbers of events from which cyclones are selected are: explosive western (E-W) = 573 cases, non-explosive western (NE-W) = 992 cases, explosive eastern (E-E) = 196 cases and non-explosive eastern (NE-E) = 793 cases. The Top50W and Top50E cyclones are excluded when constructing these subpopulations. In Figure 8(a) and (c) the grid points with statistically significant (95% Monte Carlo test) deviations are shown as counts relative to the ten samples. The count over southwest Greenland in Figure 8(a) depicts that the signal (cyclonic RWB) is very stable for explosive cyclones over the western NA at lag 0 (up to nine out of ten times). Similarly, an intensified upstream jet is also present the same number of times. At lag +2 (not shown), enhanced (cyclonic) RWB over southern Greenland is also found, but no stable signal of RWB activity is found over Europe. On the contrary, neither anomalous RWB activity nor an accelerated jet is detected for the RNE50W cyclones at lag 0 (Figure 8(c)). Over the eastern NA, the enhanced RWB activity over eastern Greenland and subtropical latitudes at lag 0 is also very stable (Figure 8(b)). The jet stream anomalies are also very robust and the position of the higher counts is consistent with an intensified and extended jet over the eastern NA. This extension of the jet is also associated with the decreased RWB occurrence detected over the European continent (blue contours). Whereas the enhanced (cyclonic) RWB activity over eastern Greenland peaks at lag 0, its southern counterpart does at lag +2 (not shown), providing evidence that both RWB anomalies evolve differently. Regarding the RNE50E cyclones, the signal of enhanced RWB vanishes at all lags and it shows only the signature of an extended jet stream and its associated decreased RWB activity (Figure 8(d)). Thus, we conclude that our results for random explosive and random non-explosive cyclones are robust.

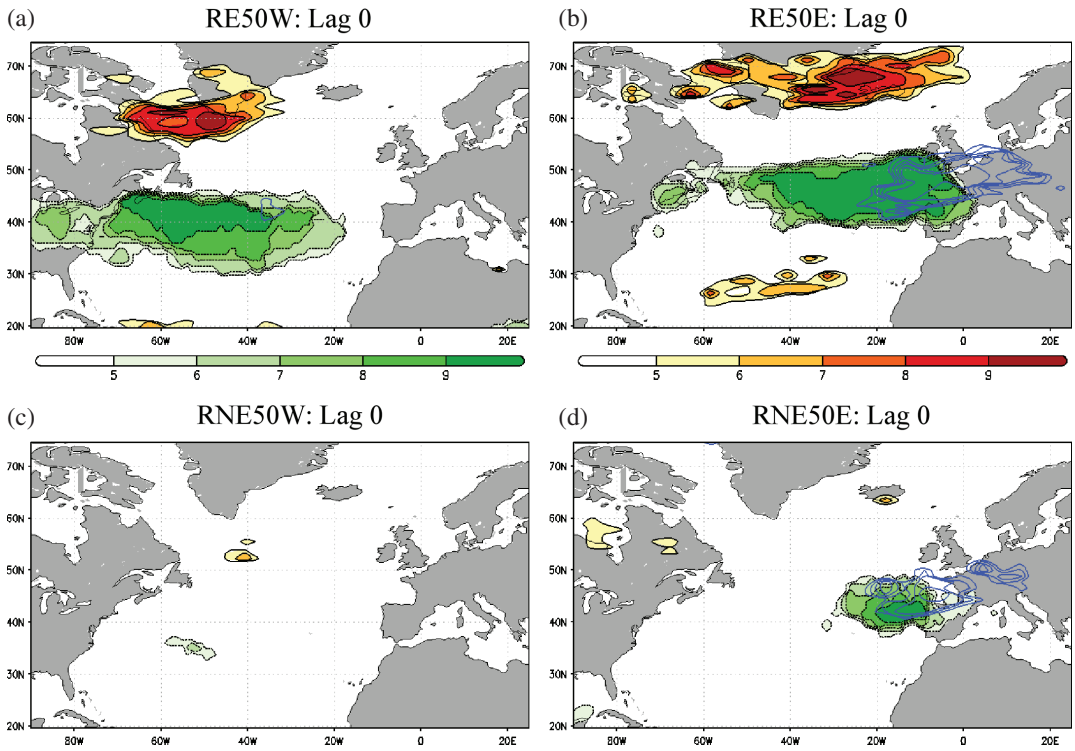

Figure 8. Summary of results at lag 0 from ten different populations of 50 cyclones each: (a) RE50W, (b) RE50E, (c) RNE50W and (d) RNE50E. Plots show the number of the ten samples with statistically significant (95% Monte Carlo test) deviations at each grid point. Rossby wave-breaking (RWB) enhanced activity in solid black contours (light-yellow to dark-red filled), RWB decreased activity in blue contours and jet stream's intensity (positive anomalies) in black dotted contours (light- to dark-green filled). Total events from which cyclones are selected (excluding Top50): E-W = 573, NE-W = 992, E-E = 196 and NE-E = 793.

Table 2. Occurrence of RWB as a precursor to cyclogenesis. Daily frequencies of RWB in the western and eastern NA (in % of days): (i) climatology using all days (top); (ii) as a precursor to cyclogenesis (by taking subsets of days with lags −2 to 0).

Samples	RWB occurrence	West (%)	East (%)
Climatology	North (cyclonic)	12.05 (22.68)	6.41 (14.70)
	South (anticyclonic)	1.52 (3.98)	3.15 (7.22)
	Both	0.15 (0.97)	0.35 (1.27)
Non-explosive cyclones (west: 992 cases; east: 793 cases)	North (cyclonic)	12.35 (22.42)	**7.47 (16.42)**
	South (anticyclonic)	1.86 (4.34)	3.58 (7.98)
	Both	0.17 (1.03)	0.41 (1.33)
Explosive cyclones (west: 623 cases; east: 246 cases)	North (cyclonic)	**18.97 (32.57)**	**12.43 (24.56)**
	South (anticyclonic)	**2.18** (3.99)	**6.87 (11.55)**
	Both	**0.48** (1.33)	**0.88 (2.92)**
Top 50 cyclones	North (cyclonic)	**22.00 (42.00)**	**19.59 (33.78)**
	South (anticyclonic)	1.33 (2.67)	**12.56 (16.89)**
	Both	0.00 (0.00)	**2.70 (5.41)**

Significant (positive) deviations from the climatological values in bold (using a 95% Monte Carlo test). Values in parentheses use the relaxed area criterion.

3.6. *Characterisation of non-local-instantaneous RWB*

In previous sections we have diagnosed anomalies in RWB occurring around the times of explosive cyclogenesis over the NA. Here we count the number of RWB events within particular regions in order to generate summary statistics, for example on the percentage of RWB events that are related to explosive cyclogenesis, and vice versa. The specific questions intended to be answered through this analysis are:

(1) How often is a large cyclonic RWB over western Greenland associated with the intensification of an explosive cyclone in the western NA?
(2) How often are both cyclonic RWB to the north and anticyclonic RWB to the south present for explosive cyclogenesis dates over the eastern NA?
(3) How often does a single breaking episode trigger explosive intensification over the eastern NA?

To answer these questions we combine RWB events over particular regions to derive frequencies of occurrence of RWB anywhere within the regions. Minimum thresholds of RWB area have been imposed, based on the assumption that the larger the RWB, the greater influence over the mean NA circulation regime is expected. As a sensitivity test, two different area thresholds, one more restrictive than the other, have been considered for cyclonic and anticyclonic RWB event selection. In the western NA, cyclonic events occurring within the latitude–longitude box (55–75°N, 90–40°W) with an area larger than 250 deg.lat.^{2} (relaxed criterion: 150 deg.lat.^{2}) have been selected for study. In a similar way, anticyclonic RWB events occurring over the western subtropical NA (20–40°N, 90–40°W) with an area larger than 125 deg.lat.^{2} (relaxed criterion: 75 deg.lat.^{2}) have also been considered. For the eastern NA, the latitude–longitude boxes for RWB event selection are (55–75°N, 50°W–0°E) and (20–40°N, 50°W–0°E), respectively. The minimum threshold area for selection of subpolar RWB events is thus twice the size (in deg.lat.^{2}) of the subtropical ones. This is based on the mean area

Table 3. Cyclogenesis preceded by RWB. Percentage of cyclones (top 50, explosive (including top 50) and non-explosive) preceded by any type of RWB (lags −2 to 0).

Cyclones	RWB occurrence	West (%)	East (%)
Top 50	North (cyclonic)	38.00 (70.00)	34.00 (52.00)
	South (anticyclonic)	4.00 (6.00)	24.00 (28.00)
	Both	0.00 (0.00)	4.00 (10.00)
Explosive (west: 623 cases; east: 246 cases)	North (cyclonic)	35.31 (52.17)	24.39 (42.68)
	South (anticyclonic)	5.30 (8.99)	14.63 (24.39)
	Both	1.28 (3.37)	2.03 (6.91)
Non-explosive (west: 992 cases; east: 793 cases)	North (cyclonic)	21.47 (37.10)	15.38 (29.63)
	South (anticyclonic)	3.53 (8.47)	8.83 (17.53)
	Both	0.40 (2.42)	1.01 (2.90)

Values in parentheses use the relaxed area criterion.

of the observed RWB positive anomalies in the previous figures. The limited zonal extension of both analysed boxes ensures that simultaneous RWB occurs over the same area of the NA (i.e. western, eastern). North cyclonic and south anticyclonic RWB events over each side of the NA are considered as simultaneous when they coexist on the same day.

The resulting frequencies of RWB over these areas are given in Table 2, with results derived from the relaxed area criterion provided in parentheses. The first few lines give the climatological frequencies of the different RWB types in these regions, for comparison. Demanding a greater area of RWB acts to reduce the frequencies considerably, but both thresholds show the same relative features in the climatology; that north cyclonic RWB is more frequent in the western NA and south anticyclonic RWB is more frequent in the eastern NA. In both regions and for both thresholds the occurrence of simultaneous RWB on both sides of the jet is rare, at most occurring on 1% of days.

The relative frequency of RWB occurrence on days prior to the intensification of cyclones over the eastern and western NA is also given in Table 2. This is done by forming subsets of days within lags −2 to 0 of cyclogenesis and then calculating the RWB frequency of these subsets. The subsets are initially of size $N \times 3$, where N is the number of cyclogenesis events, and then any double counting of days arising from the proximity of cyclogenesis events is removed. In general, these frequencies are consistent with the features observed in the RWB analysis from the local-instantaneous perspective (Section 3.4): that RWB occurrence is enhanced on days prior to explosive cyclogenesis in the NA. Significant (positive) deviations from the climatological values (bold numbers, using a 95% Monte Carlo test) are consistent with enhanced cyclonic RWB activity over the western subpolar NA as precursor of explosive cyclogenesis over the western NA. Likewise, enhanced cyclonic and anticyclonic RWB occurrence is observed over the subpolar and subtropical eastern NA on days prior to explosive cyclones affecting Europe.

In Table 3 a different approach is used to provide information about the percentage of cyclones preceded by any type of RWB. Here RWB is considered as precursor if an event is identified for at least one day within lags −2 to 0 of each cyclone. Note that Tables 2 and 3 cannot be compared directly, as the latter provides information on occurrence/non-occurrence of RWB during a 3-day period and thus persistent RWB events lasting several days are counted only once. In Table 3, percentages are lower for the cyclone sets with weaker intensities, showing that the most intense cyclones are particularly associated with RWB. For example, north cyclonic RWB is present for up to 70% of Top50W cyclones and 52% of Top50E cyclones. South anticyclonic RWB shows elevated frequencies for the eastern NA cyclones, occurring on up to 28% of Top50E cyclones, but is less important for the western NA cyclones. Simultaneous RWB events are rare as precursors of any type of cyclogenesis over both NA sectors. Their occurrence is greatest over the eastern NA, in particular up to 4% (10%) of the Top50E cyclones by using the restrictive (relaxed) area size criterion. However, for the majority of explosive cyclones over the eastern NA there is only one RWB precursor. In terms of intensity and deepening rate, over this area explosive cyclones evolving under simultaneous RWB events feature a higher maximum $\nabla^2 p$ (2.34 hPa deg.lat.$^{-2}$) and *NDR* (1.55 Bergeron) compared with cyclones preceded by a single RWB event (northern RWB, 2.16 hPa deg.lat.$^{-2}$/1.39 Bergeron; southern RWB, 2.20 hPa deg.lat.$^{-2}$/1.38 Bergeron; for independent subpopulations). This is consistent with a stronger influence of simultaneous RWB on the jet stream. These differences, however, are statistically significant only for the *NDR* (above 95%, Monte Carlo test). This is somewhat expected given that this study is based on lagged days that are centred on the date of maximum *NDR*, not $\nabla^2 p$. Thus, in some cases a decoupling in the timing of both variables could arise and thus explain the observed differences.

Table 4. Rossby wave-breaking leading to explosive cyclogenesis: percentage of RWB events that lead to explosive cyclogenesis (within lags 0 to +2) over the western and eastern NA.

	Frequency (%)	
RWB events	Western NA (Climatology: 20.67%)	Eastern NA (Climatology: 8.54%)
North cyclonic [250 (150) deg.lat.^{2}]	32.54 (29.68)	16.57 (14.27)
South anticyclonic [125 (75) deg.lat.^{2}]	29.51 (20.69)	18.65 (13.67)
Both [250/125 (150/75) deg.lat.^{2}]	40.00 (28.20)	21.43 (19.61)

Values in parentheses use the relaxed area criterion.

Conversely, we now investigate how often the RWB precursors are indeed followed by explosive cyclogenesis. The percentage of identified RWB events leading to explosive cyclogenesis over the western (623 cyclones considered, including the Top50W) and eastern (246 cyclones, including the Top50E) NA is considered. Those RWB episodes fostering explosive cyclogenesis are selected if the maximum intensification date of any cyclone occurs within lags 0 to +2 days with respect to the RWB event. The mean frequencies of explosive cyclogenesis occurrence over the whole time period by this measure are 20.67% in the western NA and 8.54% in the eastern NA. These values are effectively the percentage of all days in the dataset that have an explosive cyclogenesis event within the following 0–2 days. Table 4 shows that these likelihoods are clearly increased for most of the breaking event types, with the exception of south anticyclonic RWB events over the western NA for the relaxed criteria. As an example, the probability of an explosive western NA cyclone is increased by a factor of 1.5 if north cyclonic RWB is present. Similarly the probability of an explosive eastern NA cyclone is roughly doubled if simultaneous RWB occurs.

We have provided evidence that the likelihood of explosive cyclogenesis occurrence is sensitive to the minimum area size of RWB events. In particular, this relationship appears to be

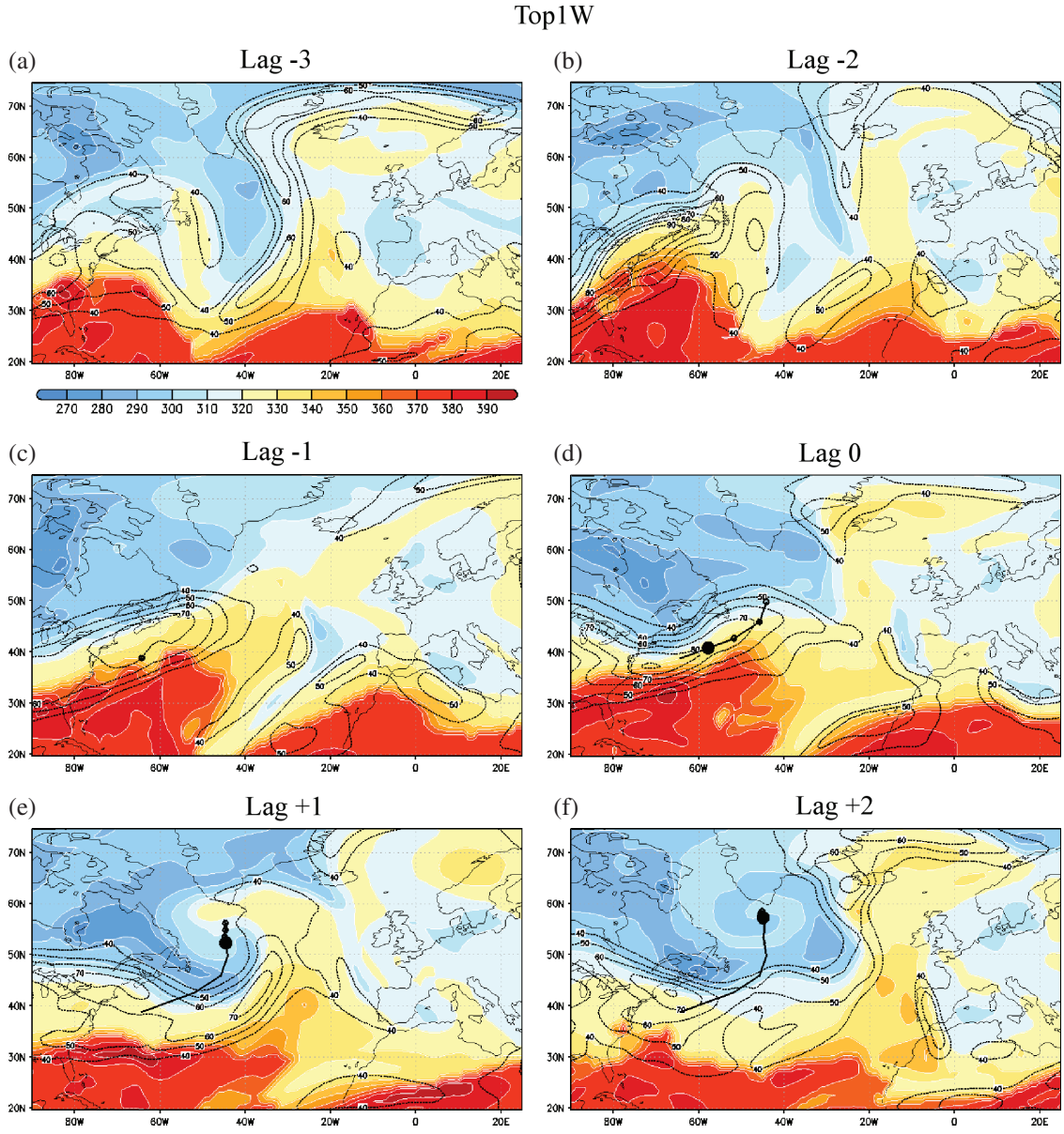

Figure 9. Case study of the most intense western cyclone (in terms of maximum Laplacian of Pressure). ((a) – (f)) Wind intensity at 250 hPa (starting from 40 m s^{-1}, interval 10 m s^{-1}) in black dotted contours. θ on the 2 PVU surface in dark red to dark blue shadings (in K). Full trajectory of the cyclone until 1800 UTC of each lagged day in a thick black contour. The cyclone position at 0000 UTC on each day is represented by a large dot. The three forthcoming positions on the same date (0600, 1200 and 1800 UTC) are marked with small black open circles. Time interval: 4 February to 9 February 1959. Fields are plotted at 0000 UTC of each day.

stronger for the south anticyclonic RWB events. Simultaneous RWB typically leads to the most intense explosive cyclogenesis. As seen in Tables 2 and 3, these situations are very rare. However, individual RWB events occur more commonly and it has been shown that these considerably raise the likelihood of subsequent explosive cyclogenesis.

3.7. Case studies

In order to document how the proposed mechanisms for explosive cyclogenesis in the NA occur, two illustrative examples of explosive cyclones are selected (Figures 9 and 10). The first example is the most intense explosive cyclone in the western NA.

Figure 9 displays θ on the 2 PVU surface and wind intensity at 250 hPa at 0000 UTC of each lagged day relative to the start of explosive development (lag 0). The cyclone position at 0000 UTC on each day is represented by a large dot. The three forthcoming positions on the same date (0600, 1200, 1800 UTC) are marked with small black open circles. The cyclone was first detected by the tracking scheme on 6 February 1959 (Figure 9(c)), underwent explosive intensification on 7 February (Figure 9(d)) and disappeared 4 days later after landfalling over eastern Greenland (not shown). On the days prior to the explosive development (Figure 9(a)–(c)), a large poleward extrusion of high θ air is evident over the eastern NA. Although this extrusion largely breaks anticyclonically over Europe, an area of cyclonic wave breaking can also be identified over southwest Greenland. At lag 0, RWB to the north squeezes the jet, which was already quite intense and confined over the western NA in previous lags, and accelerates it (Figure 9(d)). The cyclone starts to intensify and encounters very favourable upper-level conditions for explosive development. As Figure 9(e) shows, at lag +1 the cyclone leaves the jet core from the left-exit region and induces a strong cyclonic RWB south of Greenland. The breaking associated with such an intense cyclone at lag +2 completely disrupts the westerly flow and a large mass of high θ air is advected from the subtropics towards the eastern subpolar NA (Figure 9(f)). This air mass acts to reinforce the existing ridge and leads one day later to the onset of a Scandinavian blocking event (not shown). This is consistent with the eddy-forcing and maintenance theories for blocking of Shutts (1983) and Nakamura and Wallace (1993).

This example first provides evidence of how the RWB fosters explosive cyclogenesis over the western NA and second how the cyclogenesis acts as a precursor of Scandinavian blocking (see also Michel *et al.*, 2012). This situation of a large subtropical air mass extending polewards downstream of an explosive cyclogenesis

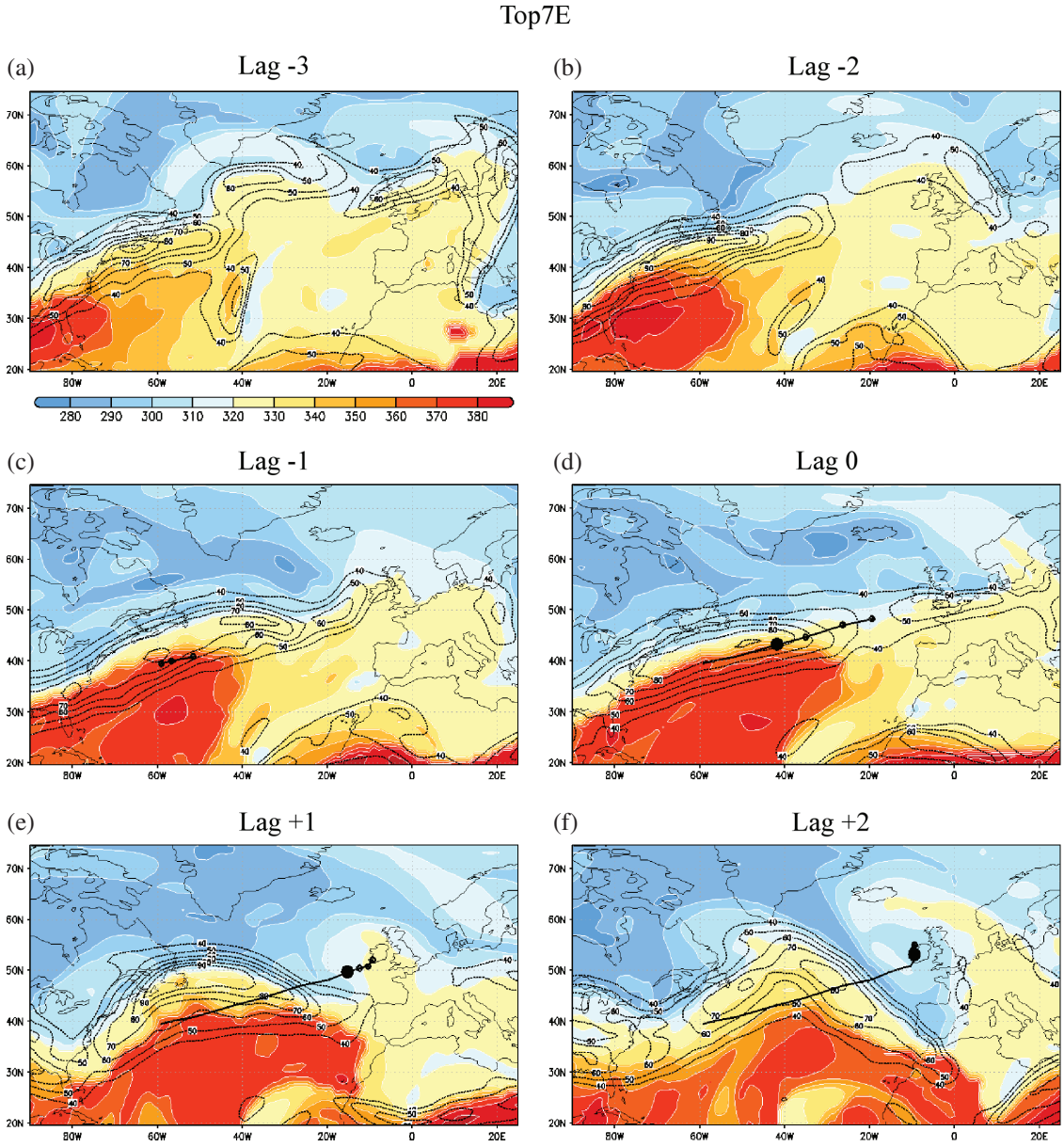

Figure 10. As Figure 9, but for an eastern cyclone. Time interval: 30 January to 4 February 1994 at 0000 UTC.

seems very sensitive in that two very different regime transitions could occur: (i) the subtropical air could break anticyclonically, leading to blocking over Europe as in this case; or (ii) it could break cyclonically over Greenland, leading to NAO- (Benedict *et al.*, 2004–see the E feature on lag −3 in their figure 6).

One of the most intense cyclones evolving over the eastern NA has also been selected (30 January to 4 February 1994) for analysis (Figure 10). On days prior to the explosive development, two simultaneous areas of cyclonic RWB to the north and anticyclonic to the south of the jet position are identified (Figure 10(a)–(c)). The combined effect of both breakings over the jet can be clearly observed in Figure 10(d). As the jet is squeezed by both RWB events, it is accelerated and shifted towards the European continent. In this case, the cyclone again encounters very favourable conditions for explosive growth at lag 0 and reaches western Ireland at lag +1 (Figure 10(e)). On this day a cyclonic RWB probably associated with the cyclone takes place over northwest Europe. Unlike the previous case, this event does not dramatically alter the large-scale circulation over the NA (Figure 10(e) and (f)).

It is interesting to note that the two case studies show a simultaneous occurrence of cyclonic (to the north) and anticyclonic (to the south) RWB. However, the cyclonic RWB clearly dominates in the former, while the anticyclonic RWB dominates in the latter (note that the anticyclonic RWB over the western NA is not detected in Table 3 due to its small size), consistent with the preferred locations of these types of breaking (e.g. Gabriel and Peters, 2008).

4. Concluding remarks

In this study the two-way relationship between Rossby wave-breaking (RWB) and intensification of extratropical cyclones in the North Atlantic (NA) has been analysed. For this purpose, two indices based on potential temperature have been used to identify (*B* index) and classify (*DB* index) cyclonic and anticyclonic RWB events from the ERA-40 period.

Evidence was provided that most intense cyclones (maximum $\nabla^2 p$) in the western NA (Top50W) are preceded by enhanced cyclonic RWB activity over western Greenland on days prior to their maximum intensification. Through the mechanism proposed in this article, the jet is squashed on its northern side by the breaking events and thus accelerated over the western NA. Such favourable upper-level conditions, associated with enhanced baroclinicity in the jet area, increase the potential for the occurrence of explosive cyclogenesis over that area (up to 70% of the Top50W cyclones are preceded by this Greenland cyclonic RWB precursor depending on the choice of area). For the most intense cyclones over the eastern NA (the Top50E), two distinct areas of enhanced RWB are found

over eastern Greenland (cyclonic) and subtropical (anticyclonic) NA. Simultaneous occurrence of north cyclonic and south anticyclonic RWB events accounts for only 10% of the cyclone cases. Explosive cyclones evolving under such conditions have higher mean intensity and larger deepening rates than cyclones preceded by a single RWB event. Nevertheless, when RWB acts as a dynamical precursor it is mainly through a single breaking event (60% of the Top50E cyclones are preceded by a single RWB precursor). The dynamical mechanism for cyclone development is analogous to that described for the western region. The RWB preceding explosive cyclogenesis events may be associated in some cases to previous cyclonic development in this region, but more generally arises from interactions between Rossby waves of varying temporal and spatial scales in the upper troposphere (McIntyre and Palmer, 1983; Nakamura and Wallace, 1993; Tomikawa *et al.*, 2006). Although these waves are ultimately forced by baroclinic development (Edmon *et al.*, 1980; Thorncroft *et al.*, 1993) their linear and nonlinear behaviour at upper levels is complex and often modelled independently of the baroclinic source (Randel and Held, 1991; Delsole, 2001; Barnes and Hartmann, 2011).

In addition, it has also been found that the cyclone's maximum intensity, deepening rate and location in the NA is sensitive to the occurrence and spatial extent of RWB events on days previous to their maximum intensification day. Composite analysis of explosive and non-explosive cyclogenesis has shown that for explosive non-top cyclones (RE50) the observed common RWB patterns are analogous (but weaker) compared with the most intense cyclones (Top50), whereas the non-explosive ones (RNE50) show no clear relationship to RWB enhanced activity. Thus, the mechanisms proposed in this article hold only for explosive cyclones in the NA, and their occurrence clearly depends on the intensity of the cyclone.

In the frame of the extensive existing literature on explosive cyclogenesis, the presence of strong upper-level winds is considered as one of several physical mechanisms contributing to rapid cyclone growth (e.g. Fink *et al.*, 2012). In this context, numerous studies have already shown the importance of a strong upper-level forcing (Bosart and Lin, 1984; Sanders, 1986; Reader and Moore, 1995; Gyakum and Danielson, 2000), a highly destabilised low-level environment (Manobianco, 1989), a strong latent heat release (Fosdick and Smith, 1991) and surface fluxes (Davis and Emanuel, 1988). As noted in previous sections, an intensified polar jet is also associated with increased baroclinicity in the jet area, thus raising the potential for explosive growth as conceptually described by Hoskins *et al.* (1985). In addition, the presence of strong divergence in the right-entrance and left-exit regions of the jet core contributes to deep vertical atmospheric destabilisation (Uccellini, 1990; Rivière and Joly, 2006a, 2006b). Finally, it has also been reported that upper-level waves can interact with the jet stream, thus creating an environment of multiple jet streaks (as observed during Klaus' intensification; Liberato *et al.*, 2011) very favourable for rapid cyclone intensification (Reed and Albright, 1986).

In this study, it has also been observed that the timing is crucial in the relationship between RWB and cyclone development (lead-lag analysis). On days following the explosive development of the most intense cyclones in the western NA (Top50W, lag +2), a common RWB pattern of cyclonic breaking over southern Greenland and anticyclonic over Europe has been identified. This result is in line with Michel *et al.* (2012), who provided evidence that the presence of very intense cyclones south of Greenland can potentially lead to the onset of Scandinavian blocking.

These findings may help in the improvement of forecasting of such hazardous phenomenon over the Euro-Atlantic sector. Given the observed persistence (3–4 days) of the identified RWB events that may foster explosive cyclogenesis in the western and eastern NA, a comprehensive analysis of RWB and the occurrence of clusters of extreme cyclones (e.g. Vitolo *et al.*, 2009) will be an interesting path for future research.

Acknowledgements

We are indebted to the ECMWF for providing the ERA-40 reanalysis data. This work is supported by national funds (Ministry of Economy and Competitiveness – Government of Spain) under the research projects DE VIAJE (CGL2009-06944) and TRACS (CGL2009-10285). IG was supported by TRACS during his visit in 2012 at the Institute for Geophysics and Meteorology of the University of Cologne, Germany. We thank Sven Ulbrich (University of Cologne) for help with the cyclone statistics, and João A. Santos (University of Trás-os-Montes e Alto Douro, Portugal) for discussions. Finally, we would like to thank the two anonymous reviewers for their helpful comments and suggestions, which contributed to improve this manuscript.

Supporting information

The following supporting information is available as part of the online article:

Figure S1. Scatter plot of cyclone populations (*NDR* vs. maximum Laplacian of pressure).

Figure S2. Mean maximum Laplacian of pressure of cyclone populations.

Figure S3. Mean *NDR* of cyclone populations.

References

Allen JT, Pezza AB, Black MT. 2010. Explosive cyclogenesis: a global climatology comparing multiple reanalyses. *J. Climate* **23**: 6468–6484.

Barnes EA, Hartmann D. 2011. Rossby wave scales, propagation, and the variability of eddy-driven jets. *J. Atmos. Sci.* **68**: 2893–2908.

Barnston AG, Livezey RE. 1987. Classification, seasonality and persistence of low-frequency atmospheric circulation patterns. *Mon. Wea. Rev.* **115**: 1083–1126.

Benedict JJ, Lee S, Feldstein SB. 2004. Synoptic view of the North Atlantic Oscillation. *J. Atmos. Sci.* **61**: 121–144.

Blessing S, Fraedrich K, Junge M, Kunz T, Lunkeit F. 2005. Daily North-Atlantic Oscillation (NAO) index: Statistics and its stratospheric polar vortex dependence. *Meteorol. Z.* **14**: 763–769.

Bosart LF, Lin SC. 1984. A diagnostic analysis of the Presidents' Day storm of February 1979. *Mon. Wea. Rev.* **112**: 2148–2177.

Champion AJ, Hodges KI, Bengtsson LO, Keenlyside NS, Esch M. 2011. Impact of increasing resolution and a warmer climate on extreme weather from Northern Hemisphere extratropical cyclones. *Tellus A.* **63A**: 893–906.

Chang EK. 2009. Are band-pass variance statistics useful measures of storm track activity? Re-examining storm track variability associated with the NAO using multiple storm track measures. *Clim. Dyn.* **33**: 277–296.

Colucci SJ. 1985. Explosive cyclogenesis and large-scale circulation changes: implications for atmospheric blocking. *J. Atmos. Sci.* **42**: 2701–2717.

Dacre HF, Gray SL. 2009. The spatial distribution and evolution characteristics of North Atlantic cyclones. *Mon. Wea. Rev.* **137**: 99–115.

Dacre HF, Gray SL. 2013. Quantifying the climatological relationship between extratropical cyclone intensity and atmospheric precursors. *Geophys. Res. Lett.* **40**: 2322–2327. DOI: 10.1002/grl.50105.

Davis CA, Emanuel KA. 1988. Observational evidence for the influence of surface heat fluxes on maritime cyclogenesis. *Mon. Wea. Rev.* **116**: 2649–2659.

DelSole T. 2001. A simple model for transient eddy momentum fluxes in the upper troposphere. *J. Atmos. Sci.* **58**: 3019–3035.

Donat MG, Leckebusch GC, Pinto JG, Ulbrich U. 2010. Examination of wind storms over central Europe with respect to circulation weather types and NAO phases. *Int. J. Climatol.* **30**: 1289–1300.

Edmon HJ, Hoskins BJ, McIntyre ME. 1980. Eliassen–Palm cross sections for the troposphere. *J. Atmos. Sci.* **37**: 2600–2616.

Feldstein SB. 2003. The dynamics of NAO teleconnection pattern growth and decay. *Q. J. R. Meteorol. Soc.* **129**: 901–924.

Fink AH, Brücher T, Ermert V, Krüger A, Pinto JG. 2009. The European storm Kyrill in January 2007: Synoptic evolution and considerations with respect to climate change. *Nat. Hazards Earth Syst. Sci.* **9**: 405–423.

Fink AH, Pohle S, Pinto JG, Knippertz P. 2012. Diagnosing the influence of diabatic processes on the explosive deepening of extratropical cyclones. *Geophys. Res. Lett.* **39**: L07803 DOI: 10.1029/2012GL051025.

Fosdick EK, Smith PJ. 1991. Latent heat release in an extratropical cyclone that developed explosively over the southeastern United States. *Mon. Wea. Rev.* **119**: 193–207.

Franzke C, Lee S, Feldstein SB. 2004. Is the North Atlantic Oscillation a breaking wave? *J. Atmos. Sci.* **61**: 145–160.

Gabriel A, Peters D. 2008. A diagnostic study of different types of Rossby wave breaking events in the northern extratropics. *J. Met. Soc. Jpn.* **86**(5): 613–631.

Gyakum JR, Danielson RE. 2000. Analysis of meteorological precursors to ordinary and explosive cyclogenesis in the western North Pacific. *Mon. Wea. Rev.* **128**: 851–863.
Hanley J, Caballero R. 2012. The role of large-scale atmospheric flow and Rossby wave breaking in the evolution of extreme windstorms over Europe. *Geophys. Res. Lett.* **39**: L21708. DOI: 10.1029/2012GL053408.
Hoskins BJ, Valdes PJ. 1990. On the existence of storm-tracks. *J. Atmos. Sci.* **47**: 1854–1864.
Hoskins BJ, McIntyre ME, Robertson AW. 1985. On the use and significance of isentropic potential vorticity maps. *Q. J. R. Meteorol. Soc.* **111**: 877–946.
Hurrell JW, Kushnir Y, Ottersen G, Visbeck M. 2003. The North Atlantic Oscillation: climate significance and environmental impact. *Geophys. Monograph. Ser.* **134**: 279 pp.
Kuwano-Yoshida A, Asuma Y. 2008. Numerical study of explosively developing extratropical cyclones in the northwestern Pacific region. *Mon. Wea. Rev.* **136**: 712–740.
Liberato MLR, Pinto JG, Trigo IF, Trigo RM. 2011. Klaus – an exceptional winter storm over northern Iberia and southern France. *Weather* **66**: 330–334.
Manobianco J. 1989. Explosive east coast cyclogenesis over the west-central North Atlantic Ocean: A composite study derived from ECMWF operational analyses. *Mon. Wea. Rev.* **117**: 2365–2383.
Masato G, Hoskins BJ, Woollings TJ. 2012. Wave-breaking characteristics of midlatitude atmospheric blocking. *Q. J. R. Meteorol. Soc.* **138**: 1285–1296.
Masato G, Hoskins BJ, Woollings TJ. 2013. Wave-breaking characteristics of Northern Hemisphere winter blocking: a two-dimensional approach. *J. Clim.* DOI: 10.1175/JCLI-D-12-00240.1.
McIntyre ME, Palmer TM. 1983. Breaking planetary waves in the stratosphere. *Nature* **305**: 593–600.
Michel C, Rivière G. 2011. The link between Rossby wave breakings and weather regime transitions. *J. Atmos. Sci.* **68**: 1730–1748.
Michel C, Rivière G, Terray L, Joly B. 2012. The dynamical link between surface cyclones, upper-tropospheric Rossby wave breaking and the life cycle of the Scandinavian blocking. *Geophys. Res. Lett.* **39**: L10806. DOI:10.1029/2012GL051682.
Murray RJ, Simmonds I. 1991. A numerical scheme for tracking cyclone centres from digital data. Part I: development and operation of the scheme. *Aust. Meteorol. Mag.* **39**: 155–166.
Nakamura H, Wallace JM. 1993. Synoptic behavior of baroclinic eddies during the blocking onset. *Mon. Wea. Rev.* **121**: 1892–1903.
Nakamura H, Sampe T, Tanimoto Y, Shimpo A. 2004. Observed associations among storm tracks, jet streams and midlatitude oceanic fronts. In *Earth's Climate: The Ocean–Atmosphere Interaction*, Wang C, Xie S-P, Carton JA (eds). Geophysical Monograph Series 147, American Geophysical Union: Washington, DC; 329–345.
Neu U, Akperov MG, Bellembaum N, Benestad R, Blender R, Caballero R, Cocozza A, Dacre HF, Feng Y, Fraedrich K, Grieger J, Gulev S, Hanley J, Hewson T, Inatsu M, Keay K, Kew SF, Kindem I, Leckebusch GC, Liberato MLR, Lionello P, Mokhov II, Pinto JG, Raible CC, Reale M, Rudeva I, Schuster M, Simmonds I, Sinclair M, Sprenger M, Tilinina ND, Trigo IF, Ulbrich S, Ulbrich U, Wang XL, Wernli H. 2013. IMILAST: A community effort to intercompare extratropical cyclone detection and tracking algorithms. *Bull. Am. Meteorol. Soc.* **94**: 529–547. DOI: 10.1175/BAMS-D-11-00154.1.
Orlanski I, 2003. Bifurcation in eddy life cycles: Implications for storm track variability. *J. Atmos. Sci.* **60**: 993–1023.
Pelly JL, Hoskins BJ. 2003. A new perspective on blocking. *J. Atmos. Sci.* **60**: 743–755.
Pinto JG, Raible CC. 2012. Past and recent changes in the North Atlantic oscillation. *Wiley Interdisc. Rev. Climate Change* **3**: 79–90. DOI:10.1002/wcc.150.
Pinto JG, Spangehl T, Ulbrich U, Speth P. 2005. Sensitivities of cyclone detection and tracking algorithm: individual tracks and climatology. *Meteorol. Z.* **14**: 823–838.
Pinto JG, Ulbrich U, Leckebusch GC, Spangehl T, Reyers M, Zacharias S. 2007. Changes in storm track and cyclone activity in three SRES ensemble experiments with the ECHAM5/MPI-OM1 GCM. *Clim. Dyn.* **29**: 195–210.
Pinto JG, Zacharias S, Fink AH, Leckebusch GC, Ulbrich U. 2009. Factors contributing to the development of extreme North Atlantic cyclones and their relationship with the NAO. *Clim. Dyn.* **32**: 711–737.
Pinto JG, Karremann MK, Born K, Della-Marta PM, Klawa M. 2012. Loss potentials associated with European windstorms under future climate conditions. *Clim. Res.* **54**: 1–20.
Raible CC. 2007. On the relation between extremes of midlatitude cyclones and the atmospheric circulation using ERA40. *Geophys. Res. Lett.* **34**: L07703. DOI:10.1029/2006GL029084.
Raible CC, Yoshimori M, Stocker TF, Casty C. 2007. Extreme midlatitude cyclones and their implications to precipitation and wind speed extremes in simulations of the Maunder Minimum versus present day conditions. *Clim Dyn.* **28**: 409–423.
Randel WJ, Held IM. 1991. Phase speed spectra of transient eddy fluxes and critical layer absorption. *J. Atmos. Sci.* **48**: 688–697.
Reader MC, Moore GWK. 1995. Stratosphere–troposphere interactions associated with a case of explosive cyclogenesis in the Labrador Sea. *Tellus A.* **47**: 849–863.
Reed RJ, Albright MD. 1986. A case study of explosive cyclogenesis in the eastern Pacific. *Mon. Wea. Rev.* **114**: 2297–2319.
Rivière G, Joly A. 2006a. Role of the low-frequency deformation field on the explosive growth of extratropical cyclones at the jet exit. Part I: barotropic critical region. *J. Atmos. Sci.* **63**: 1965–1981.
Rivière G, Joly A. 2006b. Role of the low-frequency deformation field on the explosive growth of extratropical cyclones at the jet exit. Part II : baroclinic critical region. *J. Atmos. Sci.* **63**: 1982–1995.
Rivière G, Orlanski I. 2007. Characteristics of the Atlantic storm-track eddy activity and its relation with the North Atlantic Oscillation. *J. Atmos. Sci.* **64**: 241–266.
Rivière G, Arbogast P, Maynard K, Joly A. 2010. The essential ingredients leading to the explosive growth stage of the European wind storm 'Lothar' of Christmas 1999. *Q. J. R. Meteorol. Soc.* **136**: 638–652.
Rivière G, Arbogast P, Lapeyre G, Maynard K. 2012. A potential vorticity perspective on the motion of a mid-latitude winter storm. *Geophys. Res. Lett.* **39**: L12808. DOI:10.1029/2012GL052440.
Roebber PJ. 2009. Planetary waves, cyclogenesis, and the irregular breakdown of zonal motion over the North Atlantic. *Mon. Wea. Rev.* **137**: 3907–3917.
Roebber PJ, Schumann MR. 2011. Physical processes governing the rapid deepening tail of maritime cyclogenesis. *Mon. Wea. Rev.* **139**: 2776–2789.
Sanders F. 1986. Explosive cyclogenesis in the west-central North Atlantic Ocean. Part I: Composite structure and mean behaviour. *Mon. Wea. Rev.* **114**: 1781–1794.
Sanders F, Gyakum JR. 1980. Synoptic-dynamic climatology of the bomb. *Mon. Wea. Rev.* **108**: 1589–1606.
Schwierz C, Köllner-Heck P, Zenklusen Mutter E, Bresch DN, Vidale PL, Wild M, Schär C. 2010. Modelling European winter wind storm losses in current and future climate. *Climatic Change* **101**(3–4): 485–514. DOI:10.1007/s10584-009-9712-1.
Shutts GJ. 1983. The propagation of eddies in diffluent jet streams: Eddy vorticity forcing of 'blocking' flow fields. *Q. J. R. Meteorol. Soc.* **109**: 737–761. DOI: 10.1002/qj.49710946204.
Simmonds I, Murray RJ, Leighton RM. 1999. A refinement of cyclone tracking methods with data from FROST. *Aust. Meteorol. Mag. Special Edition:* 35–49.
Strong C, Magnusdottir G. 2008a. How Rossby wave breaking over the Pacific forces the North Atlantic Oscillation. *Geophys. Res. Lett.* **35**: L10706. DOI: 10.1029/2008GL033578.
Strong C, Magnusdottir G. 2008b. Tropospheric Rossby wave breaking and the NAO/NAM. *J. Atmos. Sci.* **65**: 2861–2876.
Thorncroft CD, Hoskins BJ, McIntyre ME. 1993. Two paradigms of baroclinic wave life-cycle behaviour. *Q. J. R. Meteorol. Soc.* **119**: 17–55.
Tomikawa Y, Sato K, Shepherd TG. 2006. A diagnostic study of waves on the tropopause. *J. Atmos. Sci.* **63**: 3315–3332.
Trigo IF. 2006. Climatology and interannual variability of storm-tracks in the Euro-Atlantic sector: a comparison between ERA-40 and NCEP/NCAR reanalyses. *Clim. Dyn.* **26**: 127–143.
Uccellini LW. 1990. Processes contributing to the rapid development of extratropical cyclones. In *Extratropical Cyclones: The Erik Palmen Memorial Volume*, Newton C, Holopainen EO (eds). American Meteorological Society: Washington, DC; 81–105.
Uppala SM, KÅllberg PW, Simmons AJ, Andrae U, Bechtold VDC, Fiorino M, Gibson JK, Haseler J, Hernandez A, Kelly GA, Li X, Onogi K, Saarinen S, Sokka N, Allan RP, Andersson E, Arpe K, Balmaseda MA, Beljaars ACM, Berg LVD, Bidlot J, Bormann N, Caires S, Chevallier F, Dethof A, Dragosavac M, Fisher M, Fuentes M, Hagemann S, Hólm E, Hoskins BJ, Isaksen L, Janssen PAEM, Jenne R, Mcnally AP, Mahfouf JF, Morcrette JJ, Rayner NA, Saunders RW, Simon P, Sterl A, Trenberth KE, Untch A, Vasiljevic D, Viterbo P, Woollen J. 2005. The ERA-40 re-analysis. *Q. J. R. Meteorol. Soc.* **131**: 2961–3012. doi: 10.1256/qj.04.176.
van Loon H, Rogers JC. 1978. The seesaw in winter temperatures between Greenland and northern Europe. Part I: General description. *Mon. Wea. Rev.* **106**: 296–310.
Vitolo R, Stephenson DB, Cook IM, Mitchell-Wallace K. 2009. Serial clustering of intense European storms. *Meteorol. Z.* **18**: 411–424.
Walker GT. 1924. Correlations in seasonal variations of weather, IX. *Mem. India Meteorol. Dept.* **24**: 275–332.
Wallace JM, Gutzler DS. 1981. Teleconnections in the geopotential height field during the Northern Hemisphere winter. *Mon. Wea. Rev.* **109**: 784–812.
Wang CC, Rogers JC. 2001. A composite study of explosive cyclogenesis in different sectors of the North Atlantic. Part I: Cyclone structure and evolution. *Mon. Wea. Rev.* **129**: 1481–1499.
Wanner H, Bronnimann S, Casty C, Gyalistras D, Luterbacher J, Schmutz C, Stephenson DB, Xoplaki E. 2001. North Atlantic Oscillation – concepts and studies. *Surv. Geophys.* **22**: 321–382.
Wernli H, Dirren S, Liniger MA, Zillig M. 2002. Dynamical aspects of the life-cycle of the winter storm 'Lothar' (24–26 December 1999). *Q. J. R. Meteorol. Soc.* **128**: 405–429.
Woollings T, Hoskins B, Blackburn M, Berrisford P. 2008. A new Rossby Wave-breaking interpretation of the North Atlantic Oscillation. *J. Atmos. Sci.* **65**: 609–626.
Woollings T, Pinto JG, Santos JA. 2011. Dynamical evolution of North Atlantic ridges and poleward jet stream displacements. *J. Atmos. Sci.* **68**: 954–963.

Supplementary Material for

Rossby Wave-Breaking analysis of Explosive Cyclones in the Euro-Atlantic sector

Quarterly Journal of the Royal Meteorological Society

Figure S1. Scatter plot of cyclone populations (NDR vs. maximum Laplacian of pressure).

Figure S2. Mean maximum Laplacian of pressure of cyclone populations.

Figure S3. Mean NDR of cyclone populations.

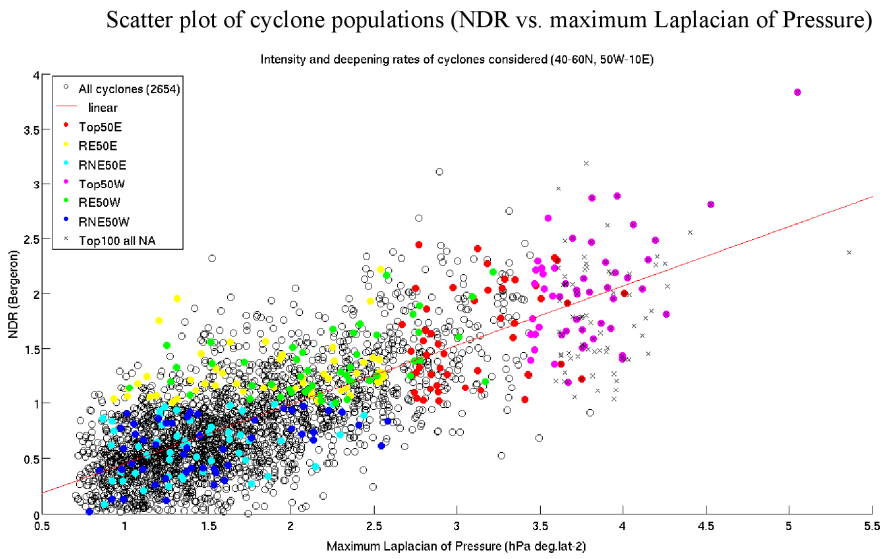

Figure S1. Scatter plot of cyclone populations (NDR vs. maximum Laplacian of pressure)

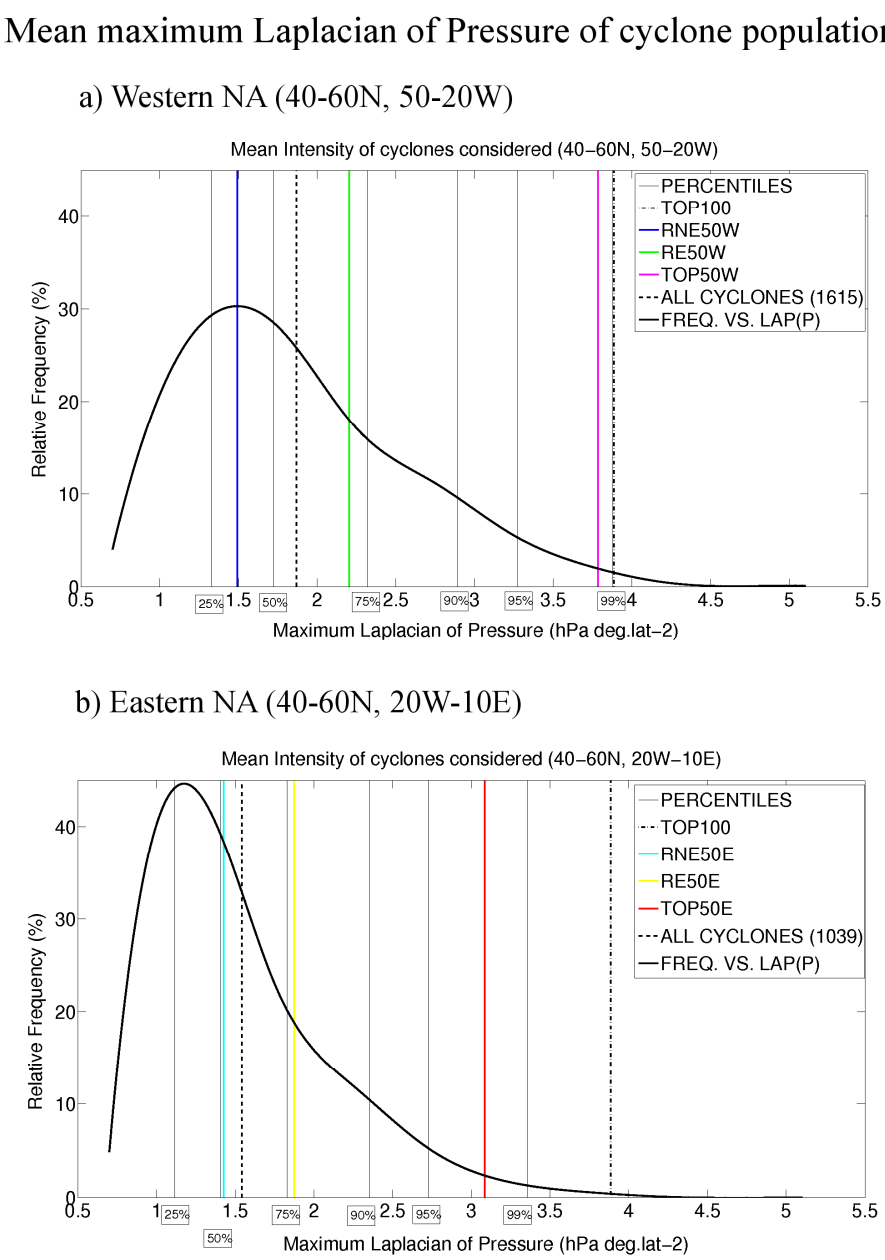

Figure S2. Mean maximum Laplacian of pressure of cyclone populations.

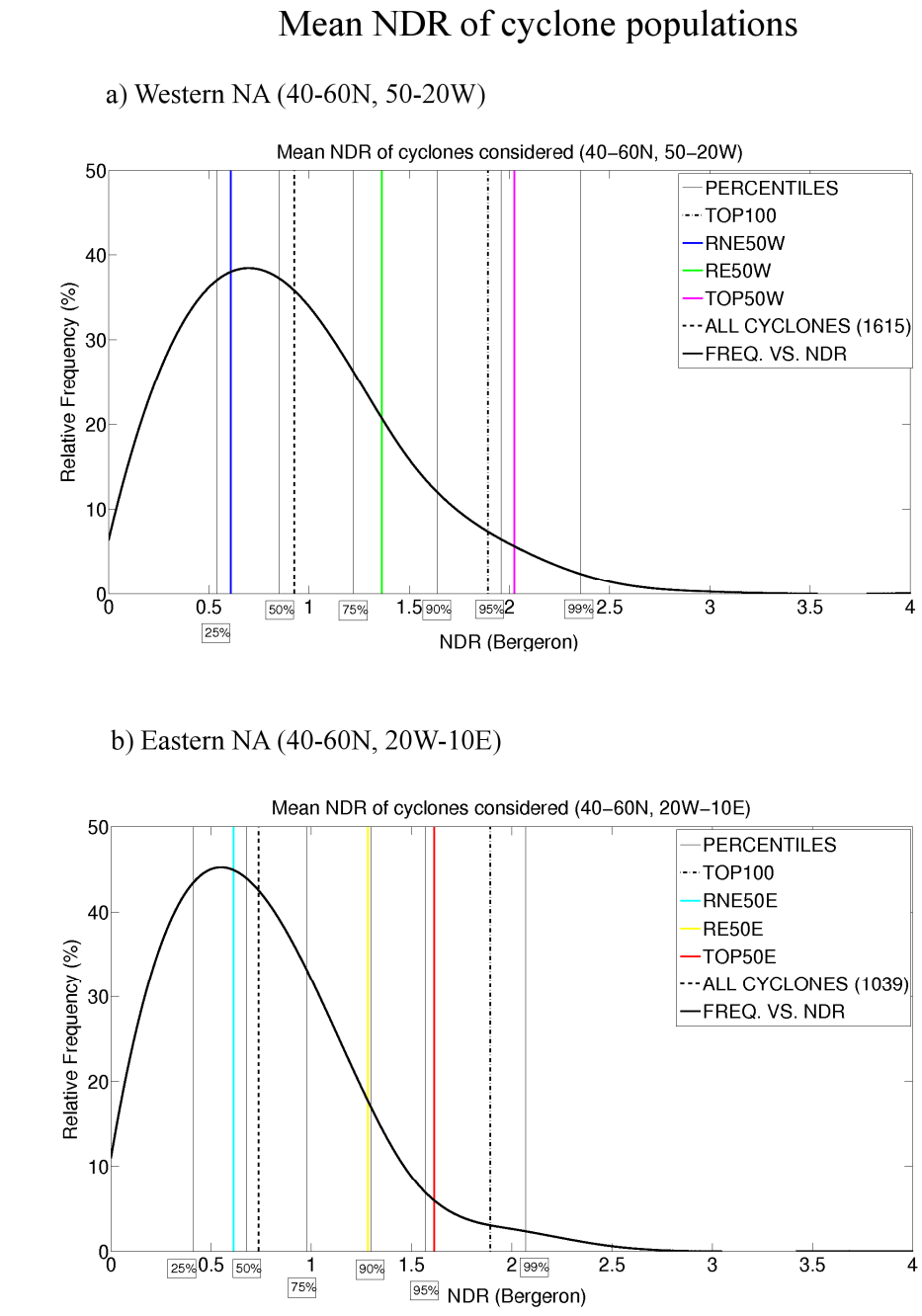

Figure S3. Mean NDR of cyclone populations.

3. Large-scale dynamics associated with clustering of extratropical cyclones affecting Western Europe

Abstract: Some recent winters in Western Europe have been characterized by the occurrence of multiple extratropical cyclones following a similar path. The occurrence of such cyclone clusters leads to large socio-economic impacts due to damaging winds, storm surges, and floods. Recent studies have statistically characterized the clustering of extratropical cyclones over the North Atlantic and Europe and hypothesized potential physical mechanisms responsible for their formation. Here we analyze 4 months characterized by multiple cyclones over Western Europe (February 1990, January 1993, December 1999, and January 2007). The evolution of the eddy driven jet stream, Rossby wave-breaking, and upstream/downstream cyclone development are investigated to infer the role of the large-scale flow and to determine if clustered cyclones are related to each other. Results suggest that optimal conditions for the occurrence of cyclone clusters are provided by a recurrent extension of an intensified eddy driven jet toward Western Europe lasting at least 1 week. Multiple Rossby wave-breaking occurrences on both the poleward and equatorward flanks of the jet contribute to the development of these anomalous large-scale conditions. The analysis of the daily weather charts reveals that upstream cyclone development (secondary cyclogenesis, where new cyclones are generated on the trailing fronts of mature cyclones) is strongly related to cyclone clustering, with multiple cyclones developing on a single jet streak. The present analysis permits a deeper understanding of the physical reasons leading to the occurrence of cyclone families over the North Atlantic, enabling a better estimation of the associated cumulative risk over Europe.

*Pinto JG, **Gómara** I, Masato G, Dacre HF, Woollings T, and Caballero R (2014) Large-scale dynamics associated with clustering of extratropical cyclones affecting Western Europe, J. Geophys. Res. Atmos., 119, 13704–13719, doi:10.1002/2014JD022305*

AGU PUBLICATIONS

JGR

Journal of Geophysical Research: Atmospheres

RESEARCH ARTICLE
10.1002/2014JD022305

Key Points:
- Analysis of physical mechanisms leading to cyclone clusters affecting Europe
- Recurrent extension of an intensified jet toward Europe leads to clustering
- Upstream secondary cyclogenesis is also strongly related to cyclone clustering

Supporting Information:
- Readme
- Figures S1–S8 and Table S1

Correspondence to:
J. G. Pinto,
j.g.pinto@reading.ac.uk

Citation:
Pinto, J. G., I. Gómara, G. Masato, H. F. Dacre, T. Woollings, and R. Caballero (2014), Large-scale dynamics associated with clustering of extratropical cyclones affecting Western Europe, *J. Geophys. Res. Atmos.*, *119*, 13,704–13,719, doi:10.1002/2014JD022305.

Received 12 JUL 2014
Accepted 20 NOV 2014
Accepted article online 25 NOV 2014
Published online 19 DEC 2014

Large-scale dynamics associated with clustering of extratropical cyclones affecting Western Europe

Joaquim G. Pinto[1,2], Iñigo Gómara[3], Giacomo Masato[1], Helen F. Dacre[1], Tim Woollings[4], and Rodrigo Caballero[5]

[1]Department of Meteorology, University of Reading, Reading, UK, [2]Institute for Geophysics and Meteorology, University of Cologne, Cologne, Germany, [3]Departamento de Geofísica y Meteorología and Instituto de Geociencias (IGEO), Universidad Complutense de Madrid, Madrid, Spain, [4]Atmospheric, Oceanic and Planetary Physics, Department of Physics, University of Oxford, Oxford, UK, [5]Department of Meteorology and Bert Bolin Centre for Climate Research, Stockholm University, Stockholm, Sweden

Abstract Some recent winters in Western Europe have been characterized by the occurrence of multiple extratropical cyclones following a similar path. The occurrence of such cyclone clusters leads to large socio-economic impacts due to damaging winds, storm surges, and floods. Recent studies have statistically characterized the clustering of extratropical cyclones over the North Atlantic and Europe and hypothesized potential physical mechanisms responsible for their formation. Here we analyze 4 months characterized by multiple cyclones over Western Europe (February 1990, January 1993, December 1999, and January 2007). The evolution of the eddy driven jet stream, Rossby wave-breaking, and upstream/downstream cyclone development are investigated to infer the role of the large-scale flow and to determine if clustered cyclones are related to each other. Results suggest that optimal conditions for the occurrence of cyclone clusters are provided by a recurrent extension of an intensified eddy driven jet toward Western Europe lasting at least 1 week. Multiple Rossby wave-breaking occurrences on both the poleward and equatorward flanks of the jet contribute to the development of these anomalous large-scale conditions. The analysis of the daily weather charts reveals that upstream cyclone development (secondary cyclogenesis, where new cyclones are generated on the trailing fronts of mature cyclones) is strongly related to cyclone clustering, with multiple cyclones developing on a single jet streak. The present analysis permits a deeper understanding of the physical reasons leading to the occurrence of cyclone families over the North Atlantic, enabling a better estimation of the associated cumulative risk over Europe.

1. Introduction

Extratropical cyclones generated in the North Atlantic storm track play a dominant role in determining the weather and climate of Western Europe. A comprehensive understanding of the controls on cyclone paths and characteristics is thus essential in order to interpret and predict the regional weather and climate [*Lamb*, 1991; *Neu et al*., 2013]. Cyclones are responsible for a large part of continental precipitation, with a contribution of 70–85% for Western and Central Europe in winter [*Hawcroft et al*., 2012], and they can cause wind damage and flooding both in coastal and inland areas [e.g., *Fink et al*., 2009; *Pfahl and Wernli*, 2012]. Intense extratropical cyclones are in fact the primary natural hazard affecting Western and Central Europe [e.g., *Della-Marta et al*., 2010; *Schwierz et al*., 2010; *Haylock*, 2011].

The winter of 2013/2014 in the North Atlantic and Europe was marked by the extremely frequent occurrence of cyclones, particularly in and around the British Isles. Over a period of about 2 months, this region was battered by a series of cyclones often occurring in quick succession and bringing strong winds, precipitation, and storm surges, leading to widespread property destruction and loss of life. Such a clustering of intense cyclones is not unprecedented: in 1990, Western Europe was affected by multiple cyclones from late January until early March [*McCallum and Norris*, 1990; *Lamb*, 1991]. Other historical cyclone clustering series occurred in 1993, 1999, and 2007 [e.g., *Ulbrich et al*., 2001; *Klawa and Ulbrich*, 2003; *Fink et al*., 2009]. Cyclone clusters are of particular concern for the insurance industry, as very high cumulative losses are incurred within the same season, placing great financial stress on insurers (insured losses due to the storm series of 1990, 1999, and 2007 were estimated at $10, $18, and $10 billion [*MunichRe*, 2010]).

Several recent studies have analyzed the serial clustering of extratropical cyclones from a statistical perspective [e.g., *Mailier et al*., 2006; *Vitolo et al*., 2009; *Pinto et al*., 2013; *Blender et al*., 2014]. These papers all show that serial clustering occurs more frequently over the eastern North Atlantic and Western Europe than would be expected by chance (Poisson process), suggesting that specific dynamical mechanisms may actively favor the occurrence of clusters. However, there has been little systematic investigation into the nature of such mechanisms so far. In this paper, we take a first step in this direction. We aim to characterize the large-scale atmospheric conditions associated with cyclone clustering and to explore how these conditions lead to this process. The following physical mechanisms have been conjectured in the literature in association with cyclone clustering [e.g., *Mailier et al*., 2006; *Hanley and Caballero*, 2012]: (i) the steering by the large-scale flow, (ii) secondary cyclogenesis of upstream developments on the trailing fronts of previous systems. Additionally, we consider a third hypothesis, (iii) downstream development of cyclones due to Rossby wave dispersion [*Simmons and Hoskins*, 1979].

The trajectories and intensity of extratropical cyclones over the North Atlantic and Europe are known to be affected by large-scale modes of variability, particularly the North Atlantic Oscillation [e.g., *Raible*, 2007; *Bader et al*., 2011; *Gómara et al*., 2014b]. For example, intense cyclones affecting Western Europe primarily occur when the eddy driven jet is (a) intensified and (b) extended toward Europe [*Pinto et al*., 2009; *Hanley and Caballero*, 2012]. Such conditions are typically associated with the occurrence of Rossby wave-breaking (RWB) on both sides of the jet, which intensifies the jet and constrains its location [*Hanley and Caballero*, 2012; *Gómara et al*., 2014a]. The relationship between the large-scale patterns (e.g., North Atlantic Oscillation) and cyclone clustering has been analyzed, e.g., by *Mailier et al*. [2006] using regression models. We hypothesize that the persistence of such large-scale conditions may lead to the steering and amplification of sequences of extratropical cyclones toward Western Europe.

Upstream growth of cyclones can lead to the occurrence of cyclone "families" (trains of cyclones with interrelated development). Such families can occur when multiple unstable waves develop and move rapidly along the trailing front in the wake of a large "parent" low [e.g., *Bjerknes and Solberg*, 1922], leading to secondary frontal cyclogenesis [e.g., *Parker*, 1998; *Rivals et al*., 1998]. Alternatively, cyclone families can be associated with downstream development, in which cyclogenesis occurs eastward of the parent cyclone due to Rossby wave dispersion [*Simmons and Hoskins*, 1979; *Chang*, 1993]. We aim to investigate the relationship between upstream and downstream development mechanisms in the formation of cyclone clusters.

In this paper, we employ an objective algorithm to detect clusters of extratropical cyclones in reanalysis data spanning the past three decades. We characterize the associated large-scale flow conditions, including jet intensity and location and Rossby wave-breaking activity. We then focus on four recent periods of cyclone clustering to study the specific mechanisms described above, namely, February 1990, January 1993, December 1999, and January 2007. Our goal in this exploratory study is not to definitively establish the dominance of any particular mechanism but rather to assess to what extent each mechanism is consistent with the observed behavior during these four periods.

The structure of the paper is as follows: Section 2 describes data and methods, while section 3 presents the selection of the periods of cyclone clustering. In section 4 the four selected months are evaluated in terms of jet intensity and location, cyclone tracks, and Rossby wave-breaking. Section 5 identifies the common features of the analyzed months in section 4 and presents a conceptual model of cyclone clustering. The summary and discussion section concludes the paper.

2. Data and Methods

The European Centre for Medium-Range Weather Forecasts Interim Re-Analysis (ERA-Interim) data set [*Dee et al*., 2011] is used. The horizontal resolution of the data set is T255 (approximately $0.75° \times 0.75°$ longitude/latitude), with 60 vertical levels from surface up to 0.1 hPa. The period considered is December to February 1980–2012 (at 6-hourly resolution).

In this study a two-dimensional RWB index from *Masato et al*. [2013a] is used, defined on the potential temperature (θ) on the dynamical tropopause (2 Potential Vorticity Units (PVU) $= 2 \times 10^{-6}$ K m^2 kg^{-1} s^{-1} surface). The temporal resolution of the index is daily (6-hourly θ fields are averaged into daily means) and the horizontal resolution is $4.5° \times 1.125°$ longitude/latitude. The index provides local-instantaneous occurrence

(*B* index) and direction of breaking (*DB* index) of large-scale RWB events (thin θ "streamers" are disregarded). The *B* index identifies regions where the mean meridional gradient of θ is reversed: if *B* is positive at a grid point, then RWB is detected at that location and time frame. Following *Gómara et al.* [2014a], no duration condition is imposed, as the focus is on instantaneous RWB. The *DB* index identifies the direction of breaking: positive and negative values of *DB* (above and below a threshold of +0.2 and −0.2) are identified as anticyclonic and cyclonic events, respectively. For further details on the RWB index, see *Pelly and Hoskins* [2003] and *Masato et al.* [2013a].

In order to identify single- and double-sided RWB events, a simple algorithm has been applied to daily two-dimensional maps (longitude versus latitude). For each day, the probability density function (PDF) of the latitude has been calculated for all grid points in the two-dimensional grid (40°W–10°E, 20°N–70°N) associated with a positive *B* index. A local maximum identification algorithm is then applied to identify the peaks of the distribution. If the distribution is bimodal, and both peaks are above a given threshold and apart by at least 20° in latitude, then the latitudes of these two peaks are retained as the locations of the double-sided RWB. If the distribution has only a single peak, the associated latitude is the location of the single-sided RWB. To exclude smaller RWBs, only the peaks exceeding a given threshold have been retained. The threshold is set as the total area underneath the PDF (i.e., the total number of *B* positive values) divided by the number of bins (i.e., the number of intervals along the *x* axis, which represents latitude values). In addition, the threshold for the single-sided RWB has been further multiplied by a factor of 5 in order to retain extensive single-sided breakings, which may likely influence the large-scale dynamics.

A cyclone identification and tracking algorithm [*Murray and Simmonds*, 1991] is applied to ERA-Interim (0.75° × 0.75°) 6-hourly data to obtain cyclone statistics over the North Atlantic (80°W–40°E, 30°N–75°N). Extratropical cyclones are identified based on the Laplacian of mean sea level pressure (MSLP) ($\nabla^2 p$), an approximation of the geostrophic relative vorticity of the system. An assignment algorithm is used to compile tracks considering the most probable trajectory of the cyclones between subsequent time frames. Basic properties of the cyclone life cycles are thus obtained (e.g., the evolution of core pressure and propagation velocity). The methodology has been adapted for Northern Hemisphere cyclone characteristics and compares well with other cyclone identification and tracking methodologies [*Pinto et al.*, 2005; *Neu et al.*, 2013]. Following *Pinto et al.* [2009], developing cyclones are selected when they verify: (i) cyclone lifetime $\geq$ 24 h; (ii) minimum MSLP $<$ 1000 hPa; (iii) maximum $(\nabla^2 p) > 0.6$ hPa degree latitude^{-2}; and (iv) maximum $\frac{\mathrm{d}}{\mathrm{d}t}\nabla^2 p \geq 0.3$ hPa degree latitude^{-2} d^{-1}. The minimum MSLP of the cyclone surface center is used as indicator of intensity in this study (cf. section 3 for further information).

Zonal and meridional wind components are used at 00 UTC of each day to analyze the position and intensity of the North Atlantic eddy driven jet. Following *Woollings et al.* [2010], the jet location is based on daily mean 850 hPa zonal wind. This choice of vertical level for the diagnostic enables a clear separation between the eddy driven jet (which extends throughout the depth of the troposphere) and the subtropical jet (which is confined to the upper troposphere). In order to focus on the eastern North Atlantic and Western Europe, the wind is averaged over the longitudes between 40°W and 10°E. The resulting field is subsequently low-pass filtered (Lanczos, 10 day cutoff frequency) and the latitudinal location of the maximum westerly wind speed is taken [cf. *Woollings et al.*, 2010]. Note that jet indices computed using 925–700 hPa provide very similar results. The choice of 40°W–10°E is justified by the focus on cyclones affecting Western Europe. The anomalies of the jet intensity are calculated by subtracting the winter (December–February, DJF) 850 hPa long-term mean.

Available weather charts from the UK Met Office are used to analyze the influence of surface fronts and secondary cyclogenesis on clustering events. The frontal positions displayed in the frontal analysis charts are made by forecasters using (i) model and observed parameters such as temperature, wind shifts, dew point, cloud cover, cloud types, visibility, and lines in precipitation patterns and (ii) (post-2000 only) an automated frontal identification algorithm based on gradients of wet-bulb potential temperature [*Hewson*, 1997, 1998]. Thus, some subjectivity is present in the frontal analysis. To relate the frontal positions with reanalysis data, the frontal positions are reprojected onto a regular latitude/longitude grid. Historical storm names are obtained from the *Freie Universität* Berlin.

Finally, daily averaged *u* and *v* winds at 300 hPa (2.5° × 2.5°) from the National Centers for Environmental Prediction (NCEP) reanalysis data [*Kalnay et al.*, 1996] are used for the Hövmoller diagrams (section 5).

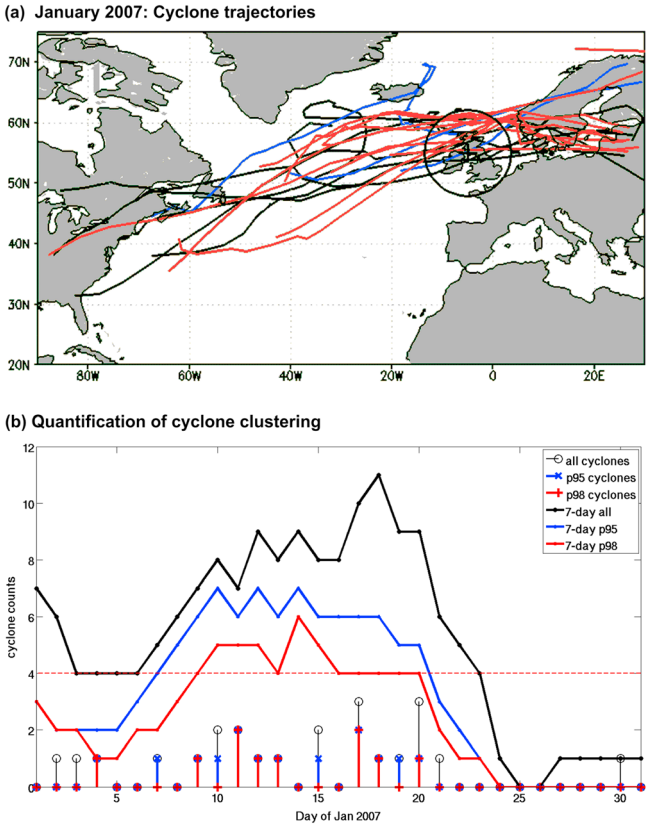

Figure 1. (a) Trajectories of all (black lines), p95 (blue lines), and p98 (red lines) cyclones crossing the circle detection area ((55°N, 5°W), $r = 700$ km) during January 2007. (b) All, p95, and p98 cyclone counts in January 2007 per calendar day (stems, see legend). Solid lines: 7 day running sums of cyclone counts. Dashed red line: threshold defined for clustering detection (four cyclones within 7 days).

3. Selection of Clustering Periods Within ERA-Interim

Identification of clustering events over Western Europe is carried out for the winter months (DJF 1980–2012). For this purpose, cyclone tracks are detected in a circular area covering the British Isles at the time where its location is nearest to the circle center (central position (55°N, 5°W), radius = 700 km). Figure 1a shows the detection area with the location of the January 2007 cyclone tracks overlaid. The cyclones tracking through the circular area are shown in three colors: red tracks indicate cyclones whose minimum core pressure within this area is below the climatological second MSLP percentile (p98 cyclones, 2% most intense) at (55°N, 5°W), blue tracks are cyclones whose core pressure is below the fifth percentile (p95, 5% most intense), and black tracks depict the remaining cyclones (all).

The method captures the majority of cyclones affecting the British Isles (Figure 1a). Further cyclones could easily be included if the area was slightly shifted south/north but obviously at the cost of losing other cyclones. The sensitivity of the results to the central position of the circular area (55°N, 5°W) has been investigated. Different locations between 45°N and 65°N with 5° increments along 5°W were tested and little difference in the major clustering periods was identified (not shown). Regarding the choice of radius (700 km), we have followed *Pinto et al.* [2013] which analyzed the sensitivity of the detection method to the choice of radius. Values between 400 and 1000 km were tested as this interval encompasses the typical range of effective radius for extratropical cyclones (computed following *Simmonds* [2000] and *Simmonds and Keay* [2000]). This range typically starts at 600 km and sometimes reaches 1000 km [*Rudeva and Gulev*, 2007]. *Pinto et al.* [2013] selected the value of 700 km as this choice of radius corresponds to a plateau of quasi-constant values of dispersion statistic (a measure of clustering), with small changes both to larger and smaller radii over most of the study area (their Figure S1).

In Figure 1b the daily counts of all, p95, and p98 cyclones in January 2007 are shown as stems. The occurrence of cyclone clustering events is quantified using a 7 day running sum of the daily counts (colored lines). A threshold of four or more consecutive cyclones within 7 days (dashed black line) is set to identify clustering periods.

Using these criteria, a period of 12 clustering days for p98 cyclones (9–20 January, red line) is identified, with a total of nine cyclones. If the criteria is used for p95 cyclones (blue line), the clustering period has a length of 14 days (7–20 January) including 14 p95 cyclones. For the other selected periods, either long clustering periods (e.g., 26 January to 5 February 1990 at the p95/p98 level) or multiple clustering periods (e.g., 6, 8–14, and 22–27 December 1999) are identified (see Table 1 for details). The values associated with the clustering periods (length, recurrence, and cyclones involved) are remarkable compared with climatology and rank among the top positions. Although January 1993 also presents above average values, cyclones over that

Table 1. Characterization of the Four Main Periods of Clustering[a]

	Clustering Periods		Length (Days)		Cyclone Counts per Event		Clustering Days per Month (%)	
	p95	p98	p95	p98	p95	p98	p95	p98
Jan 2007	7–20	9–20	**14**[4]	**12**[2]	**14**[3]	**9**[2]	**45.16**[4]	**38.71**[1]
Dec 1999	6		1		4		**45.16**[5]	19.35
	8–14		7		7			
	22–27	22–27	6	6	4	4		
Jan 1993	10–18	18	9	1	10	4	29.03	3.23
Feb 1990	26 Jan to 5 Feb	26 Jan to 5 Feb	**11**[9]	**11**[3]	**12**[5]	**12**[1]	**42.48**[6]	**24.78**[6]
	10	10	1	1	4	4		
	14	14	1	1	4	4		
	24 Feb to 2 Mar		7		6			
Climatology	Total 63	Total 43	6.03	4.46	6.86	5.46	13.16	6.65

[a]Top 10 rankings of clustering properties among each class (p95, p98 cyclones) during the whole base period (DJF 1980–2012) are highlighted in bolds and provided with superscripts. For more details, see text.

month mostly tracked further north and are thus not counted by the method. For p95 (p98) cyclones, the 1980–2012 winter long-term mean of the 7 day running sum is 1.36 (0.85) cyclones per week and the selected events represent approximately 13.16%—corresponding to 380 days (6.65%—corresponding to 192 days) of the total base period (2888 days). The total number of identified clustering events by the algorithm is 63 (43), which corresponds to 1.97 (1.34) per winter (DJF) season, with a mean length of 6.03 (4.46) days for p95 (p98) cyclones. The total number of p95 (p98) cyclones is 567 (355).

4. Characterization of Clustering Periods

The large-scale flow is analyzed during the four selected months (January 2007, December 1999, January 1993, and February 1990). In Figure 2, the jet stream latitude (black solid line) and speed anomalies (shadings) for the 850 hPa level averaged over the eastern North Atlantic (40°W–10°E) are shown. An intensified and quasi-stationary jet is observed for extended periods during each of the 4 months. This configuration is known to foster rapid intensification of individual cyclones affecting Europe [*Hanley and Caballero*, 2012; *Gómara et al.*, 2014a], as the strong upward motion of air at the right-entrance and left-exit regions of the jet core seems to promote rapid storm amplification [e.g., *Uccellini*, 1990; *Rivière and Joly*, 2006a, 2006b]. In addition, the unusual persistence of the jet location (up to 2 weeks) and its positive speed anomalies (significant values in stippling) may foster the development of multiple cyclones and thus be related to the serial windstorm clustering over Western Europe, as conditions promoting strong cyclone intensification endure for long time periods.

The influence of RWB in modulating the jet state and promoting cyclone clustering is investigated in detail for the period 6–20 January 2007. This is illustrated in Figure 3, where daily fields of θ on the dynamical tropopause (2 PVU surface shadings; 00 UTC), jet intensity at 250 hPa (dashed contours; 00 UTC) and RWB occurrence ($B > 0$; hatched fields) are provided with p95 cyclone tracks overlaid (solid lines). When known, the names of the major cyclones are provided at the top of each subpanel.

During the period of 6–20 January 2007, a cluster of cyclones (Franz, Gerhard and Hanno; 9–13 January) is characterized by two strong and consecutive large-scale anticyclonic RWB episodes over the subtropical eastern North Atlantic. In particular, the second anticyclonic event (12 January) is accompanied by large-scale cyclonic RWB to the north of the jet. Two additional and smaller scale cyclonic RWB events (likely associated with Cyclones Gerhard and Franz, respectively) can also be observed in the θ field south east of Greenland and west of Scandinavia on the same day (cf. Figure 3). These two small-scale RWB events exert some local influence on the northernmost part of the jet (not shown) but do not appear to be the main contributors of the current large-scale configuration. This is also the reason that we imposed a strict criterion on the identification of large-scale RWBs, which are particularly efficient in driving and constraining the westerly flow in the midlatitudes [*Orlanski*, 2003].

Next, a period of single-sided (poleward) RWB follows (13–16 January), and finally, a second cluster of cyclones (Kyrill and Lancelot; 17–20 January) also corresponds to two simultaneous large-scale RWBs (north cyclonic and south anticyclonic) which tighten the jet from both flanks and extend it toward Western Europe. For comparison purposes, a similar analysis is performed for the periods 22–30 December 1999 (Figure S1 in

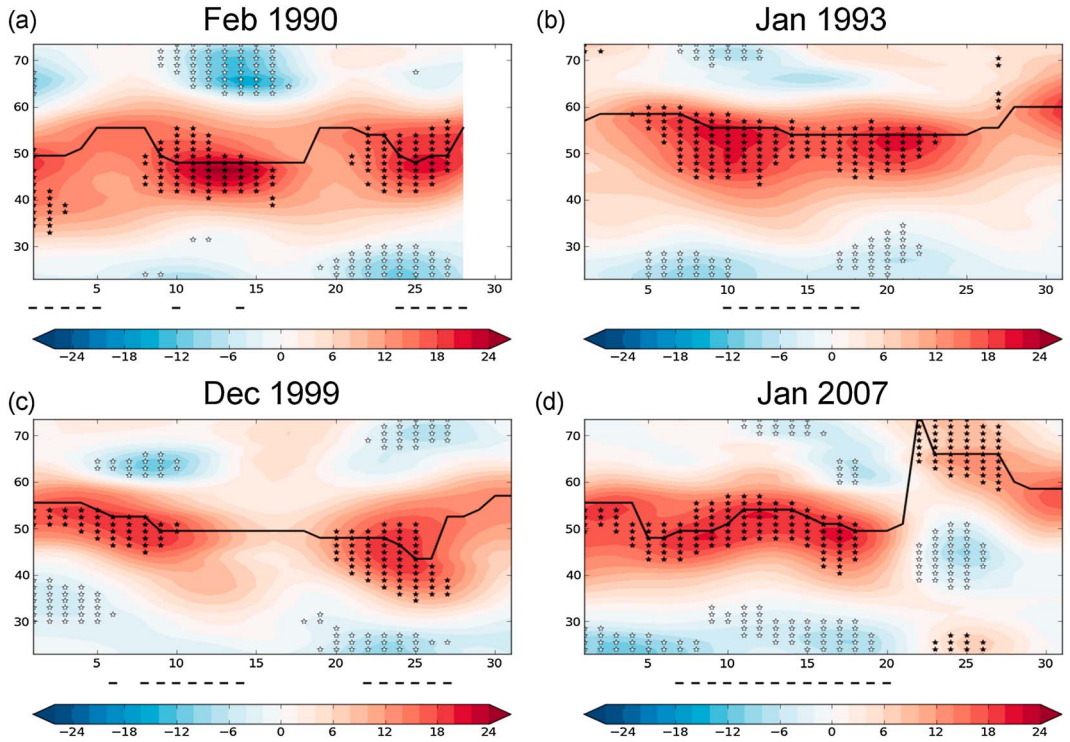

Figure 2. Jet stream (40°W–10°E) latitude (line, degrees north) and intensity at 850 hPa (colors, as anomalies to long-term mean in m s^{-1}) for February 1990, January 1993, December 1999, and January 2007, *x* axis corresponds to calendar days. Cyclone clustering periods (p95 cyclone counts) are marked by black dashed lines below each subpanel. Values above 90%/below 10% centiles are dotted (red dotted areas mean "jet significantly stronger than usual").

the supporting information), 1–30 January 1993 (Figure S2), and 1–28 February/1–2 March 1990 (Figure S3). These figures strongly suggest that the occurrence of strong, large-scale RWB events on both sides of the jet is a common feature in all clustering periods.

This phenomenon is quantified in Figure 4, where RWB amplitude (represented by the positive values in Figure 4) is averaged over (40°W–10°E) for the same periods, and the stippling indicates where the wave-breakings occur. The relative position of the RWB with respect to the jet location (black solid line) can also be inferred. For a large fraction of the considered 4 months, extensive RWB events are identified respectively to the north and to the south of the jet. The double-sided RWB periods show close correspondence to maximum positive jet speed anomalies (Figures 2a–2d). As an example, the RWB events in Figure 3 between 8 and 13 January and 16–20 January 2007 are well captured and lead to the intensified and quasi-stationary jet state reported above (Figures 2d and 4d). Nevertheless, it is important to note that the strong jet observed in Figures 2 and 4 (black solid line) is not completely stationary in time (see Figure 3 and Figures S1 to S3 for comparison), as the apparent quasi-stationarity arises from the time filtering of the wind data (cf. section 2). The recurrent occurrence of RWB events interacting with the jet at synoptic time scales (1 to 5 days) is the real cause for the emerging quasi-stationary.

Figure 5 shows the basic properties of the 850 hPa jet conditional on the occurrence of single- and double- sided RWB events and cyclone clustering for the whole reanalysis period. In Figures 5a and 5b the jet speed at 850 hPa and jet latitude probability density functions are composited considering the daily values of the two-sided RWB events. The uncertainty range is derived using a Monte Carlo method, with 100 simulations randomly extracting the data from each subsample, respectively. The total number of days considered for the long-term distribution (red) is 2876, from which 452 days exhibit double-sided RWBs (blue distribution), while the remaining 2424 do not exhibit double-sided RWB (green distribution). When compared against the climatology and nondouble-sided RWB events, the double-sided RWB events are

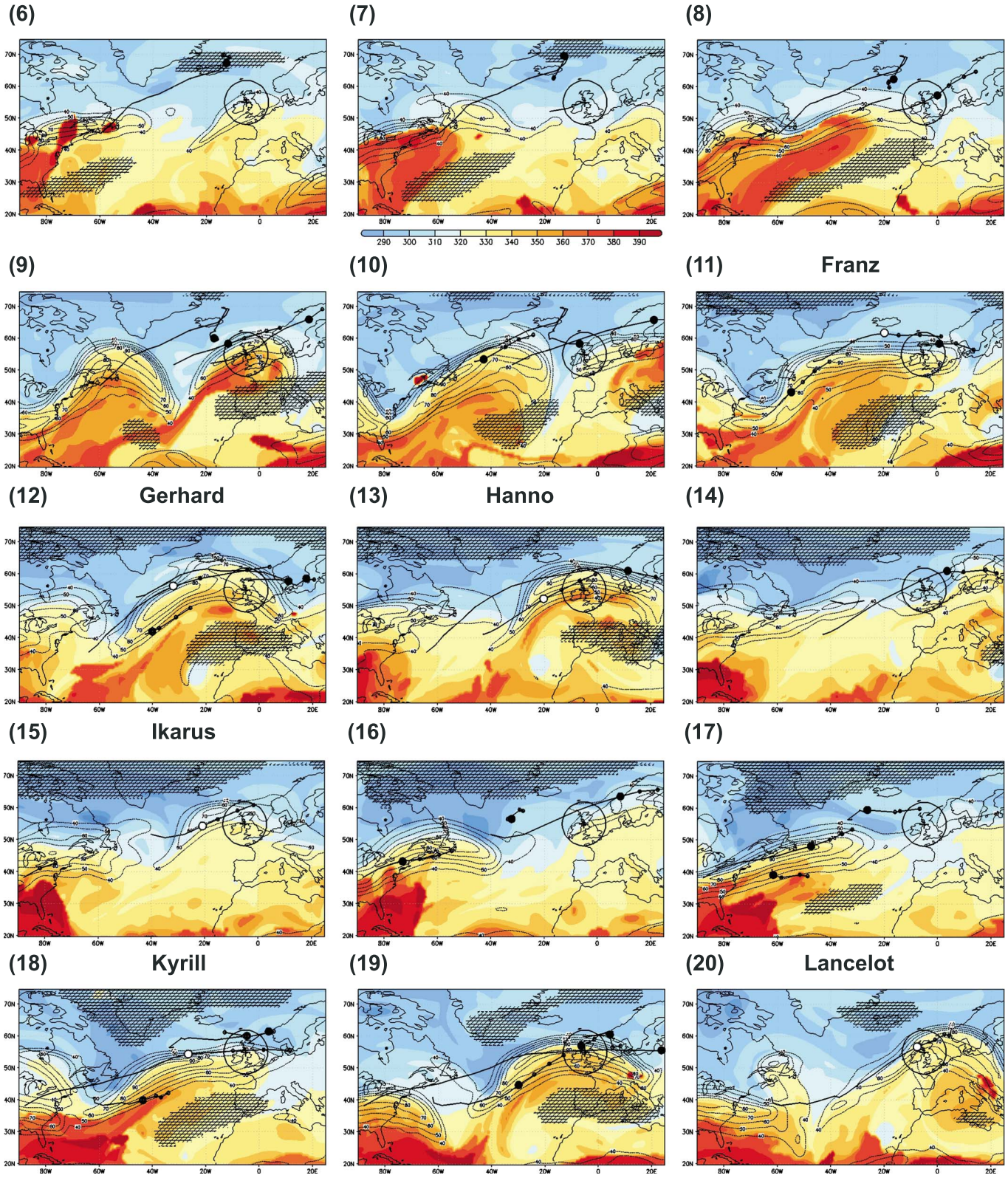

Figure 3. 6–20 January 2007. Red/blue shadings: θ on the 2 PVU surface in K (00 UTC). Hatched fields: daily RWB occurrence. Dashed contours: wind intensity at 250 hPa (m s^{-1}, 00 UTC), contours drawn from 40 m s^{-1} with 10 m s^{-1} contour intervals. Solid contour lines: Full p95 cyclone trajectories until 18 UTC of each day. Large filled black dots: Cyclone positions at 00 UTC. Small circles: three forthcoming cyclone positions on the same date. Large open white dots: Positions (00 UTC) of named historical storms crossing the detection area ((55°N, 5°W), r = 700 km) on that day.

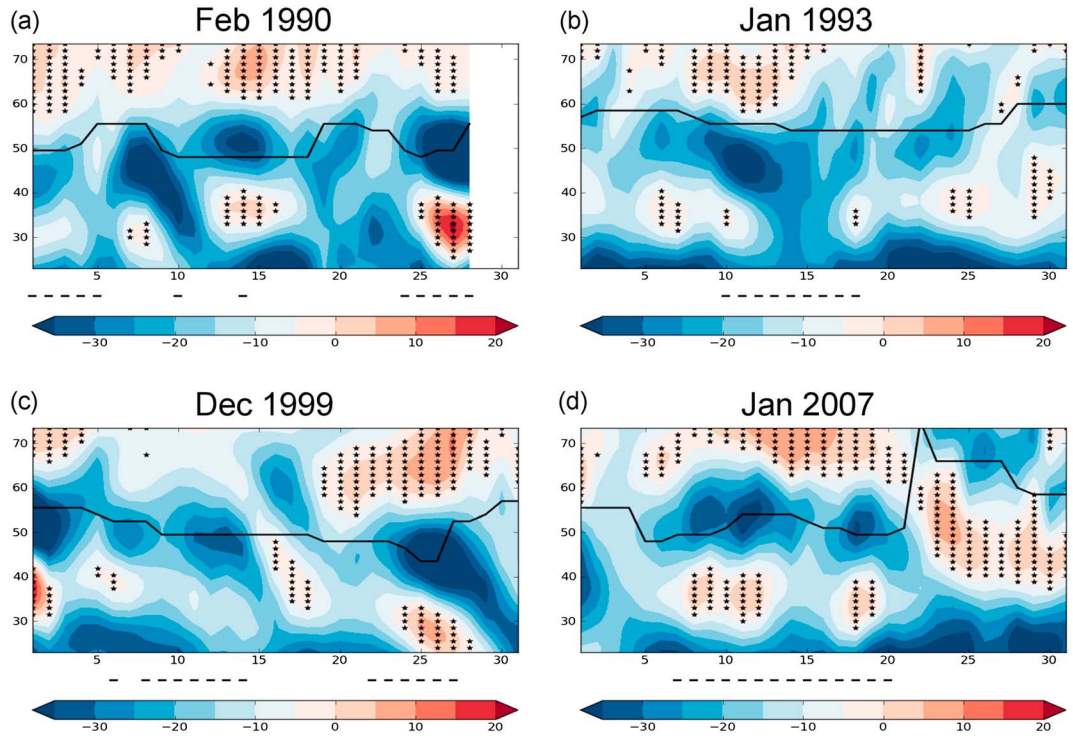

Figure 4. Jet stream (40°W–10°E) latitude (line, degrees north) for February 1990, January 1993, December 1999, and January 2007, the *x* axis corresponds to calendar days (as in Figure 2) and cyclone clustering periods (p95 cyclone counts) are marked by black dashed lines below each panel. The colors show the RWB amplitude (represented by positive values) averaged over (40°W–10°E). The black stippling indicates where the wave-breakings occur (see the text for more details).

associated with a stronger and more latitudinally constrained jet over Western Europe. Differences are up to 6 m/s and point to a more limited corridor for the jet location (45°N–55°N). Given the typical location for the occurrence of cyclonic (anticyclonic) RWB poleward (equatorward) of the eddy driven jet [e.g., *Gómara et al*., 2014a, Figures 1c and 1d], it is natural that the jet stream over the eastern North Atlantic is constrained within these latitudinal bounds if double-sided RWB occur.

In the lower panels (Figures 5c and 5d), the jet characteristics associated with the occurrence of clustering of p95 cyclones over the British Isles (55°N, 5°W) are illustrated (cf. section 3 and Figure 1). In general, the jet speed and latitudinal extent associated with these cyclones (380 of 2876 total days) are very similar to those of the double-sided RWB described above, which suggests a strong relationship between double-sided RWB and cyclone clustering. It should be pointed out that the two subsets are not entirely overlapping, as only 44% of the total storm clustering days are also characterized by the occurrence of the double-sided RWB. For this calculation a 2 day lead or lag between cyclone clustering and RWB dates is allowed (i.e., if within a 5 day period there is at least 1 day characterized by a two-sided RWB and 1 day characterized by cyclone clustering, then the central day of the period is labeled as a two-sided RWB). Also, the 29 February of every year are disregarded (thus the base period is here 2876 days instead of 2888 days). From the remaining 56%, 21% are characterized by one-sided RWB and 35% by no RWB (see Table S1). When considering the stronger (p98) cyclones as input, the number of overlapping dates increases from 44% to 48%, and the anomalous jet conditions are amplified (Figure S4 and Table S1). Here 20% of the remaining cases are characterized by one-sided RWB and 32% by no RWB. On the contrary, when considering the whole base period (DJF 1980–2012), the days without RWB clearly dominate (61% of days), and days with two-sided RWB events become rarer (16%, cf. Table S1). These numbers, together with the results in Figure 5, highlight the strong connection between double-sided RWB and cyclone clustering.

Some attention should also be paid to the effect that the clustering method itself introduces in the distributions in Figure 5. As the area of selection is a circle of 700 km radius, one might expect that the jet location (blue distribution in Figure 5d) is highly constrained around its center (55°N). According to *Mahlstein et al*. [2012], a jet

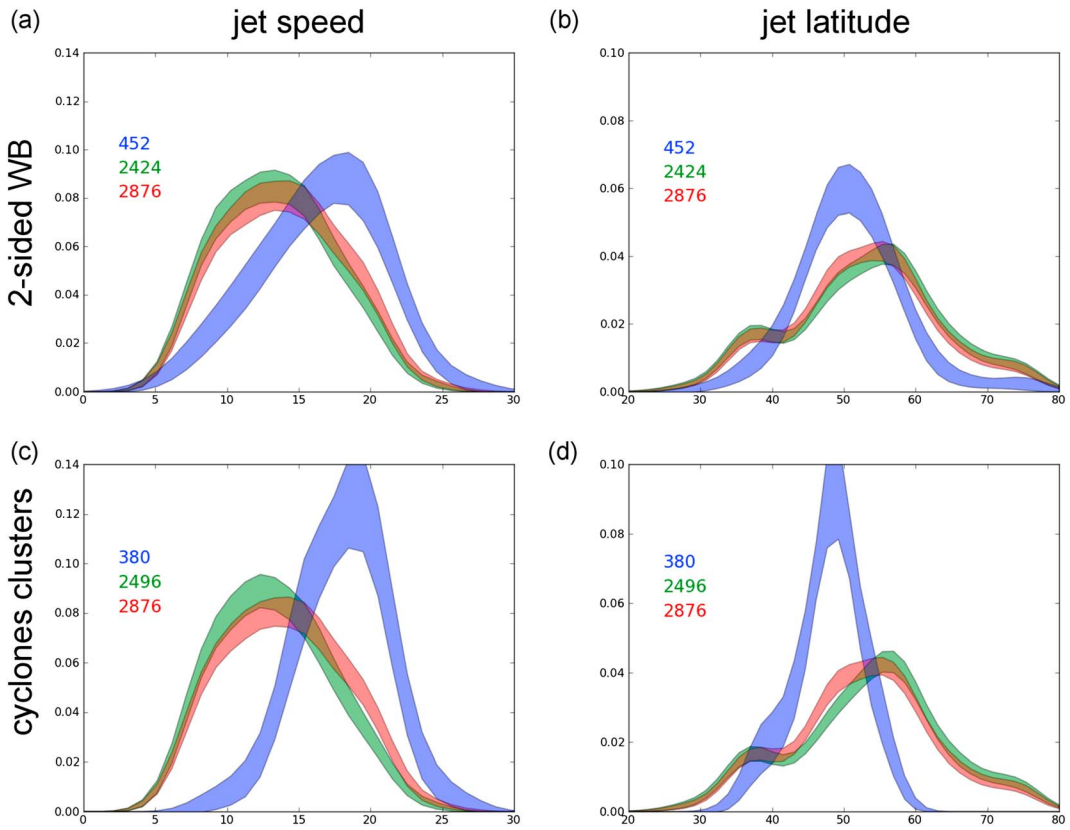

Figure 5. (a, b) Comparison for distributions with two-sided RWB (blue) versus other cases (green) and all cases (red) for low-pass filtered jet speed at 850 hPa (m s^{-1}) and jet latitude (degrees north), all for (40°W–10°E). (b, d) Same as above but for the occurrence of p95 cyclone clusters intercepting the detection area across the British Isles (55°N, 5°W). The uncertainty of the PDFs reflects the size of the data set it is associated with.

stream located around this latitude is associated with a higher chance of strong winds over the southern half of the British Isles, France, and Benelux countries. A sensitivity analysis for other latitudes than 55°N leads to comparable results for the latitude constraint, but with a slightly shifted peak of the jet distribution (not shown).

Figure 6 shows the vertical structure of the jet associated with cyclone clustering. The vertical cross section (1000–150 hPa) of the climatological jet averaged over (40°W–10°E) is shown in Figure 6a. The analogous composite for the jet associated with clustering of p95 cyclones is provided in Figure 6b and reveals very intense and latitudinally constrained upper level winds centered at 50°N with a strong signature at lower levels. In Figure 6c, the associated composite anomalies are calculated by subtracting the long-term mean. A very robust and barotropic jet structure is present at all pressure levels during clustering of p95 cyclones (5 and 95% confidence intervals in dashed contours using a Monte Carlo test of 1000 random iterations). Whereas positive anomalies are constrained around 45°N–50°N, negative anomalies are found in the ranges 25°N–30°N and 60°N–80°N. If more intense (p98) cyclones are considered, the positive jet anomalies are even stronger and more latitudinally constrained (Figure 6d). As suggested in previous studies [*Pinto et al.*, 2009; *Gómara et al.*, 2014a], a more intense jet over the eastern North Atlantic is related to enhanced baroclinicity both at upper and at lower levels and is consistent with increased storm activity.

5. Cyclone Clusters and Cyclone Families

In the previous section we have demonstrated the relationship between the large-scale flow conditions and cyclone clusters. In particular, the presence of an intense and persistent eddy driven jet is related to the occurrence of cyclone clusters over Western Europe. In this section, we investigate the relationship between selected cyclones over the Northeast Atlantic region (35°N–70°N, 15°W–20°E) within each cyclone cluster. This is done in order to enable the analysis of European windstorms following a similar path out of the

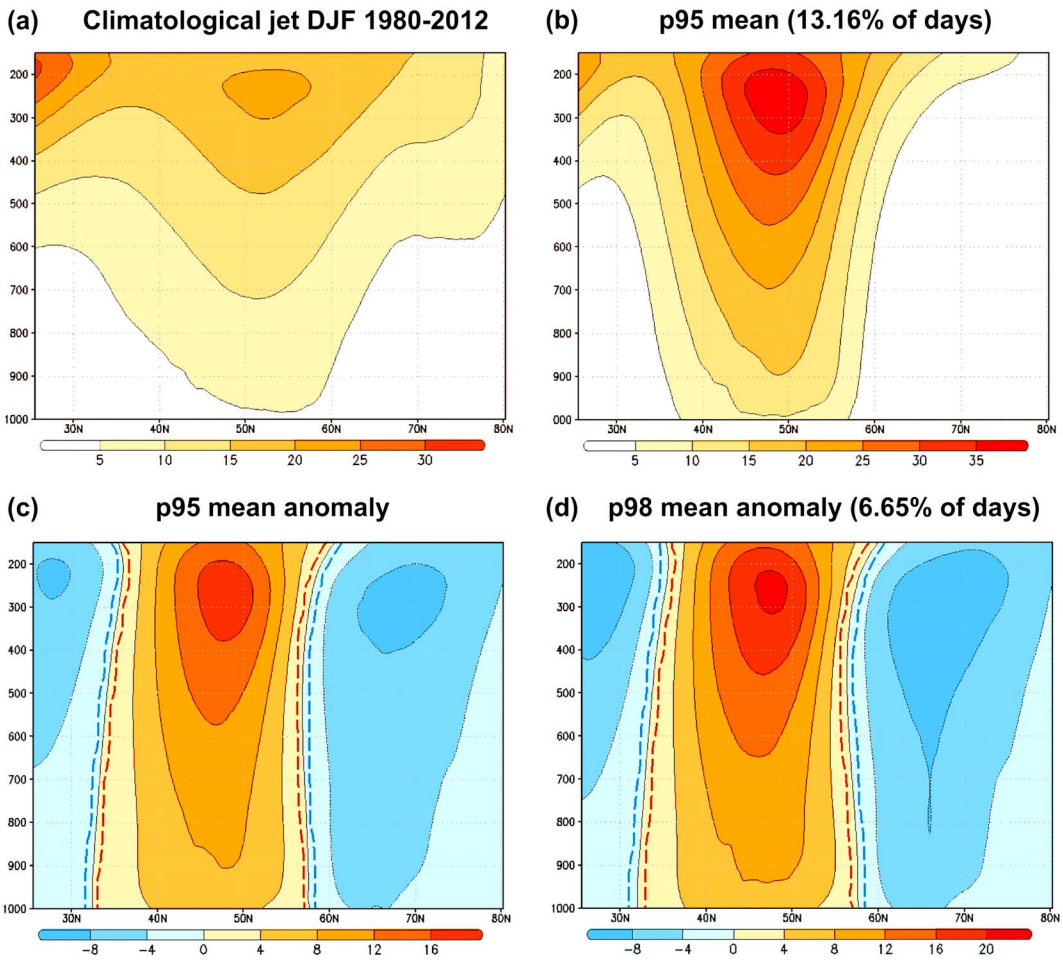

Figure 6. (a) Climatological jet (daily means): 1000 to 150 hPa pressure levels averaged over (40°W–10°E) in m s^{-1}; DJF 1980–2012. (b) Composite wind intensity during clustering dates of p95 cyclones on grid point (55°N, 5°W). (c) Same as Figure 6b but for the composite anomalies subtracting climatology. Marked with dashed red/blue contours are 5 and 95% Monte Carlo intervals (1000 random iterations). (d) Same as Figure 6c but for p98 cyclones.

detection area (e.g., Lothar and Martin, 25–28 December 1999; cf. section 3). We consider two mechanisms for linking the cyclones: (i) Upstream development of cyclones (secondary frontal cyclogenesis [e.g., *Parker*, 1998]), in which new cyclones are generated, e.g., on the trailing (cold) fronts of mature cyclones and (ii) downstream development of cyclones [e.g., *Simmons and Hoskins*, 1979], in which new cyclones form downstream (i.e., eastward) of existing cyclones due to Rossby wave dispersion.

Rather than attempting a climatological investigation, in this section we look for evidence of these two mechanisms in the 4 months focused on in this paper. The identification of a specific mechanism is contrasted with the null hypothesis that the development of cyclones within a cluster is mutually unrelated, even if they occur in quick succession, other than through the fact that they develop under the same strong, persistent, upper tropospheric jet.

Secondary frontal cyclones develop on the trailing fronts of preexisting cyclones. Although many observational and theoretical modeling studies have been carried out on the structure and evolution of secondary frontal cyclones, there is no objective method of differentiating them from other types of cyclones [*Parker*, 1998]. In general, primary frontal cyclones develop in large-scale baroclinic regions such as the polar frontal zone, where strong temperature gradients separate cold air of polar origin from tropical air. They have a typical life cycle of 3–4 days and a horizontal scale ~2000 km. Secondary frontal cyclones typically develop in more localized baroclinic regions such as the trailing cold fronts of preexisting frontal cyclones. They tend to be smaller in scale and develop over 1–2 days. Compared to primary cyclones, their

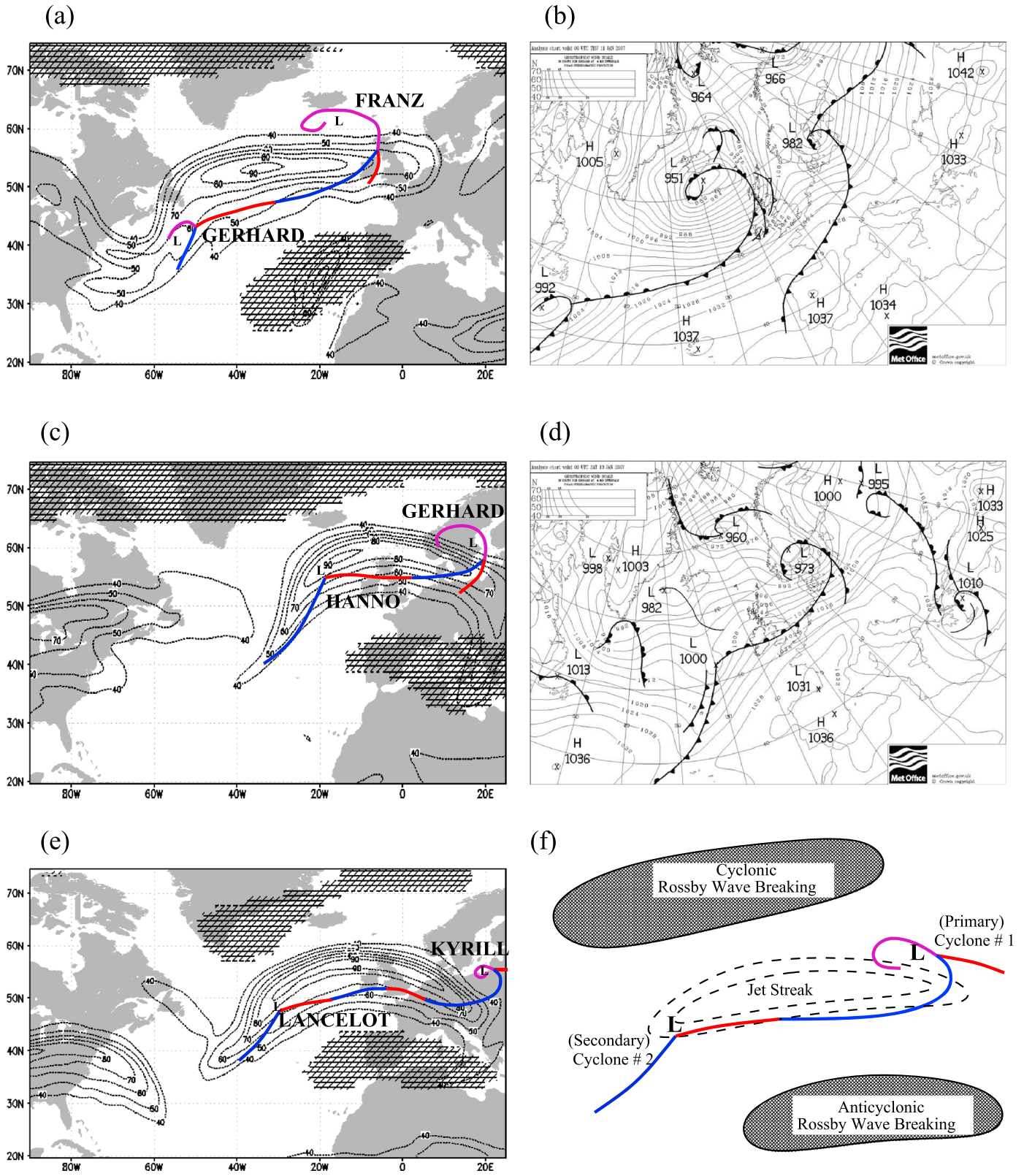

Figure 7. (a, c, and e) RWB occurrence ($B > 0$; hatched), wind intensity at 250 hPa (m s^{-1}; dashed contours drawn from 40 m s^{-1} with 10 m s^{-1} contour intervals), cyclone surface centers and fronts (from UK Met Office weather charts; red/blue/purple solid lines for warm/cold/occluded fronts) for 00 UTC on example dates 11, 13, and 19 January 2007. (b, d) Weather charts (00 UTC) on 11 and 13 January 2007. (f) Schematic summary showing relative positions of clustering cyclones with respect to jet streak location and location of RWB.

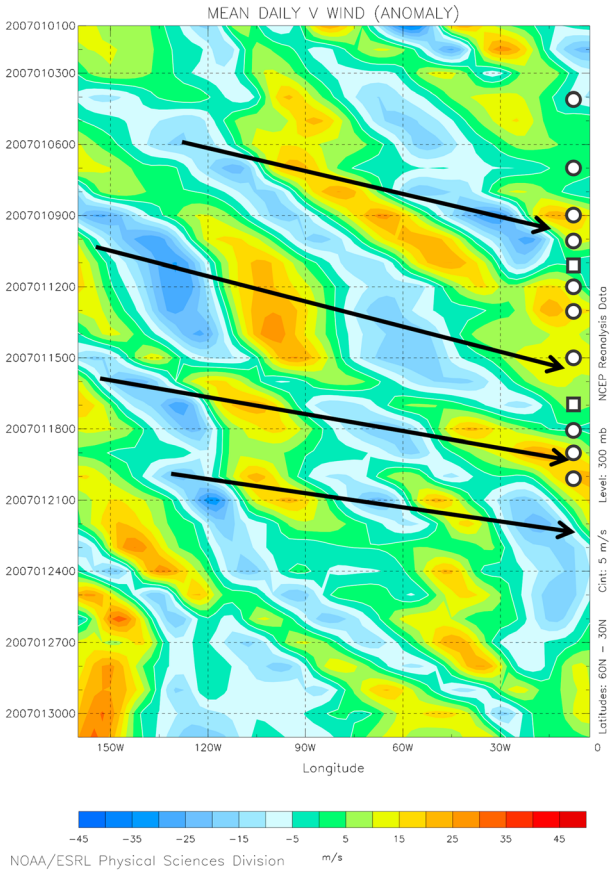

Figure 8. Hovmöller diagram of zonal wind daily speed anomalies at 300 hPa ($m\,s^{-1}$) for January 2007, averaged over latitude band to (30°N–60°N). The black arrows give subjective indications of the group velocity of some Rossby wave packets. Counts of p95 cyclones per day (see Figure 1a) crossing the meridian 5°W are provided in geometric forms (circles: one count per day; squares: two counts per day).

development is thought to be more influenced by nonbaroclinic mechanisms such as large-scale strain [*Dritschel et al.*, 1991; *Bishop and Thorpe*, 1994a, 1994b; *Renfrew et al.*, 1997; *Dacre and Gray*, 2006], frontal shear [*Chaboureau and Thorpe*, 1999; *Joly and Thorpe*, 1991], latent heat release [*Joly and Thorpe*, 1990; *Schär and Davies*, 1990; *Plant et al.*, 2003], and boundary layer friction [*Adamson et al.*, 2006]. In this paper, secondary cyclones are defined as those which develop on the trailing cold front of preexisting cyclones (as depicted on the UK Met Office frontal analysis charts).

To investigate upstream secondary frontal cyclone development, we replot Figure 3 retaining only 250 hPa wind speed and areas of RWB and add the surface central positions and fronts of cyclones as identified in daily weather charts from the UK Met-Office. Examples of such charts are presented in Figure 7, which depicts the dates 11, 13, and 19 January 2007. Cyclone names are added, and only those fronts associated with cyclones tracking over Western Europe are shown in Figure 7. In all three cases, a jet streak feature links two cyclones, with a "parent" cyclone in the left-exit region of the jet, typically already occluding (e.g., Franz in Figure 7a), while a new secondary cyclone is developing in the right-entrance region of the jet (Gerhard in the same figure). Two days later (Figure 7c), cyclone Gerhard is the occluding parent cyclone, while a new storm (Hanno) is developing in the right-entrance region of the jet streak. The pattern occurs again on the 19 January 2007 (Figure 7e), with Kyrill as a parent cyclone and Lancelot as a secondary cyclone. In all these cases, cyclonic wave-breaking is identified on the poleward side of the jet (typically northwestward), while anticyclonic wave-breaking is located on the equatorward side of the jet (typically located southeastward). The analysis of similar charts for the other 3 months studied (see Figures S5 to S7) suggests a similar pattern of upper and lower level features and thus leads to the conceptual model shown in Figure 7f. As expected from the literature [e.g., *Uccellini*, 1990], cyclones are typically generated in the right-entrance region of the upper level jet and travel toward the left-exit region. The anomalously strong upper level jet streak is related to strong wind shear and strong low-level temperature gradients through thermal wind balance, thus maintaining the high baroclinicity necessary for explosive cyclone growth. Thus, it appears that the individual cyclones within the clusters examined can be related via the upstream development mechanism. This means that secondary cyclones form upstream, on the trailing cold fronts of primary cyclones, and develop into mature cyclones following the same path.

We now investigate the possibility that the process of downstream development enhances the clustering of cyclones by enabling several cyclones to develop in rapid succession. Downstream development is a feature of the dispersive nature of Rossby wave packets [*Simmons and Hoskins*, 1979]. Relative to the surface, the group velocity of synoptic-scale wave packets is directed eastward and is faster than the phase velocity. This means that existing cyclonic and anticyclonic anomalies move eastward over the surface but new anomalies develop downstream, or further east, of these as the wave energy disperses. Hence, the development of several cyclones can be linked, with new cyclones forming downstream of their parent.

To investigate this mechanism, we have followed *Chang* [1993] in generating Hovmöller diagrams of 300 hPa meridional wind anomalies for the four winters. The diagram for January 2007 is presented in Figure 8 as an example. Note that the meridional wind has been averaged over the 30°N–60°N band of latitude, so this picture illustrates synoptic and large-scale features of the flow only. The Hövmoller shows several clear Rossby wave trains with the characteristic signature of a group velocity (indicated by black arrows) which is faster than the phase velocity at which individual wind anomalies propagate. These wave packets arrive at the Greenwich meridian between 11 and 21 January (see Figure 8), which suggests that downstream development may have played a role in the development of some of these cyclones. It is interesting to note that during this core period of clustering, phase speeds in the western and central North Atlantic are in fact close to zero (albeit interspersed with some propagation), suggesting that stationary wave activity (i.e., which does not propagate downstream) may play an important role in controlling such events. However, the occurrence of multiple cyclones over Europe does not correspond to the arrival of several cyclones from the same wave packet. This is because multiple cyclones from the same wave packet do not last long enough to cross the same meridian. The wavelength of the packets in Figure 8 is typically 4000 km (in agreement with *Chang and Yu* [1999]), yet individual anomalies typically progress eastward by only around 2000 km during their lifetime.

Analysis of the other 3 months supports this result, that the clustering of European cyclones cannot generally be linked to the arrival of several cyclones from the same Rossby wave packet. As in the null hypothesis, the intense, straight jet stream provides a favorable waveguide for the wave packets but the packets themselves may not be dynamically linked. Still, downstream development is a mechanism for cyclone growth which may have played a role in the development of some, if not all, of the individual cyclones during these anomalous seasons. This applies particularly for the first cyclones of a storm series. For example, in the December 1999 case (Figure S8), clear wave packets arrive at the Greenwich meridian around 23 and 30 of December. The period of cyclone clustering lies between these dates, suggesting that downstream development may have played a role in the early cyclones of the cluster but not in the later ones.

6. Summary and Discussion

Four winter months corresponding to the main periods of the cyclone series of 1990, 1993, 1999, and 2007 were analyzed to identify the physical mechanisms associated with their occurrence. Our results identify during these clustering episodes a recurrent extension of an intensified eddy driven jet toward Western Europe which endures at least 1 week. On a daily basis, this corresponds to the occurrence of multiple jet streak events which successively occupy this location over several weeks. Cyclonic and anticyclonic Rossby wave-breaking events to the north and south of the eddy driven jet contribute to its recurring intensification and extension toward Europe and constrain the location of the jet typically within a limited corridor around 50°N. As a consequence, the large-scale conditions promoting rapid cyclone intensification persist for long time periods and increase the likelihood of storm clustering. Our results clearly document the importance of the steering by the large-scale flow for cyclone clustering.

Regarding the interrelated behavior between RWB occurrence and the jet state, it is well known that preferred locations of wave-breaking occurrence are located to the north (cyclonic) and south (anticyclonic) flanks of the eddy driven jet due to horizontal wind shear at upper levels [*Gabriel and Peters*, 2008]. The reverse effect—RWB as a cause of the changes in the mean flow, sometimes represented by the North Atlantic Oscillation—has also been described in various studies [e.g., *Franzke et al*., 2004; *Benedict et al*., 2004; *Rivière and Orlanski*, 2007; *Strong and Magnusdottir*, 2008b; *Michel and Rivière*, 2011]. In particular, the growth and decay of the positive phase of the North Atlantic Oscillation, which projects onto the large-scale configuration fostering clustering over the UK (cf. *Gómara et al*. [2014b]; Figure 2), is suggested to be forced by Rossby wave trains traveling from the North Pacific into the North Atlantic [*Feldstein*, 2003; *Strong and Magnusdottir*, 2008a]. Visual inspection of Figures 3 and S1–S3, corroborates with this argument, as RWB occurrence appears to steer the jet configuration. For predictability purposes, the variability and origin of these waves is undoubtedly an interesting path for future research.

An intensified eddy driven jet (as identified in the 4 months studied here) is associated with enhanced vertical wind shear and hence baroclinicity at lower levels, thus increasing the probability of explosive growth of baroclinic disturbances [*Hoskins et al*., 1985; *Gyakum and Danielson*, 2000; *Dacre and Gray*, 2013]. In the traditional view, cyclones themselves present two different life cycle behaviors depending on their

contrasting upper air evolution during their decaying stage (LC1 - anticyclonic and LC2 - cyclonic [e.g., *Thorncroft et al*., 1993]), and develop under a single jet streak. In the examples studied here, jet streaks are generated by previous and unrelated Rossby wave trains with greater temporal and spatial scales than those local RWB events related to the cyclones themselves [*McIntyre and Palmer*, 1983; *Nakamura and Wallace*, 1993]. Such upper level waves interacting with the jet stream may lead to the creation of multiple jet streaks (e.g., Figure 3), each favoring rapid cyclone intensification [*Reed and Albright*, 1986]. In fact, the strong divergence in the right-entrance and left-exit regions of a jet streak further contributes to enhance cyclone growth [*Uccellini*, 1990; *Rivière and Joly*, 2006a, 2006b]. These large-scale conditions analyzed here are thus consistent with the occurrence of multiple intense cyclones.

Additionally, this study highlights the importance of cyclone families and secondary cyclogenesis, particularly of upstream developments on trailing cold fronts of preexisting mature cyclones. The manual analysis of frontal developments has allowed the establishment of a link between cyclones based on synoptic plausibility and causality. A recurring pattern is identified, in which a developing cyclone is located in the right-entrance region of the jet on the trailing front of a mature cyclone located in the left-exit region of the same jet streak (Figure 7). The new cyclone follows a similar path to the previous cyclone toward the poleward side of the jet streak. This evidence is consistent with the idea of cyclone families and secondary cyclogenesis [e.g., *Bjerknes and Solberg*, 1922; *Parker*, 1998]. In fact, many of the top ranking destructive cyclones affecting Western Europe are secondary cyclones developing in the Northeast Atlantic region [e.g., *Dacre and Gray*, 2009].

The possible role of downstream development associated with the dispersive nature of Rossby waves [*Simmons and Hoskins*, 1979] was also analyzed. While this process can lead to cyclone development to the east of the parent cyclone [e.g., *Chang and Yu*, 1999; *Riemer et al*., 2008], it cannot explain the cyclone clustering periods presented here. While Rossby wave packets are present during these periods, the wavelengths are too long to correspond to the different cyclones within the clustering families.

This exploratory study provides the first dynamical analysis of the occurrence of clusters of extratropical cyclones over the North Atlantic, focusing on the role of secondary cyclogenesis and jet dynamics, and thus permitting a better understanding of the physical mechanisms leading to the occurrence of such cyclone families. The robustness of these results should be tested in a more complete analysis for the whole reanalysis period, and on other case studies like the winter of 2013/2014, in which a cyclone series led to severe impacts particularly in the United Kingdom. An interesting question which remains to be investigated concerns the relative roles played by the synoptic-scale temperature gradient associated with the jet streak and the mesoscale temperature gradient associated with the trailing cold front of the primary cyclone in determining the rate of secondary cyclone development. In addition, a more detailed analysis quantifying the role of deformation strain, shear, and latent heat release (all thought to be important for secondary cyclone development) could be performed to further characterize the relationship between cyclone clustering and secondary cyclogenesis. Other possible lines of future research are the estimation of the implications of cyclone clustering to the seriality of windstorm losses [e.g., *Karremann et al*., 2014], and the analysis of the identified mechanisms of cyclone clustering in high-resolution general circulation models like the High-Resolution Global Environmental Model [*Shaffrey et al*., 2009] to enable a better understanding of the projected changes of cyclone clustering under future climate conditions [*Pinto et al*., 2013]. With this aim, the representation of Rossby wave-breaking and its interactions with the upper level jet in general circulation models [e.g., *Masato et al*., 2013b] are of particular interest.

Acknowledgments

We thank the European Centre for Medium-Range Weather Forecasts and the National Centers for Environmental Prediction for the reanalysis data ERA-Interim and NCEP. We also thank the UK Met Office for the weather charts and the *Freie Universität* Berlin for the storm names. Iñigo Gómara is supported by Spanish national funds (research project MULCLIVAR CGL2012-38923-C02-01). We thank Sven Ulbrich (University of Cologne) and Marc Stringer (University of Reading) for help with data processing. We are grateful to John Methven, Len Shaffrey (both University of Reading), and David Stephenson (University of Exeter) for discussions and Peter Clark (University of Reading) for providing additional synoptic charts. We also thank Olivia Martius and two anonymous reviewers for their helpful and constructive comments. The ERA-Interim Re-analysis data set is available from European Centre for Medium-Range Weather Forecasts (http://apps.ecmwf.int/datasets/). The NCEP reanalysis data set is available from the National Centers for Environmental Prediction (www.ncep.noaa.gov/). The weather charts are available from the UK Met Office (http://www.metoffice.gov.uk), and the storm names from the *Freie Universität* Berlin (http://www.met.fu-berlin.de/adopt-a-vortex/). All other data are available from the authors (j.g.pinto@reading.ac.uk).

References

Adamson, D. S., S. E. Belcher, B. J. Hoskins, and R. S. Plant (2006), Boundary layer friction in mid-latitude cyclones, *Q. J. R. Meteorol. Soc.*, *132*, 101–124.

Bader, J., M. D. S. Mesquita, K. I. Hodges, N. Keenlyside, S. Østerhus, and M. Miles (2011), A review on Northern Hemisphere sea-ice, storminess and the North Atlantic Oscillation: Observations and projected changes, *Atmos. Res.*, *101*, 809–834.

Benedict, J. J., S. Lee, and S. B. Feldstein (2004), Synoptic view of the North Atlantic Oscillation, *J. Atmos. Sci.*, *61*, 121–144.

Bishop, C. H., and A. J. Thorpe (1994a), Frontal wave stability during moist deformation frontogenesis. Part I: Linear wave dynamics, *J. Atmos. Sci.*, *51*, 852–873.

Bishop, C. H., and A. J. Thorpe (1994b), Frontal wave stability during moist deformation frontogenesis. Part II: The suppression of non linear wave development, *J. Atmos. Sci.*, *51*, 874–888.

Bjerknes, J., and H. Solberg (1922), Life cycle of cyclones and the polar front theory of atmospheric circulation, *Geofys. Publ.*, *3*, 3–18.

Blender, R., C. C. Raible, and F. Lunkeit (2014), Non-exponential return time distributions for vorticity extremes explained by fractional Poisson processes, *Q. J. R. Meteorol. Soc.*, doi:10.1002/qj.2354.

Chaboureau, J. P., and A. J. Thorpe (1999), Frontogenesis and the development of secondary wave cyclones in FASTEX, *Q. J. R. Meteorol. Soc.*, *125*, 925–940.
Chang, E. K. (1993), Downstream development of baroclinic waves as inferred from regression analysis, *J. Atmos. Sci.*, *50*, 2038–2053.
Chang, E. K., and D. B. Yu (1999), Characteristics of wave packets in the upper troposphere. Part I: Northern Hemisphere winter, *J. Atmos. Sci.*, *56*, 1708–1728.
Dacre, H. F., and S. L. Gray (2006), Life-cycle simulations of low-level frontal waves and the impact of deformation strain, *Q. J. R. Meteorol. Soc.*, *132*, 2171–2190.
Dacre, H. F., and S. L. Gray (2009), The spatial distribution and evolution characteristics of North Atlantic cyclones, *Mon. Weather Rev.*, *137*, 99–115.
Dacre, H. F., and S. L. Gray (2013), Quantifying the climatological relationship between extratropical cyclone intensity and atmospheric precursors, *Geophys. Res. Lett.*, *40*, 2322–2327, doi:10.1002/grl.50105.
Dee, D., et al. (2011), The ERA-Interim reanalysis: Configuration and performance of the data assimilation system, *Q. J. R. Meteorol. Soc.*, *137*, 553–597.
Della-Marta, P. M., M. A. Liniger, C. Appenzeller, D. N. Bresch, P. Köllner-Heck, and V. Muccione (2010), Improved estimates of the European winter windstorm climate and the risk of reinsurance loss using climate model data, *J. Appl. Meteorol. Climatol.*, *49*, 2092–2120.
Dritschel, D. G., P. H. Haynes, and M. N. Juckes (1991), The stability of a two-dimensional vorticity filament under uniform strain, *J. Fluid Mech.*, *230*, 647–665.
Feldstein, S. B. (2003), The dynamics of NAO teleconnection pattern growth and decay, *Q. J. R. Meteorol. Soc.*, *129*, 901–924.
Fink, A. H., T. Brücher, E. Ermert, A. Krüger, and J. G. Pinto (2009), The European storm Kyrill in January 2007: Synoptic evolution, meteorological impacts and some considerations with respect to climate change, *Nat. Hazards Earth Syst. Sci.*, *9*, 405–423.
Franzke, C., S. Lee, and S. B. Feldstein (2004), Is the North Atlantic Oscillation a breaking wave?, *J. Atmos. Sci.*, *61*, 145–160.
Gabriel, A., and D. Peters (2008), A diagnostic study of different types of Rossby wave breaking events in the northern extratropics, *J. Meteorol. Soc. Jpn.*, *86*, 613–631.
Gómara, I., J. G. Pinto, T. Woollings, G. Masato, P. Zurita-Gotor, and B. Rodríguez-Fonseca (2014a), Rossby wave-breaking analysis of explosive cyclones in the Euro-Atlantic sector, *Q. J. R. Meteorol. Soc.*, *140*, 738–753, doi:10.1002/qj.2190.
Gómara, I., B. Rodríguez-Fonseca, P. Zurita-Gotor, and J. G. Pinto (2014b), On the relation between explosive cyclones affecting Europe and the North Atlantic Oscillation, *Geophys. Res. Lett.*, *41*, 2182–2190, doi:10.1002/2014GL059647.
Gyakum, J. R., and R. E. Danielson (2000), Analysis of meteorological precursors to ordinary and explosive cyclogenesis in the western North Pacific, *Mon. Weather Rev.*, *128*, 851–863.
Hanley, J., and R. Caballero (2012), The role of large-scale atmospheric flow and Rossby wave breaking in the evolution of extreme windstorms over Europe, *Geophys. Res. Lett.*, *39*, L21708, doi:10.1029/2012GL053408.
Hawcroft, M. K., L. C. Shaffrey, K. I. Hodges, and H. F. Dacre (2012), How much Northern Hemisphere precipitation is associated with extratropical cyclones?, *Geophys. Res. Lett.*, *39*, L24809, doi:10.1029/2012GL053866.
Haylock, M. R. (2011), European extra-tropical storm damage risk from a multimodel ensemble of dynamically-downscaled global climate models, *Nat. Hazards Earth Syst. Sci.*, *11*, 2847–2857.
Hewson, T. D. (1997), Objective identification of frontal wave cyclones, *Meteorol. Appl.*, *4*, 311–315.
Hewson, T. D. (1998), Objective fronts, *Meteorol. Appl.*, *5*, 37–65.
Hoskins, B. J., M. E. McIntyre, and A. W. Robertson (1985), On the use and significance of isentropic potential vorticity maps, *Q. J. R. Meteorol. Soc.*, *111*, 877–946.
Joly, A., and A. J. Thorpe (1990), Frontal instabilities generated by tropospheric potential vorticity anomalies, *Q. J. R. Meteorol. Soc.*, *116*, 525–560.
Joly, A., and A. J. Thorpe (1991), The stability of time-dependent flows: An application to fronts in developing baroclinic waves, *J. Atmos. Sci.*, *48*, 163–182.
Kalnay, E., et al. (1996), The NCEP/NCAR 40-Year Reanalysis Project, *Bull. Am. Meteorol. Soc.*, *77*, 437–471.
Karremann, M. K., J. G. Pinto, P. J. Von Bomhard, and M. Klawa (2014), On the clustering of winter storm loss events over Germany, *Nat. Hazards Earth Syst. Sci.*, *14*, 2041–2052.
Klawa, M., and U. Ulbrich (2003), A model for the estimation of storm losses and the identification of severe winter storms in Germany, *Nat. Hazards Earth Syst. Sci.*, *3*, 725–732.
Lamb, H. H. (1991), *Historic Storms of the North Sea, British Isles, and Northwest Europe*, Cambridge Univ. Press, Cambridge, U. K.
Mahlstein, I., O. Martius, C. Chevalier, and D. Ginsbourger (2012), Changes in the odds of extreme events in the Atlantic basin depending on the position of the extratropical jet, *Geophys. Res. Lett.*, *39*, L22805, doi:10.1029/2012GL053993.
Mailier, P. J., D. B. Stephenson, C. A. T. Ferro, and K. I. Hodges (2006), Serial clustering of extratropical cyclones, *Mon. Weather Rev.*, *134*, 2224–2240.
Masato, G., B. J. Hoskins, and T. Woollings (2013a), Wave-breaking characteristics of Northern Hemisphere winter blocking: A two-dimensional approach, *J. Clim.*, *26*, 4535–4549.
Masato, G., B. J. Hoskins, and T. Woollings (2013b), Winter and summer Northern Hemisphere blocking in CMIP5 models, *J. Clim.*, *26*, 7044–7059.
McCallum, E., and W. J. T. Norris (1990), The storms of January and February 1990, *Meteorol. Mag.*, *119*, 201–210.
McIntyre, M. E., and T. M. Palmer (1983), Breaking planetary waves in the stratosphere, *Nature*, *305*, 593–600.
Michel, C., and G. Rivière (2011), The link between Rossby wave breakings and weather regime transitions, *J. Atmos. Sci.*, *68*, 1730–1748.
Munich Re (2010), Significant European winter storms 1980−June 2010. Overall losses [in German]. [Available at www.munichre.com.]
Murray, R. J., and I. Simmonds (1991), A numerical scheme for tracking cyclone centres from digital data. Part I: Development and operation of the scheme, *Aust. Meteorol. Mag.*, *39*, 155–166.
Nakamura, H., and J. M. Wallace (1993), Synoptic behavior of baroclinic eddies during the blocking onset, *Mon. Weather Rev.*, *121*, 1892–1903.
Neu, U., et al. (2013), IMILAST—A community effort to intercompare extratropical cyclone detection and tracking algorithms, *Bull. Am. Meteorol. Soc.*, *94*, 529–547.
Orlanski, I. (2003), Bifurcation in eddy life cycles: Implications for storm track variability, *J. Atmos. Sci.*, *60*, 993–1023.
Parker, D. J. (1998), Secondary frontal waves in the North Atlantic region: A dynamical perspective of current ideas, *Q. J. R. Meteorol. Soc.*, *124*, 829–856.
Pelly, J. L., and B. J. Hoskins (2003), A new perspective on blocking, *J. Atmos. Sci.*, *60*, 743–755.
Pfahl, S., and H. Wernli (2012), Quantifying the relevance of cyclones for precipitation extremes, *J. Clim.*, *25*, 6770–6780.
Pinto, J. G., T. Spangehl, U. Ulbrich, and P. Speth (2005), Sensitivities of a cyclone detection and tracking algorithm: Individual tracks and climatology, *Meteorol. Z.*, *14*, 823–838.

Pinto, J. G., S. Zacharias, A. H. Fink, G. C. Leckebusch, and U. Ulbrich (2009), Factors contributing to the development of extreme North Atlantic cyclones and their relationship with the NAO, *Clim. Dyn.*, *32*, 711–737.
Pinto, J. G., N. Bellenbaum, M. K. Karremann, and P. M. Della-Marta (2013), Serial clustering of extratropical cyclones over the North Atlantic and Europe under recent and future climate conditions, *J. Geophys. Res. Atmos.*, *118*, 12,476–12,485, doi:10.1002/2013JD020564.
Plant, R. S., G. C. Craig, and S. L. Gray (2003), On a threefold classification of extratropical cyclogenesis, *Q. J. R. Meteorol. Soc.*, *129*, 2989–3012.
Raible, C. C. (2007), On the relation between extremes of midlatitude cyclones and the atmospheric circulation using ERA40, *Geophys. Res. Lett.*, *34*, L07703, doi:10.1029/2006GL029084.
Reed, R. J., and M. D. Albright (1986), A case study of explosive cyclogenesis in the eastern Pacific, *Mon. Weather Rev.*, *114*, 2297–2319.
Renfrew, I. A., A. J. Thorpe, and C. H. Bishop (1997), The role of the environmental flow in the development of secondary frontal cyclones, *Q. J. R. Meteorol. Soc.*, *123*, 1653–1675.
Riemer, M., S. C. Jones, and C. A. Davis (2008), The impact of extratropical transition on the downstream flow: An idealized modelling study with a straight jet, *Q. J. R. Meteorol. Soc.*, *134*, 69–91.
Rivals, H., J. P. Cammas, and I. A. Renfrew (1998), Secondary cyclogenesis: The initiation phase of a frontal wave observed over the eastern Atlantic, *Q. J. R. Meteorol. Soc.*, *124*, 243–267.
Rivière, G., and A. Joly (2006a), Role of the low-frequency deformation field on the explosive growth of extratropical cyclones at the jet exit. Part I: Barotropic critical region, *J. Atmos. Sci.*, *63*, 1965–1981.
Rivière, G., and A. Joly (2006b), Role of the low-frequency deformation field on the explosive growth of extratropical cyclones at the jet exit. Part II: Baroclinic critical region, *J. Atmos. Sci.*, *63*, 1982–1995.
Rivière, G., and I. Orlanski (2007), Characteristics of the Atlantic storm-track eddy activity and its relation with the North Atlantic Oscillation, *J. Atmos. Sci.*, *64*, 241–266.
Rudeva, I., and S. K. Gulev (2007), Climatology of cyclone size characteristics and their changes during the cyclone life cycle, *Mon. Weather Rev.*, *135*, 2568–2587.
Schär, C., and H. C. Davies (1990), An instability of mature cold fronts, *J. Atmos. Sci.*, *47*, 929–950.
Schwierz, C., et al. (2010), Modelling European winter wind storm losses in current and future climate, *Clim. Change*, *101*, 485–514.
Shaffrey, L. C., et al. (2009), UK-HiGEM: The new UK High Resolution Global Environment Model. Model description and basic evaluation, *J. Clim.*, *22*, 1861–1896.
Simmonds, I. (2000), Size changes over the life of sea level cyclones in the NCEP reanalysis, *Mon. Weather Rev.*, *128*, 4118–4125.
Simmonds, I., and K. Keay (2000), Mean Southern Hemisphere extratropical cyclone behavior in the 40-year NCEP–NCAR reanalysis, *J. Clim.*, *13*, 873–885.
Simmons, A. J., and B. J. Hoskins (1979), The downstream and upstream development of unstable baroclinic waves, *J. Atmos. Sci.*, *36*, 1239–1254.
Strong, C., and G. Magnusdottir (2008a), How Rossby wave breaking over the Pacific forces the North Atlantic Oscillation, *Geophys. Res. Lett.*, *35*, L10706, doi:10.1029/2008GL033578.
Strong, C., and G. Magnusdottir (2008b), Tropospheric Rossby wave breaking and the NAO/NAM, *J. Atmos. Sci.*, *65*, 2861–2876.
Thorncroft, C. D., B. J. Hoskins, and M. E. McIntyre (1993), Two paradigms of baroclinic-wave life-cycle behaviour, *Q. J. R. Meteorol. Soc.*, *119*, 17–55.
Uccellini, L. W. (1990), Processes contributing to the rapid development of extratropical cyclones, in *Extratropical Cyclones: The Erik Palmen Memorial Volume*, edited by C. Newton and E. O. Holopainen, pp. 81–105, Am. Meteorol. Soc., Boston, Mass.
Ulbrich, U., A. H. Fink, M. Klawa, and J. G. Pinto (2001), Three extreme storms over Europe in December 1999, *Weather*, *56*, 70–80.
Vitolo, R., D. B. Stephenson, I. M. Cook, and K. Mitchell-Wallace (2009), Serial clustering of intense European storms, *Meteorol. Z.*, *18*, 411–424.
Woollings, T., A. Hannachi, and B. Hoskins (2010), Variability of the North Atlantic eddy-driven jet stream, *Q. J. R. Meteorol. Soc.*, *136*, 856–868.

Supplementary Material for

Large-scale dynamics associated with clustering of extra-tropical cyclones affecting Western Europe

Journal of Geophysical Research - Atmospheres

The auxiliary material consists of one PDF document with 8 figures and 1 table.

Figure S1: 1-28 February and 1-2 March 1990. Red/blue shadings: theta on 2PVU in K (00 UTC). Hatched fields: daily RWB occurrence. Dashed contours: wind intensity at 250 hPa (m s-1, 00 UTC). Solid contour lines: Full cyclone p95 trajectories until 18 UTC of each day. Large filled black dots: Cyclone positions at 00 UTC. Small circles: 3 forthcoming cyclone positions on the same date. Large open white dots: Positions (00 UTC) of named historical storms crossing the detection area ([55°N, 5°W], r=700 km) on that day.

Figure S2: As Figure S1 but for 1-30 January 1993.

Figure S3: As Figure S1 but for 22-30 December 1999

Figure S4: Upper: Comparison for distributions with two sided RWB (blue) vs. other cases (green) and all cases (red) for jet speed (m s-1) and jet latitude (degrees north), all for [40°W-10°E]. Lower: same as above but for the occurrence of p98 cyclone clusters intercepting the detection area across the British Isles [55°N, 5°W]. The uncertainty of the PDFs reflects the size of the data-set it is associated with.

Figure S5: RWB (B>0), jet stream at 250 hPa (dashed contours; m s-1), cyclone positions and fronts (from UK Met Office weather charts; red/blue/purple solid lines for warm/cold/occluded fronts) for 12Z on (a) 7, (b) 11 and (c) 26 February 1990.

Figure S6: Same as Figure S5 for 12Z on (a) 10 and (b) 21 January 1993.

Figure S7: Same as Figure S5 for 00Z on (a) 25 and (b) 26 December 1999.

Figure S8: Hovmöller diagram of zonal wind daily speed anomalies at 300 hPa (m s-1) for December 1999, averaged over latitude band to [30°-60°N]. The black arrows give subjective indications of the group velocity of some Rossby wave packets. Counts of p95 cyclones per day (see Figure 1a) crossing the meridian 5°W are provided in geometric forms (circles: 1 count per day; squares: 2 counts per day; pentagons: 3 counts per day).

Table S1: The table shows the percentages of RWB relative to the climatology and the cyclone clustering sub-samples, with and without the lead-lag criterion imposed (see text for more details). The numbers in the climatology for the 2 days lag are dependent on the p95/p98 sub-sample, and those relative to p95 are shown here. However, their variation is minimal, of the order of 2-3%.

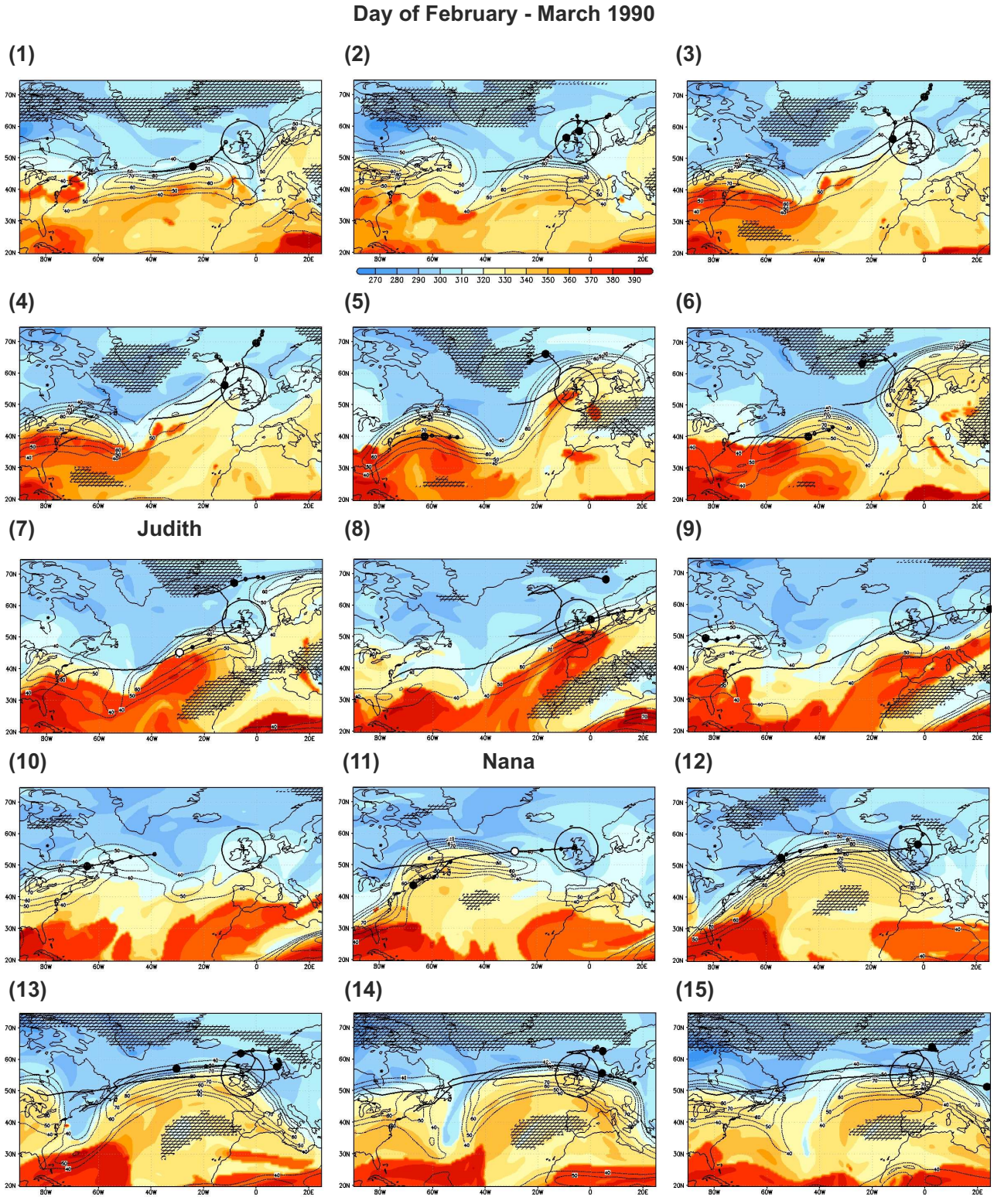
Day of February - March 1990
(1)
(2)
(3)
270 280 290 300 310 320 330 340 350 360 370 380 390
(4)
(5)
(6)
(7)
Judith
(8)
(9)
(10)
(11)
Nana
(12)
(13)
(14)
(15)

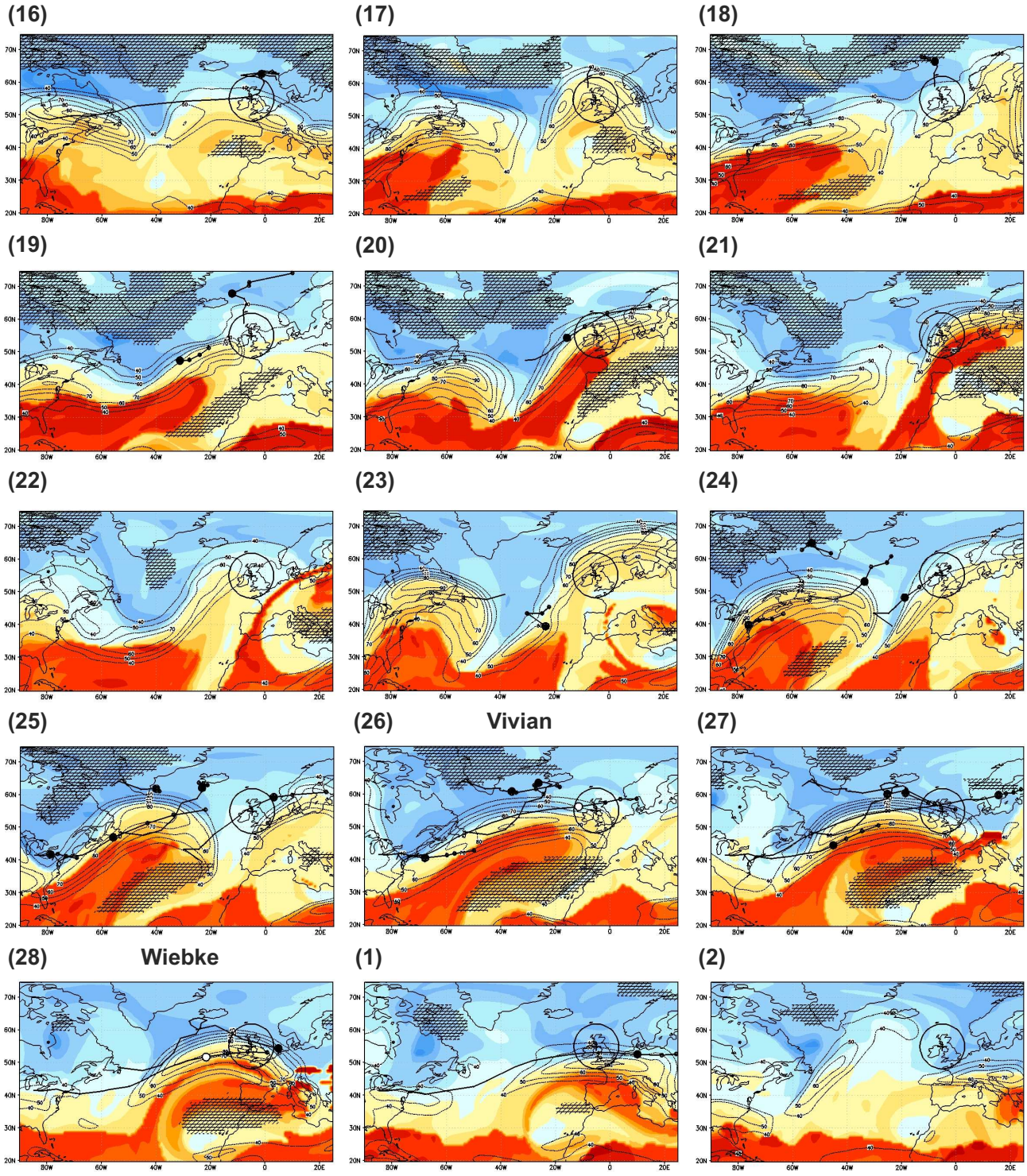

Figure S1: 1-28 February and 1-2 March 1990. Red/blue shadings: θ on 2PVU in K (00 UTC). Hatched fields: daily RWB occurrence. Dashed contours: wind intensity at 250 hPa (m s^{-1}, 00 UTC) (contours drawn from 40 m s^{-1} with 10 m s^{-1} contour intervals, 00 UTC). Solid contour lines: Full cyclone p95 trajectories until 18 UTC of each day. Large filled black dots: Cyclone positions at 00 UTC. Small circles: 3 forthcoming cyclone positions on the same date. Large open white dots: Positions (00 UTC) of named historical storms crossing the detection area ([55°N, 5°W], r=700 km) on that day.

Day of January 1993

(1)

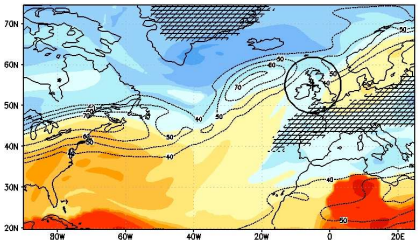

(2)

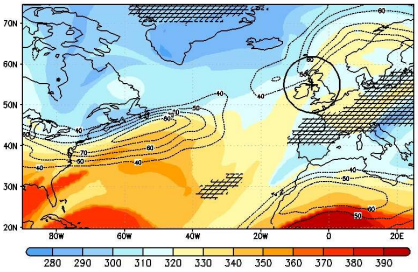

(3)

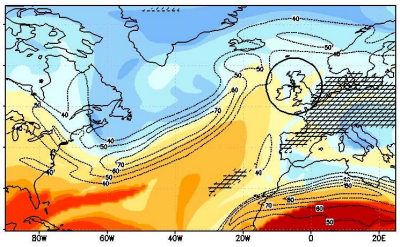

(4)

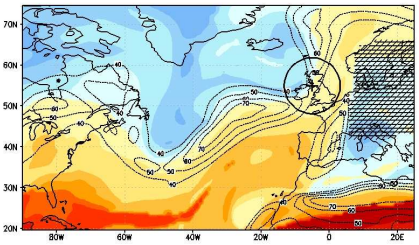

(5)

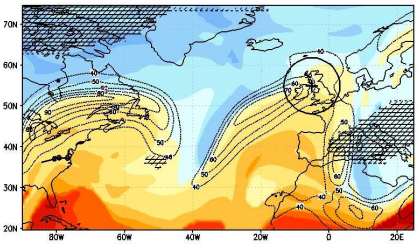

(6)

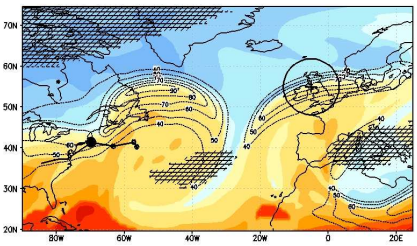

(7)

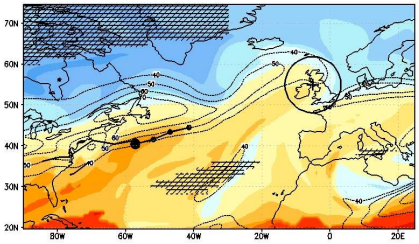

(8)

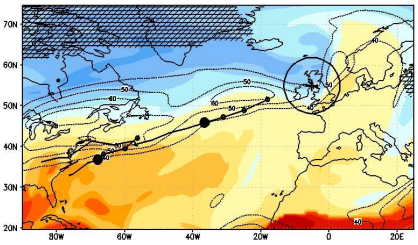

(9)

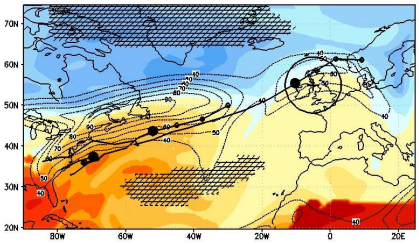

(10)

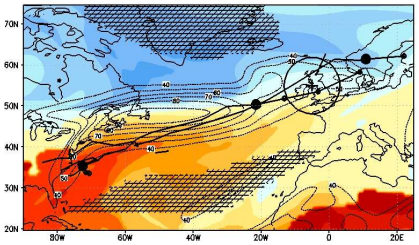

(11)

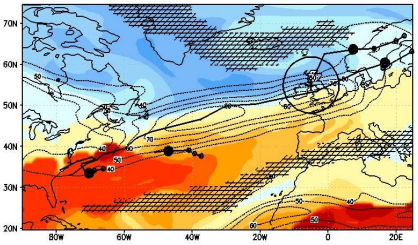

(12)

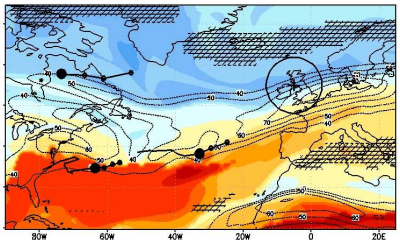

(13) Verena

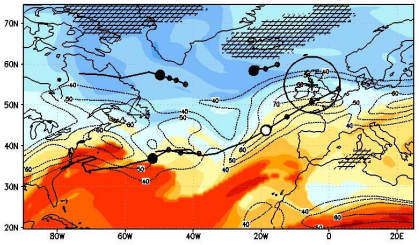

(14)

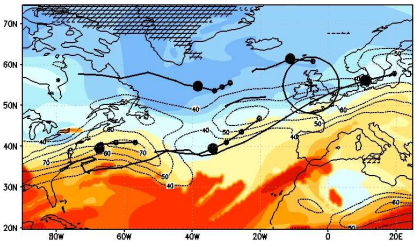

(15)

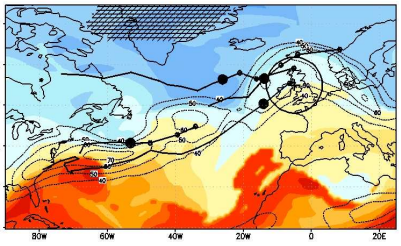

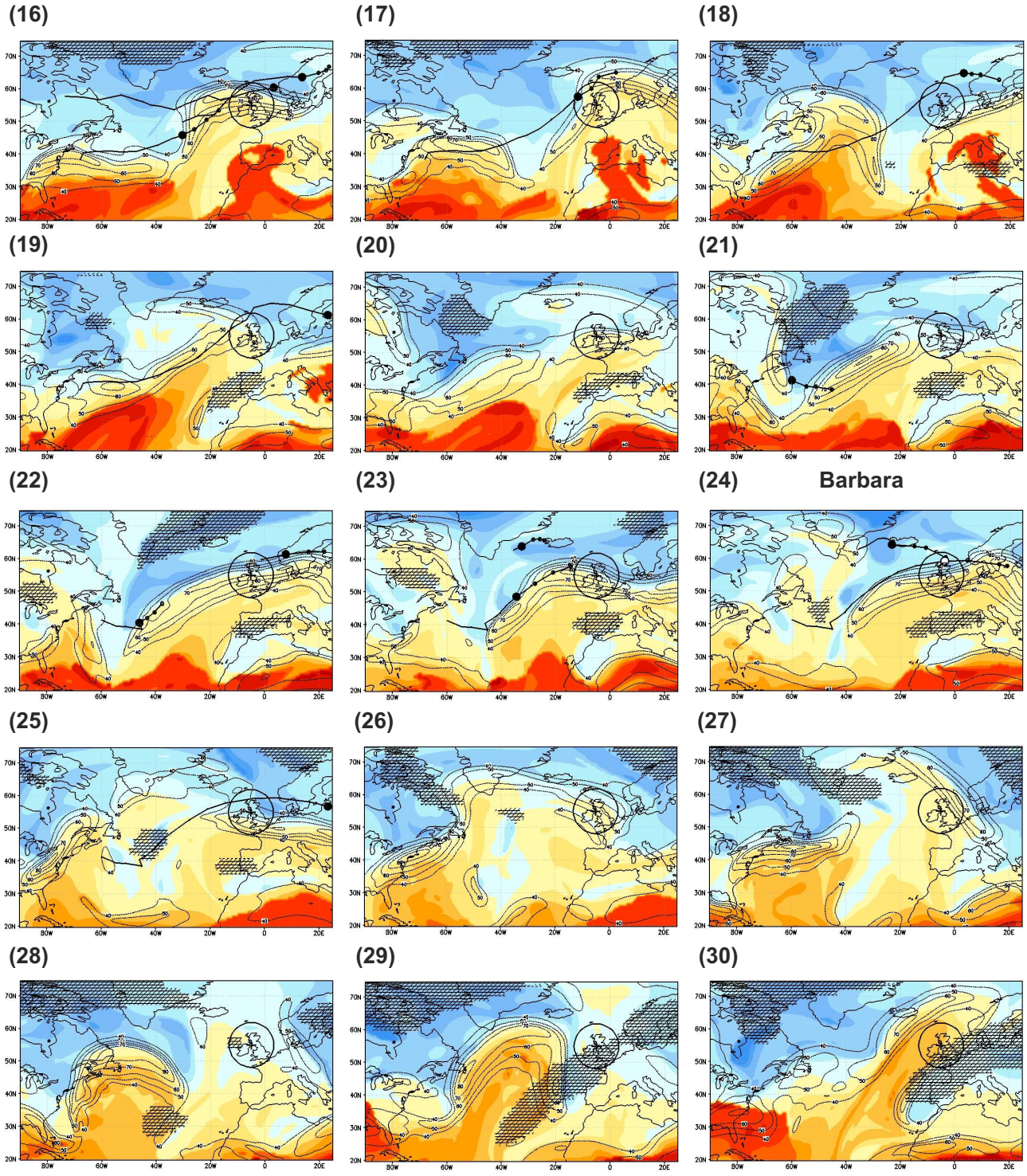

Figure S2: As Figure S1 but for 1-30 January 1993.

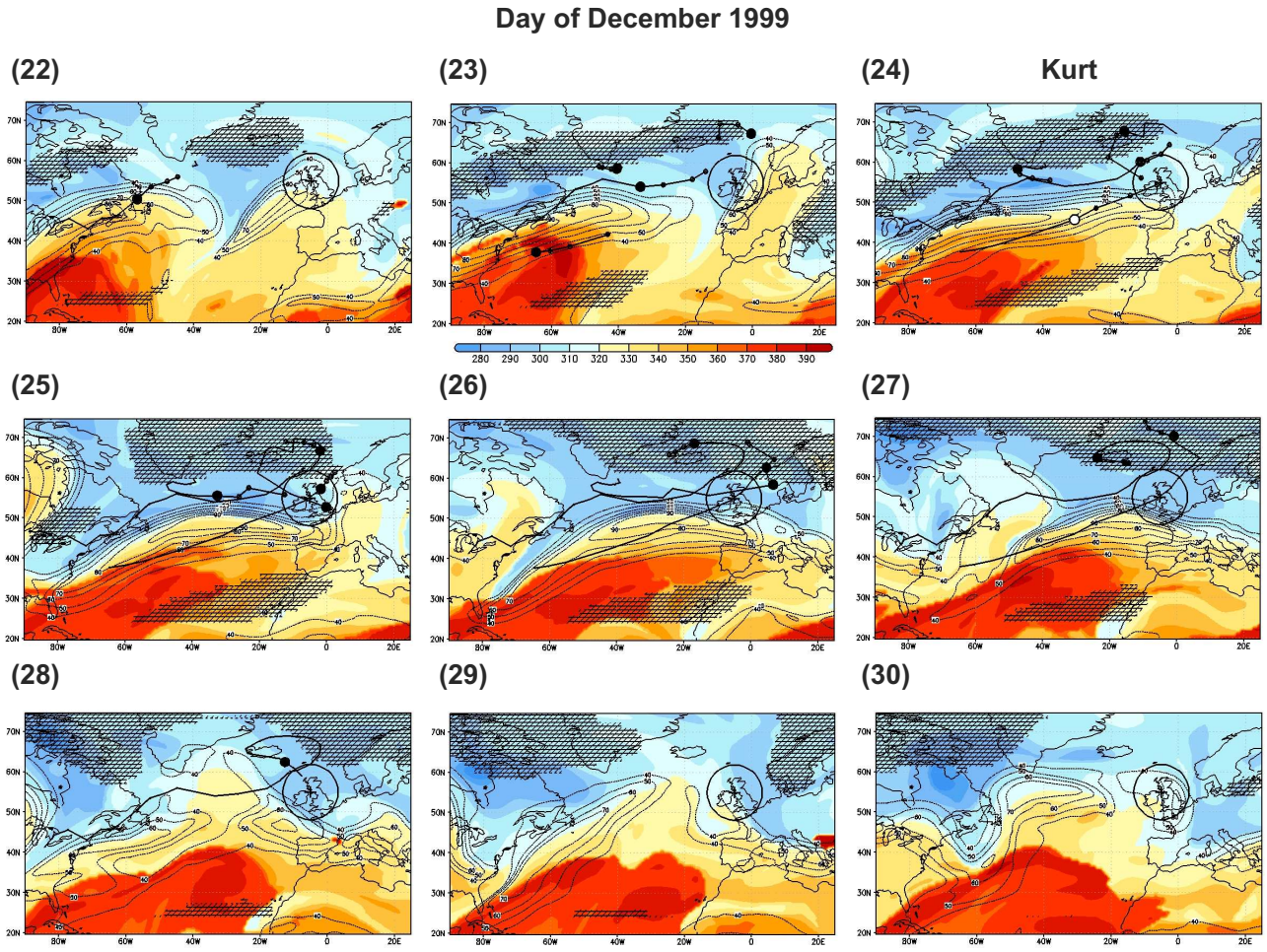

Figure S3: As Figure S1 but for 22-30 December 1999.

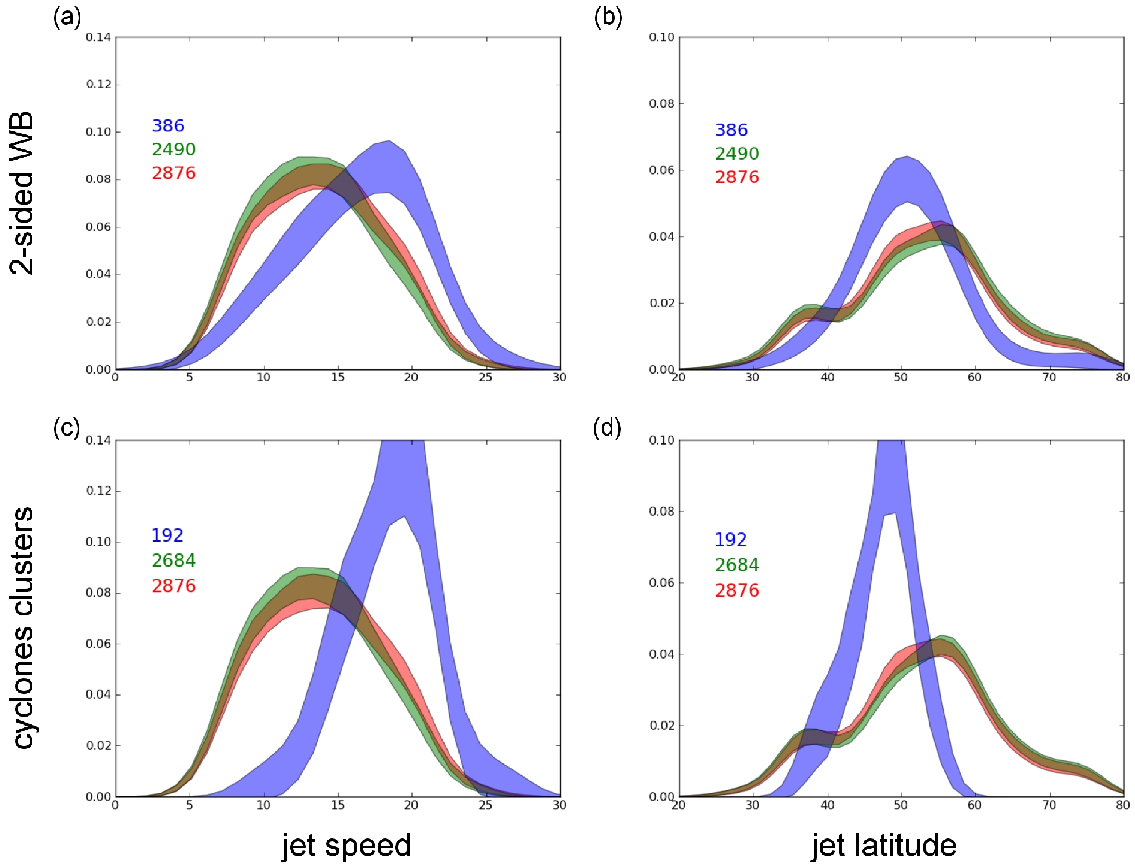

Figure S4: Upper: Comparison for distributions with two sided RWB (blue) vs. other cases (green) and all cases (red) for jet speed (m s^{-1}) and jet latitude (degrees north), all for [40°W-10°E]. Lower: same as above but for the occurrence of p98 cyclone clusters intercepting the detection area across the British Isles [55°N, 5°W]. The uncertainty of the PDFs reflects the size of the data-set it is associated with.

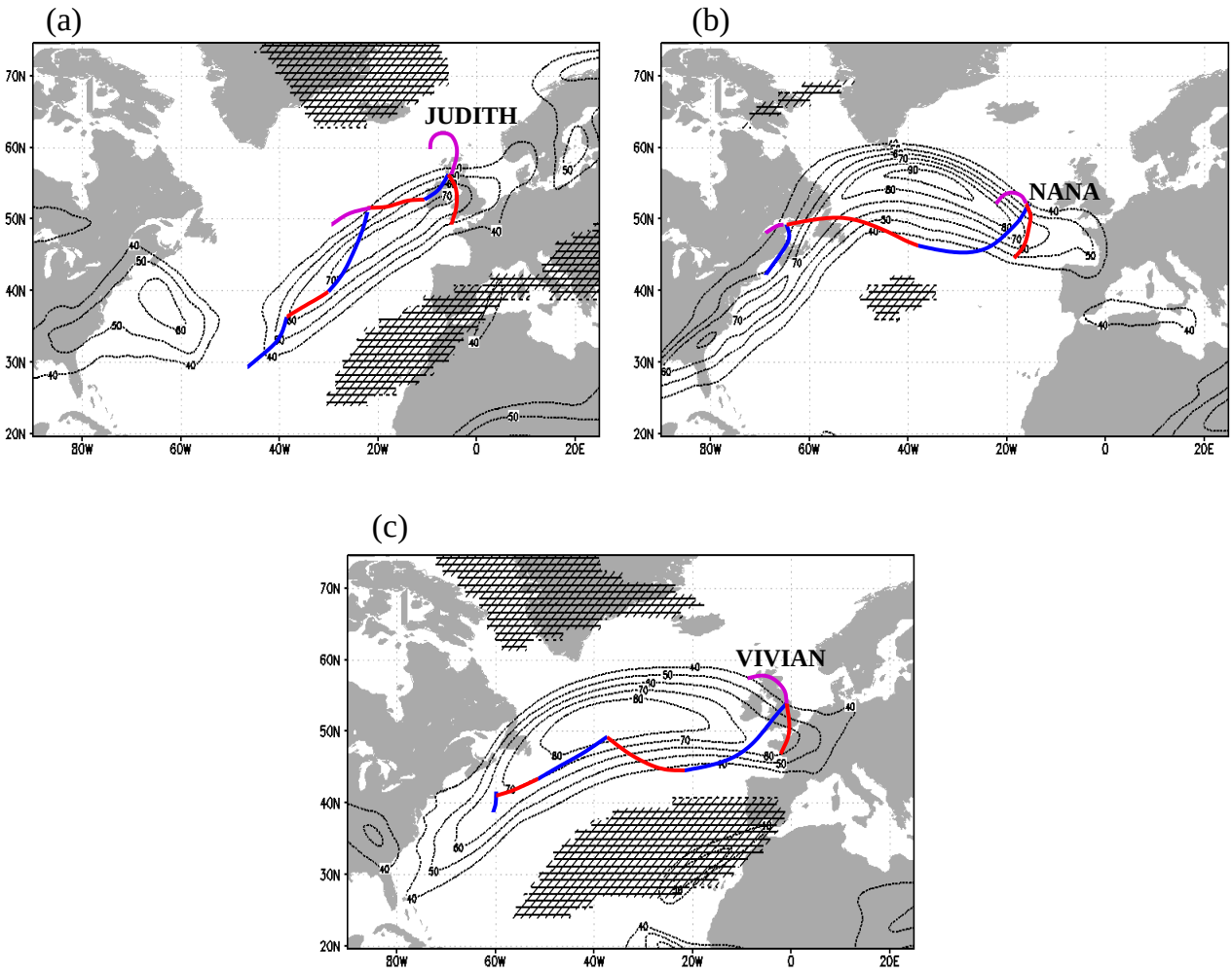

Figure S5: RWB (B> 0), jet stream at 250 hPa (dashed contours; m s^{-1}), cyclone positions and fronts (from UK Met Office weather charts; red/blue/purple solid lines for warm/cold/occluded fronts) for 12Z on (a) 7, (b) 11 and (c) 26 February 1990.

Description: February 1990 contained multiple cyclone families, all associated with a distinct jet streak. Figure S7(a) shows a jet streak that occurred between 5-8 February 1990 and 3 related cyclones. Figure S7(b) shows the following jet streak, which occurred between 10-12 February 1990. A family of 3 cyclones, of which 2 are shown here, were associated with this jet streak. Finally, Figure S7(c) shows a jet streak that occurred between 23-28 February 1990. A family of 5 cyclones formed on this jet streak, of which 3 are shown here. For all of these cases, double-sided RWB is evident.

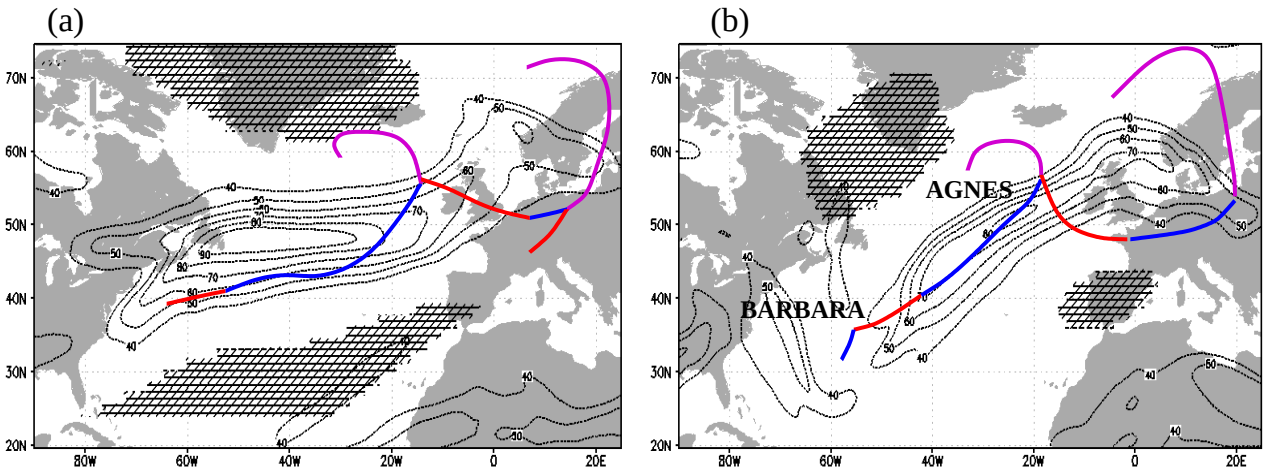

Figure S6: Same as Figure S5 for 12Z on (a) 10 and (b) 21 January 1993.

Description: Between 7-12 January 1993 a cluster of 5 cyclones forms between cyclonic and anticyclonic RWB regions. Figure S6(a) shows 3 of these cyclones. Between 20-24 January 1993 a cluster of 4 cyclones forms along the same jet streak of which 3 cyclones are shown in figure S6(b). The region of cyclonic RWB to the poleward side of the jet is less extensive than for other clustering events studied.

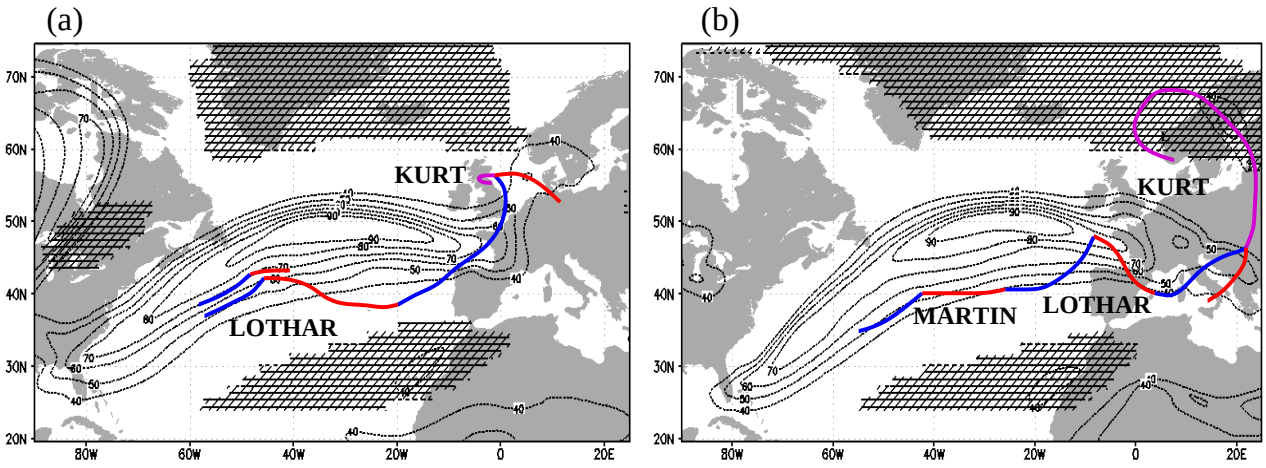

Figure S7: Same as Figure S5 for 00Z on (a) 25 and (b) 26 December 1999.

Description: Between 24-28 December 1999 a cluster of cyclones occurs between cyclonic and anticyclonic RWB regions. Kurt, Lothar and Martin all form in the right entrance region of the upper-level jet and then travel towards the left exit region. Frontal waves form on their trailing cold fronts and develop into cyclones which follow the same path.

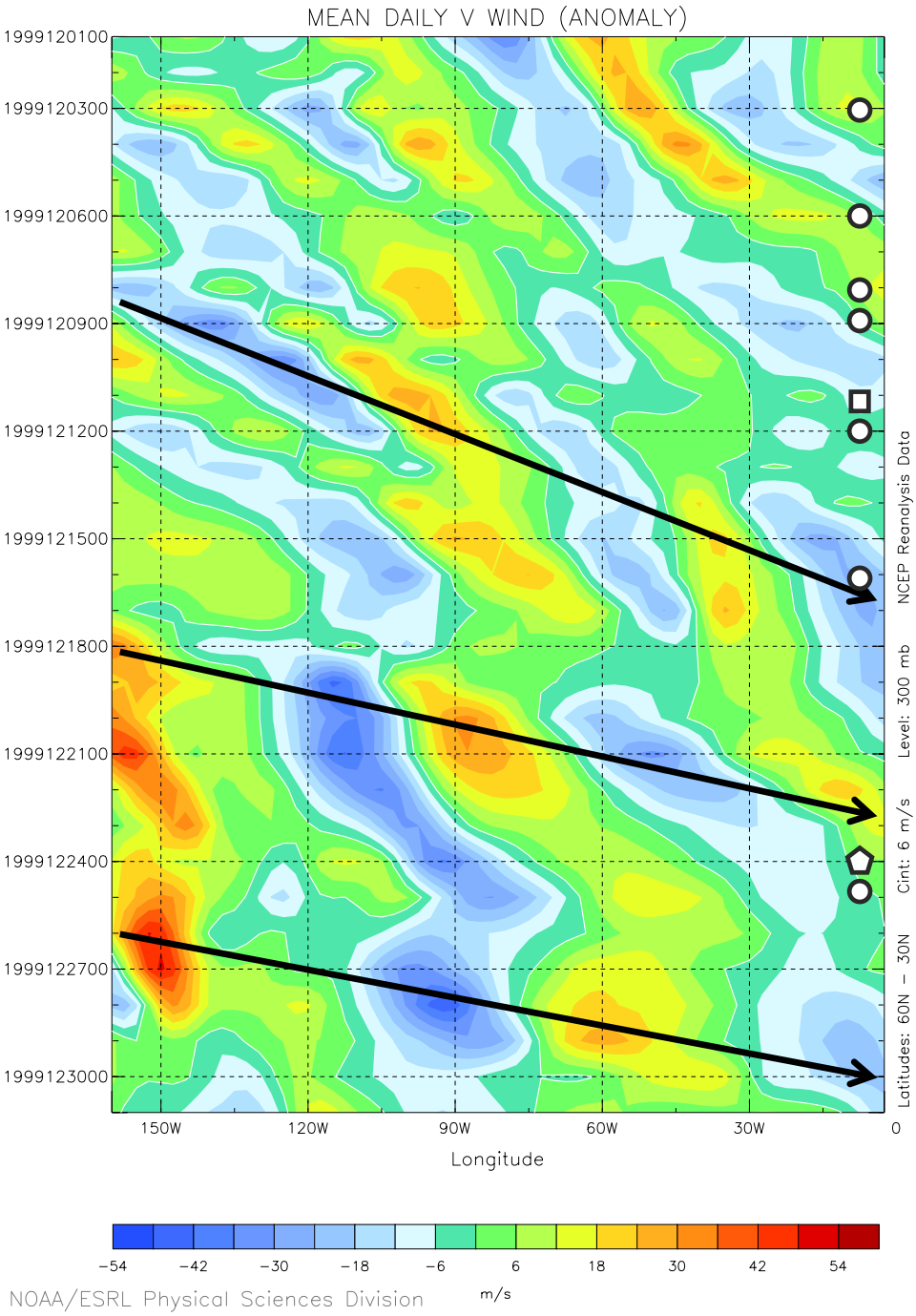

Figure S8: Hovmoller diagram of zonal wind daily speed anomalies at 300 hPa (m s-1) for December 1999, averaged over latitude band to [30°-60°N]. The black arrows give subjective indications of the group velocity of some Rossby wave packets. Counts of p95 cyclones per day (see Figure 1a) crossing the meridian 5°W are provided in geometric forms (circles: 1 count per day; squares: 2 counts per day; pentagons: 3 counts per day).

no lag	**climatology**	**p95**	**p98**
2-s RWB	10%	18%	20%
1-s RWB	25%	31%	34%
No RWB	65%	51%	46%
2 days lag	**climatology**	**p95**	**p98**
2-s RWB	16%	44%	48%
1-s RWB	23%	21%	20%
No RWB	61%	35%	32%

Table S8: The table shows the percentages of RWB relative to the climatology and the cyclone clustering sub-samples, with and without the lead-lag criterion imposed (see text for more details). The numbers in the climatology for the 2 days lag are dependent on the p95/p98 sub-sample, and those relative to p95 are shown here. However, their variation is minimal, of the order of 2-3%.

4. Abrupt transitions in the variability of explosive cyclones over the North Atlantic

Abstract: Explosive cyclones are intense extra-tropical low pressure systems with large deepening rates. In the Euro-Atlantic sector, they are a major source of life-threatening weather impacts due to their associated strong wind gusts, heavy precipitation and storm surge events. The variability of the North Atlantic cyclonic activity is modulated by the North Atlantic Oscillation (NAO). In this study, we investigate abrupt transitions in time focusing on the high-frequency (1-11 yr.) climate variability of explosive North Atlantic cyclones. Therefore, winter explosive cyclones from two reanalysis datasets (NCEP and ERA-40) and an atmosphere/ocean coupled general circulation model (ECHAM5/MPIOM1) are analyzed. The leading mode of variability of explosive cyclone track density is characterized by a strengthening/weakening pattern between Newfoundland and Iceland. This pattern is found for most of the time periods, but for specific periods (of about 20-25 years) it abruptly changes shape both in NCEP and ECHAM5/MPIOM1. These changes are accompanied by rapid modifications of the NAO influence on explosive cyclogenesis, and decreased baroclinicity over the sub-polar North Atlantic. The influence of the ocean is found important for both the occurrence and persistence of such periods. This study evidences the low-frequency control for the time-evolving high-frequency climate variability of explosive cyclogenesis in the North Atlantic. These results permit a better understanding of explosive cyclogenesis variability on different timescales.

***Gómara** I, Rodríguez-Fonseca B, Zurita-Gotor P, Ulbrich S, and Pinto JG (2015) Abrupt transitions in the variability of explosive cyclones over the North Atlantic, Clim. Dyn. (under review, CLDY-D-15-00358). 'Revision in progress' version of 25 September 2015.*

Abrupt transitions in the variability of explosive cyclones over the North Atlantic

Iñigo Gómara · Belén Rodríguez-Fonseca · Pablo Zurita-Gotor · Sven Ulbrich · Joaquim G. Pinto

Submitted: 26 June 2015. 'Revision in progress' version of 25 September 2015

Abstract Explosive cyclones are intense extra-tropical low pressure systems with large deepening rates. In the Euro-Atlantic sector, they are a major source of life-threatening weather impacts due to their associated strong wind gusts, heavy precipitation and storm surge events. The variability of the North Atlantic cyclonic activity is modulated by the North Atlantic Oscillation (NAO). In this study, we investigate abrupt transitions in time focusing on the high-frequency (1-11 yr.) climate variability of explosive North Atlantic cyclones. Therefore, winter explosive cyclones from two reanalysis datasets (NCEP and ERA-40) and an atmosphere/ocean coupled general circulation model (ECHAM5/MPIOM1) are analyzed. The leading mode of variability of explosive cyclone track density is characterized by a strengthening/weakening pattern between Newfoundland and Iceland. This pattern is found for most of the time periods, but for specific periods (of about 20-25 years) it abruptly changes shape both in NCEP and ECHAM5/MPIOM1. These changes are accompanied by rapid modifications of the NAO influence on explosive cyclogenesis, and decreased baroclinicity over the sub-polar North Atlantic. The influence of the ocean is found important for both the occurrence and persistence of such periods.

This study evidences the low-frequency control for the time-evolving high-frequency climate variability of explosive cyclogenesis in the North Atlantic. These results permit a better understanding of explosive cyclogenesis variability on different timescales.

Keywords Extra-tropical cyclones; Explosive cyclogenesis; NAO; Jet stream; Ocean; Non-stationary Teleconnections

1 Introduction

The wintertime variability in the mid-latitudes of both hemispheres is dominated by the occurrence of sub-weekly baroclinic disturbances (Blackmon et al. 1977; Lau 1978). Such disturbances typically grow in the vicinity of the planetary stationary troughs, where the gradients of temperature and humidity are maximum (Hoskins and Valdes 1990), and terminate near the regions of stationary ridges (Lau 1988). In the northern hemisphere, these areas (so called 'storm tracks') extend from the Eastern Asian and North American coast lines towards Western North America and Europe, respectively (Hoskins and Valdes 1990). In both oceanic basins, the storm track maximum lies northeast of the upper-level polar jet stream core, which is semi-permanently located over Japan and eastern North America, respectively (Chang and Orlanski 1993; Woollings et al. 2010). Such a configuration is consistent with surface baroclinic disturbances crossing the jet core from the right-entrance toward the left-exit regions, where strong upward motion of air fosters further cyclone amplification (Uccellini 1990; Rivière and Joly 2006). Additionally, upper-level mobile troughs (Bosart and Lin 1984; Sanders 1986; Reader and Moore 1995; Gyakum and Danielson 2000), and surface sensible and latent heat fluxes (Fosdick and Smith 1991; Davis and Emmanuel 1988) also contribute to extra-tropical cyclone intensification. The characteristics of these dynamical precursors and their relative vertical position (Hoskins et al. 1985) typically determine the deepening rate (Pettersen and Smebye 1971; Fink et al. 2012) and life cycle of cyclones (Bjerknes and

Iñigo Gómara · B. Rodríguez-Fonseca · P. Zurita-Gotor
Dpto. Geofísica y Meteorología, Universidad Complutense de Madrid, Facultad de CC. Físicas, Ciudad Universitaria s/n. 28040 Madrid, Spain. E-mail: i.gomara@ucm.es

S. Ulbrich
Institute for Geophysics and Meteorology, University of Cologne, Cologne, Germany

J. G. Pinto
Department of Meteorology, University of Reading, Reading, United Kingdom

Institute for Geophysics and Meteorology, University of Cologne, Cologne, Germany

Solberg 1922; Shapiro and Keyser 1990). In the literature, surface cyclones featuring strong intensification rates (equal or above 24 hPa day^{-1} at 60°N, or equivalent) are denominated 'explosive cyclones' or 'bombs' (Sanders and Gyakum 1980). These explosive cyclones are associated with strong impacts like wind gusts, heavy precipitation and storm surge events (Bosart and Lin 1984; Wernli et al. 2002; Ludwig et al. 2014).

Over the North Atlantic, the most prominent pattern of climate variability is the North Atlantic Oscillation (hereafter NAO; cf. Wanner et al. 2001). It represents a redistribution of air masses between sub-tropical and sub-polar latitudes, and modulates the strength and latitudinal location of the westerly flow (Marshall et al. 2001). Under its positive phase, the polar jet stream is accelerated and shifted to the northeast compared with its 'average' position. Under the negative phase, the jet stream is decelerated, constrained upstream in the North Atlantic and shifted to the south. The changed mean flow induces a latitudinal displacement of storm trajectories (Hurrell et al. 2003; Trigo 2006; Santos et al. 2013), and modulates their intensification rates (Gómara et al. 2014b). In this regard, the positive NAO phase is associated with stronger and more extensive baroclinicity over the North Atlantic. Under these conditions, the number of strong cyclones in the North Atlantic is higher (Pinto et al. 2009).

The synoptic temporal evolution of the NAO seems to be dominated by stochastic processes (Feldstein 2003), such as Rossby Wave-Breaking (RWB; Benedict et al. 2004; Woollings et al. 2008; Strong and Magnusdottir 2008). RWB appears to significantly control explosive cyclogenesis (Hanley and Caballero 2012; Gómara et al. 2014a) and cyclone families over Western Europe (Pinto et al. 2014) at synoptic timescales by accelerating and constraining the jet.

There has been discussion on the literature whether the lower-frequency NAO variability (James and James 1989; Wunsch 1999; Schneider et al. 2003; Raible et al. 2005) arises from pure climate noise (Stephenson et al. 2000), or is forced by external factors such as: (i) the ocean variability in the North Atlantic (Raible et al. 2001; Visbeck et al. 2003; Rodríguez-Fonseca et al. 2006; Chen et al. 2015) and tropical Pacific (Trenberth et al. 1998; Müller et al. 2008; Zhang et al. 2015); (ii) the stratosphere (Baldwin and Dunkerton 2001; Reichler et al. 2012); (iii) solar variability (Shindell et al. 2001); (iv) the mid-latitude western flow from the North Pacific (Honda et al. 2001; Pinto et al. 2011; Drouard et al. 2015); and (v) the Indian ocean (Hoerling et al. 2001; 2004), among others. Additionally, the role of anthropogenic climate change is another factor to consider. For example, there is some evidence of an intensification and eastward shift of the NAO dipole over the last decades of the 20th century (Hurrell et al. 2003; Jung et al. 2003). However, it is still unclear whether such evolution is primarily due to global warming (Ulbrich and Christoph 1999; Osborn et al. 1999; Bader et al. 2011), decadal natural variability of the NAO (Wang et al. 2012; Pinto and Raible 2012; Raible et al. 2014) and/or the storm track itself (Rogers 1997; Lu and Greatbach 2002).

The characterization of the low-frequency changes in the dominant teleconnection patterns, such as NAO, and their associated impacts has been assessed in previous studies: e.g., in European precipitation: Raible et al. (2004), Vicente-Serrano and López-Moreno (2008); in the North Atlantic Storm track: Luksch et al. (2005); Pinto et al. (2011). Such low-frequency changes (either atmospheric or oceanic) often lead to non-stationary teleconnections between remote regions (López-Parages and Rodríguez-Fonseca 2012), thus providing enhanced forecast skill of relevant phenomena during specific periods of time (Rodríguez-Fonseca et al. 2009; Losada et al. 2012).

Based on our current state of knowledge, the study of 'bomb' variability at climatic timescales (1-11 yr.) and its relation with multi-decadal variability (>33 yr.; Woollings et al. 2015) is still largely unexplored in the literature. Therefore, this study aims to address the following (and still unresolved) questions:

- What drives explosive cyclogenesis climatic (1-11 yr.) variability?
- Is the relationship between the NAO and the number of explosive cyclones over the North Atlantic diagnosed in recent papers (e.g., Pinto et al. 2009; Gómara et al. 2014b) also systematic at climatic timescales?
- Does it depend on the studied period?

To address these questions, winter track-density data of explosive North Atlantic cyclones is used from reanalysis and a long-term run (505 yr.) of an ocean-atmosphere coupled model. In sections 2 and 3 the data and methods used in this study are described. Sections 4 and 5 include results based respectively on reanalysis and Global Climate Model (GCM) data. A short discussion and summary conclude this article.

2 Data

Both reanalysis and GCM data are considered for this study. The first reanalysis dataset is provided by the *National Centers for Environmental Prediction* (NCEP; Kalnay et al. 1996). The data used has a 6-hr resolution and extends from January 1948 to February 2012. The spectral spatial resolution is T62 (approximately 2.5°x2.5°) and extends from the surface up to 3 hPa (28 vertical levels). Additionally, data from the *European Centre for Medium-*

Range Weather Forecasts (ECMWF) ERA-40 (Uppala et al. 2005) is considered. The data starts in September 1957, ends in March 2002, and is available 6-hourly with a spectral spatial resolution of T159 (~1.125°x1.125°). The 60 vertical levels reach 0.1 hPa.

The sea surface temperature (SST) and sea ice data from the *Met Office Hadley Centre* (HadISST) are used. This monthly global dataset starts in 1870 and has a 1°x1° resolution (Rayner et al. 2003). The ocean heat content is estimated from the integrated temperature from 0 to 300 m from the Simple Ocean Data Assimilation (SODA) reanalysis. The monthly fields have a horizontal resolution of 0.5˚x0.5˚ and span 1950-2009 (Carton and Giese 2008).

A coupled 505-yr control simulation with perpetual 1860 external forcing conditions performed with the ECHAM5/MPIOM1 (hereafter ECHAM5; Roeckner et al. 2003; Jungclaus et al. 2006) GCM is used. The atmospheric (oceanic) model has a spatial resolution of T63 (T31), with 31 (40) vertical levels from the surface up (down) to 10 hPa (5720 m). Oceanic and atmospheric models are coupled without further flux adjustments. The tropical SST variability is found realistic (Jungclaus et al. 2006). The storm track and NAO variability have also been evaluated in previous studies (e.g., Bengtsson et al. 2006; Pinto et al. 2011).

3 Methods

Climate indices

Climate indices are based on winter seasonal averages (DJF) using anomalies from the long term mean. A 31-point high-pass Lanczos filter with 11-yr cut-off frequency is applied to the ECHAM5 data. Filtering is not applied to reanalysis data due to the constraints posed by the short time series. Still, most of the spectral power density is concentrated within the band of 1 to 11-yr (cf. Section 4). The following indices are considered:

- The NAO index (Figs. S1a-c), defined as the leading EOF of 500-hPa geopotential height (z500) winter seasonal anomalies over the area (20-80˚N, 80˚W-40˚E; Barnston and Livezey 1987).

- The Arctic Oscillation (AO, Figs. S1d-f) and Pacific North American Pattern (PNA, Figs. S1g-i), defined as the two leading EOFs of z500 winter hemispheric anomalies north of 20ºN (NOAA CPC definition).

- The Niño-34 index (Figs. S1j-l), based on winter averaged high-pass filtered (1-13 yr) SST anomalies over the area (5ºS-5ºN, 170º-120ºW; Trenberth 1997).

- The Atlantic Multi-decadal Oscillation (AMO, Figs. S1m-o) index, defined as the leading EOF of SST winter seasonal low-pass filtered anomalies (>33-yr; detrended) over the area (95˚W-30˚E, 0-70˚N; Mohino et al. 2011).

All indices are normalized. Additionally, the upper-level (500-300 hPa) and lower-level (850-700 hPa) maximum Eady Growth Rate (*bi*; Hoskins and Valdes 1990) is used as indicator of the large-scale baroclinicity and potential wave growth (1):

$$bi = 0.31 \left(\frac{f}{N}\right) \left|\frac{\mathrm{dv}}{\mathrm{dz}}\right|, \quad (1)$$

where f is the Coriolis parameter, N is the static stability, z the vertical coordinate and v the horizontal wind vector.

Cyclones

A cyclone identification and tracking scheme (Murray and Simmonds 1991), adapted and validated for the Northern Hemisphere storm track (Pinto et al. 2005), is applied to 6-hourly winter (DJF) MSLP data. Cyclones are identified using the Laplacian of MSLP, an indicator of its geostrophic relative vorticity. Derived cyclone statistics compare well with other tracking schemes (Raible et al. 2008; Neu et al. 2013). Systems are selected based on the following criteria (Pinto et al. 2009): (i) cyclone lifetime ≥ 24 h; (ii) minimum MSLP (p) < 1000 hPa; (iii) Max. (∇^2 p) > 0.6 hPa deg.lat.$^{-2}$; and (iv) Max. d/dt ∇^2 p ≥ 0.3 hPa deg.lat.$^{-2}$ day^{-1}. The maximum normalized deepening rate (NDR) is used as a measure of cyclone's intensity (2):

$$NDR = \frac{\Delta P}{24} \frac{\sin 60°}{\sin \emptyset} \quad (2)$$

where ΔP is the pressure fall (hPa) and Φ the mean latitude of the cyclone's surface centre over a period of 24 hours. Depending on their maximum *NDR*, cyclones are separated into two 2 different subsets: (i) explosive cyclones (EC; *NDR* ≥ 1 Bergeron); and (ii) non explosive cyclones (*NDR* < 1 Bergeron). Cyclone track-densities are constructed by counting the number of cyclones intercepting a circle of radius of 7.5˚ for each grid point over time, providing combined information of cyclone numbers and track lengths.

Statistics

Different methods are applied for statistical hypothesis testing (von Storch and Zwiers 1999): (i) a two tailed t test that accounts for autocorrelation of the series (Bretherton et al. 1999); (ii) a t test for a difference in mean; (iii) a Mann-Whitney U test; and (iv) a Fisher's test for a difference in variance. The confidence intervals chosen are 95% or 99%.

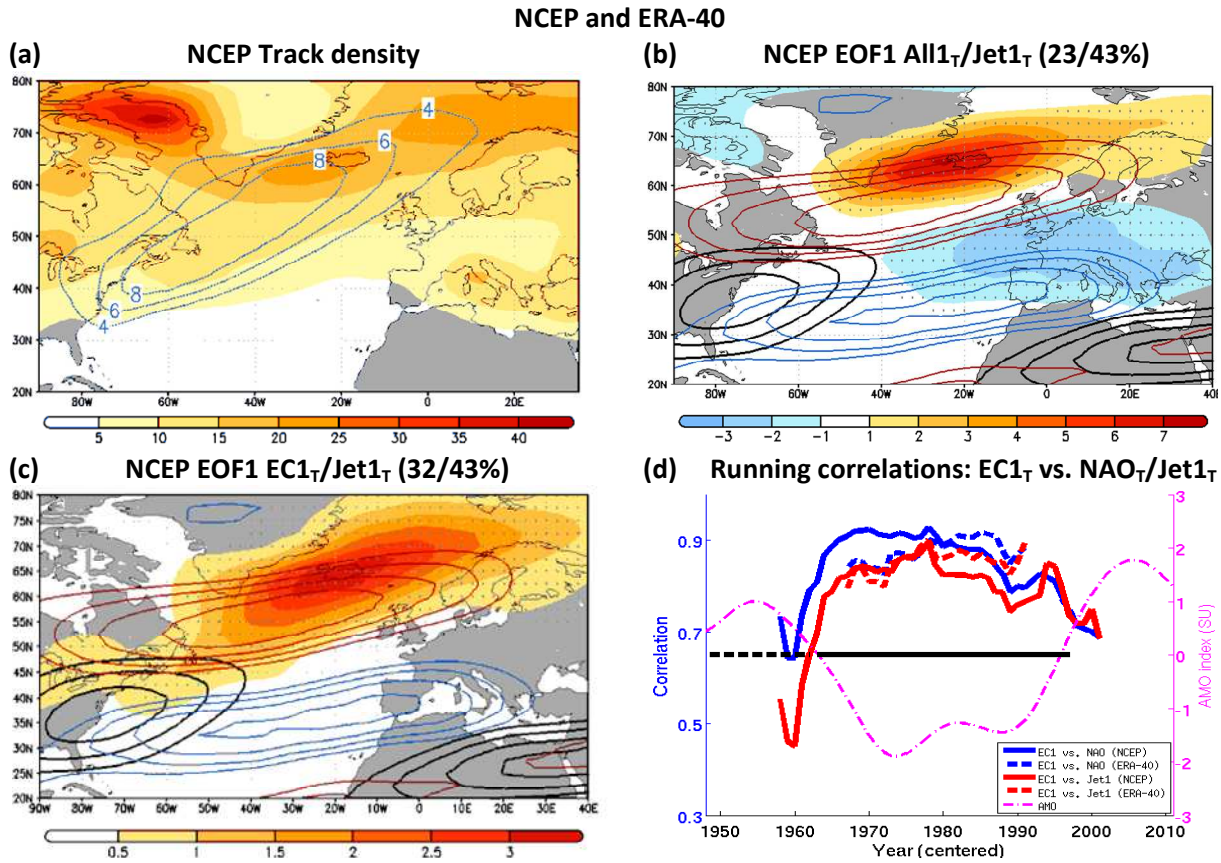

Fig. 1 (a) Mean track density plots (in counts per 7.5° radius circle area per DJF season) of explosive (contours) and non-explosive (shadings) cyclones based on NCEP (base period 1948-2011). (b) EOF1 and explained variance (%) of DJF all cyclones (explosive + non-explosive) anomalous track density fields (ALL1$_T$; shadings - 99% significance in stippling) and u250 (Jet1$_T$; red/blue contours, in m s^{-1} per std, starting from 2.5 in 0.5 m s^{-1} intervals) based on NCEP. The climatological jet stream core is shown in thick black contours (starting from 30 m s^{-1} with 5 m s^{-1} intervals). (c) Same as (b) but for explosive track density fields only. (d) 21-yr running correlations (centered) of EC1$_T$ vs. NAO$_T$ (blue lines) and EC1$_T$ vs. Jet1$_T$ (red lines) for NCEP (solid lines) and ERA40 (dashed lines). All correlations are significant (95% confidence interval, two side t test). The magenta line is the AMO index. 1948-1962 and 1963-1997 periods denoted with black dashed and black solid horizontal lines.

4 Results of the reanalysis data sets

A) High-frequency variability of explosive cyclone tracks

In this section results for both reanalyses are presented. The focus is set to the NCEP reanalysis as it spans a longer time period than ERA-40. ERA-40 results are discussed where appropriate. The mean track densities of explosive (EC) and non-explosive (NoEC) cyclones are shown in Fig. 1a (NCEP 1948-2011). For EC, a maximum extending from Newfoundland to Iceland is identified.

This maximum is consistent with cyclogenesis over the region of strongest baroclinicity near the Gulf Stream (Sanders and Gyakum 1980; Hoskins and Valdes 1990), and the subsequent intensification of storms, which typically cross the eddy driven jet from the right-entrance to the left-exit regions (Uccellini 1990). For NoEC, the area of maximum density is shifted northeastward, extending between southeast Greenland, northwest of the British Isles and Scandinavia.

In order to characterize the variability of cyclone activity, the leading Empirical Orthogonal Function (EOF) of cyclone track density is determined for the entire North Atlantic [20º-80ºN; 90ºW-40ºE] using NCEP reanalysis (Fig. 1b). This analysis includes all cyclones, i.e., explosive and non-explosive ones. The EOF pattern is hereafter labeled with the subscript $_T$ (total). The leading pattern (All1$_T$) represents a latitudinal shift of cyclone trajectories between Iceland and Western Europe. Overlaid in Fig. 1b is the leading EOF of the 250-hPa zonal wind anomalies (Jet1$_T$). The climatological jet core is also highlighted in the figure. The Jet1$_T$ pattern is consistent with the NAO variability, i.e., with a northeastward (southwestward) latitudinal displacement and intensification (weakening) of the extra-tropical jet. The spatial correspondence between All1$_T$ and Jet1$_T$ latitudinal nodes is evident in Fig. 1b, and implies the steering of cyclone trajectories by the NAO (e.g., Hurrell et al. 2003; Pinto and Raible 2012).

Table 1: Correlation coefficients between climate indices in NCEP/ERA-40/ECHAM5

Corr.	NAO	AO	PNA	Niño-34	$Jet1_T$	$Jet2_T$
$All1_T$	**0.91/0.90/0.84**	**0.78/0.79/0.56**	-0.23/-0.23/**-0.17**	-0.15/-0.08/**-0.17**	**0.92/0.90/0.84**	-0.06/-0.12/**-0.16**
$EC1_T$	**0.78/0.88/0.66**	**0.63/0.74/0.38**	-0.16/-0.25/**-0.32**	-0.11/-0.27/**-0.13**	**0.72/0.85/0.59**	0.21/0.19/**0.29**
$All2_T$	0.08/0.10/**0.21**	-0.14/-0.18/**0.14**	0.04/-0.29/**0.17**	0.04/0.14/0.04	0.03/0.06/**0.15**	**0.55/0.55/0.36**
$EC2_T$	-0.12/-0.04/**-0.36**	**-0.26**/-0.21/**-0.19**	-0.05/**-0.44**/0.02	0.04/0.20/**0.17**	-0.22/-0.21/**-0.53**	**0.65/0.78/0.50**

Significant values (95%, t test) are provided in bold numbers. Shaded cells denote significant correlation coefficients for all datasets.

The stronger center of action over Iceland (Fig. 1b) suggests increased cyclone activity over the sub-polar region under the positive NAO phase (Pinto et al. 2009). The leading EOF of explosive cyclone tracks ($EC1_T$, Fig. 1c) is compared to the $Jet1_T$ and the jet core. The $EC1_T$ pattern is consistent with $Jet1_T$, as the jet and NAO variability appear to intensify/weaken explosive cyclone activity along their climatological trajectories rather than change the cyclone pathways. Under a positive NAO and $Jet1_T$ phase, baroclinicity over the North Atlantic is stronger and larger (Pinto et al. 2009). In addition, EC forming over Eastern North America typically cross the upper-level jet from the right-entrance to the left-exit regions, and explosively amplify (Uccellini 1990). In contrast, a weaker, less extended and southerly displaced jet is obviously less efficient for explosive intensification.

For completeness, the second leading EOFs of all cyclones ($All2_T$) and explosive cyclones ($EC2_T$) are provided as supplementary material in Figs. S2a-b. $All2_T$ represents a north to south dipole of cyclone trajectories between northern Europe and the Mediterranean (Fig. S2a). $EC2_T$ reveals a different pattern, with an intensification/extension of the explosive tracks between the east cost of the US and the British Isles and a weakening northeast of Iceland (Fig. S2b). $EC2_T$ is consistent with $Jet2_T$ (250-hpa zonal wind EOF2), a large-scale configuration known to foster the occurrence of explosive cyclogenesis and storm families over Western and Central Europe (Fig. S2b; Hanley and Caballero 2012; Pinto et al. 2014).

$All1_T$/$EC1_T$ are significantly (95% confidence interval) correlated with $Jet1_T$ (0.92/0.72), the NAO (0.91/0.78) and the AO (0.78/0.63) for NCEP (Table 1). Likewise, $All2_T$ and $EC2_T$ also significantly correlate with $Jet2_T$. Most of the spectral power for these modes is concentrated within the range of periods 1-11yr (Fig. S2c for EC1, not shown for the rest) and the modes are well separated (Fig. S2d; North et al. 1982).

For comparison, the mean track density pattern and corresponding EOF modes of $ALL1_T$/$ALL2_T$, $EC1_T$/$EC2_T$, and $Jet1_T$/$Jet2_T$ are also calculated for 1957-2001 using ERA-40 (Fig. S3). The ERA-40 track density pattern (Fig. S3a) is very similar to NCEP, but with a greater total number of cyclone counts. This may be associated with the higher horizontal resolution of ERA-40 (Pinto et al. 2005). The EOFs are also similar to NCEP (Fig S3b-e) and represent the same variability (Table 1). The modes are well separated (Fig. S2d). In general terms, the linear correlation between $EC1_T$ and $Jet1_T$ agree well in both reanalysis (Table 1), with slightly lower values for NCEP (ERA-40: 0.85; NCEP: 0.72). However, if the same time period is considered, the values are almost identical (NCEP: 0.83).

B) Analysis of stationarity

In order to assess the stationarity of the relation between the NAO and explosive cyclogenesis, 21-year running correlations between the leading Principal Components (PCs) of $EC1_T$ and NAO_T/$Jet1_T$ are shown in Fig. 1d for NCEP and ERA-40. The analysis suggests a non-stationary link between the NAO_T/$Jet1_T$ variability and $EC1_T$ in NCEP. Specifically, the NAO_T/$Jet1_T$ influence on $EC1_T$ is particularly weak at the beginning of the period, increases abruptly in the 60s and remains large to the late 90s (see solid and dashed horizontal black lines in Fig. 1d). In ERA-40 (Fig. 1d; dashed blue/red curves), the time series are too short to detect any change in the correlation. Nevertheless, the ERA-40 results are consistent with NCEP between the 60s and 90s.

In order to analyze possible dynamical differences between the two NCEP periods, EOFs are calculated independently for winters 1948-1962 (labeled as 50s; e.g. $EC1_{50s}$/$Jet1_{50s}$) and 1963-1997 (labeled as 80s). All EOFs are standardized with respect to the PC for the full period. Figs. 2a-b show that the leading mode of explosive cyclone track density is sensitive to the choice of period. The 1948-1962 EOF1 for explosive cyclones ($EC1_{50s}$; Fig. 2a) is constrained over the western North Atlantic, showing a strengthening/weakening of the cyclone tracks between Eastern North America and southern Greenland. The structure of the associated $Jet1_{50s}$ depicts a latitudinal jet variability also constrained to the westernmost part of the basin (Fig. 2a).

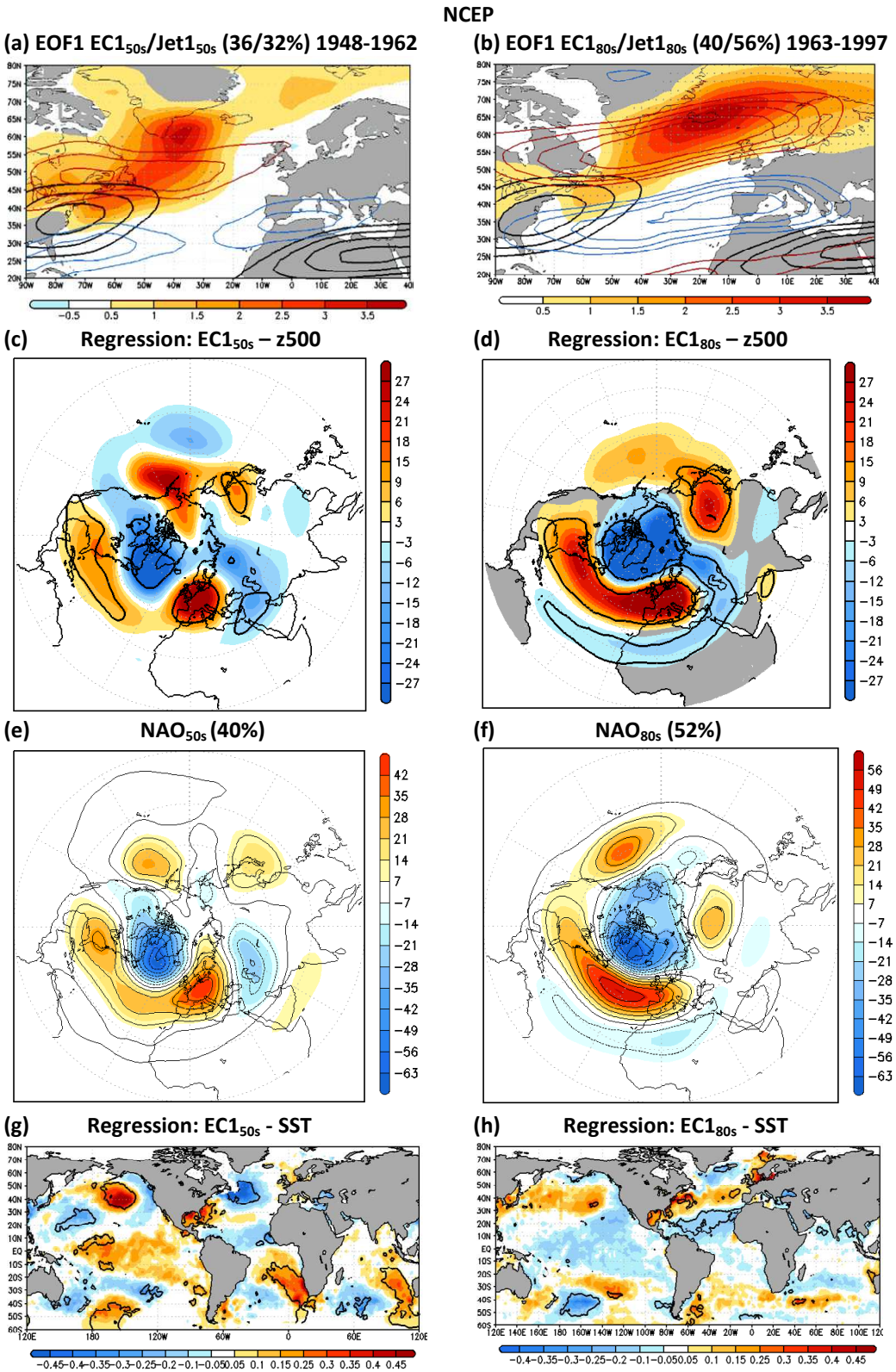

Fig. 2 (a) Same as Fig. 1(c) but for the re-calculated EOFs for the base period 1948-1962. (b) Same as (a) but for 1963-1997. (c) Regression (shadings, in gpm std^{-1}) and correlation (contours, 95% confidence interval) of EC1$_{50s}$ onto z500 winter anomalies for the period 1948-1962. (d) Same as (c) but for EC1$_{80s}$ (base period 1963-1997). (e) Re-calculated NAO pattern (NAO$_{50s}$; shadings in gpm std^{-1}) and explained variance (in %) for the base period DJF 1948-1962. (f) Same as (e) but for 1963-1997 (NAO$_{80s}$). (g) Same as (c) but for SST winter anomalies onto EC1$_{50s}$ for the period 1948-1962 (in K std^{-1}; based on HadISST). (h) Same as (g) but for EC1$_{80s}$ (base period 1963-1997).

In contrast, the spatial structure of $EC1_{80s}$ is similar to $EC1_T$ (Fig. 2b) and explains more variability (40 vs. 36%). The $EC1_{80s}$ pattern is centered over the northeastern North Atlantic, with a maximum over Iceland.

For the jet variability ($Jet1_{80s}$; Fig. 2b), both latitudinal nodes are stronger than for $Jet1_{50s}$ and span all over the North Atlantic basin, explaining a much larger fraction of variance (56 vs. 32%). The corresponding PCs are regressed on the z500 anomalies of each period (Figs. 2c-d, respectively). A pattern consisting of three centers of action over the North Atlantic is found for the first period, with positive anomalies over the western sub-tropical North Atlantic and Western Europe, and a negative anomaly south-west of Greenland. On the contrary, the second period features a very clear NAO/AO hemispheric structure with significant seesaw anomalies expanding over the whole North Atlantic.

Differences in the NAO patterns calculated independently for each period (NAO_{50s} vs. NAO_{80s}, Figs. 2e-f) are consistent with differences in the regressed z500 patterns (Moore et al. 2013). In particular, the sub-tropical NAO center of action appears weaker over the central North Atlantic in the first period, and two separated maxima are found over Eastern North America and Europe (Fig. 2e). The positive maximum over Europe may hinder the extension of cyclone tracks over the eastern North Atlantic in $EC1_{50s}$ (Fig. 2a). The spatial correlation of NAO_{50s} vs. NAO_T is only 0.50. These findings are consistent with Raible et al. (2014), where the teleconnectivity of z500 is shown to be dominant between Baffin Island and the western North Atlantic during the period 1940-1969 on 20CR reanalysis (cf. their Fig. 5b).

For the second period, a very strong, extensive, zonally symmetric and eastward displaced NAO is observed (Fig. 2f), which is consistent with enhanced cyclone activity over the eastern sub-polar North Atlantic (Fig. 2b). This NAO_{80s} pattern shows a much higher spatial correlation with the total period NAO_T (0.86).

The corresponding PCs of EC are regressed on the winter SST anomalies of each period (Figs. 2g-h). A significant cooling over the sub-tropical and sub-polar North Atlantic is associated with the positive phase of $EC1_{80s}$ (Fig. 2h) and with warming in the central part of the basin. This Atlantic SST tripole pattern is associated with the positive phase of the NAO, whose subtropical part is found to have predictive skill (Czaja and Frankignoul 1999; Rodríguez-Fonseca et al. 2006; Losada et al. 2007). The positive correlation between winter tropical Pacific and sub-tropical north Atlantic SSTs is well accepted in the literature (Wang 2002), and impacts NAO evolution during the late winter season (Sung et al. 2013). During the 50's period, a stronger connection with the North Pacific SSTs is evident (Fig. 2g). This is consistent with previous analyses on this topic (Raible et al. 2001; 2004). A noticeable feature (despite the scarce SST observations in this time period) is the absence of the positive relationship between the equatorial Pacific and the sub-tropical North Atlantic during the 50's period (Fig. 2g), coinciding with the decoupling between NAO and $EC1_{50s}$.

C) Impact of multi-decadal variability

The possible influence of the lower-frequency multi-decadal variability on the connection between explosive cyclogenesis and the NAO is investigated based on the inter-decadal evolution of the jet and maximum Eady Growth Rate. The latter is an indicator of baroclinicity and potential cyclone growth (Hoskins and Valdes 1990). The climatological values of the jet intensity and Maximum Eady Growth Rate in the upper (500-300 hPa; bi400) and lower (850-700 hPa; bi775) troposphere are presented in Figs. S4a-b (NCEP). Both variables partly overlap (especially for bi400), which is consistent with higher potential growth of cyclones in the regions where the vertical wind shear is larger (Pinto et al. 2009). Differences between the two periods (1948-1962 vs. 1963-1997) are shown in Fig. 3a. The early period is characterized by a weaker jet and decreased baroclinicity (bi400) over large parts of the sub-polar North Atlantic compared with the second period. The sub-tropical NA conditions are more suitable for cyclone formation during the early period. For the lower level baroclinicity (bi775; Fig. S4c), large differences are observed over western Greenland. Thus, this is a hint that the strong low level baroclinicity over Western Greenland in the first period is related to the deflected EC trajectories toward this region in the $EC1_{50s}$ pattern (cf. Fig. 2a). In addition, no significant change of bi775 is observed between periods over the sub-tropical North Atlantic. This is in contrast to the results of bi400 (compare Figs. 3a and S4c), and may be related to changes in the sub-tropical jet intensity, which is confined to the upper troposphere.

To analyze the decadal jet and NAO variability for the NCEP period, a Hovmöller diagram of low-pass filtered (>33 yr.) u250 anomalies averaged between 100°W-20°W, an index of the latitudinal location of the maximum positive jet anomalies and the decadal NAO index (>33-yr) are presented in Fig. 3b. The latter is shifted and rescaled to have the same mean and standard deviation as the latitude index. The period of lowest correlation between $EC1_T$ and $Jet1_T/NAO_T$ (1948-1962) is characterized by a minimum in the jet latitude index and decadal NAO values, with negative u250 anomalies over the latitude band 40˚-60˚N (Fig. 3b). In contrast, a more intense and poleward shifted jet is observed in the latter period, together with a more positive decadal NAO.

The influence of inter-decadal changes in the ocean is analyzed through the winter SSTs and integrated (0-300 m) ocean temperature. Climatologies of these variables are shown in Fig. S4d.

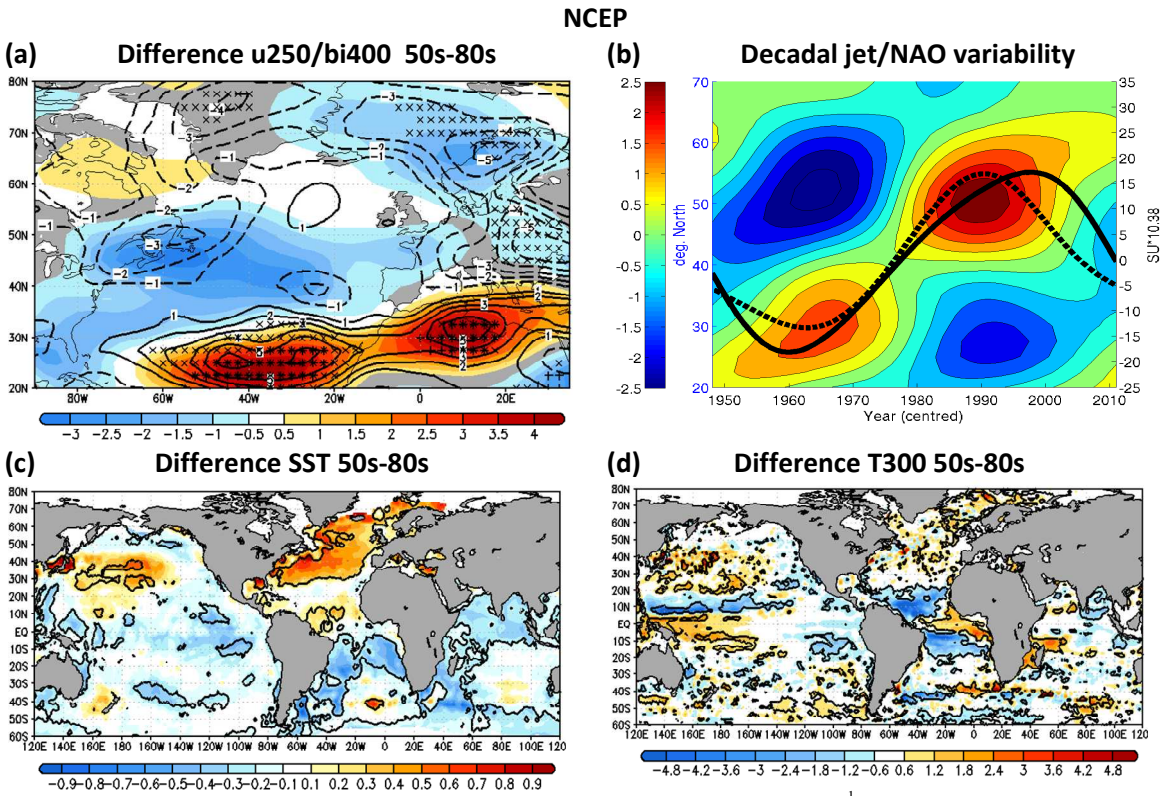

Fig. 3 (a) Difference of u250 intensity between 1948-1962 and 1963-1997 in red/blue shadings (m s^{-1}; 95% confidence interval marked with +). Difference of 300-500 hPa Eady Growth rate (bi400) in contours (day^{-1}; 95% confidence interval marked with *x*). For the differences the means of the second period are subtracted to the first one. (b) Low pass filtered (> 33-yr) u250 anomalies averaged between 100°W-20°W in red/blue shadings (m s^{-1}). The thick black line follows the latitudinal location of the maximum u250 positive anomalies. The thick dashed line is the decadal NAO index (> 33 yr.). Both indices are centered in the Y-axis and have the same standard deviation (the corresponding of the jet latitude index) to allow comparison. (c) Same as (a) but for the winter SST in red/blue shadings (in K, 95% confidence interval in contours). (d) Same as (c) but for the integral of ocean temperature from 0 to 300 m (in °C $*10^{-2}$ m). The years 1948 and 1949 are missing from the first period data, as the used version of SODA dataset starts in 1950.

Fig. 3c shows the winter SST difference between the two periods: a positive anomaly pattern apparently reminiscent of the Atlantic Multi-decadal Oscillation (AMO; Knight et al. 2005) is found over the North Atlantic. Indeed, running-correlations appear to be 180 degrees out of phase with this oceanic multi-decadal pattern (Fig. 1d). Thus, a strengthening and eastern propagation of EC in the second period (Fig. 2b) is consistent with a more negative AMO phase and a potential slowdown of the Meridional Overturning Circulation (MOC), both possibly driven by their common internal variability or greenhouse gas forcing (Woollings et al. 2012).

The difference in winter integral temperature (0-300 m) is calculated in Fig. 3d as indicator of ocean heat content above the thermocline. The emerging pattern looks consistent with the MOC circulation, with an important cooling in the sub-tropics (Wang and Zhang 2013). These results suggest an important role of the ocean in driving the explosive storm track activity over the North Atlantic.

We hypothesize that decadal variations of the jet and the ocean contribute to modulate the high-frequency climate variability of explosive cyclone tracks in the North Atlantic. However, the robustness of these results is difficult to establish given the short time series. In particular, it is not clear if the variability in EC activity is triggered by natural decadal variability, anthropogenic climate change (e.g., the eastern NAO shift during the late 20th century, a slowdown of the MOC, etc.) or just a coincidence by chance. These facts put forward the necessity of using long control simulations in order to better infer a robust hypothesis about the mechanisms involved.

5 Coupled model results

A) High-frequency variability of explosive cyclone tracks

In order to test the robustness of the results, a 505-yr control simulation of ECHAM5/MPIOM1 is analyzed. Cyclone track density of EC and NoEC are shown in Fig. 4a. Just like NCEP, the maximum in EC activity is located between Newfoundland and Iceland. For NoEC cyclones, the shape and counts are similar to NCEP over the North Atlantic.

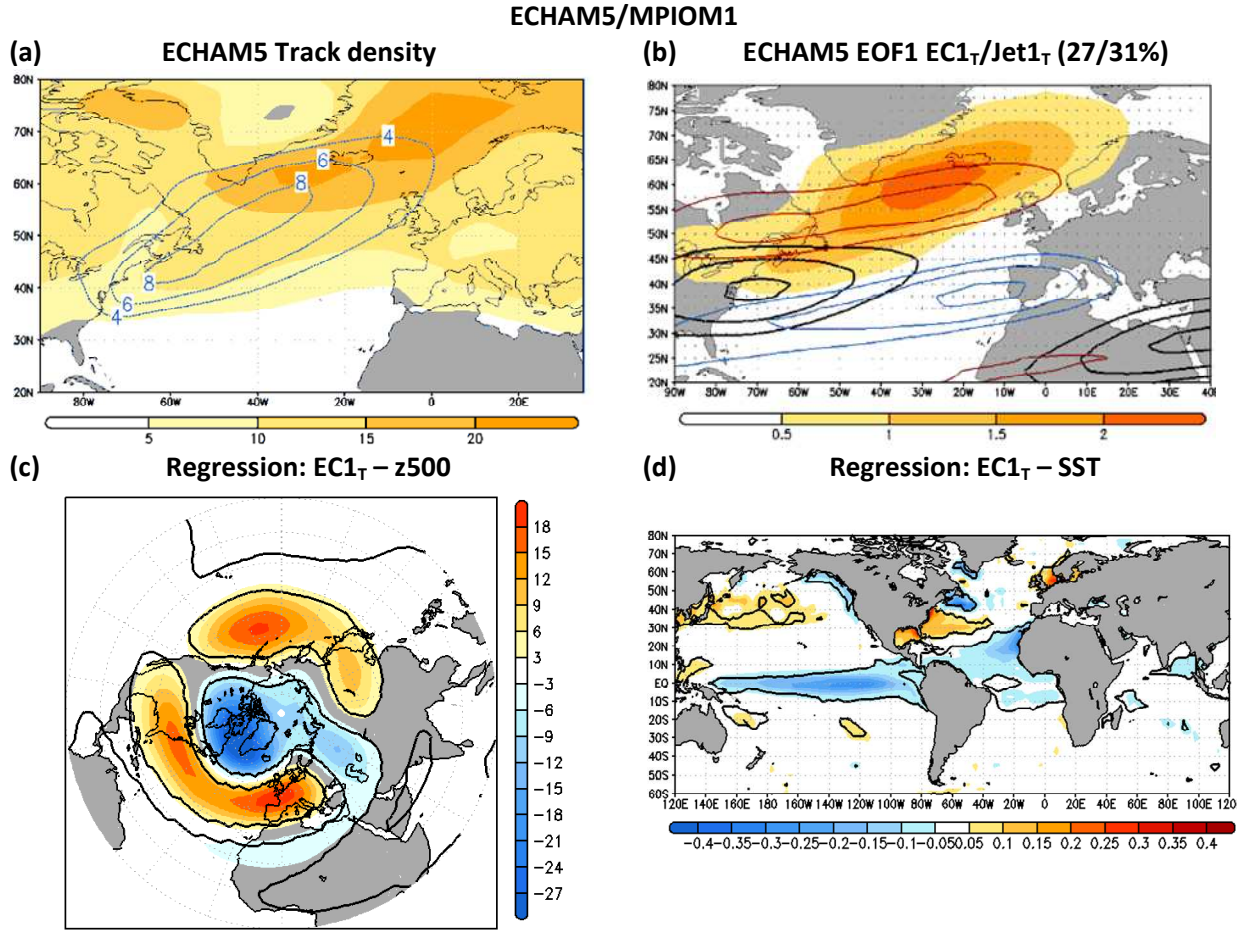

Fig. 4 (a) Same as Fig. 1(a) but for ECHAM5 (base period DJF 1-505 model years). (b) Same as Fig. 1(c) but for ECHAM5. (c) Regression (shadings, in gpm std^{-1}) and correlation (contours, 95% confidence interval) of z500 winter anomalies onto $EC1_T$ for the total period of study on ECHAM5 (years 1-505). (d) Regression (shadings, in K std^{-1}) and correlation (contours, 95% confidence interval) of SST winter anomalies onto $EC1_T$ for the total period of study on ECHAM5 (years 1-505).

The difference between ECHAM5 and NCEP for EC cyclones (Fig. S5a) shows that ECHAM5 tracks are too zonal - a systematic bias in climate models (e.g., Zappa et al. 2014; Seiler and Zwiers 2015). The same is found for NoEC cyclones (not shown). The leading EOF of explosive cyclones for the whole period ($EC1_T$) represents a strengthening/weakening of the climatological pattern between Newfoundland and Iceland (Fig. 4b), also consistent with EOF1 of u250 ($Jet1_T$).

The $EC1_T$-PC is regressed on the winter anomalies of z500 for the total ECHAM5 period (Fig. 4c), revealing again a very clear AO/NAO pattern (cf. Table 1). This pattern is very similar to that obtained for the second NCEP period (Fig. 2d). $EC1_T$-PC is also regressed on the winter SST anomalies (Fig. 4d), resulting in a pattern very similar to the second NCEP period (Fig. 2h). In particular, both the North Atlantic tripole pattern and La Niña-type variability appear to be significantly correlated with the leading mode of variability (positive phase) of explosive cyclone tracks. The model could overestimate the ENSO-like connection with EC as in the observations this is not so clear (not significant - Fig. 2h). The remaining EOFs ($All1_T$, $All2_T$, $EC2_T$) are provided in Figs. S5b-d. These are again in good agreement with NCEP and ERA-40.

B) Analysis of stationarity

To investigate whether the NCEP results are reproduced by the GCM and to what extent these results are caused by natural variability of the climate system, the time-dependent relation between $EC1_T$ and the $Jet1_T/NAO_T$ variability is analyzed. Fig. 5a shows the 21-yr running correlations between the principal components (PCs) of $EC1_T$ and the $NAO_T/Jet1_T$. $EC1_T$ and NAO_T are highly correlated most of the time, but appear to be less correlated or 'decoupled' in specific periods. The same is found for $EC1_T$ vs. $Jet1_T$ PCs. Hereupon we refer to the periods of low correlation as 'decoupling periods' (51 years in total, model years 182-209 and 305-327; Fig. 5a).

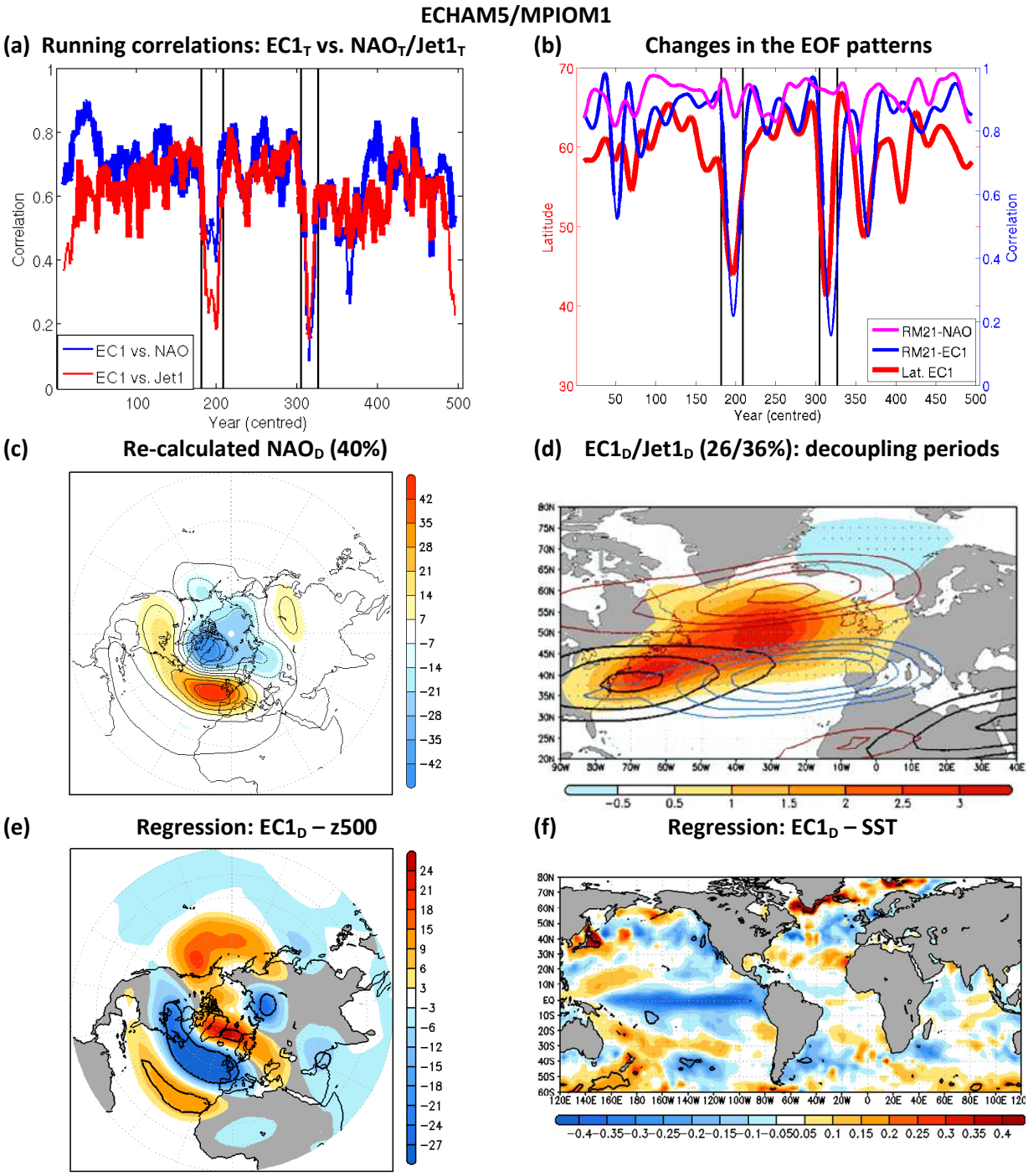

Fig. 5 (a) 21-yr running correlations (centered) of $EC1_T$ vs. NAO_T PCs (blue line) and $EC1_T$ vs. $Jet1_T$ PCs (red) on ECHAM5. Significant values highlighted with thicker red/blue segments (95% confidence interval, two tailed t test). 'Decoupling periods' denoted with vertical bars. (b) *Magenta line:* Spatial correlation of NAO_T vs. the 485 running NAO patterns (based on 21-yr. sliding window EOFs). *Blue line:* Same as the magenta line but for the 485 EC1 patterns vs. $EC1_T$. *Red line:* Latitudinal location (in deg. N; averaged over 90˚W-40˚E) of the center of action (maximum positive values) of each of the 485 EC1 patterns. (c) Same as Fig. 2(e) but for the decoupling periods on ECHAM5 (model years 182-209 and 305-327). (d) Same as Fig. 2(a) but for the decoupling periods on ECHAM5. (e) Same as Fig. 2(c) but for the decoupling periods on ECHAM5. (f) Same as Fig. 2(g) but for the decoupling periods on ECHAM5.

Although slightly smoothed, the 'decoupling periods' can still be detected in the running correlations if the window length is increased to 41-yr.

We analyze the change of the leading patterns of variability during the simulation with running EOFs. If the EC or NAO variability changes during specific periods, the EOFs for those periods are expected to look differently. With this aim, we compute the EOFs in 21-yr sliding

windows (485 patterns for 505 years) with a consistent polarity for all calculations.

The spatial correlation between each of the 485 NAO patterns and the total period NAO_T is shown in Fig. 5b. There are no abrupt changes in the correlations during the decoupling periods, suggesting that the NAO spatial structure remain largely unchanged. Moreover, the NAO pattern calculated only for the decoupling dates (Fig. 5c; hereafter NAO_D) is not much different from the total period NAO_T (Fig. S1c; spatial correlation of 0.91). Regarding the intensity of the nodes, it is noticeable the strengthening of the southern lobe of NAO_D (Fig. 5c) compared with NAO_T (Fig. S1c).

With respect to the leading mode of explosive cyclones, the spatial correlation between the time-varying and total-period modes is non-stationary in time and changes abruptly during the decoupling periods (Fig. 5b). This suggests that the occurrence of the decoupling periods is due to a different spatial structure of the leading EC variability. A zonal average (90˚W-40˚E) of each of the 485 EC1 regression patterns is performed to characterize these changes. An index with the latitudinal location of the maximum positive center of action for each EC1 pattern is displayed in Fig. 5b, and shows an abrupt southward shift of this center of action (from ~60˚N to 45˚N) during the decoupling periods. This is confirmed when the specific EOF1 of explosive cyclone track density anomalies is calculated solely for the decoupling dates ($EC1_D$; Fig. 5d). Here, $EC1_D$ represents a strengthening/weakening of the explosive cyclone track between the North American seaboard and Western Europe, a pattern shifted south relative to the total period $EC1_T$ (compare Figs. 4b and 5d). Finally, the corresponding second leading EOF ($EC2_D$) depicts an intensifying/weakening pattern quite restricted over the Icelandic area (Fig. S5e). This suggests that the two leading EOFs change order during the decoupling periods.

Although most of the variability of EC track density is explained by a pattern confined over the northern sub-polar regions, the variability shifts south for specific periods and this cannot be explained by the EOFs deduced for the full period ($EC1_T$ and NAO_T). Unlike NCEP, these changes do not appear to be associated with a longitudinal shift of the NAO nodes. The potential changes in the interannual forcing during the decoupling periods are investigated through the regression of $EC1_D$-PC on z500 and SST winter anomalies (Figs. 5e-f). During these periods, the z500 pattern associated with the variability of EC is characterized by a belt of low pressure anomalies extending from Newfoundland to Western Europe between 40°-60°N (Fig. 5e). This anomaly is accompanied by positive anomalies of z500 between Greenland and Scandinavia and over the eastern sub-tropical North Atlantic (~30˚N). The sign and shape of the z500 anomalies does not resemble the NAO+/AO+ pattern observed in Fig. 4c. Indeed, the correlation between $EC1_D$ and $Jet1_D/NAO_D$ is -0.62/-0.49 (99% confidence interval). Therefore, explosive cyclones appear to predominantly promote from NAO- during the decoupling periods. In this line, it seems plausible that the baroclinicity associated with the negative NAO years during the decoupling periods is stronger and more extensive over the North Atlantic than the corresponding of the positive years (in contrast with climatology - Pinto et al. 2009). In Figs. S6b and S6c the NAO index is regressed on bi400 (climatology in Fig. S6a). As observed, the negative values (associated with NAO-) are more extensive than the positive (NAO+) during the decoupling periods (Figs. S6c-d).

Regarding the SST anomalies, no significant regression pattern is found (Fig. 5f), nor a hint of the North Atlantic SST tripole during the decoupling periods.

C) Impact of multi-decadal variability

The potential role of the low-frequency variability as modulator of the high-frequency EC variability (1-11 yr.) is analyzed in the following. During the decoupling periods, EC is anomalously frequent in the corridor between the eastern US and Western Europe, while their numbers are reduced from southern Greenland to Western Scandinavia (Fig. 6a). A similar structure is observed in the variance, with an increase of variability to the south and a decrease to the north. This is consistent with greater variability in the areas where EC are more frequent. In contrast, no significant differences are observed in the mean or in the variance of the North Pacific storm track (not shown). This suggests that the westerly flow from the North Pacific does not play an important role in the occurrence of the decoupling periods.

This brings us again to the question of why EC tracks shift south during long and persistent periods of time (~20-25 years each). The long term anomalies of the jet intensity and the upper-level maximum Eady Growth Rate are calculated for the decoupling periods (Fig. 6b). The climatological means for ECHAM5 are provided in Fig. S6a for comparison. The overlapping between both variables is evident, although with a much more zonal structure than for NCEP. During the decoupling periods both the jet and bi400 significantly shift south (Fig. 6b), with positive anomalies over the sub-tropical North Atlantic and negative values over the Newfoundland-Iceland area. The same is observed for bi775 (not shown). Thus, the long-term upper-level conditions become more efficient for cyclone growth between the eastern US and Western Europe at the expense of the sub-polar North Atlantic.

The low-pass filtered (>33-yr) u250 anomalies averaged between 100˚-20˚W are used to highlight the latitude of the maximum positive jet anomalies in Fig. 6c. The decadal NAO index (>33-yr) is added.

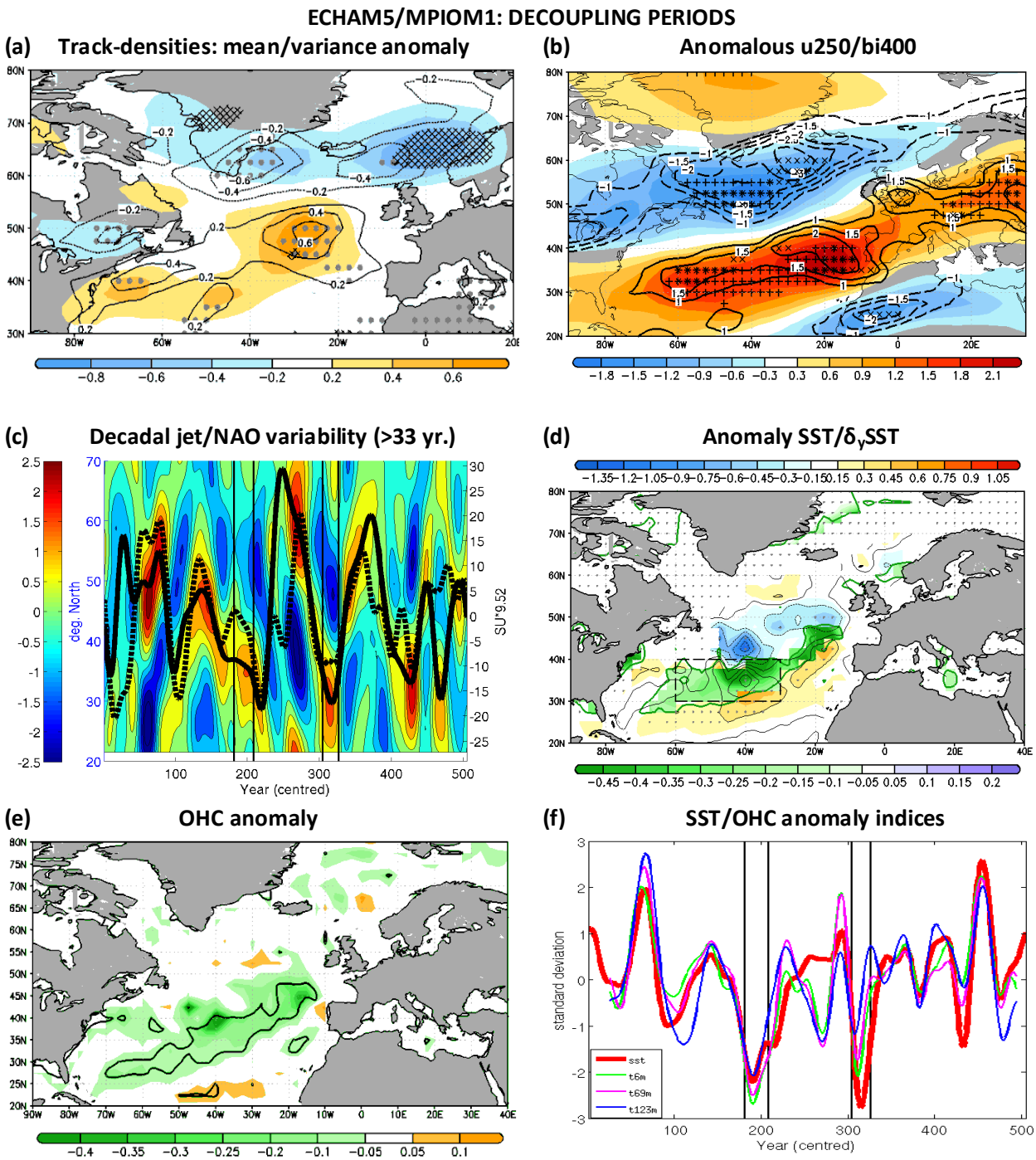

Fig. 6 (a) Explosive track density anomaly for the decoupling periods (shadings; 95% confidence interval - hatched) and standard deviation anomaly (contours; standard units, 95% confidence interval - filled dots). (b) Winter u250 anomaly (red/blue shadings in m s^{-1}, 95% confidence interval marked with +) and 300-500 hPa Eady Growth rate anomaly (bi400, contours in day^{-1}, 95% confidence interval marked with *x*) during the decoupling periods. (c) Same as Fig. 3(b) but for ECHAM5. Decoupling periods marked with vertical bars. (d) Winter SST significant anomalies (magenta-positive/green-negative shadings in K, 95% confidence interval, Mann–Whitney U test) and meridional SST gradient anomaly (δ_ySST; red-positive/blue-negative shadings in K per 1000 km, 95% confidence interval in stippling) during the decoupling periods. (e) Ocean heat content anomaly (shadings, in 10^9 J m^{-2}) during the decoupling periods (95% confidence interval in contours) between the surface and 123 m in ocean depth. (f) Low pass filtered water temperature anomalies (> 33 yr.; in SU) averaged over the area [30˚-40˚N, 60˚-30˚W, dashed rectangle in Fig. 6d] at different ocean depth levels (0, 6, 69 and 123 meters - see legend).

The polar jet exhibits strong multi-decadal variability, with multiple oscillations in the latitude range 30˚-65˚N.

It is remarkable that both decoupling periods feature a persistent and remarkably equatorward shifted jet. Moreover, weakened upper-level winds are identified around 45˚-60˚N (consistent with Fig. 6b). Although the

low-frequency variability of the NAO and the jet appear similar in Fig. 6c, it is surprising that the decadal NAO index hardly changes during the decoupling periods. Therefore, it is plausible to assume the existence of an additional and independent potential forcing co-responsible for the extremely southern position of the jet in these situations.

To find this potential modulator, the SST anomalies over the North Atlantic are analyzed. Eddy-driven jets tend to be collocated with areas with maximum meridional SST gradients (cf. Fig. S6e; Minobe et al. 2008; Nakamura et al. 2008). Therefore, we hypothesize that if the North Atlantic SST gradient shifts in latitude during specific periods, then the extra-tropical jet and baroclinicity fields might also react to this forcing (Dong et al. 2013). This is observed for the SST and meridional SST gradient anomalies during the decoupling periods (Fig. 6d). During these periods, an extensive cold SST anomaly is present across the North Atlantic. The presence of this negative SST anomaly induces an attenuation of the meridional gradient over the Gulf Stream area and an increase over the sub-tropical North Atlantic. Such a SST anomaly pattern is thought to: (i) trigger the establishment of positive extra-tropical jet intensity and baroclinicity anomalies over the sub-tropical North Atlantic; and (ii) support the persistence of these anomalies through a positive feedback process. A southerly shifted storm track cools the waters beneath, that act to reinforce the pre-existing SST anomaly (Dong et al. 2013). To investigate whether the negative SST anomaly is originally triggered from the ocean depth or by the lower atmosphere, the ocean heat content above the thermocline (from 0 to 123 m) and its anomaly for the decoupling periods are calculated (Fig. 6e; climatology in Fig. S6f). The value of 123 m is selected based on a calculation of the mean thermocline depth over the sub-tropical north Atlantic area in MPIOM1 (not shown). Indeed, the negative SST anomaly during the decoupling periods (Fig. 6d) is also identified in the ocean's mixed layer and thermocline (Fig. 6e). Several indices of temperature anomaly in this layer are constructed for the North Atlantic area (30˚-40˚N, 60˚-30˚W). The selected area for the indices overlaps well the region of negative SST anomalies during the decoupling periods (Fig. 6d). Fig. 6f shows the low pass filtered (> 33yr.) indices of temperature anomaly, revealing exceptional negative anomalies in this area. These temperature anomalies extend through the ocean depth and even below the thermocline region (cf. Fig. S6g). These results support the idea that the multi-decadal variability of the ocean itself also contributes to the occurrence of the reported decoupling periods on ECHAM5 by pushing the extra-tropical jet equatorward.

6 Summary and conclusions

This study explores the modulating role of the low-frequency oceanic and atmospheric variability (>33-yr) on the high-frequency climate variability (1-11 yr) of explosive cyclogenesis over the North Atlantic in wintertime. For this purpose, the track density of explosive and non-explosive cyclones from two reanalysis datasets and a long control Global Climate Model (GCM) simulation are analyzed. An Empirical Orthogonal Function (EOF) approach is used to characterize the preferred modes of variability in the North Atlantic.

Results show that the leading mode of the high-frequency climate variability for all cyclones ($All1_T$) represents primarily a latitudinal shift of cyclone trajectories between Iceland and Western Europe (Fig. 1b). This pattern is consistent with previous studies (e.g., Rogers 1997; Lu and Greatbach 2002). However, the leading variability mode of explosive cyclone tracks ($EC1_T$) consists of a strengthening/weakening pattern extending from Newfoundland to Iceland (Fig. 1c). Although these two patterns are different, both modes are significantly correlated with the North Atlantic Oscillation (NAO) during most time periods in all three datasets (cf. Table 1). This results from the influence of the NAO in modulating cyclone's trajectories ($All1_T$; cf. Wanner et al. 2001) and cyclone intensification rates ($EC1_T$; cf. Pinto et al. 2009). However, during specific decades of NCEP and ECHAM5 the EC1-NAO correlation abruptly changes.

On NCEP, this fluctuating relationship seems to be associated with multi-decadal changes in the NAO shape and location. In particular, between 1948 and 1962 the NAO-EC1 correlation is 0.68. In this period the NAO pattern is more confined over the western North Atlantic (Raible et al. 2014). Contrastingly, the period 1963-1997 is characterized by an eastward extension and intensification of the NAO centers of action (especially the sub-tropical node; Jung et al. 2003). In this interval the NAO-EC1 correlation raises up to 0.89. The changes in the NAO structure are consistent with the changes in EC1 between periods. Thus, EC1 is more confined west in the basin during the mid 20th century, whereas for the last decades it appears stronger and more extended towards Northern Europe (cf. Fig. 2). These changes in NAO and EC1 variability between decades are also consistent with changes in the AMO phase (Woollings et al. 2012).

On ECHAM5, the NAO-EC1 connection is systematic and robust for most of the simulation excepting two periods of about 20-25 yr. each. During these periods (so called 'decoupling periods') a strong decrease in the running 21 yr. correlations is observed (please note that these correlations are smoothed by the running windows - Fig. 5a). Indeed, if the specific EOF patterns are calculated solely for these periods, there exists strong and significant (95% confidence level) EC1-NAO anti-correlation (-0.49).

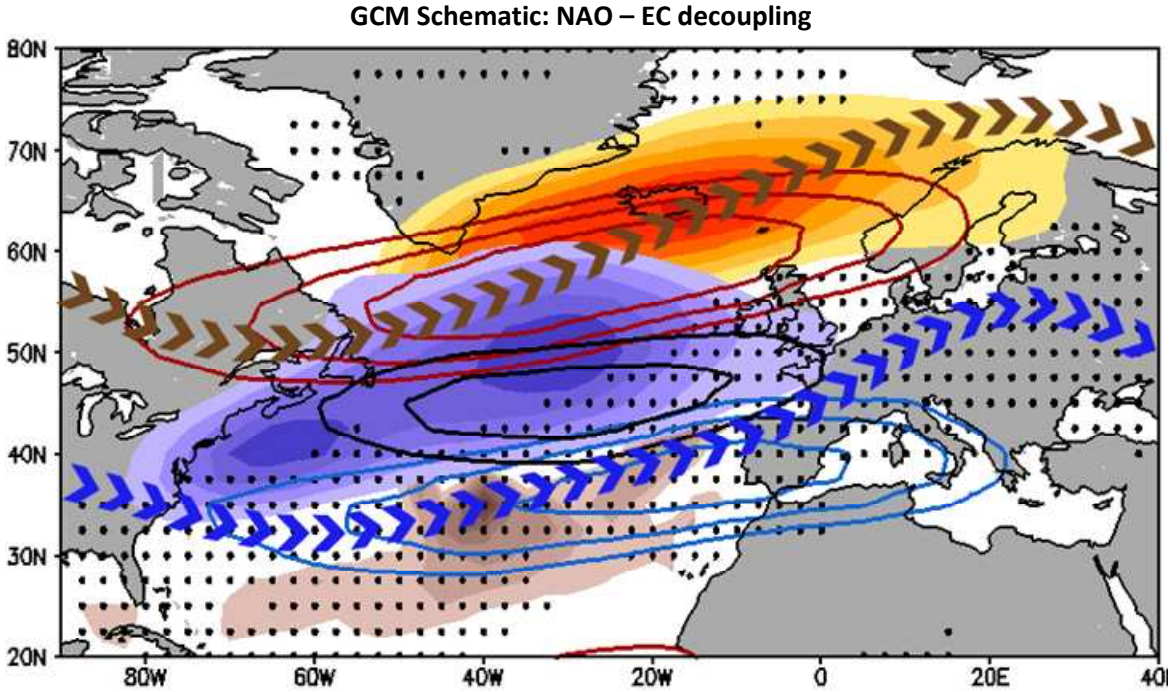

Fig. 7 Schematic of the mechanism leading to abrupt fluctuations in the climate variability of explosive cyclogenesis on ECHAM5/MPIOM1. *High-frequency features (1-11yr.)*: Leading EOFs of winter EC track density (shadings; red-'normal conditions'; purple-'decoupling periods') and u250 (contours; red-positive/blue-negative phases of EOF1/NAO; black - EOF2 positive phase) data. *Low-frequency fields (> 33 yr.):* Multi-decadal positions of the Jet (arrows; red - NAO+; blue - 'decoupling periods'), enhanced baroclinicity (stippling - 'decoupling periods') and enhanced meridional SST gradient (brown shadings - 'decoupling periods').

Such change in correlation is triggered by an abrupt equatorward displacement of the EC1 main centre of action during the decoupling periods. In Fig. 7 this abrupt shift can be easily observed (compare red – 'normal conditions' vs. purple – 'decoupling periods' shadings). Not surprisingly, during these decades the extra-tropical jet is remarkably shifted south from its average position and enhanced baroclinicity is present over the sub-tropical North Atlantic (Fig. 7). Such jet configuration is accompanied by a stronger SST gradient over the sub-tropical North Atlantic. As a consequence, explosive cyclone tracks shift south (cf. Fig. 6a). Regarding the NAO pattern, no remarkable change is observed in its structure within the decoupling periods, apart from an intensification of its southern node. Nevertheless, during these periods the baroclinicity associated with NAO- is stronger and more extensive than the associated with NAO+ (Figs. S6b-d). This behavior is exactly the opposite of what is observed in climatology (ECHAM5) and reanalysis (Pinto et al. 2009). Therefore, during the decoupling periods explosive cyclones appear to promote from NAO- and their main variability mode is thus shifted south.

A second mechanism potentially explaining the occurrence of the ECHAM5 decoupling periods is associated with the existence of intense ascent of air in the right-entrance an left-exit regions of the jet core (Uccellini 1990; Riviére and Joly 2006). Under a positive NAO phase (normal conditions), low pressure systems forming over the eastern North American seaboard (Fig. S7a) cross the jet from the right-entrance toward the left-exit regions and explosively amplify (Fig. 7; cf. Uccellini 1990). Under a negative NAO phase, baroclinic disturbances do not encounter favorable upper level conditions and explosive cyclogenesis is mitigated over the sub-polar North Atlantic. This mechanism might hold for most of the periods studied in all 3 data-sets, and rely on the alternate succession of north and central/south jet positions during consecutive winters (cf. contours in Fig. 7; Woollings et al. 2010). In particular, the number of years with a northern jet location can be an important factor in triggering the leading variability mode of explosive cyclone tracks, as a high fraction of variance can be introduced during the NAO+ years in the timeseries. On the contrary, if the jet is repeatedly situated over the central or sub-tropical North Atlantic (i.e. a marked southerly shifted multi-decadal jet), the variance associated with NAO+ years is absent and other modes of variability (not necessary related to NAO+) can emerge. These correspond to abrupt transitions in the EC variability.

However, the mechanism above is only valid if the regions of strong genesis do not significantly vary with the NAO. To prove/reject this assumption, the NAO_T-PC is regressed on the winter explosive genesis density fields of ECHAM5 (Fig. S7b).

Despite the NAO phases appear to slightly influence the main regions of explosive cyclogenesis in the North Atlantic (Hoskins and Hodges 2002), the changes in total genesis counts are low (max. ~15%). In this line, the influence over the Eastern North American genesis area is almost negligible.

The present results evidence the importance of the low-frequency control for the time-evolving high-frequency climate variability of explosive cyclone tracks in the North Atlantic. This modulation leads to a non-stationary connection between the NAO and EC activity both in reanalysis and GCM data (Raible et al. 2014). Moreover, an unsteady connection between EC leading variability (positive phase) and La Niña is also found in the GCM data, though of weaker magnitude (Luksch et al. 2005). The current results can potentially contribute to an improvement of the multi-decadal predictions of extreme cyclones in the North Atlantic (e.g., Lee et al. 2012; Nissen et al. 2014). A clear example of this multi-decadal variability is the observed increased storm activity over Northern and Western Europe during the recent decades (Feser et al. 2015). This study also suggests that year-to-year predictions of EC activity in the North Atlantic shall consider a time-evolving forecast skill of the NAO (Scaife et al. 2014) and ENSO (Barnston et al. 2012) in their analyses.

Regarding the potential role of anthropogenic climate change in the results observed on NCEP, it must be noted that abrupt changes in the variability of explosive cyclogenesis are also observed in the pre-industrial simulation, so these transitions appear to be internally driven. Finally, as this study is mainly focused on explosive cyclogenesis, an extended analysis for all cyclones and its time-varying relation with the NAO will be an interesting path for future research through the use of a larger set of control and forced simulations (e.g., CMIP5 models).

Acknowledgments We thank the *National Centers for Environmental Prediction* and the *European Centre for Medium-Range Weather Forecasts* for the NCEP and ERA-40 reanalysis. We thank the *Met Office Hadley Centre* for the SST and sea ice data (HadISST) and the *University of Maryland* for the Simple Ocean Data Assimilation (SODA) reanalysis. We are indebted to the *Max Plank Institute* and the *Deutsches Klimarechenzentrum* (DKRZ) for the ECHAM5/MPIOM1 data. In particular, we thank Hans Winter, Hannes Thiemann, Helmuth Haak and Monika Esch for help with the MPIOM1 data. IG is supported by the research projects MULCLIVAR (CGL-2012-38923-C02-01 - Spanish Ministry of Economy and Competitiveness) and PREFACE (EUFP7/2007–2013 grant agreement 603521). We thank Irene Polo, Marta Martín-Rey, Jorge López-Parages, Rubén Banderas, Tim Woollings, Christoph Raible and Gwendal Rivière for constructive comments.

References

Bader J, Mesquita MDS, Hodges KI, Miles M, Osterhus S, Keenlyside N (2011) A Review on Northern Hemisphere Sea-Ice, Storminess and the North Atlantic Oscillation: Observations and Projected Changes. Atmos Res 101: 809-834. doi:10.1016/j.atmosres.2011.04.007 .

Baldwin MP, Dunkerton TJ (2001) Stratospheric Harbingers of Anomalous Weather Regimes. Science 294 (5542): 581-584. DOI:10.1126/science.1063315

Barnston AG, Livezey RE (1987) Classification, Seasonality and Persistence of Low-Frequency Atmospheric Circulation Patterns. Mon Wea Rev 115: 1083–1126. doi: 10.1175/1520-0493(1987)115<1083:CSAPOL>2.0.CO;2

Barnston AG, Tippett MK, L'Heureux ML, Li S, DeWitt DG (2012) Skill of Real-Time Seasonal ENSO Model Predictions during 2002–11: Is Our Capability Increasing? Bull Amer Meteor Soc 93: 631–651, doi: http://dx.doi.org/10.1175/BAMS-D-11-00111.1

Benedict JJ, Lee S, Feldstein SB (2004) Synoptic view of the North Atlantic Oscillation. J Atmos Sci 61: 121 - 144.

Bengtsson L, Hodges KI, Roeckner E, Brokopf R (2006) On the natural variability of the pre-industrial European climate. Clim Dyn 27:743–760.

Bjerknes J, Solberg H (1922) Life cycle of cyclones and the polar front theory of atmospheric circulation. Geofys Publ 3: 3-18.

Blackmon ML, Wallace JM, Lau NC, Mullen SL (1977) An Observational Study of the Northern Hemisphere Wintertime Circulation. J Atmos Sci 34: 1040-1053. doi: 10.1175/1520-0469(1977)034<1040:AOSOTN>2.0.CO;2

Bosart LF, Lin SC (1984) A diagnostic analysis of the Presidents' Day storm of February 1979. Mon Wea Rev 112: 2148 - 2177.

Branstator G (2002) Circumglobal teleconnections, the jet stream wave-guide, and the North Atlantic Oscillation. J Climate 15: 1893-1910.

Bretherton CS, Widmann M, Dymnikov VP, Wallace JM, Blade I (1999) Effective number of degrees of freedom of a spatial field. J Climate 12: 1990-2009.

Carton JA, Giese BS (2008) A Reanalysis of Ocean Climate Using Simple Ocean Data Assimilation (SODA). Mon Weather Rev 136: 2999-3017

Chang EKM, Orlanski I (1993) On the Dynamics of a Storm Track. J Atmos Sci 50: 999–1015. doi: 10.1175/1520-0469(1993)050<0999:OTDOAS>2.0.CO;2

Chen S, Wu R, Chen W (2015) The Changing Relationship between Interannual Variations of the North Atlantic Oscillation and Northern Tropical Atlantic SST. J Climate 28: 485–504. doi: 10.1175/JCLI-D-14-00422.1

Czaja A, Frankignoul C (1999) Influence of the North Atlantic SST on the atmospheric circulation. Geophys Res Lett 26 (19): 2969-2972. DOI: 10.1029/1999GL900613

Davis CA, Emanuel KA (1988) Observational evidence for the influence of surface heat fluxes on maritime cyclogenesis. Mon Wea Rev 116: 2649 - 2659.

Dong B, Sutton RT, Woollings T, Hodges K (2013) Variability of the North Atlantic summer storm track: mechanisms and impacts on European climate. Environ Res Lett 8: 034037. doi:10.1088/1748-9326/8/3/034037

Drouard M, Rivière G, Arbogast P (2015) The Link between the North Pacific Climate Variability and the North Atlantic Oscillation via Downstream Propagation of Synoptic Waves. J Climate 28: 3957-3976. doi: 10.1175/JCLI-D-14-00552.1

Feldstein SB (2003) The dynamics of NAO teleconnection pattern growth and decay. Q J R Meteorol Soc 129: 901-924.

Feser F, Barcikowska M, Krueger O, Schenk F, Weisse R, Xia L (2015) Storminess over the North Atlantic and northwestern Europe-A review. Q J R Meteorol Soc 141: 350-382. doi: 10.1002/qj.2364

Fink AH, Pohle S, Pinto JG, Knippertz P (2012) Diagnosing the influence of diabatic processes on the explosive deepening of extratropical cyclones. Geophys Res Lett 39: L07803. doi:10.1029/2012GL051025.

Fosdick EK, Smith PJ (1991) Latent Heat Release in an Extratropical Cyclone that Developed Explosively over the Southeastern United States. Mon Wea Rev 119: 193-207.

Gómara I, Pinto JG, Woollings T, Masato G, Zurita-Gotor P, Rodríguez-Fonseca B (2014a) Rossby Wave-Breaking analysis of Explosive Cyclones in the Euro-Atlantic sector. Q J R Meteorol Soc 140: 738–753. . doi: 10.1002/qj.2190

Gómara I, Rodríguez-Fonseca B, Zurita-Gotor P, Pinto JG (2014b) On the relation between explosive cyclones affecting Europe and the North Atlantic Oscillation. Geophys Res Lett 41: 2182-2190. doi:10.1002/2014GL059647.

Gyakum JR, Danielson RE (2000) Analysis of meteorological precursors to ordinary and explosive cyclogenesis in the western North Pacific. Mon Wea Rev 128: 851 - 863.

Hanley J, Caballero R (2012) The role of large-scale atmospheric flow and Rossby wave breaking in the evolution of extreme windstorms over Europe. Geophys Res Lett 39: L21708, doi:10.1029/2012GL053408

Hoerling MP, Hurrell JW, Xu T (2001) Tropical origin for recent North Atlantic climate change. Science 292: 90- 92

Hoerling MP, Hurrell JW, Xu T, Bates GT, Phillips A (2004) Twentieth century North Atlantic climate change. Part II: Understanding the effect of Indian Ocean warming. Clim Dyn 23: 391-405, doi:10.1007/s00382-004-0433-x

Honda M, Nakamura H, Ukita J, Kousaka I, Takeuchi K (2001) Interannual Seesaw between the Aleutian and Icelandic Lows. Part I: Seasonal Dependence and Life Cycle. J Climate 14: 1029-1042. doi: 10.1175/1520-0442(2001)014<1029:ISBTAA>2.0.CO;2

Hoskins BJ, McIntyre ME, Robertson AW (1985) On the use and significance of isentropic potential vorticity maps. Q J R Meteorol Soc 111: 877-946.

Hoskins BJ, Valdes PJ (1990) On the Existence of Storm-Tracks. J Atmos Sci 47: 1854-1864. doi: 10.1175/1520-0469(1990)047<1854:OTEOST>2.0.CO;2

Hoskins BJ, Ambrizzi T (1993) Rossby wave propagation on a realistic longitudinally varying flow. J Atmos Sci 50: 1661–1671.

Hoskins BJ, Hodges KI (2002) New perspectives on the Northern Hemisphere winter storm tracks. J. Atmos. Sci., 59 (6), 1041-1061.

Hurrell JW, Kushnir Y, Ottersen G, Visbeck M (2003) The North Atlantic Oscillation: climate significance and environmental impact. Geophys. Monogr. Series 134: 279pp.

James IN, James PM (1989) Ultra-low-frequency variability in a simple atmospheric circulation model. Nature 342: 53-55

Jung T, Hilmer M, Ruprecht E, Kleppek S, Gulev SK, Zolina O (2003) Characteristics of the Recent Eastward Shift of Interannual NAO variability. J Clim 16:3371-3382.

Jungclaus JH, Botzet M, Haak H, Keenlyside N, Luo JJ, Latif M, Marotzke J, Mikolajewicz U, Roeckner E (2006) Ocean circulation and tropical variability in the coupled model ECHAM5/MPI-OM. J Clim 19:3952-3972.

Kalnay E, and co-authors (1996) The NCEP/NCAR 40-Year Reanalysis Project, Bull the Am Meteorol Soc 77: 437-471.

Knight JR, Allan RJ, Folland CK, Vellinga M, Mann ME (2005) A signature of persistent natural thermohaline circulation cycles in observed climate. Geophys Res Lett 32: L20708. doi:10.1029/2005GL024233.

Lau NC (1978) On the Three-Dimensional Structure of the Observed Transient Eddy Statistics of the Northern Hemisphere Wintertime Circulation. J Atmos Sci 35: 1900–1923. doi: 10.1175/1520-0469(1978)035<1900:OTTDSO>2.0.CO;2

Lau NC (1988) Variability of the Observed Midlatitude Storm Tracks in Relation to Low-Frequency Changes in the Circulation Pattern. J Atmos Sci 45: 2718–2743. doi: http://dx.doi.org/10.1175/1520-0469(1988)045<2718:VOTOMS>2.0.CO;2

Lee SS, Lee JY, Wang B, Ha KJ, Jin FF, Straus DM, Shukla J (2012) Interdecadal changes in the storm track activity over the North Pacific and North Atlantic. Clim Dyn 39: 313-327. doi:10.1007/s00382-011-1188-9. IPRC-817.

López-Parages J, Rodríguez-Fonseca B (2012) Multidecadal modulation of El Niño influence on the Euro-Mediterranean rainfall. Geophys Res Lett 39: L02704. doi:10.1029/2011GL050049.

Losada T, Rodríguez-Fonseca B, Mechoso CR, Ma HY (2007) Impacts of SST anomalies on the North Atlantic atmospheric circulation: a case study for the northern winter 1995/1996. Clim Dyn 29 (7-8): 807-819.

Losada T, Rodriguez-Fonseca B, Mohino E, Bader J, Janicot S, Mechoso CR (2012) Tropical SST and Sahel rainfall: A non-stationary relationship. Geophys Res Lett 39: L12705 doi:10.1029/2012GL052423.

Lu J, Greatbatch RJ (2002) The changing relationship between the NAO and northern hemisphere climate variability. Geophys Res Lett 29 (7) doi: 10.1029/2001GL014052.

Ludwig P, Pinto JG, Reyers M, Gray SL (2014) The role of anomalous SST and surface fluxes over the southeastern North Atlantic in the explosive development of windstorm Xynthia. Q J R Meteorol Soc 140: 1729–1741. doi: 10.1002/qj.2253

Luksch U, Raible CC, Blender R, Fraedrich K (2005) Decadal Cyclone Track Variability in the North Atlantic. Metorol Z special issue 14:747-753

Marshall J, and coauthors (2001) North Atlantic climate variability: Phenomena, impacts and mechanisms. Int J Climatol 21: 1863-1898.

Minobe S, Kuwano-Yoshida A, Komori N, Xie SP, Small RJ (2008) Influence of the Gulf Stream on the troposphere. Nature 452 (7184): 206–209

Mohino E, Janicot S, Bader J (2011) Sahel rainfall and decadal to multi-decadal sea surface temperature variability. Climate Dynamics 37(3):419-440. DOI:10.1007/s00382-010-0867-2

Moore GWK, Renfrew IA, Pickart RS (2013) Multidecadal mobility of the North Atlantic Oscillation, J Climate 26: 2453–2466.

Müller WA, Frankignoul C, Chouaib N (2008). Observed decadal tropical Pacific–North Atlantic teleconnections. Geophys Res Lett 35: L24810. doi:10.1029/2008GL035901

Murray RJ, Simmonds I (1991) A numerical scheme for tracking cyclone centers from digital data. Part I: development and operation of the scheme. Austr Meteorol Mag 39: 155-166.

Nakamura H, Sampe T, Goto A, Ohfuchi W, Xie SP (2008) On the importance of mid-latitude oceanic frontal zones for the mean state and dominant variability in the tropospheric circulation. Geophys Res Lett 35. doi:10.1029/2008GL034,010

Neu U, and co-authors (2013) IMILAST: A Community Effort to Intercompare Extratropical Cyclone Detection and Tracking Algorithms. Bull Amer Meteor Soc 94: 529-547. doi: 10.1175/BAMS-D-11-00154.1

Nissen KM, Ulbrich U, Leckebusch GC, Kuhnel I (2014) Decadal windstorm activity in the North Atlantic-European sector and its relationship to the meridional overturning circulation in an ensemble of simulations with a coupled climate model. Clim Dyn 43(5-6): 1545-1555. doi:10.1007/s00382-013-1975-6

North GR, Bell TL, Cahalan RF, Moeng FJ (1982) Sampling errors in the estimation of empirical orthogonal functions. Mon Weather Rev 110: 699-706. doi:10.1175/1520-0493(1982)110<0699:SEITEO> 2.0.CO;2

Osborn TJ, Briffa KR, Tett SFB, Jones PD, Trigo RM (1999) Evaluation of the North Atlantic oscillation as simulated by a coupled climate model. Clim Dyn 15:685-702.

Petterssen S, Smebye SJ (1971) On the development of extratropical cyclones. Q J R Meteorol Soc 97: 457-482. doi: 10.1002/qj.49709741407

Pinto JG, Spangehl T, Ulbrich U, Speth P (2005) Sensitivities of

cyclone detection and tracking algorithm: individual tracks and climatology. Meteorol Z 14: 823-838.

Pinto JG, Zacharias S, Fink AH, Leckebusch GC, Ulbrich U (2009) Factors contributing to the development of extreme North Atlantic cyclones and their relationship with the NAO. Clim Dyn 32: 711-737.

Pinto JG, Reyers M, Ulbrich U (2011) The variable link between PNA and NAO in observations and in multi-century CGCM simulations. Clim Dyn 36 (1-2): 337-354. doi: 10.1007/s00382-010-0770-x

Pinto JG, Raible CC (2012) Past and recent changes in the North Atlantic oscillation. Wiley Interdisciplinary Reviews: Climate Change 3: 79-90. doi:10.1002/wcc.150

Pinto JG, Gómara I, Masato G, Dacre HF, Woollings T, Caballero R (2014) Large-scale dynamics associated with clustering of extratropical cyclones affecting Western Europe. J Geophys Res Atmos 119, 13,704–13,719, doi:10.1002/2014JD022305.

Raible CC, Luksch U, Fraedrich K, Voss R (2001) North Atlantic decadal regimes in a coupled GCM simulation. Clim Dyn 18: 321-330

Raible CC, Luksch U, Fraedrich K (2004) Precipitation and Northern Hemisphere Regimes. Atmos Sci Lett 5: 43-55, DOI: 10.1016/j.atmoscilet.2003.12.001

Raible C C, Stocker TF, Yoshimori M, Renold M, Beyerle U, Casty C, Luterbacher J (2005) Northern Hemispheric trends of pressure indices and atmospheric circulation patterns in observations, reconstructions, and coupled GCM simulations. J Climate 18: 3968-3982

Raible CC, Della-Marta P, Schwierz C, Wernli H, Blender R (2008) Northern Hemisphere extratropical cyclones: A comparison of detection and tracking methods and different reanalyses. Mon Wea Rev 136: 880-897.

Raible CC, Lehner F, Gonzalez-Rouco JF, Fernandez-Donado L (2014) Changing correlation structures of the Northern Hemisphere atmospheric circulation from 1000 to 2100 AD, Climate of the Past 10: 537-550, doi:10.5194/cp-10-537-2014.

Rayner NA, Parker DE, Horton EB, Folland CK, Alexander LV, Rowell DP, Kent EC, Kaplan A (2003) Global analyses of sea surface temperature, sea ice, and night marine air temperature since the late nineteenth century. J Geophys Res 108 (14): 4407. doi: 10.1029/2002JD002670

Reader MC, Moore GWK (1995) Stratosphere-troposphere interactions associated with a case of explosive cyclogenesis in the Labrador Sea. Tellus A 47: 849-863.

Reichler T, Kim J, Manzini E, Kröger J (2012) A stratospheric connection to Atlantic climate variability. Nature Geoscience 5: 783-787. doi:10.1038/ngeo1586.

Rivière G, Joly A (2006) Role of the low-frequency deformation field on the explosive growth of extratropical cyclones at the jet exit. Part I: Barotropic critical region. J Atmos Sci 63: 1965-1981.

Rodríguez-Fonseca B, Polo I, Serrano E, Castro M (2006) Evaluation of the North Atlantic SST forcing on the European and North African Winter climate. Int J Climatol 25. DOI 10.1002/7joc.1234

Rodríguez-Fonseca B, Polo I, García-Serrano J, Losada T, Mohino E, Mechoso CR, Kucharski F (2009) Are Atlantic Niños enhancing Pacific ENSO events in recent decades? Geophys Res Lett 36: L20705. doi:10.1029/2009GL040048.

Roeckner E, and coauthors (2003) The atmospheric general circulation model ECHAM 5. PART I: model description. MPI Report 349.

Rogers JC (1997) North Atlantic Storm Track Variability and Its Association to the North Atlantic Oscillation and Climate Variability of Northern Europe. J Climate 10 1635-1647. doi: 10.1175/1520-0442(1997)010<1635:NASTVA>2.0.CO;2

Sanders F, Gyakum JR (1980) Synoptic-Dynamic climatology of the bomb. Mon Wea Rev 108: 1589-1606.

Sanders F (1986) Explosive cyclogenesis in the west-central North Atlantic Ocean. Part I: Composite structure and mean behavior. Mon Wea Rev 114: 1781-1794.

Santos JA, Woollings T, Pinto JG (2013) Are the Winters 2010 and 2012 Archetypes Exhibiting Extreme Opposite Behavior of the North Atlantic Jet Stream? Mon Wea Rev 141: 3626–3640. doi: http://dx.doi.org/10.1175/MWR-D-13-00024.1.

Scaife AA, and co-authors (2014) Skillful long-range prediction of European and North American winters. Geophys Res Lett, 41, 2514–2519, doi:10.1002/2014GL059637.

Schneider EK, Bengtsson L, Hu ZZ (2003) Forcing of Northern Hemisphere climate trends. J Atmos Sci 60: 1504-1521

Seiler C, Zwiers FW (2015) How well do CMIP5 climate models reproduce explosive cyclones in the extratropics of the Northern Hemisphere? Clim Dyn 10.1007/s00382-015-2642-x

Shapiro MA, Keyser D (1990) Extratropical Cyclones: The Erik Palmen memorial volume, chapter 10. Amer. Meteorol. Soc.

Shindell DT, Schmidt GA, Mann ME, Rind D, Waple A (2001) Solar forcing of regional climate change during the Maunder Minimum. Science 294: 2149-2152. doi:10.1126/science.1064363.

Stephenson DB, Pavan V, Bojariu R (2000) Is the North Atlantic Oscillation a random walk? Int J Climatol 20:1–18

Strong C, Magnusdottir G (2008) How Rossby wave breaking over the Pacific forces the North Atlantic Oscillation. Geophys Res Lett 35: L10706. doi: 10.1029/2008GL033578.

Sung MK, Ham YG, Kug JS, An SI (2013) An alterative effect by the tropical North Atlantic SST in intraseasonally varying El Nino teleconnection over the North Atlantic. Tellus A 65.

Trenberth KE (1997) The Definition of El Niño. Bull the Am Meteorol Soc 78: 2771-2777.

Trenberth KE, Branstator GW, Karoly D, Kumar A, Lau NC, Ropelewski C (1998) Progress during TOGA in understanding and modeling global teleconnections associated with tropical sea surface temperatures. J Geophys Res, 103(C7): 14,291–14,324. doi:10.1029/ 97JC01444.

Trigo IF (2006) Climatology and interannual variability of storm-tracks in the Euro-Atlantic sector: a comparison between ERA-40 and NCEP/NCAR reanalyses. Clim Dyn 26: 127-143.

Uccellini LW (1990) Processes contributing to the rapid development of extratropical cyclones. Extratropical Cyclones: The Erik Palmen Memorial Volume, C. Newton and E. O. Holopainen, Eds., American Meteorological Society, 81-105.

Ulbrich U, Christoph M (1999) A shift of the NAO and increasing storm track activity over Europe due to anthropogenic greenhouse gas forcing. Clim Dyn 15:551–559

Uppala SM, and co-authors (2005) The ERA-40 re-analysis. Q J R Meteorol Soc 131: 2961-3012.

Vicente-Serrano SM, López-Moreno JI (2008) Differences in the non-stationary influence of the North Atlantic Oscillation on European precipitation under different scenarios of greenhouse gas concentrations. Geophys Res Lett 35: L18710. doi:10.1029/2008GL034832.

Visbeck M, Chassignet E, Curry R, Delworth T, Dickson B, Krahmann G (2003) The Ocean's response to North Atlantic oscillation variability. In: Hurrell, J.W., Kushnir, Y., Ottersen, G., Visbeck, M. (Eds.), The North Atlantic Oscillation. AGU, pp. 113–146.

von Storch H, Zwiers F (1999) Statistical analysis in Climate research Cambridge University press, Cambridge

Wang C (2002) Atlantic Climate Variability and Its Associated Atmospheric Circulation Cells. J Climate 15: 1516-1536. doi: 10.1175/1520-0442(2002)015<1516:ACVAIA>2.0.CO;2

Wang C, Zhang L (2013) Multidecadal Ocean Temperature and Salinity Variability in the Tropical North Atlantic: Linking with the AMO, AMOC, and Subtropical Cell. J Climate 26: 6137-6162. doi: http://dx.doi.org/10.1175/JCLI-D-12-00721.1

Wang, YH, Magnusdottir G, Stern H, Tian X, Yu Y (2012) Decadal variability of the NAO: Introducing an augmented NAO index. Geophys Res Lett 39: L21702. doi:10.1029/2012GL053413.

Wanner H, Bronnimann S, Casty C, Gyalistras D, Luterbacher J,

Schmutz C, Stephenson DB, Xoplaki E (2001) North Atlantic Oscillation-concepts and studies. Surv Geophys 22: 321-382.

Wernli H, Dirren S, Liniger MA, Zillig M (2002) Dynamical aspects of the life-cycle of the winter storm "Lothar" (24–26 December 1999). Q J R Meteorol Soc 128: 405-429.

Woollings T, Hoskins B, Blackburn M, Berrisford P (2008) A New Rossby Wave-breaking Interpretation of the North Atlantic Oscillation. J Atmos Sci 65: 609-626.

Woollings T, Hannachi A, Hoskins B (2010) Variability of the North Atlantic eddy-driven jet stream. Q J R Meteorol Soc 136: 856-868. doi: 10.1002/qj.625

Woollings T, Gregory JM, Pinto JG, Reyers M, Brayshaw DJ (2012) Response of the North Atlantic storm track to climate change shaped by ocean-atmosphere coupling. Nature Geoscience 5:313-317.

Woollings T, Franzke C, Hodson DLR, Dong B, Barnes EA, Raible CC, Pinto JG (2015) Contrasting interannual and multi-decadal NAO variability. Clim Dyn 45:539-556. doi:10.1007/s00382-014-2237-y

Wunsch C (1999) The interpretation of short climate records, with comments on the North Atlantic and Southern Oscillations. Bull Amer Meteor Soc 80: 245–255

Zappa G, Masato G, Shaffrey L, Woollings T, Hodges K (2014) Linking Northern Hemisphere blocking and storm track biases in the CMIP5 climate models. Geophys Res Lett 41: 135-139. doi:10.1002/2013GL058480.

Zhang W, Wang L, Xiang B, Qi L, He J (2015) Impacts of two types of La Niña on the NAO during boreal winter. Clim Dyn 44: 1351-1366.

Supplementary Material for

Abrupt transitions in the variability of explosive cyclones over the North Atlantic

Climate Dynamics

Fig. S1: Regression patterns (shadings in gpm std^{-1}; K std^{-1}) and explained variance (in %) of (a)-(c) the North Atlantic Oscillation (NAO); (d)-(f) the Arctic Oscillation (AO); (g)-(i) the Pacific North American (PNA) pattern; (j)-(l) el Niño-34 pattern; and (m)-(o) the Atlantic Multi-decadal Oscillation (AMO) pattern. Left/central/right columns are for NCEP-HadISST/ERA-40-HadISST/ECHAM5-MPIOM1. Further information on the construction of the indices is available in section 3 of the manuscript.

Fig. S2: (a) EOF2 and explained variance (%) of DJF all cyclones (explosive + non-explosive) anomalous track density fields ($ALL2_T$; shadings - 99% significance in stippling) and u250 ($Jet2_T$; red/blue contours, in m s^{-1} std^{-1}, starting from 2.5 in 0.5 m s^{-1} std^{-1} intervals) on NCEP (base period 1948-2011). The climatological jet stream core is shown in thick black contours (starting from 30 m s^{-1} with 5 m s^{-1} intervals). (b) Same as (a) but for explosive track density fields only. (c) Spectral power density of $EC1_T$ and 95% confidence interval from red noise on NCEP. (d) 3 leading eigenvalues (crosses) and sampling errors (bars) of $EC1_T$/$EC2_T$/$EC3_T$ on ECHAM5, NCEP and ERA40.

Fig. S3: (a) Mean track density fields (in counts per 7.5° radius circle area per DJF season) of explosive (contours) and non-explosive (shadings) cyclones on ERA-40 (base period 1957-2001). (b) EOF1 and explained variance (%) of DJF all cyclones (explosive + non-explosive) anomalous track density fields ($All1_T$; shadings - 99% significance in stippling) and u250 ($Jet1_T$; red/blue contours, in m s^{-1} std^{-1}, starting from 2.5 in 0.5 m s^{-1} std^{-1} intervals) on ERA-40. The climatological jet stream core is shown in thick black contours (starting from 30 m s^{-1} with 5 m s^{-1} intervals). (c) Same as (b) but for explosive track density fields. (d) Same as (b) but for the second leading EOFs of all cyclones and the jet. (e) Same as (b) but for the second leading EOFs of explosive cyclogenesis and the jet.

Fig. S4: (a) Climatological winter zonal wind at 250 hPa (u250, contours in m s^{-1}) and 300-500 hPa maximum Eady Growth rate (bi400, shadings in day^{-1}) on NCEP. (b) Same as (a) but for 850-700 maximum Eady Growth rate (bi775; shadings). (c) Difference of u250 intensity between 1948-1962 and 1963-1997 in red/blue shadings (m s^{-1}; 95% confidence interval marked with *+*). Difference of 700-850 hPa Eady Growth rate (bi775) in contours

(in day^{-1}; 95% confidence interval marked with *x*). For the differences the means of the second period are subtracted to the first one. (d) Climatology of integrated temperature between the ocean surface and 300 m (red/blue shadings, in degrees C * 10^{-2} m) on SODA (base period DJF 1950-2009). Climatology of SSTs (contours, in degrees C) on HadISST (base period 1948-2011).

Fig. S5: (a) Difference in mean explosive track-densities: ECHAM5 minus NCEP (shadings). Hatched areas depict significant differences (95% confidence interval, t test for a difference in mean). (b) EOF1 and explained variance (%) of DJF all cyclones (explosive + non-explosive) anomalous track density fields ($All1_T$; shadings - 99% significance in stippling) and u250 ($Jet1_T$; red/blue contours, in m s^{-1} std^{-1}, starting from 2.5 in 0.5 m s^{-1} std^{-1} intervals) on ECHAM5 (base period DJF 1-505 years). (c) Same as (b) but for the second leading EOFs of all cyclones and the Jet ($All2_T$/$Jet2_T$). (d) Same as (b) but for the second leading EOFs of explosive cyclones and the Jet ($EC2_T$/$Jet2_T$). (e) Same as (b) but for the second leading EOFs of explosive cyclones and the jet during the decoupling periods ($EC2_D$/$Jet2_D$).

Fig. S6: (a) Climatological winter zonal wind at 250 hPa (u250, contours in m s^{-1}) and 300-500 hPa maximum Eady Growth rate (bi400, shadings in day^{-1}) on ECHAM5. (b) Regression of NAO_T onto winter bi400 anomalies (in day^{-1} std^{-1}) for the whole ECHAM5 period (95% confidence interval in stippling). (c) Same as (b) but for the regression of NAO_D during the decoupling periods. (d) Difference of (c) minus (b). (e) Climatological winter SSTs in degrees C (shadings) and associated meridional SST gradient (contours, δ_ySST in degrees C per 1000 km) in MPIOM1. (f) Mean oceanic heat content (OHC) from 0 to 123 m (thermocline depth over the sub-tropical North Atlantic) in MPIOM1 (in 10^9 J m^{-2}). (g) Oceanic vertical temperature profile over the area [30˚-40˚N, 60˚-30˚W; MPIOM1]. *Black line*: climatology. *Blue dashed line*: decoupling periods.

Fig. S7: (a) Mean genesis density fields of explosive cyclones (in counts per 7.5° radius circle area per DJF season) in ECHAM5/MPIOM1. (b) Regression of NAO_T on winter anomalies of explosive cyclone genesis density fields (shadings in counts std^{-1}, 95% confidence interval in contours).

ELECTRONIC SUPPLEMENTARY MATERIAL FOR

'Abrupt transitions in the variability of explosive cyclones over the North Atlantic'

Iñigo Gómara[1,2*], Belén Rodríguez-Fonseca[1,2], Pablo Zurita-Gotor[1,2], Sven Ulbrich[3], and Joaquim G. Pinto[4,3]

[1] *Dpto. Geofísica y Meteorología, Universidad Complutense de Madrid, Madrid, Spain*

[2] *Instituto de Geociencias (IGEO), UCM, CSIC, Madrid, Spain*

[3] *Institute for Geophysics and Meteorology, University of Cologne, Cologne, Germany*

[4] *Department of Meteorology, University of Reading, Reading, United Kingdom*

Submitted to Climate Dynamics

26 June 2015

'Revision in Progress' version of 25 September 2015

[*]**Correspondence to:** Iñigo Gómara, Dpto. Geofísica y Meteorología, Universidad Complutense de Madrid, Facultad de CC. Físicas, Ciudad Universitaria s/n. 28040 Madrid, Spain. E-mail: i.gomara@ucm.es

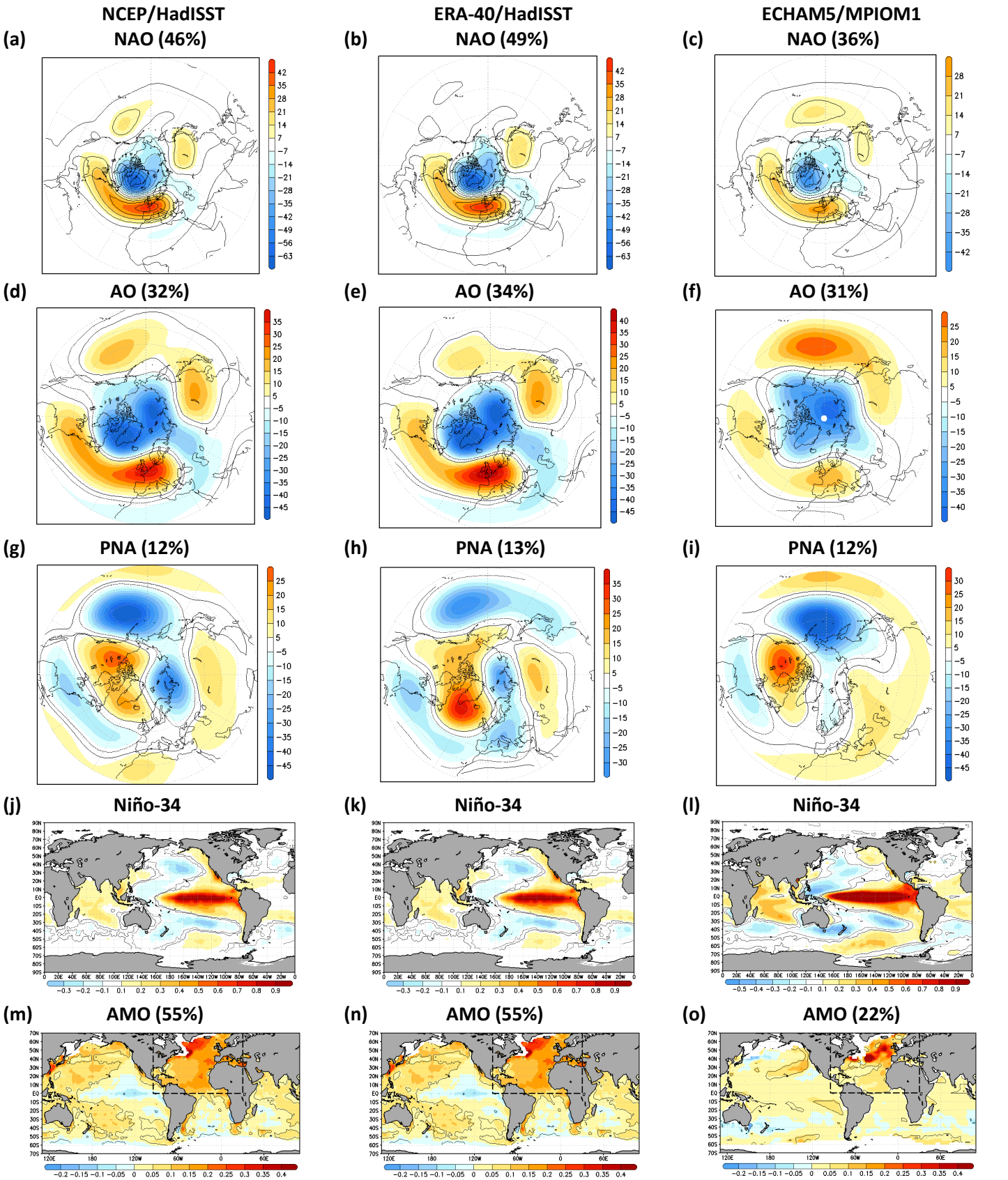

Fig. S1: Regression patterns (shadings in gpm std^{-1}; K std^{-1}) and explained variance (in %) of (a)-(c) the North Atlantic Oscillation (NAO); (d)-(f) the Arctic Oscillation (AO); (g)-(i) the Pacific North American (PNA) pattern; (j)-(l) el Niño-34 pattern; and (m)-(o) the Atlantic Multi-decadal Oscillation (AMO) pattern. Left/central/right columns are for NCEP-HadISST/ERA-40-HadISST/ECHAM5-MPIOM1. Further information on the construction of the indices is available in section 3 of the manuscript.

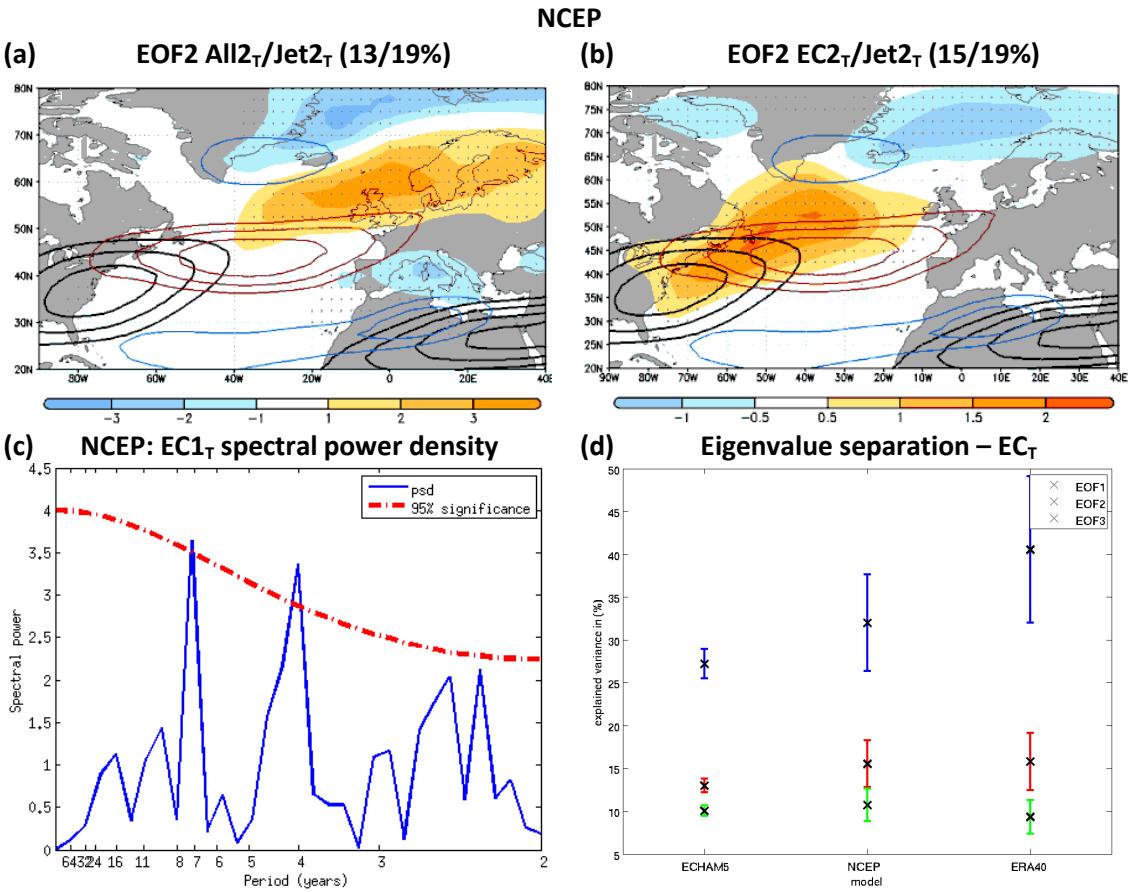

Fig. S2: (a) EOF2 and explained variance (%) of DJF all cyclones (explosive + non-explosive) anomalous track density fields ($ALL2_T$; shadings - 99% significance in stippling) and u250 ($Jet2_T$; red/blue contours, in m s^{-1} std^{-1}, starting from 2.5 in 0.5 m s^{-1} std^{-1} intervals) on NCEP (base period 1948-2011). The climatological jet stream core is shown in thick black contours (starting from 30 m s^{-1} with 5 m s^{-1} intervals). (b) Same as (a) but for explosive track density fields only. (c) Spectral power density of $EC1_T$ and 95% confidence interval from red noise on NCEP. (d) 3 leading eigenvalues (crosses) and sampling errors (bars) of $EC1_T$/$EC2_T$/$EC3_T$ on ECHAM5, NCEP and ERA40.

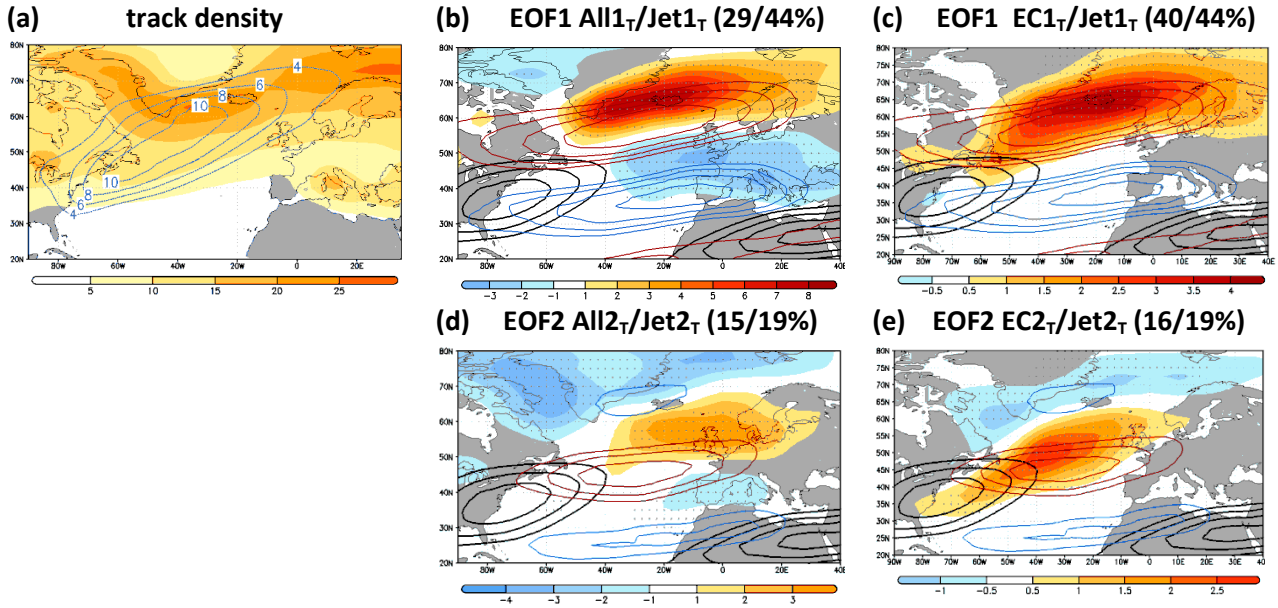

Fig. S3: (a) Mean track density fields (in counts per 7.5° radius circle area per DJF season) of explosive (contours) and non-explosive (shadings) cyclones on ERA-40 (base period 1957-2001). (b) EOF1 and explained variance (%) of DJF all cyclones (explosive + non-explosive) anomalous track density fields (All1$_T$; shadings - 99% significance in stippling) and u250 (Jet1$_T$; red/blue contours, in m s^{-1} std^{-1}, starting from 2.5 in 0.5 m s^{-1} std^{-1} intervals) on ERA-40. The climatological jet stream core is shown in thick black contours (starting from 30 m s^{-1} with 5 m s^{-1} intervals). (c) Same as (b) but for explosive track density fields. (d) Same as (b) but for the second leading EOFs of all cyclones and the jet. (e) Same as (b) but for the second leading EOFs of explosive cyclogenesis and the jet.

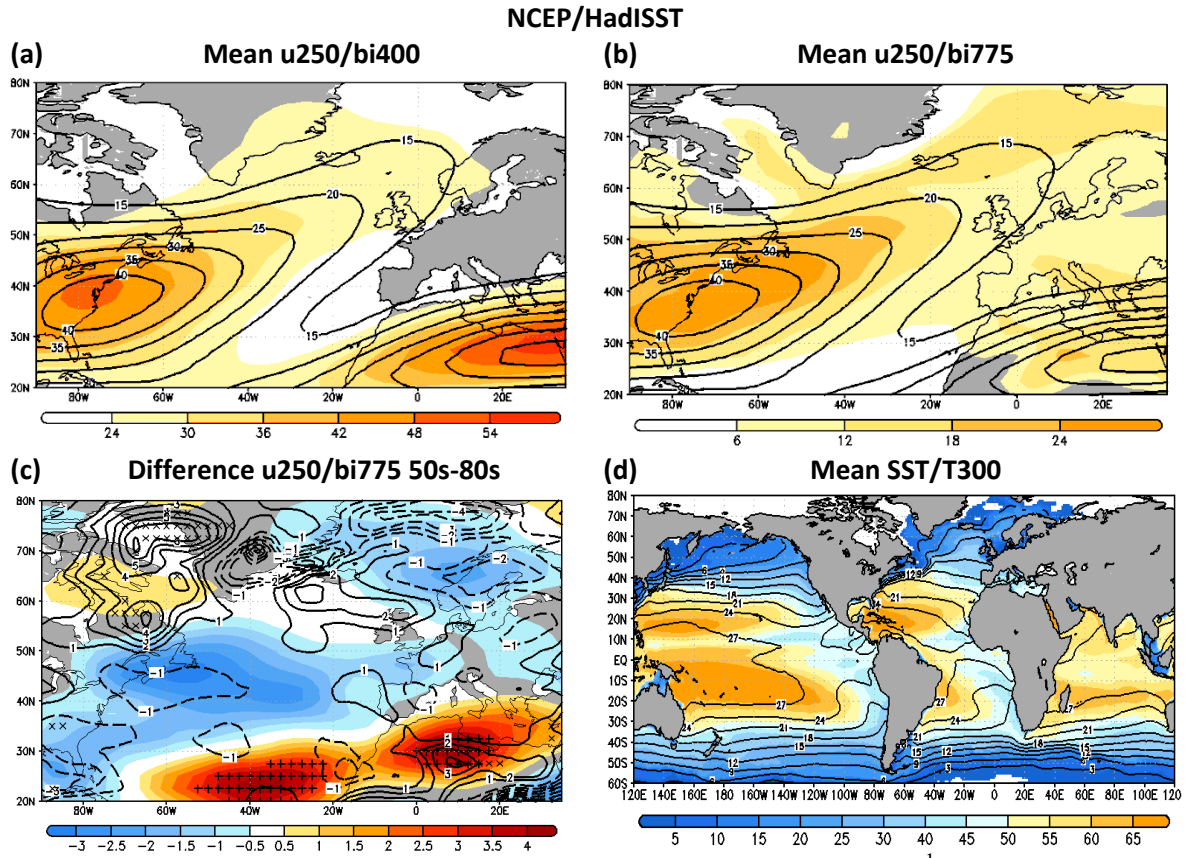

Fig. S4: (a) Climatological winter zonal wind at 250 hPa (u250, contours in m s^{-1}) and 300-500 hPa maximum Eady Growth rate (bi400, shadings in day^{-1}) on NCEP. (b) Same as (a) but for 850-700 maximum Eady Growth rate (bi775; shadings). (c) Difference of u250 intensity between 1948-1962 and 1963-1997 in red/blue shadings (m s^{-1}; 95% confidence interval marked with +). Difference of 700-850 hPa Eady Growth rate (bi775) in contours (in day^{-1}; 95% confidence interval marked with *x*). For the differences the means of the second period are subtracted to the first one. (d) Climatology of integrated temperature between the ocean surface and 300 m (red/blue shadings, in degrees C * 10^{-2} m) on SODA (base period DJF 1950-2009). Climatology of SSTs (contours, in degrees C) on HadISST (base period 1948-2011).

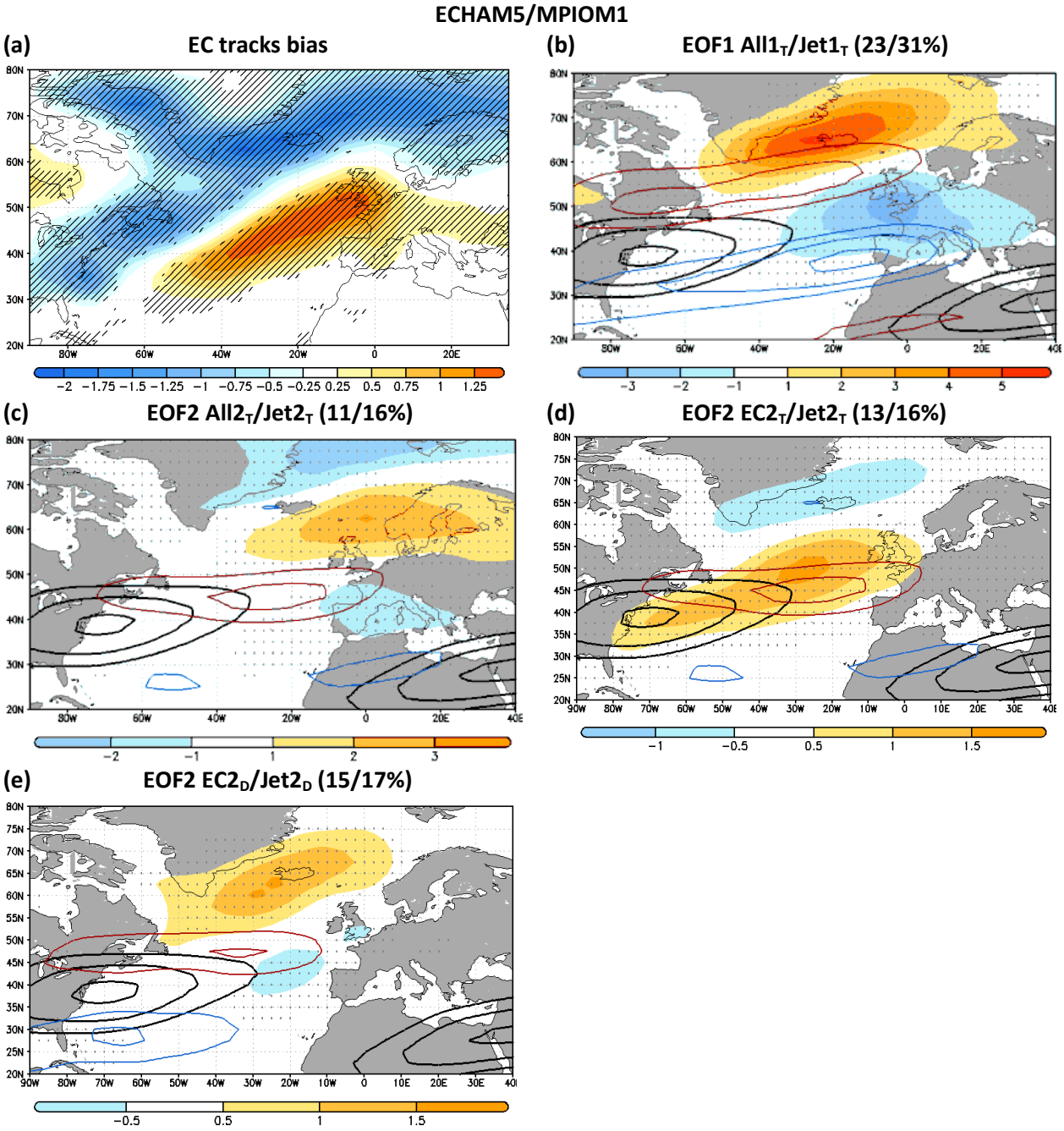

Fig. S5: (a) Difference in mean explosive track-densities: ECHAM5 minus NCEP (shadings). Hatched areas depict significant differences (95% confidence interval, t test for a difference in mean). (b) EOF1 and explained variance (%) of DJF all cyclones (explosive + non-explosive) anomalous track density fields ($All1_T$; shadings - 99% significance in stippling) and u250 ($Jet1_T$; red/blue contours, in m s^{-1} std^{-1}, starting from 2.5 in 0.5 m s^{-1} std^{-1} intervals) on ECHAM5 (base period DJF 1-505 years). (c) Same as (b) but for the second leading EOFs of all cyclones and the Jet ($All2_T$/$Jet2_T$). (d) Same as (b) but for the second leading EOFs of explosive cyclones and the Jet ($EC2_T$/$Jet2_T$). (e) Same as (b) but for the second leading EOFs of explosive cyclones and the jet during the decoupling periods ($EC2_D$/$Jet2_D$).

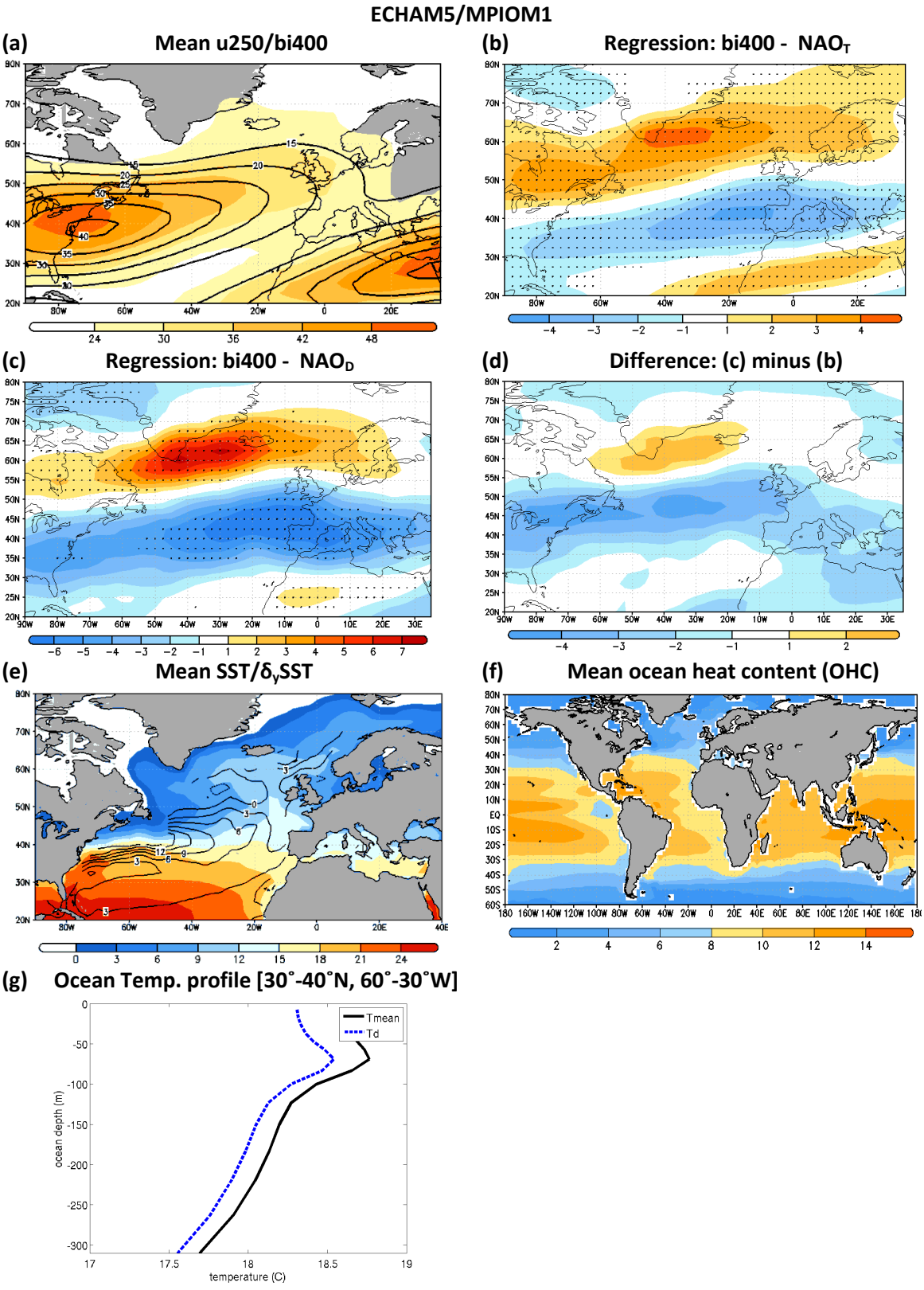

Fig. S6: (a) Climatological winter zonal wind at 250 hPa (u250, contours in m s^{-1}) and 300-500 hPa maximum Eady Growth rate (bi400, shadings in day^{-1}) on ECHAM5. (b) Regression of NAO_T onto winter bi400 anomalies (in day^{-1} std^{-1}) for the whole ECHAM5 period (95% confidence interval in stippling). (c) Same as (b) but for the regression of NAO_D during the decoupling periods. (d) Difference of (c) minus (b). (e) Climatological winter SSTs in degrees C (shadings) and associated meridional SST gradient (contours, δ_ySST in degrees C per 1000 km) in MPIOM1. (f) Mean oceanic heat content (OHC) from 0 to 123 m (thermocline depth over the sub-tropical North Atlantic) in MPIOM1 (in 10^9 J m^{-2}). (g) Oceanic vertical temperature profile over the area [30°-40°N, 60°-30°W; MPIOM1]. *Black line*: climatology. *Blue dashed line*: decoupling periods.

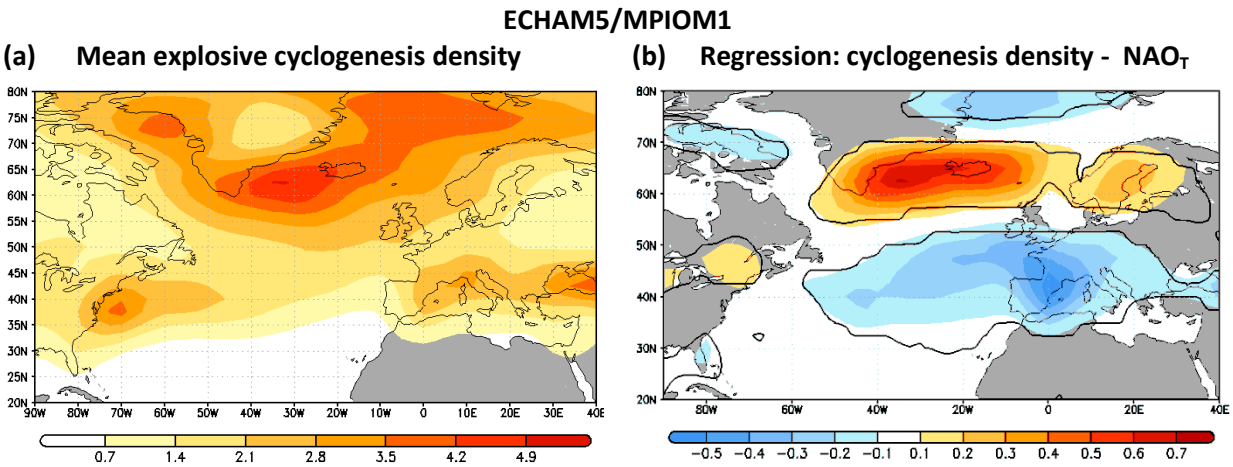

Fig. S7: (a) Mean genesis density fields of explosive cyclones (in counts per 7.5° radius circle area per DJF season) in ECHAM5/MPIOM1. (b) Regression of NAO_T on winter anomalies of explosive cyclone genesis density fields (shadings in counts std^{-1}, 95% confidence interval in contours).

VI. DISCUSSION

'The more violent the storm, the quicker it passes.'

Paulo Coelho (lyricist and novelist; 1947-nowadays)

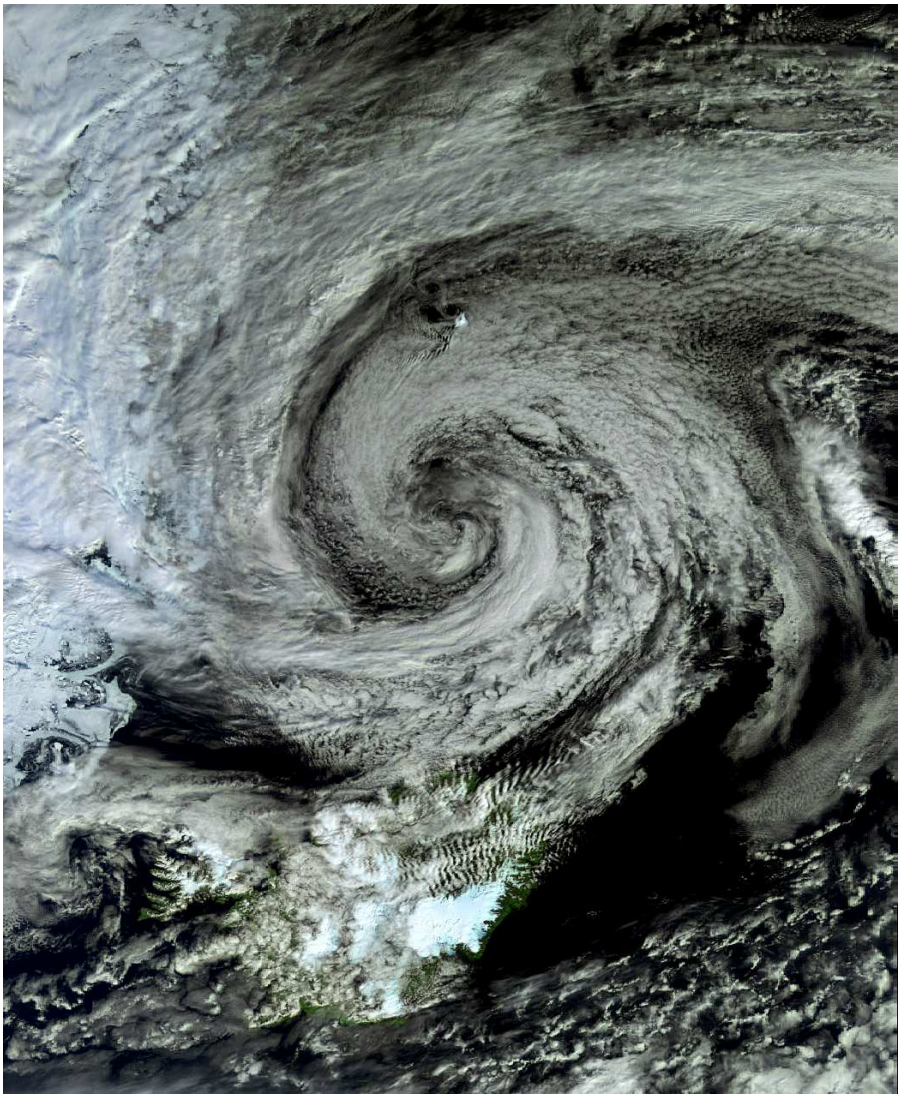

VI. Discussion

The studies presented in this thesis analyze the large-scale dynamics and variability associated with explosive cyclogenesis over the North Atlantic. This is done to potentially improve the predictability of these rapid deepening extra-tropical low-pressure systems, both in terms of operational and climate forecasting, due to the strong weather impacts they often produce on socio-economic activity [e.g., cyclones Klaus and Xynthia in January 2009 and February 2010; *Aon Benfield*, 2010]. Additional to the associated weather impacts, extra-tropical cyclones are also an important factor in determining the day-to-day local weather in Europe [*Ulbrich et al.*, 2009].

As described previously in this thesis, the NAO predominantly controls the climate variability in the North Atlantic [*Wanner et al.*, 2001]. Despite this oscillation is mainly governed by stochastic processes [*Feldstein*, 2003], yet some information can be attained from the NAO behavior to forecast cyclone activity. Under NAO+ (NAO-) the jet is accelerated (decelerated) and shifted northeastward (southwestward) in the North Atlantic [*Hurell et al.*, 2003]. This leads to a northward (southward) shift and intensification of extra-tropical cyclone activity over the North Atlantic [*Pinto et al.*, 2009]. As a consequence, the occurrence of strong cyclones over the North Atlantic is predominantly associated with a positive NAO phase [*Raible*, 2007; *Pinto et al.*, 2009]. A similar result holds for the occurrence of windstorms over Central Europe, which appear to predominantly promote from a moderately positive NAO [*Donat et al.*, 2010]. However, the robustness of this relation for a large set of cyclones of different intensities affecting this continent remained largely unexplored.

To address this question, in *Gómara et al.* [2014b; Section V.1] two subsets of explosive (424) and non-explosive (1665) cyclones affecting Europe are considered on NCEP reanalysis. The large-scale flow is characterized through a daily NAO index [*Blessing et al.*, 2005] and daily anomalies of z500/u250. As the results show, on days prior to cyclone maximum intensification and impact over Europe (3-4 days), the large-scale conditions over the North Atlantic are contrasting for explosive and non-explosive cyclones (cf. Figs. 6.1a and 6.1e). On one hand, explosive cyclones predominantly develop under a downstream propagating north-negative and south-positive composite structure of z500 anomalies, typically accompanied by an accelerated eddy-driven jet over Western Europe (Fig. 6.1a-b).

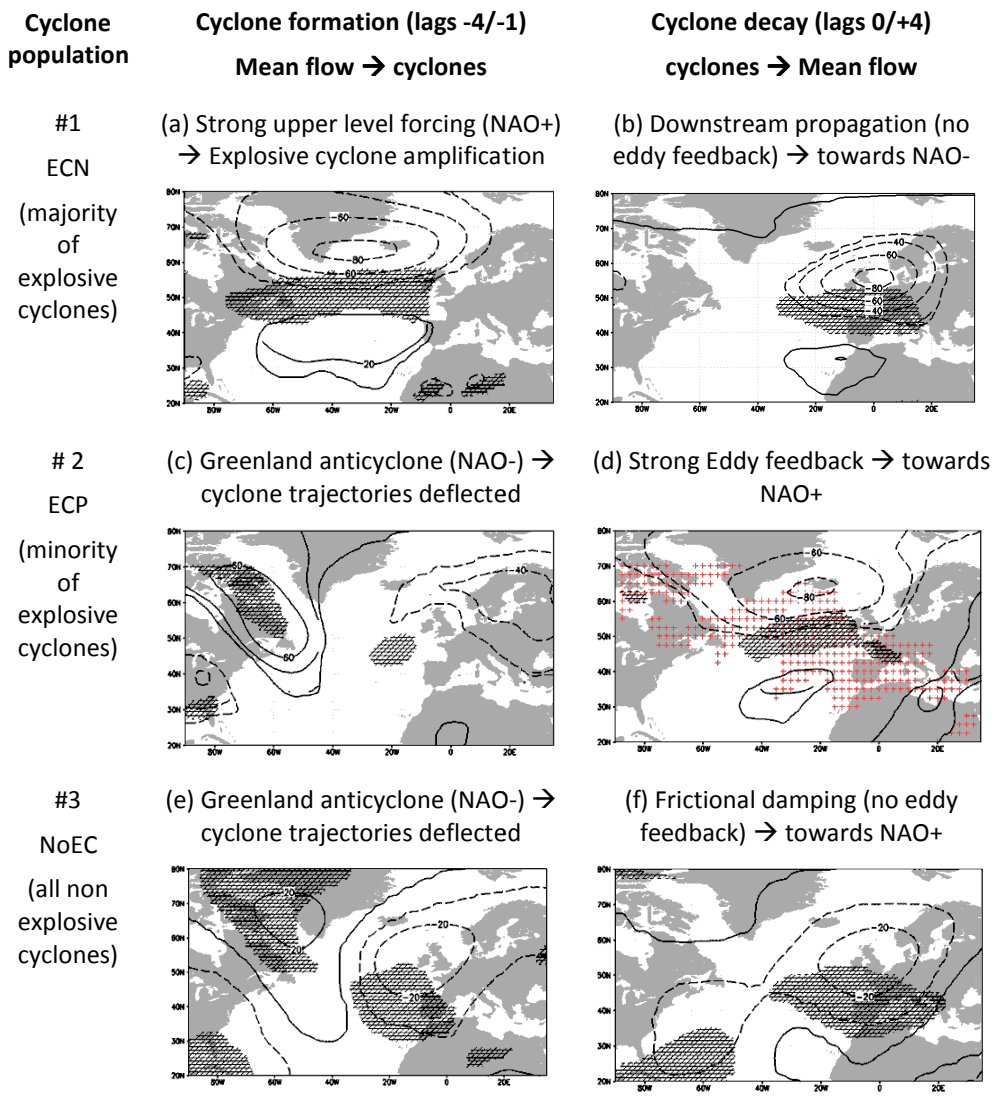

Fig. 6.1: Schematic of the two-way relation between the mean flow and different cyclone populations affecting Europe. Contours represent z500 composite anomalies (in gpm). Hatched areas denote significant positive anomalies of the jet intensity. Red crosses denote areas of enhanced positive momentum fluxes during cyclone's decay (averaged between lags 0/+4). 99% confidence interval, Monte Carlo test. Figure adapted from *Gómara et al.* [2014b].

This pattern resembles the positive NAO phase and is known to support rapid eddy amplification in the vicinity of Europe [*Pinto et al.*, 2009; *Hanley and Caballero*, 2012]. On the other hand, non-explosive cyclones tend to develop under a negative NAO phase, typically characterized by positive z500 anomalies

over Greenland and negative over eastern North America and north-western Europe (Fig. 6.1e). Although this structure does not resemble the NAO pattern, it projects more onto NAO- due to the positive z500 anomalies over Greenland. In this case, the large-scale circulation does not appear to promote cyclone intensification, but to deflect low pressure systems toward Europe due to the relative 'high pressures' over Greenland. This large-scale pattern is very similar to the Greenland anticyclone weather type from *Vautard* [1990]. Provided that the composite analysis is based on cyclones spreading over a wide area, the broad lows in Fig. 6.1 might be affected by the cyclone's imprint at 500 hPa. To minimize this potential effect, a 5-day running mean smoothing was applied to the daily z500 fields. In addition, the large scale patterns presented in Fig. 6.1 extend hemispherically (not shown) and display a similar structure at negative cyclone lags (-4/-3), when cyclones are incipient and located far away to each other (cf. Figs. S1g, S1h, and S1i - Section V.1).

The timing in cyclone formation is another crucial factor in the NAO/cyclones relation. For the majority of the strongest cyclones impacting Europe (ECN), the associated north-negative and south-positive z500 pattern rapidly propagates downstream in the North Atlantic, with an associated abrupt growth and decay of the NAO phase in a period of around 12 days (Fig. 6.1a-b). Contrastingly, the z500 structure associated with non-explosive cyclones is more stationary in time and therefore appears to be driven by different dynamical processes (Fig. 6.1e-f). To further investigate this contrasting behavior in timing, in the second part of *Gómara et al.* [2014b] the variation of the daily NAO index on days after the maximum intensification period of cyclones is analyzed. The choice of positive cyclone lags instead of negative (where lag 0 is the date when a cyclone features its maximum intensification) is based on the potential influence that cyclones themselves appear to exert onto the large-scale flow during their decay. In this context, a few analyses of case studies and specific cyclone populations have shown the impact of the former onto the mean flow via high-frequency eddy momentum fluxes (either positive or negative) [*Riviére and Orlanski*, 2007; *Michel et al.*, 2012]. The question why a single storm can be associated with positive or negative momentum fluxes depends on its life-cycle. From a classic perspective, cyclones themselves present two different types of life-cycles depending on their structure in the upper-levels [e.g., LC1 and LC2; *Thorncroft et al.*, 1993]. During their decay, LC1 cyclones tend to break anticyclonically and are associated with positive momentum fluxes, which typically induce a poleward shift of the jet and a tendency towards NAO+. On the contrary, LC2 cyclones break cyclonically, are associated with negative momentum fluxes and promote NAO-. A clear example

of this relation was the March 1993 Superstorm [*Riviére and Orlanski*, 2007]. The storm was associated with strong positive momentum fluxes over the North Atlantic during its decay, and produced an abrupt increase in the daily NAO index in a short period of time (4-5 days). As a consequence, the NAO phase remained in positive values until the equilibrium was reached a couple of weeks later. According to case studies, the influence that a single cyclone can exert onto the mean flow appears to be sensitive to the cyclone's maximum intensity. As an application of these strong but infrequent eddy feedbacks, some predictability can be added on short-term NAO variability. This is supported by the contrasting characteristic timescales of the processes involved in the growth and decay of the atmospheric anomalies. Whereas eddy feedbacks (growth) can alter the atmospheric state in question of few days [*Riviére and Orlanski*, 2007; *Pinto et al.*, 2009], weak frictional damping acts to mitigate the existing anomalies in weekly timescales [decay; *Lorenz and Hartmann*, 2001].

In order to further characterize the relation above, and additional to the evolution of the daily NAO index, a comprehensive analysis of momentum fluxes associated with European cyclones is carried out in *Gómara et al.* [2014b]. In particular, a focus on contrasting explosive vs. non explosive cyclones at positive lags (0 to +4) is laid. Not surprisingly, explosive cyclones tend to produce stronger variations in the daily NAO index during their decay, both positive and negative, although for different reasons. The dynamical mechanisms producing the negative variations are not associated with eddy feedback of the cyclones involved whatsoever. In this case, the downstream propagation of the NAO+ like structure contributing to rapid cyclone intensification reduces its projection onto the loading NAO pattern in time (Fig. 6.1a-b). This mechanism holds for a large number of cyclones (ECN; 169/424, e.g., cyclone Kyrill). Contrastingly, a lower number of cyclones (ECP; 103/424) is associated with strong and extensive enhanced positive momentum fluxes during their decay, and appear to promote NAO+ (Fig. 6.1d). These cyclones predominantly intensify under a weak upper-level forcing and the role of moist adiabatic processes appears to be more important in their amplification [Fig. 6.1c; *Fink et al.*, 2012]. Therefore, some NAO-like short term predictability can be attained from the dynamics associated with this cyclone population. A good archetype of this cyclone subset was cyclone Xynthia [*Ludwig et al.*, 2014].

In summary, the results from *Gómara et al.* [2014b] clearly show that the links between the NAO and European cyclones are sensitive to cyclone's intensity and timing. Despite the analysis provides very valuable information regarding the two-way relation between extra-tropical cyclones and the mean flow in the North

Atlantic, it suffers from the geographical constraints applied to the cyclones to prioritize their weather impacts over Europe. As a consequence, in *Gómara et al.* [2014a] a deeper and more general description of this bi-directional relation is provided. For this purpose, a comprehensive data set of cyclones of different intensities and locations over the North Atlantic is used on ERA-40. In addition, the large-scale circulation is no longer represented by a fixed spatial mode (e.g., the NAO), but by local-instantaneous Rossby wave-breaking occurrence.

As mentioned before, Rossby wave-breaking (RWB) processes are defined as the irreversible overturning of potential temperature contours on the tropopause, and their underlying dynamics are consistent with eddy feedback and momentum fluxes [i.e., high-frequency non-linear processes; *McIntyre and Palmer*, 1983]. The role of RWB in mediating the relation between weather extremes and the mean flow has been addressed in previous studies. In particular, blocking events over the North Atlantic appear to be closely related with the occurrence of a common RWB pattern [*Pelly and Hoskins*, 2003; *Santos et al.*, 2009; *Woollings et al.*, 2011; *Masato et al.*, 2013a; 2013b]. In addition, RWB activity is also suggested to influence large-scale circulation transitions in the North Atlantic [*Michel and Riviére*, 2011], including the positive and negative phases of the NAO [as previously observed under an eddy momentum flux perspective; *Franzke et al.*, 2004; *Woollings et al.*, 2008; *Strong and Magnusdottir*, 2008a; 2008b]. Related with cyclonic activity, *Hanley and Caballero* [2012] have recently shown the existence of a simultaneous cyclonic/anticyclonic RWB pattern that appears to promote rapid cyclone intensification in the vicinity of Europe. Under the mechanism they propose, the eddy-driven jet over Western Europe is squashed and intensified from both flanks by simultaneous RWB events (Fig. 6.2a). The imprint of such mechanism is indeed indirectly observed in some results from *Gómara et al.* [2014b; Section V.1]. In particular, the observed sharp growth in the NAO index during negative cyclone lags is suggestive of high-frequency RWB processes (Fig. 3b - Section V.1), and the jet structure promoting cyclone intensification over Western Europe (Fig. 6.1a) is similar to *Hanley and Caballero's* [2012]. Therefore, in *Gómara et al.* [2014a; Section V.2] the robustness of this mechanism using a comprehensive cyclone data set and a RWB index is subsequently analyzed. In particular, the role of cyclone's intensity, trajectory and location in the North Atlantic is assessed. With this aim, six different populations of cyclones of varying intensities over the western [40˚-60˚N, 50˚-20˚W] and eastern [40˚-60˚N, 20˚W-10˚E] North Atlantic are considered: (i-ii) top 50 strongest cyclones; (iii-iv) 50 random explosive non-top cyclones; and (v-vi) 50 random non-explosive cyclones.

Over the eastern North Atlantic for the strongest 50 cyclones on days prior to maximum cyclone intensity, a north-cyclonic and south-anticyclonic common RWB pattern arises (Fig. 5a-c - Section V.2). This pattern is very similar to *Hanley and Caballero's* [2012] and is also accompanied by positive anomalies of the jet intensity over the eastern North Atlantic (cf. Fig. 6.2a). An intensified eddy-driven jet is associated with increased vertical wind shear and baroclinicity below, thus enhancing the potential for explosive growth of baroclinic disturbances at lower levels [*Gyakum and Danielson*, 2000; *Dacre and Gray*, 2013]. If a relatively slightly weaker population of explosive cyclones is used, a pattern of enhanced simultaneous cyclonic/anticyclonic RWB also arises, but the anomalies are smaller and weaker (Fig. 6ac - Section V.2).

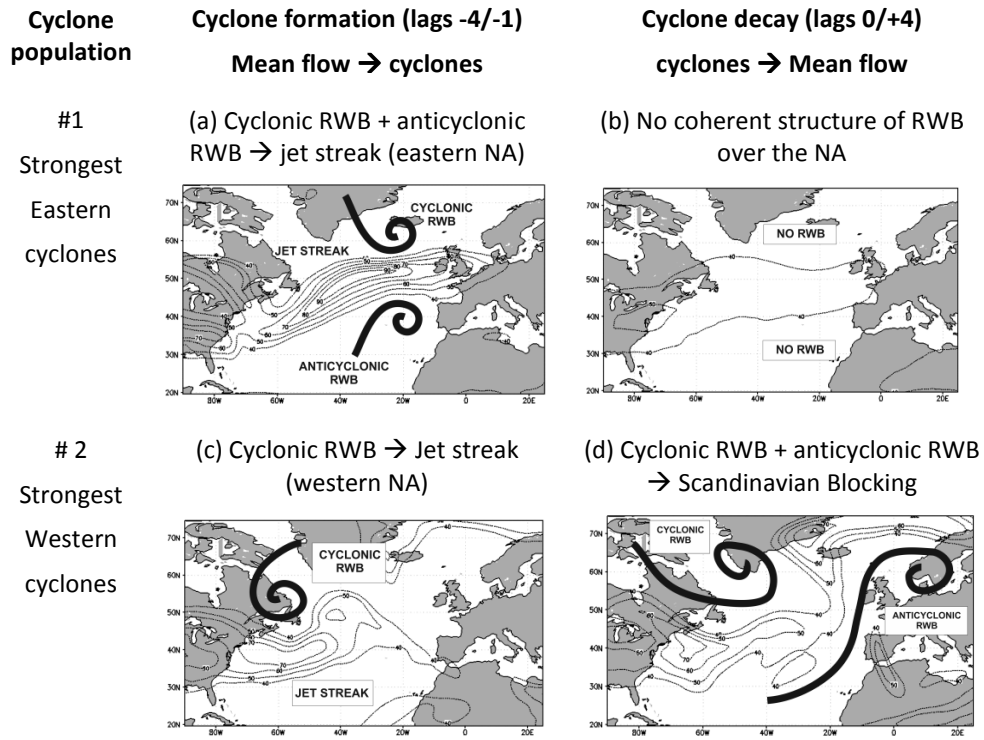

Fig. 6.2: Schematic of the two-way relation between the mean flow and intense extra-tropical cyclones over different areas of the North Atlantic (NA). Shaded contours represent the jet stream state (in m s^{-1}). Solid contours represent RWB occurrence and direction of breaking. Figures adapted from *Gómara et al.* [2014a].

Lastly, if non-explosive cyclones are considered, no coherent structure of enhanced RWB is observed (Fig. 6bd - Section V.2). In order to generate summary

statistics, the numbers of north-cyclonic and south-anticyclonic RWB events (over particular regions and minimum size thresholds) on days previous to eastern cyclones are calculated. This is done to investigate how frequent simultaneous RWB events are. As the results show (Tables 2-4 - Section V.2), north-cyclonic and south-anticyclonic simultaneous RWB events are indeed very rare and only account for 10% of the top 50 strongest eastern cyclone cases. However, explosive cyclones developing under such conditions are significantly stronger than the rest. On the contrary, single RWB events (especially north-cyclonic) are much more common precursors of these cyclones (60% of times). As expected, these numbers clearly decrease for cyclone populations of lower intensities.

For the western North Atlantic cyclones a similar RWB behavior is observed, although with some differences. For the strongest cyclones, the common RWB pattern promoting explosive cyclone growth has only one node. In this case only cyclonic RWB over western Greenland is present and the extra-tropical jet is squeezed and intensified from its northern flank over the western North Atlantic (Fig. 6.2c). As a consequence, western cyclones encounter profitable conditions for rapid growth. Consistent with the eastern cyclones, the size, frequency and strength of this common RWB pattern is directly proportional to the cyclone's maximum intensity, and non-existent for non-explosive cyclones. For the strongest cyclones over this area, a single cyclonic RWB precursor is present 70% of times, whereas simultaneous RWB events are absent.

Attending to the influence of RWB types in cyclone formation, over the western North Atlantic cyclonic RWB clearly dominates, whereas anticyclonic raises its importance east in the basin. These results are consistent with the preferred locations of RWB types in the North Atlantic [e.g., *Gabriel and Peters*, 2008]. Regarding the potential origin of the RWB events preceding explosive cyclogenesis, in some cases these events may be associated with previous cyclonic development. However, the size and persistence (3-5 days) of the RWB events observed suggests that these may be more generally associated with upper-level Rossby waves of varying spatial and temporal scales travelling from the North Pacific [*Nakamura and Wallace*, 1993; *Delsole*, 2001; *Barnes and Hartmann*, 2011].

In this context, the capacity of cyclone populations to alter the large-scale flow through RWB processes is also investigated in *Gómara et al.* [2014a]. As on *Gómara et al.* [2014b], positive cyclone lags (o to +4) are selected. As the results show, only the strongest cyclones over the western North Atlantic are able to drastically modify the circulation conditions over the North Atlantic.

On positive lags of the 50 western strongest cyclones, enhanced cyclonic RWB south of Greenland and anticyclonic over Europe are present (Fig. 6.2d). Cyclones themselves appear to be responsible of the strong and extensive cyclonic RWB near Greenland. Such RWB completely disrupts the zonal flow and a large mass of high potential temperature is advected from the sub-tropics toward the eastern sub-polar North Atlantic, potentially leading to the onset of Scandinavian blocking [*Michel et al.*, 2012]. On positive lags of the 50 eastern strongest cyclones, no clear sign of enhanced RWB is observed (Fig. 6.2b). This result is consistent with a lower mean intensity of eastern North Atlantic cyclones, but partially contrasts with the outcome from *Gómara et al.* [2014b], where a not negligible number of decaying cyclones appears to be associated with positive eddy momentum fluxes and promote NAO+ (Fig. 4f - Section V.1). The question of why no enhanced anticyclonic RWB is associated with eastern decaying cyclones in *Gómara et al.* [2014a] may be associated with the strong criterion imposed by the index on the scale of wave-breaking (two boxes of 14.625˚ latitude each). As a consequence, some small-scale potential temperature streamers associated with these cyclones might be disregarded in *Gómara et al.* [2014a]. In addition, in *Gómara et al.* [2014a] no further separation between different explosive cyclone dynamics is performed. Thus, the RWB associated with the decaying of few cyclones could be masked by the dynamics of the rest. In summary, in *Gómara et al.* [2014a] evidence is given that the links between large-scale RWB and cyclogenesis over the North Atlantic are sensitive to the cyclone's intensity, location and timing.

Regarding the interconnected evolution between the eddy-driven jet and RWB, it is well known that the preferred areas of cyclonic (anticyclonic) RWB lie further north (south) of the jet core due to strong horizontal wind shear at upper-levels [*Gabriel and Peters*, 2008]. The contrary effect, in which RWB acts to modulate the jet characteristics, is suggested in *Gómara et al.* [2014a] and in many other previous articles of NAO variability and atmospheric blocking [*Benedict et al.*, 2004; *Woollings et al.*, 2008; *Strong and Magnusdottir*, 2008a; 2008b; *Michel and Rivière*, 2011]. However, atmospheric causality is a hard question to discriminate in this context. Supporting the assumptions presented in this thesis, that RWB is the cause and the acceleration of the jet is the consequence, in Figs. 9 and 10 from *Gómara et al.* [2014a; Section V.2] two different case studies of RWB, jet intensification and cyclone amplification over the western North Atlantic are provided. As visual inspection of these figures depicts, the timing of RWB and jet intensification is consistent with the

mechanism suggested, as RWB tends to occur 1-2 days in advance of the jet modifications.

Another question of pivotal interest is the persistence (3-5 days) of the identified NAO+ [*Gómara et al.*, 2014b] and RWB [*Gómara et al.*, 2014a] events leading to explosive cyclogenesis over Western Europe. As previously explained in this thesis, strong low pressure systems often appear individually, but in some occasions a quick succession of events occurs over the same area [*Ulbrich et al.*, 2001]. These are the so-called 'storm families' or 'storm clustering' events. Over Western Europe, several storm clustering events have occurred within the last decades (e.g., December 1999, January 2007, winter 2013/2014, etc.), leading to strong impacts on normal socio-economic activity and high cumulative property losses [*MunichRe*, 2010].

Thus, in *Pinto et al.* [2014; Section V.3] the dynamical mechanisms responsible for the occurrence of storm clustering over Western Europe are analyzed. In particular, the role of RWB in the evolution of the polar jet and occurrence of storm families near the UK is carefully investigated. In addition, the potential influence of upstream and downstream secondary cyclogenesis is also assessed. For this purpose a complete cyclone dataset, a RWB/jet latitude index, and weather charts from the UK Met-Office are used on ERA-Interim. The identification of cyclone families is performed through an objective algorithm that detects successive cyclone passages in the vicinity of the British Isles (circle detection area; centre 55˚N-5˚W, radius 700 km). Based on this criterion, four main clustering periods are selected as illustrative in the article (e.g., February 1990, January 1993, December 1999 and January 2007).

Not surprisingly, evidence of a strong connection between RWB, jet dynamics and cyclone clustering is provided in Figs. 1-6 of *Pinto et al.* [2014]. During these periods, extensive and recurrent north-cyclonic and south-anticyclonic RWB events take place at both sides of the jet. As a consequence, the jet is recurrently accelerated over Western Europe during periods of 1-2 weeks and surface disturbances in the eastern North Atlantic encounter very favorable upper-level conditions for rapid amplification. However, for the occurrence of storm clustering, the supportive upper-level conditions need to be fueled by surface disturbances upstream in the North Atlantic. In the literature, several articles have described the occurrence of trains of multiple unstable waves that develop and propagate in the wake of a large parent low [*Bjerknes and Solberg*, 1922; *Parker*, 1998; *Rivals et al.*, 1998]. As a result, the potential role of secondary upstream cyclogenesis and its relation with the upper-level circulation is also investigated in the frame of storm clustering. Through a manual analysis of frontal

developments, a recurring pattern of secondary cyclogenesis is identified in *Pinto et al.* [2014], in which a developing cyclone is located in the right-entrance region of the jet, on the trailing cold front of a mature cyclone situated in the left-exit region of the same jet streak (Fig. 6.3). Subsequently, the incipient cyclone explosively intensifies under the jet streak and follows a similar path to the parent cyclone, thus leading to a quick succession of low pressure systems over the same area.

In addition, the role of downstream secondary cyclogenesis is also analyzed in *Pinto at al.* [2014]. Due to the dispersive nature of Rossby waves, in some cases developing cyclones tend to form east of a parent low [*Simmons and Hoskins*, 1979; *Chang*, 1993]. The role of this potential mechanism is analyzed during the main clustering periods over Western Europe (e.g., February 1990, January 1993, December 1999 and January 2007). Opposite to the previous mechanisms, secondary downstream cyclogenesis does not appear to be responsible of the clustering events analyzed. Despite Rossby wave packets are present during these periods, their wave-lengths are exceedingly long to correspond to the different cyclones within the storm families (Fig. 8 – Section V.3).

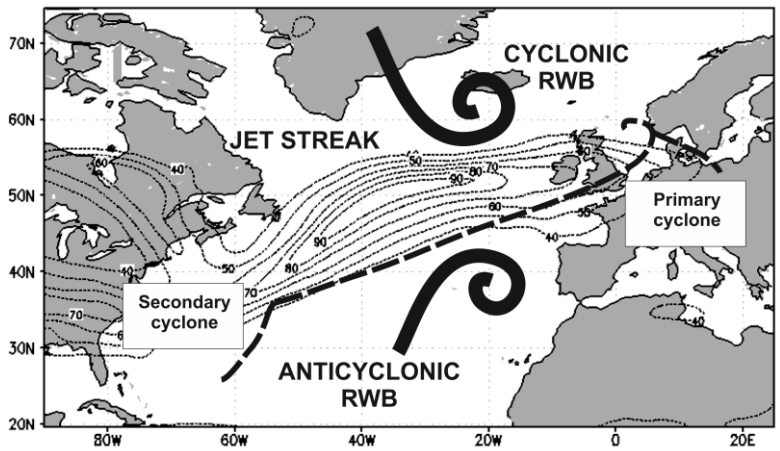

Fig. 6.3: Schematic summary showing the positions and fronts of clustered cyclones (thick dashed lines), and the dynamical precursors (RWB - solid lines, jet streak - thin dashed lines - and secondary upstream cyclogenesis) leading to their occurrence. Figure adapted from *Pinto et al*. [2014].

Hence, the exploratory study of *Pinto et al.* [2014] provides a first physical interpretation of the occurrence of storm families over the North Atlantic. The intention of the article is not to definitely establish the dominance of any physical

mechanism, but to investigate storm clustering from a dynamical perspective instead of a more statistical approach [*Mailier et al.*, 2006; *Vitolo et al.*, 2009; *Pinto et al.*, 2013; *Blender et al.*, 2015]. As potential paths for future research, the robustness of these results should be tested in a longer reanalysis data set and in high-resolution climate models [e.g., *Shaffrey et al.*, 2009]. In this direction, an assessment of storm clustering in historical and future CMIP5 model simulations has recently been released by *Economou et al.* [2015]. At the light of the current fruitful debate on the potential drivers of the 2013/2014 stormy winter over the UK [*Huntingford et al.*, 2014; *van Oldenborgh et al.*, 2015], another interesting topic to follow may be the study of role played by RWB in such anomalous winter, as well as the variability and origin of these waves.

So far, the two-way relation between extra-tropical cyclones and the large-scale circulation at synoptic timescales has been described in the three first articles of this thesis. These studies permit a better understanding of the physical mechanisms leading to the occurrence of explosive cyclogenesis and storm clustering over the North Atlantic, and may help to improve their operational forecasting. However, these studies are mainly focused on the role played by the upper level circulation in rapid cyclone amplification. In the literature, other physical factors such as strong latent heat release [*Fosdick and Smith*, 1991], sensible fluxes [*Davis and Emmanuel*, 1988], low-level baroclinicity [*Hoskins and Valdes*, 1990; *Hoskins et al.*, 1985] and air-sea interactions [*Sanders*, 1986; *Ludwig et al.*, 2014] are also suggested to be decisive for sudden cyclone intensification, both at synoptic and longer timescales.

In order to provide a more complete view of this phenomenon, in *Gómara et al.* [2015] the high-frequency climate variability (1-11 years) of explosive North Atlantic cyclones is characterized. In addition, the potential drivers of this variability are also investigated. For this purpose, the winter-track density data of explosive and non-explosive cyclones from two reanalysis data sets (NCEP and ERA-40) and a long control simulation of ECHAM5/MPIOM1 are used. According to the differences observed in the variability and dynamics between explosive and non-explosive cyclones at synoptic scales in the previous articles of this thesis, a question of prime interest is to investigate whether the variability associated with these cyclones is remarkably different as well at climatic timescales (1-11 yr.). With this aim, an Empirical Orthogonal Function (EOF) approach is applied to cyclone data and other variables (e.g., u250, z500) to characterize the preferred modes of variability in the North Atlantic.

Results show that the leading variability mode for all cyclones (All1; including explosive and non-explosive cyclones) predominantly represents a shift

in cyclone trajectories between Iceland and Western Europe [Fig. 1b – section V.4; *Rogers*, 1997; *Dong et al.*, 2013]. On the contrary, the leading mode of explosive cyclone tracks (EC1) represents a strengthening/weakening pattern extending from Newfoundland to Iceland (Fig. 1c – section V.4). Despite both modes have different structure, they share the same atmospheric variability, which is stirred by the leading variability mode of the jet, and the NAO (cf. Table 1 - Section V.4). Thus, the NAO not only acts as a wave-guide of surface baroclinic disturbances, but also as a boost (under its positive phase) for rapid cyclone intensification [*Pinto et al.*, 2009; *Gómara et al.*, 2014b]. In the ocean, the projection of such variability leads to the Atlantic tripole pattern [*Czaja and Frankignoul*, 1999]. In addition, some prediction skill could be added from the tropical pacific SST, as a significant anti-correlation is found between ENSO and the positive phase of EC1 (this is only valid on ECHAM5/MPIOM1 - Fig. 4d - Section V.4).

For completeness, the second leading EOFs of explosive cyclone tracks (EC2) and the extra-tropical jet are also calculated in *Gómara et al.* [2015]. Not surprisingly, both EOFs are well correlated and represent a strengthening/weakening pattern between eastern North America and Western Europe (Figs. S2b and S3e - Section V.4). This large-scale configuration is indeed very similar to the associated with explosive cyclogenesis and storm clustering over Western Europe, which is know to be mainly driven by RWB at synoptic timescales [*Gómara et al.*, 2014a; 2014b; *Pinto et al.*, 2014]. Regarding the role played by the NAO for the occurrence of explosive cyclogenesis over Western Europe, it must be noted that the area used for cyclone selection in *Gómara et al.* [2014b] spans over [30˚-65˚N, 20˚W-10˚E]. As a consequence, the results in *Gómara et al.* [2014b] can be understood as a combination of the two leading EOFs of explosive cyclone tracks from Gómara et al. [2015] (compare Fig. 1b – Section V.1 and Figs. 1c and S2b – Section V.4). In terms of the NAO phase, EC1 (positive phase) is associated with a markedly positive NAO, whereas EC2 is linked with neutral to slightly positive NAO phases. The combination of both modes thus leads to a moderately positive NAO, as obtained in *Gómara et al.* [2014b].

After the characterization of the explosive cyclone track variability modes, the time-evolving connection between explosive cyclogenesis leading variability (EC1) and the NAO is investigated in *Gómara et al.* [2015]. On one hand, this is motivated by the slightly different results in correlation between EC1 and the NAO on reanalysis data sets covering different time periods (NCEP vs. ERA-40; cf. Table 1 - Section V.4). On the other hand, this is also incited by the existing literature on non-stationary teleconnections between remote regions [*Pinto et al.*, 2011; *López-Parages and Rodríguez-Fonseca*, 2012], which are able to provide enhanced

forecast skill of relevant phenomena during specific periods of time [*Jung et al.*, 2003; *Rodríguez-Fonseca et al.*, 2009; *Losada et al.*, 2012]. As a result, a (21 yr.) running correlation between EC1 and NAO is performed on NCEP, ERA-40 and ECHAM5/MPIOM1. Evidence is given that the relation between EC1 and NAO is non-stationary in time, and remarkably fluctuates within different time periods. For instance, the period 1963-1997 is characterized in NCEP and ERA-40 by a strong correlation between EC1 and the NAO. This period is associated with atmospheric and oceanic multi-decadal anomalies: (i) a strong positive multi-decadal NAO phase with an eastward shift of its centers of action [*Ulbrich and Christoph*, 1999; *Jung et al.*, 2003; *Pinto and Raible*, 2012]; (ii) enhanced baroclinicity over the sub-polar North Atlantic; and (iii) a strong negative AMO phase [*Woollings et al.*, 2012]. The conjunction of these factors leads to more prominent variability of explosive cyclone tracks in the area between Iceland and Scandinavia. On the contrary, the period 1948-1962 is characterized by opposite attributes of the NAO/AMO, and enhanced baroclinicity over western Greenland and the sub-tropical North Atlantic. As a result, the leading variability mode of EC appears constrained over the western north Atlantic and western Greenland.

Despite the results from reanalysis are clear, the use of short time series for the purposes of this analysis is insufficient. In addition, the potential roles played by natural climate variability and/or anthropogenic climate change are difficult to distinguish. Thus, in order to better infer a robust hypothesis about the mechanisms involved, a long control simulation of ECHAM5/MPIOM1 is used. On ECHAM5, the NAO-EC1 connection is systematic and robust for most of the simulation excepting two periods of about 20-25 yr. each. During these periods (so called ‘decoupling periods’) a strong decrease in the running 21 yr. correlations is observed (please note that these correlations are smoothed by the use of running windows; cf. Fig. 5a - section V.4). Indeed, if the specific EOF patterns are calculated solely for these periods, there exists strong and significant (95% confidence level) EC1-NAO anti-correlation (-0.49).

Such change in correlation is triggered by an abrupt equatorward displacement of the EC1 main centre of action during the decoupling periods. In Fig. 6.4 this abrupt shift can be easily observed (compare light – ‘normal conditions’ vs. dark – ‘decoupling periods’ shadings). As expected, during these decades the extra-tropical jet is southerly displaced from its average position and enhanced baroclinicity extends over the sub-tropical North Atlantic (Fig. 6.4 - stippling). Such jet configuration is accompanied by a stronger SST gradient over the sub-tropical North Atlantic.

Regarding the NAO pattern, no remarkable change is observed in its structure within the decoupling periods. However, during these periods the baroclinicity associated with NAO- is stronger and more extensive than the associated with NAO+ (Figs. S6b-d - Section V.4). This 'odd' behavior is the opposite of what is observed in climatology (ECHAM5) and previous studies [*Pinto et al.*, 2009]. Therefore, during the decoupling periods explosive cyclones appear to predominantly promote from NAO- and their main variability mode is thus shifted south.

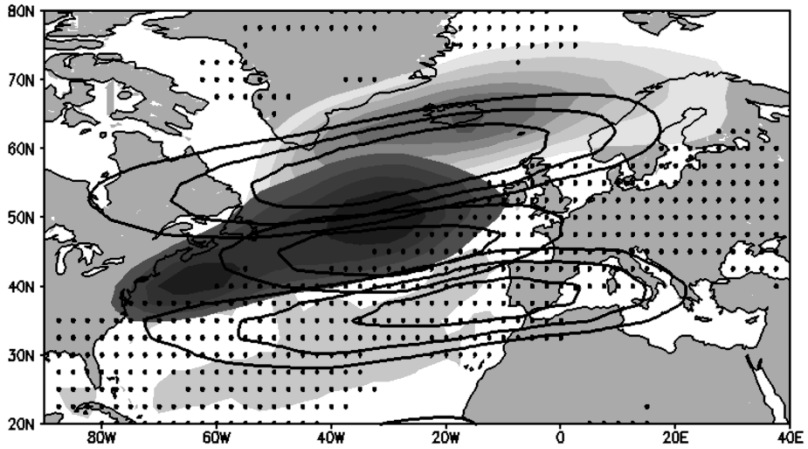

Fig. 6.4: Schematic of the mechanism leading to a decoupling between the NAO and explosive cyclogenesis leading variability (EC1) in ECHAM5/MPIOM1. Three preferred positions of the winter jet (1-11 yr.) in solid contours. Areas of enhanced multi-decadal (> 33 yr.) baroclinicity in stippling. EC1 pattern during normal conditions (decoupling periods) in light (dark) grey. Enhanced meridional SST gradient over the sub-tropical North Atlantic (decoupling periods) in light grey. Figure adapted from *Gómara et al.* [2015].

In addition, the connection between the NAO and EC1 could also be well established during those decades in which the eddy-driven jet alternates its position between the sub-polar and central/sub-tropical latitudes in the North Atlantic (contours in Fig. 6.4). These are the so-called three preferred positions of the interannual winter jet [*Woollings et al.*, 2010]. This second potential mechanisms relies on the existence of strong upper level divergence over the right-entrance and left-exit regions of the jet core [*Uccellini*, 1990]. During NAO+ years (poleward shifted jet) baroclinic disturbances forming over Eastern North America are able to cross the areas of strong upper level divergence and explosively amplify. These NAO+ years therefore introduce strong variance in the track density data as the number of explosive cyclones is remarkably increased.

However, a weaker, less extended and southerly shifted jet (NAO-) is obviously less efficient for explosive intensification and explosive cyclone activity is mitigated over the North Atlantic. If the jet is repeatedly situated over the central or sub-tropical North Atlantic (i.e. a marked southerly shifted multi-decadal jet), the variance associated with NAO+ years is absent and other modes of variability (not necessary related to NAO+) can emerge. These may explain the abrupt transitions in the EC variability and also rely on the apparent low influence of the NAO phases on the explosive genesis area situated over the Eastern North American coast line (cf. Fig. S7 – section V.4).

Gómara et al. [2015] provides evidence of the modulating role of low frequency oceanic and atmospheric variability (>33 yr.) onto the high-frequency climate variability (1-11 yr.) of explosive cyclogenesis in the North Atlantic. In addition, it highlights the importance of the extra-tropical jet evolution as the leading precursor and modulator of explosive cyclone growth at climatic timescales. The novel results of this study may contribute to improve multi-decadal predictions of extreme cyclones in the North Atlantic [*Nissen et al.*, 2014; *Feser et al.*, 2015]. The current analysis only focuses on explosive cyclogenesis. Thus, an analogous study considering all cyclones for a larger set of control simulations (e.g., CMIP5 models) might be an interesting path for future research. An analysis of the decadal occurrence of RWB [*Woollings et al.*, 2015] and its potential influence over EC2 would be another interesting topic to follow. Hopefully, the outcome of these proposed investigations might help in the better understanding of the 2013/2014 stormy winter over the British Isles.

In summary, this thesis provides evidence that explosive cyclones affecting Europe predominantly develop under NAO+ events lasting several days [*Gómara et al.*, 2014b]. These events are triggered by RWB processes [*Gómara et al.*, 2014a], and appear to promote single and multiple cyclone occurrences over Western Europe [*Pinto et al.*, 2014]. The dynamics of explosive and non-explosive cyclones over the North Atlantic are contrasting at synoptic timescales. The same is observed for climatic timescales, where a non-stationary connection between the NAO and explosive cyclogenesis leading variability is found [*Gómara et al.*, 2015]. Evidence is provided that this relation appears to be modulated by multi-decadal variability of the ocean-atmosphere coupled system.

VII. CONCLUSIONS, IMPLICATIONS AND OUTLOOK

'Science never solves a problem without creating ten more.'

George Bernard Shaw (playwright; 1856-1950)

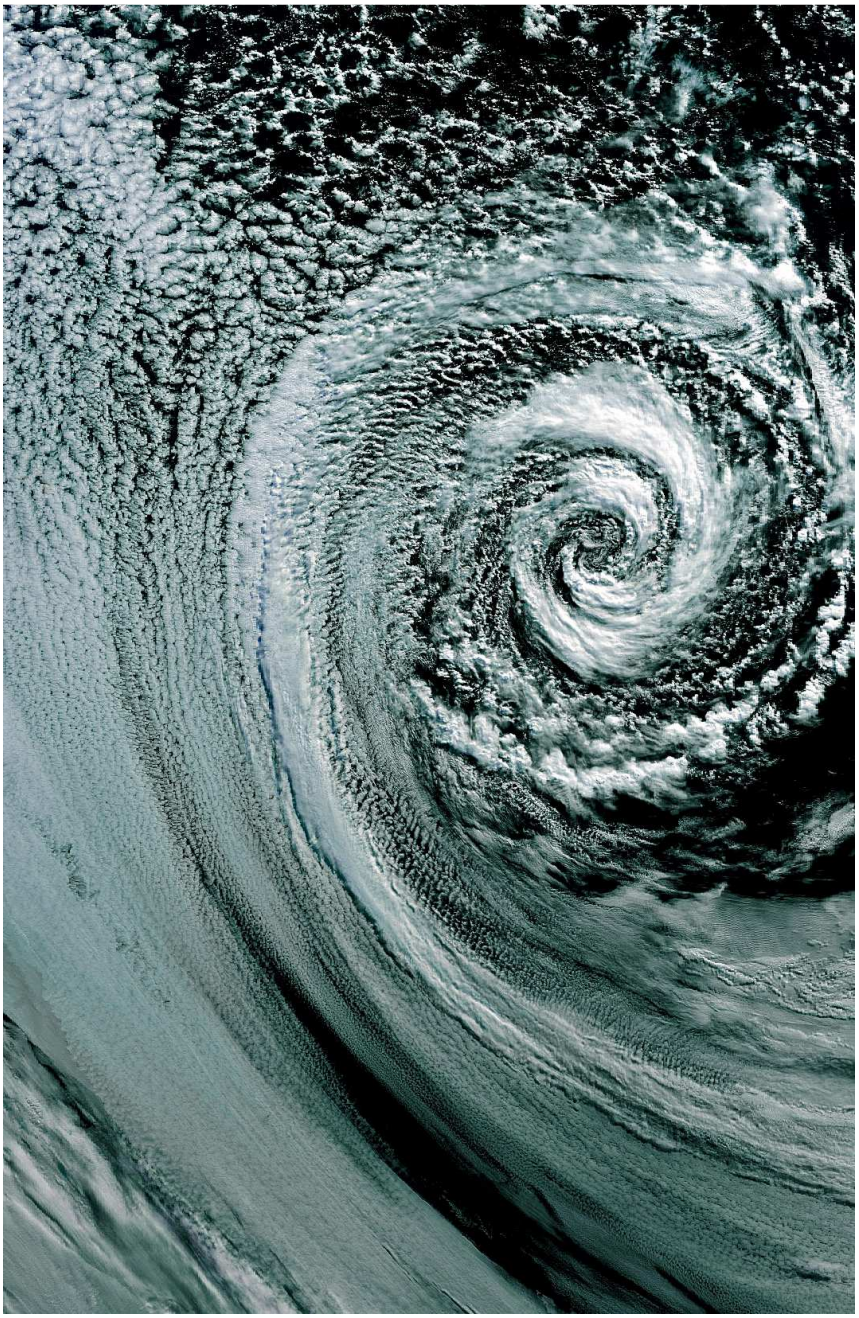

VII. Conclusions, Implications and Outlook

In this thesis the large-scale dynamics and variability associated with explosive cyclogenesis over the North Atlantic have been analyzed. On one hand, the two-way relation between the large-scale circulation and extra-tropical cyclones at synoptic timescales has been assessed. Within this context, the sensitivity of this relation to cyclone's intensity and cyclone clustering has been investigated. On the other hand, the climate variability (1-11 yr.) of explosive cyclones over the North Atlantic has been characterized, and the potential external forcings to this variability have been identified. The conclusions of this thesis are enumerated below. These are divided into four different blocks, each one corresponding to the outcomes of each scientific publication attached in the Results chapter. For consistency, the main objectives and open questions posed in the Objectives chapter are acknowledged here, together with the main implications of each study. The potential paths for future research of this thesis (as a whole) are described in the final paragraphs of this chapter.

1. On the relation between explosive cyclones affecting Europe and the North Atlantic oscillation [*Gómara et al.*, 2014b]

- **Objective:** To analyze the bi-directional relation between the large-scale mean flow (mostly explained by the North Atlantic Oscillation) and explosive and non-explosive cyclones affecting Western and Central Europe.

- **Open Questions:** *Which NAO phase is more favorable for the occurrence of explosive cyclones over Western and Central Europe? How is characterized the associated large-scale flow? What is the influence of explosive cyclones affecting Europe over the large-scale mean flow and the NAO? Are these relations sensitive to storm's intensity?*

- **Conclusions:**

  1. Evidence is given that explosive and non-explosive cyclones affecting Europe predominantly develop under different large-scale circulation conditions:

a. Non-explosive cyclones develop more frequently under negative and neutral NAO phases. These cyclones are linked to a tripole pattern (wave-like, arched in the North Atlantic) of z500 anomalies, with negative anomalies over eastern North America and north-western Europe, and a positive anomaly over south-western Greenland. These mean flow anomalies, which project more onto NAO- due to the Greenland center of action, do not appear to promote rapid cyclone intensification, but to deflect the cyclone trajectories toward Europe.

b. The number of explosive cyclones is larger under a positive NAO phase. These cyclones tend to develop under a downstream propagating north-negative and south-positive pattern of z500 anomalies. This z500 structure is accompanied by an intensified jet stream over Western Europe, which acts to promote rapid cyclone intensification over this area.

2. After cyclone's peak intensity, contrasting NAO behavior is observed for explosive and non-explosive cyclones:

a. Non-explosive cyclones do not appear to produce any eddy-related influence onto the large-scale flow. During cyclone's decline, the NAO anomalies appear to decay due to frictional damping processes (similar to climatology).

b. Explosive cyclones produce strong variations in the daily NAO index, both positive and negative, and the large-scale circulation.

i. The negative variations are due to the downstream propagation of the z500/jet structure (NAO+ like) over the North Atlantic described in point 1.b. This is due to the lower projection of the anomalies onto the canonical NAO pattern used to compute the daily NAO index.

ii. The positive variations are due to enhanced positive eddy momentum fluxes associated with the explosive cyclones. These positive fluxes appear to promote the NAO positive phase during cyclone lysis.

- **Main implications:** This study may contribute to improve predictions (lags -4/-3) of explosive cyclones impacting Europe and enhance the predictability on short-term NAO-like variability.

2. Rossby wave-breaking analysis of explosive cyclones in the Euro-Atlantic sector [*Gómara et al.*, 2014a]

- **Objective:** To provide a deeper and more general description of the two-way relationship between cyclones and the large-scale circulation in the North Atlantic through the analysis of Rossby Wave-Breaking processes.

- **Open questions:** *Is there a common pattern of RWB upstream (downstream) and prior to (after) explosive cyclogenesis over the North Atlantic? Is RWB dependent on the cyclone's intensity? Is RWB sensitive to the cyclone's trajectory and location (and vice-versa)?*

- **Conclusions:**

1. The most intense cyclones in the western North Atlantic are preceded by enhanced cyclonic RWB activity over western Greenland on days prior to their maximum intensification. Under these conditions, the extra-tropical jet is squashed on its northern side by the RWB events and thus accelerated over the western North Atlantic. Such favorable upper level conditions for cyclone growth increase the potential for the occurrence of explosive cyclones over that area.

2. The most intense cyclones over the eastern North Atlantic are preceded by two distinct areas of enhanced RWB: cyclonic RWB over eastern Greenland and anticyclonic over the sub-tropical North

Atlantic. Both RWB events squeeze the jet from both flanks and accelerate it over Western Europe. The probability of an explosive eastern cyclone is roughly doubled if simultaneous RWB occurs.

3. On days following the explosive development of the most intense cyclones in the western North Atlantic, a common RWB pattern of cyclonic breaking over southern Greenland and anticyclonic over Europe is identified. This RWB structure appears to lead the onset of Scandinavian Blocking.

4. Non-explosive cyclones depict no sign of enhanced RWB over the whole North Atlantic area, either at days prior or following their maximum intensification period.

5. The links between RWB and cyclogenesis over the Euro-Atlantic sector are sensitive to cyclone's maximum intensity, deepening rate, timing and location.

- **Main implications:** These findings have contributed to a better understanding of the large-scale conditions leading to the occurrence of explosive cyclones affecting Western Europe, and may help to improve their forecast over the Euro-Atlantic sector.

3. Large-scale dynamics associated with clustering of extratropical cyclones affecting Western Europe [*Pinto et al.*, 2014]

- **Objective:** To provide the first dynamical analysis of the occurrence of cyclone families over Western Europe, focusing on the role of Rossby Wave-Breaking, jet dynamics and secondary cyclogenesis.

- **Open questions:** *Which are the potential physical mechanisms responsible for the occurrence of storm families over Western Europe? What is the role of the steering by the large-scale flow? Are upstream and downstream secondary cyclogenesis processes important? To what extent is the*

occurrence of these physical precursors sensitive to the intensity of the clustered cyclones involved (and vice-versa)?

- **Conclusions:**

  1. Optimal conditions for the occurrence of cyclone clusters are provided by a recurrent extension of an intensified eddy-driven jet over Western Europe lasting at least 1 week. Multiple RWB occurrences on both the poleward and equatorward flanks of the jet contribute to the development of these favorable anomalous large-scale conditions for cyclone growth.

  2. The connection between cyclone clustering and double-sided RWB is tighter for the most intense storm series.

  3. Secondary upstream cyclogenesis plays an important role in the occurrence of cyclone families over Western Europe. A recurring pattern during cyclone clustering events is identified: a developing cyclone is located in the right-entrance region of the jet on the trailing cold front of a mature cyclone. The mature cyclone is situated in the left-exit region of the same jet-streak. Next, the new cyclone rapidly intensifies and follows a similar path to the previous cyclone.

  4. Secondary downstream cyclogenesis may play a role in some of the cyclone clustering events observed over Western Europe. However, it cannot explain solely the major episodes of February 1990, January 1993, December 1999 and January 2007.

- **Main implications:** This study permits a better understanding of the physical mechanisms leading to the occurrence of cyclone families over Western Europe, thus potentially enabling a better quantification of the associated cumulative risk over this area.

5. <u>Abrupt transitions in the variability of explosive cyclones over the North Atlantic [*Gómara et al.*, 2015]</u>

- **Objective:** To characterize the high-frequency climate variability (1-11 yr.) of explosive cyclogenesis in the North Atlantic and analyze the potential modulating role of the ocean-atmosphere coupled system multi-decadal variability.

- **Open questions:** *Is the climate (1-11yr.) variability of explosive cyclogenesis over the North Atlantic similar to the observed for all cyclones? What is the role of the NAO and the extra-tropical jet stream in steering the climate variability of explosive cyclones? Is the connection with the NAO stationary in time? Does El Niño play an important role influencing explosive cyclogenesis? What is the potential role of the atmospheric/oceanic multi-decadal variability modulating the high-frequency climate behavior of explosive cyclogenesis?*

- **Conclusions:**

1. The leading variability mode (1-11 yr.) of explosive cyclogenesis is different from the associated with the whole storm track:

    a. EOF1 of explosive cyclogenesis represents a strengthening (EC1+) / weakening (EC1-) pattern of cyclone track density between Newfoundland and Iceland.

    b. EOF1 of the whole storm track (including explosive and non-explosive cyclones) predominantly represents a latitudinal shift of storm trajectories between Iceland and Western Europe.

2. The NAO is significantly and positively correlated with EC1+. Under NAO+, baroclinicity is enhanced over the North Atlantic and surface disturbances forming near Newfoundland cross the jet from the right-entrance toward the left-exit regions. These conditions promote explosive intensification of cyclones. This mechanism holds for the majority of the periods studied in NCEP, ERA-40 and ECHAM5/MPIOM1.

3. During specific periods of NCEP and ECHAM5/MPIOM1 the correlation between EC1+ and the NAO rapidly fluctuates. Therefore, the connection between the NAO and explosive cyclogenesis is non-stationary in time.

4. El Niño variability appears to be anti-correlated with EC1+ in NCEP (not statistically significant) and ECHAM5/MPIOM1 (95% confidence level). The influence of El Niño is also non-stationary in time.

5. Evidence is given on the importance of the multi-decadal oceanic/atmospheric variability for the non-stationary behavior of explosive cyclone tracks in the North Atlantic:

    a. The decades of increased (decreased) NAO-EC1 correlation are characterized by enhanced (decreased) baroclinicity over the sub-polar (sub-tropical) North Atlantic. These periods agree with multi-decadal changes of the jet latitude.

    b. The ocean state is found important for the occurrence and persistence of decadal fluctuations in the NAO-EC1 connection.

- **Main implications:** This study may contribute to improve multi-decadal predictions of explosive cyclones over specific areas of the North Atlantic.

Potential paths for future research

The potential paths for future research of this thesis are individually described in each publication of the Results chapter. Despite several topics are acknowledged as the thesis progresses, others still remain unresolved. In the following the most compelling topics for potential future research are described:

The robustness of the results in section V.3 (storm clustering over Western Europe) should be tested in a more complete analysis for the whole reanalysis period, including the storm series over the British Isles during the winter of 2013/2014 [*Huntingford et al.*, 2014; *van Oldenborgh et al.*, 2015]. This is currently under way at the University of Reading. Another interesting question is the relative role played by the synoptic-scale temperature gradient associated with the jet streak and the mesoscale temperature gradient associated with the cold front of the primary cyclone in determining the rate of secondary cyclogenesis. The importance of the deformation strain, shear, and latent heat release in secondary cyclogenesis are also important aspects to consider. Other lines of future research include similar analyses in high-resolution general circulation models [*Shaffrey et al.*, 2009] and the estimation of windstorm losses associated to cyclone clustering [*Karremann et al.*, 2014]. This aspect is also a part of the current ongoing work at the University of Reading. For predictability purposes, a study of the variability and origin of the Rossby wave-trains leading to explosive cyclogenesis and cyclone clustering over Western Europe is undoubtedly a very interesting path for future research.

The results in section V.4 (climate variability of explosive cyclone tracks in the North Atlantic) should be tested in a larger set of control experiments with different GCMs (e.g., from CMIP3 and CMIP5). In addition, the potential non-stationary connection between the whole storm track and the NAO would also be interesting path for subsequent research. This work is programmed to start at the Complutense University of Madrid during the next months. An analysis of the decadal occurrence of RWB [*Woollings et al.*, 2015] and its influence over the second leading variability mode of explosive cyclone tracks would be another interesting topic to follow.

References

Adamson DS, Belcher SE, Hoskins BJ, and Plant RS (2006) Boundary layer friction in mid-latitude cyclones, Q. J. R. Meteorol. Soc., 132, 101-124.

Allen JT, Pezza AB, and Black MT (2010) Explosive Cyclogenesis: A Global Climatology Comparing Multiple Reanalyses, J. Climate., 23, 6468 - 6484.

Aon Benfield (2010) Impact Forecasting report: European Winter Storms: Traditional Perils Posing New Challenges. Available at:

http://www.aon.com/attachments/reinsurance/traditional_perils_new_challenges.pdf

Bader J, Mesquita MDS, Hodges KI, Keenlyside N, Østerhus S, and Miles M (2011) A review on Northern Hemisphere sea-ice, storminess and the North Atlantic Oscillation: observations and projected changes, Atmos. Res., 101, 809-834.

Baldwin MP, and Dunkerton TJ (2001) Stratospheric Harbingers of Anomalous Weather Regimes, Science, 294 (5542), 581-584, DOI:10.1126/science.1063315

Barnes EA, and Hartmann D (2011) Rossby Wave Scales, Propagation, and the Variability of Eddy-Driven Jets, J. Atmos. Sci., 68, 2893 - 2908.

Barnston AG, and Livezey RE (1987) Classification, seasonality and persistence of low-frequency atmospheric circulation patterns, Mon. Weather Rev., 115, 1083 - 1126.

Barnston AG, Tippett MK, L'Heureux ML, Li S, and DeWitt DG (2012) Skill of Real-Time Seasonal ENSO Model Predictions during 2002–11: Is Our Capability Increasing? Bull. Amer. Meteor. Soc., 93, 631-651, doi: http://dx.doi.org/10.1175/BAMS-D-11-00111.1.

Barriopedro D, García-Herrera R, Lupo AR, and Hernández E (2006) A Climatology of Northern Hemisphere Blocking, Journal of Climate, 19, 6, 1042-1063, doi: 10.1175/JCLI3678.1

Benedict JJ, Lee S, and Feldstein SB (2004) Synoptic view of the North Atlantic Oscillation, J. Atmos. Sci., 61, 121 - 144.

Bengtsson L, Hodges KI, Roeckner E, and Brokopf R (2006) On the natural variability of the pre-industrial European climate, Clim. Dyn., 27, 743–760

Bishop CH, and Thorpe AJ (1994a) Frontal wave stability during moist deformation frontogenesis. Part I: Linear wave dynamics, J. Atmos. Sci., 51, 852-873.

Bishop CH, and Thorpe AJ (1994b) Frontal wave stability during moist deformation frontogenesis. Part II: The suppression of non linear wave development, J. Atmos. Sci., 51, 874-888.

Bjerknes J, and Solberg H (1922) Life cycle of cyclones and the polar front theory of atmospheric circulation, Geofys. Publ., 3, 3–18.

Bjerknes J (1966) A possible response of the atmospheric Hadley circulation to anomalies of ocean temperature, Tellus, 18, 820–829.

Blackmon ML, Wallace JM, Lau NC, and Mullen SL (1977) An Observational Study of the Northern Hemisphere Wintertime Circulation, J. Atmos. Sci., 34, 1040-1053, doi: 10.1175/1520-0469(1977)034<1040:AOSOTN>2.0.CO;2

Bladé I, Newman M, Alexander MA, and Scott JD (2008) The late fall extratropical response to ENSO: sensitivity to coupling and convection in the tropical West Pacific, J. Climate, 21(23), 6101-6118.

Blender R, Raible CC, and Lunkeit F (2015) Non-exponential return time distributions for vorticity extremes explained by fractional Poisson processes, Q. J. R. Meteorol. Soc., 141: 249–257. doi: 10.1002/qj.2354.

Blessing S, Fraedrich K, Junge M, Kunz T, and Lunkeit F (2005) Daily North-Atlantic Oscillation (NAO) index: Statistics and its stratospheric polar vortex dependence, Meteorol. Z., 14, 763 - 769.

Bosart LF, and Lin SC (1984) A diagnostic analysis of the Presidents' Day storm of February 1979, Mon. Weather Rev., 112, 2148 - 2177.

Branstator G (2002) Circumglobal teleconnections, the jet stream wave-guide, and the North Atlantic Oscillation, J. Climate, 15, 1893-1910.

Bretherton CS, Widmann M, Dymnikov VP, Wallace JM, and Blade I (1999) Effective number of degrees of freedom of a spatial field, J. Climate, 12, 1990-2009.

Broecker WS (1991) *The great ocean conveyor,* Oceanography, 4(2), 79-89.

Brönnimann S (2007) Impact of El Niño-Southern Oscillation on European climate, Reviews of Geophysics, 45, RG3003, doi:10.1029/2006RG000199

Carton JA, Giese BS, and Grodsky SA (2005) Sea level rise and the warming of the oceans in the SODA ocean reanalysis, J. Geophys. Res., 110, doi: 10.1029/2004JC002817

Carton JA, and Giese BS (2008) A Reanalysis of Ocean Climate Using Simple Ocean Data Assimilation (SODA), Mon. Weather Rev., 136, 2999-3017.

Cassou C, and Terray L (2001) Dual influence of Atlantic and Pacific SST anomalies on the North Atlantic/Europe winter climate, Geophys. Res. Lett., 28, 3195–3198.

Chaboureau JP, and Thorpe AJ (1999) Frontogenesis and the development of secondary wave cyclones in FASTEX, Q. J. R. Meteorol. Soc., 125, 925-940.

Champion AJ, Hodges KI, Bengtsson LO, Keenlyside NS, and Esch M (2011) Impact of increasing resolution and a warmer climate on extreme weather from Northern Hemisphere extratropical cyclones, Tellus A., 63A, 893 - 906.

Chang EKM (1993) Downstream development of baroclinic waves as inferred from regression analysis, J. Atmos. Sci., 50, 2038-2053.

Chang EKM, and Orlanski I (1993) On the Dynamics of a Storm Track, J. Atmos. Sci., 50, 999–1015, doi: 10.1175/1520-0469(1993)050<0999:OTDOAS>2.0.CO;2

Chang EKM, and Yu DB (1999) Characteristics of wave packets in the upper troposphere. Part I: Northern hemisphere winter, J. Atmos. Sci., 56, 1708-1728.

Chang EKM (2009) Are band-pass variance statistics useful measures of storm track activity? Re-examining storm track variability associated with the NAO using multiple storm track measures, Clim. Dyn., 33, 277 - 296.

Chen S, Wu R, and Chen W (2015) The Changing Relationship between Interannual Variations of the North Atlantic Oscillation and Northern Tropical Atlantic SST, J. Climate, 28, 485–504, doi: 10.1175/JCLI-D-14-00422.1

Colucci SJ (1985) Explosive Cyclogenesis and Large-Scale Circulation Changes: Implications for Atmospheric Blocking, J. Atmos. Sci., 42, 2701 - 2717.

Compo, and co-authors (2011) The Twentieth Century Reanalysis Project, Quart. J. Roy. Meteor. Soc., 137, 1-28, DOI:10.1002/qj.776

Czaja A, and Frankignoul C (1999) Influence of the North Atlantic SST on the atmospheric circulation, Geophys. Res. Lett., 26, 19, 2969-2972, DOI: 10.1029/1999GL900613

Dacre HF, and Gray SL (2006) Life-cycle simulations of low-level frontal waves and the impact of deformation strain, Q. J. R. Meteorol. Soc., 132, 2171-2190.

Dacre HF, and Gray SL (2009) The Spatial Distribution and Evolution Characteristics of North Atlantic Cyclones, Mon. Weather Rev., 137, 99 - 115.

Dacre HF, and Gray SL (2013) Quantifying the climatological relationship between extratropical cyclone intensity and atmospheric precursors, Geophys. Res. Lett., doi: 10.1002/grl.50105

Davis CA, and Emanuel KA (1988) Observational evidence for the influence of surface heat fluxes on maritime cyclogenesis, Mon. Weather Rev., 116, 2649 - 2659.

Dee DP, and Uppala S (2009) Variational bias correction of satellite radiance data in the ERA-Interim reanalysis, Q.J.R. Meteorol. Soc., 135, 1830–1841, doi: 10.1002/qj.493

Dee DP, and co-authors (2011) The ERA-Interim reanalysis: configuration and performance of the data assimilation system, Q.J.R. Meteorol. Soc., 137, 553–597, doi: 10.1002/qj.828

Della-Marta PM, Liniger MA, Appenzeller C, Bresch DN, Köllner-Heck P, and Muccione V (2010) Improved estimates of the European winter windstorm climate and the risk of reinsurance loss using climate model data, J. Appl. Meteorol. Climatol., 49, 2092–2120.

DelSole T (2001) A Simple Model for Transient Eddy Momentum Fluxes in the Upper Troposphere, J. Atmos. Sci., 58, 3019 - 3035.

Donat MG, Leckebusch GC, Pinto JG, and Ulbrich U (2010) Examination of Wind Storms over Central Europe with respect to Circulation Weather Types and NAO phases, Int. J. of Climatology, 30, 1289 - 1300.

Dong B, Sutton RT, Woollings T, and Hodges K (2013) Variability of the North Atlantic summer storm track: mechanisms and impacts on European climate, Environ. Res. Lett., 8, 034037, doi:10.1088/1748-9326/8/3/034037

Dritschel DG, Haynes PH, and Juckes MN (1991) The stability of a two-dimensional vorticity filament under uniform strain, J. Fluid Mech., 230, 647-665.

Drouard M, Rivière G, and Arbogast P (2013) The North Atlantic Oscillation Response to Large-Scale Atmospheric Anomalies in the Northeastern Pacific, J. Atmos. Sci., 70, 2854–2874, doi: http://dx.doi.org/10.1175/JAS-D-12-0351.1

Drouard M, Rivière G, and Arbogast P (2015) The Link between the North Pacific Climate Variability and the North Atlantic Oscillation via Downstream Propagation of Synoptic Waves, J. Climate 28, 3957-3976, doi: 10.1175/JCLI-D-14-00552.1

Duchon CE (1979) Lanczos Filtering in One and Two Dimensions, J. Appl. Meteor., 18, 1016–1022,

doi: http://dx.doi.org/10.1175/1520-0450(1979)018<1016:LFIOAT>2.0.CO;2

Economou T, Stephenson DB, Pinto JG, Shaffrey LC, and Zappa G (2015) Serial clustering of extratropical cyclones in historical and future CMIP5 model simulations, Quart. J. R. Meteorol. Soc., doi:10.1002/qj.2591

Edmon HJ, Hoskins BJ, and McIntyre ME (1980) Eliassen–Palm cross sections for the troposphere, J. Atmos. Sci., 37, 2600 - 2616.

Feldstein SB (2003) The dynamics of NAO teleconnection pattern growth and decay, Q.J.R. Meteorol. Soc., 129, 901 - 924.

Fernández J, Sáenz J, Zorita E (2003) Analysis of wintertime atmospheric moisture transport and its variability over southern Europe in the NCEP Reanalyses, Climate Research, 23, 195-215, doi:10.3354/cr023195.

Feser F, Barcikowska M, Krueger O, Schenk F, Weisse R, and Xia L (2015) Storminess over the North Atlantic and northwestern Europe-A review, Q.J.R. Meteorol. Soc., 141, 350-382, doi: 10.1002/qj.2364

Fink AH, Brücher T, Ermert V, Krüger A, and Pinto JG (2009) The European Storm Kyrill in January 2007: Synoptic Evolution and Considerations with Respect to Climate Change, Nat. Hazards Earth Sys. Sci., 9, 405-423.

Fink AH, Pohle S, Pinto JG, and Knippertz P (2012) Diagnosing the influence of diabatic processes on the explosive deepening of extratropical cyclones, Geophys. Res. Lett., 39, L07803, DOI: 10.1029/2012GL051025.

Fosdick EK, and Smith PJ (1991) Latent Heat Release in an Extratropical Cyclone that Developed Explosively over the Southeastern United States, Mon. Weather Rev., 119, 193 - 207.

Frankignoul C, and Kestenare E (2005) Observed Atlantic SST anomaly impact on the NAO: An update, Journal of climate, 18(19), 4089-4094.

Franzke C, Lee S, and Feldstein SB (2004) Is the North Atlantic Oscillation a breaking wave? J. Atmos. Sci., 61, 145 - 160.

Gabriel A, and Peters D (2008) A diagnostic study of different types of Rossby wave breaking events in the northern extratropics, J. Met. Soc. Japan, 86(5), 613 - 631.

García-Serrano J, Rodríguez-Fonseca B, Bladé I, Zurita-Gotor P, and Cámara A (2011) Rotational atmospheric circulation during North Atlantic-European winter: the influence of ENSO, Clim. Dyn., 37(9-10), 1727–1743, doi:10.1007/s00382-010-0968-y

Gastineau G, and Frankignoul C (2012) Cold-season atmospheric response to the natural variability of the Atlantic meridional overturning circulation. Clim. Dyn., 39(1-2), 37-57.

Gómara I, Rodríguez-Puebla C, Rodríguez-Fonseca B, and Yagüe C (2010) Study of extra-tropical cyclone Klaus: posible connections with the NAO, Meteorology and Renewable energies: Spanish Meteorological Society, ISSN: 978 – 84 – 613 -9596 – 5.

Gómara I, Pinto JG, Woollings T, Masato G, Zurita-Gotor P, and Rodríguez-Fonseca B (2014a) Rossby wave-breaking analysis of explosive cyclones in the Euro-Atlantic sector, Q.J.R. Meteorol. Soc., 140, 738–753, doi: 10.1002/qj.2190

Gómara I, Rodríguez-Fonseca B, Zurita-Gotor P, and Pinto JG (2014b) On the relation between explosive cyclones affecting Europe and the North Atlantic Oscillation, Geophys. Res. Lett., 41, 2182–2190, doi:10.1002/2014GL059647.

Gómara I, Rodríguez-Fonseca B, Zurita-Gotor P, Ulbrich S, and Pinto JG (2015) Abrupt transitions in the variability of explosive cyclones over the North Atlantic, Clim. Dyn., (under review, CLDY-D-15-00358).

Greatbatch RJ, Lu J, and Peterson KA (2004) Nonstationary impact of ENSO on Euro-Atlantic winter climate, Geophys. Res. Lett., 31, L02208. doi:10.1029/2003GL018542

Gyakum JR (1983) On the evolution of the QE II Storm. II: Dynamic and thermodynamic structure, Mon. Weather Rev., 111, 1156-1173, DOI: 10.1175/1520-0493.

Gyakum JR, and Danielson RE (2000) Analysis of meteorological precursors to ordinary and explosive cyclogenesis in the western North Pacific, Mon. Weather Rev., 128, 851 - 863.

Hanley J, and Caballero R (2012) The role of large-scale atmospheric flow and Rossby wave breaking in the evolution of extreme windstorms over Europe, Geophys. Res. Lett., 39, L21708. doi:10.1029/2012GL053408

Harris BA, and Kelly G (2001) A satellite radiance-bias correction scheme for data assimilation, Q. J. R. Meteorol. Soc., 127, 1453–1468.

Hawcroft MK, Shaffrey LC, Hodges KI, and Dacre HF (2012) How much Northern Hemisphere precipitation is associated with extratropical cyclones? Geophys. Res. Lett., 39, L24809.

Haylock MR (2011) European extra-tropical storm damage risk from a multimodel ensemble of dynamically-downscaled global climate models, Nat. Hazards Earth Syst. Sci., 11, 2847–2857.

Hewson TD (1997) Objective identification of frontal wave cyclones, Meteorol. Appl., 4, 311–315.

Hewson, TD (1998) Objective fronts, Meteorol. Appl., 5, 37–65.

Hoerling MP, Hurrell JW, and Xu T (2001) Tropical origin for recent North Atlantic climate change, Science, 292, 90-92.

Hoerling MP, Hurrell JW, Xu T, Bates GT, and Phillips A (2004) Twentieth century North Atlantic climate change. Part II: Understanding the effect of Indian Ocean warming, Clim. Dyn., 23, 391-405, doi:10.1007/s00382-004-0433-x.

Honda M, Nakamura H, Ukita J, Kousaka I, and Takeuchi K (2001) Interannual Seesaw between the Aleutian and Icelandic Lows. Part I: Seasonal Dependence and Life Cycle, J. Climate, 14, 1029-1042, doi: 10.1175/1520-0442(2001)014<1029:ISBTAA>2.0.CO;2

Hoskins BJ, James IN, and White GH (1983) The shape, propagation and mean-flow interaction of large-scale weather, J. Atmos. Sci., 40, 1595–1612.

Hoskins BJ, McIntyre ME, and Robertson AW (1985) On the use and significance of isentropic potential vorticity maps, Q. J. R. Meteorol. Soc., 111, 877 - 946.

Hoskins BJ, and Valdes PJ (1990) On the existence of storm-tracks, J. Atmos. Sci., 47, 1854 - 1864.

Hoskins B, and Ambrizzi T (1993) Rossby wave propagation on a realistic longitudinally varying flow, J. Atmos. Sci., 50, 1661–1671.

Hoskins BJ, and Hodges KI (2002) New perspectives on the Northern Hemisphere winter storm tracks, J. Atmos. Sci., 59, 1041–1061.

Huntingford C, and co-authors (2014) Nature Clim. Change, 4, 769–777.

Hurrell JW, Kushnir Y, Ottersen G, and Visbeck M (2003) The North Atlantic Oscillation: climate significance and environmental impact, Geophysical monograph. Series., 134, 279pp.

IPCC (2007) Climate Change 2007: The Physical Science Basis. Contribution of Working Group I to the Fourth Assessment Report of the Intergovernmental Panel on Climate Change [Solomon, S., D.

Qin, M. Manning, Z. Chen, M. Marquis, K.B. Averyt, M.Tignor and H.L. Miller (eds.)]. Cambridge University Press, Cambridge, United Kingdom and New York, NY, USA.

James IN, and James PM (1989) Ultra-low-frequency variability in a simple atmospheric circulation model, Nature, 342, 53-55.

Jin EK, Kinter JL, Wang B, Park CK, Kang IS, Kirtman BP, Kug JS, Kumar A, Luo JJ, Schemm J, Shukla J, and Yamagata T (2008) Current status of ENSO prediction skill in coupled ocean–atmosphere models, Clim. Dyn., 31, 0930-7575. 10.1007/s00382-008-0397-3

Joly A, and Thorpe AJ (1990) Frontal instabilities generated by tropospheric potential vorticity anomalies, Q. J. R. Meteorol. Soc., 116, 525-560.

Joly A, and Thorpe AJ (1991) The stability of time-dependent flows: An application to fronts in developing baroclinic waves, J. Atmos. Sci., 48, 163-182.

Jung T, Hilmer M, Ruprecht E, Kleppek S, Gulev SK, and Zolina O (2003) Characteristics of the Recent Eastward Shift of Interannual NAO variability, J. Clim., 16, 3371–3382.

Jungclaus JH, Botzet M, Haak H, Keenlyside N, Luo JJ, Latif M, Marotzke J, Mikolajewicz U, and Roeckner E (2006) Ocean circulation and tropical variability in the coupled model ECHAM5/MPI-OM, J. Clim., 19, 3952–3972.

Kalnay E, and co-authors (1996) The NCEP / NCAR 40-year reanalysis project, Bull. Amer. Meteor. Soc., 77, 437-471.

Karremann MK, Pinto JG, Von Bomhard PJ, and Klawa M (2014) On the clustering of winter storm loss events over Germany, Nat. Hazards Earth Syst. Sci., 14, 2041-2052.

Klawa M, and Ulbrich U (2003) A model for the estimation of storm losses and the identification of severe winter storms in Germany, Nat. Hazards Earth Syst. Sci., 3, 725–732.

Knight JR, Allan RJ, Folland CK, Vellinga M, and Mann ME (2005) A signature of persistent natural thermohaline circulation cycles in observed climate, Geophys. Res. Lett., 32, L20708. doi:10.1029/2005GL024233.

Kobayashi S, and co-authors (2015) The JRA-55 Reanalysis: General Specifications and Basic Characteristics, 93, doi: 10.2151/jmsj.2015-001.

Kuwano-Yoshida A, and Asuma Y (2008) Numerical Study of Explosively Developing Extratropical Cyclones in the Northwestern Pacific Region, Mon. Weather Rev., 136, 712 - 740.

Lamb HH (1991) Historic Storms of the North Sea, British Isles, and Northwest Europe, Cambridge University Press, Cambridge, UK.

Lau NC (1978) On the Three-Dimensional Structure of the Observed Transient Eddy Statistics of the Northern Hemisphere Wintertime Circulation, J. Atmos. Sci., 35, 1900–1923, doi: 10.1175/1520-0469(1978)035<1900:OTTDSO>2.0.CO;2

Lau NC (1988) Variability of the Observed Midlatitude Storm Tracks in Relation to Low-Frequency Changes in the Circulation Pattern, J. Atmos. Sci., 45, 2718–2743, doi: http://dx.doi.org/10.1175/1520-0469(1988)045<2718:VOTOMS>2.0.CO;2

Lee SS, Lee JY, Wang B, Ha KJ, Jin FF, Straus DM, and Shukla J (2012) Interdecadal changes in the storm track activity over the North Pacific and North Atlantic, Clim. Dyn., 39, 1-2, 313-327, doi:10.1007/s00382-011-1188-9. IPRC-817.

Li X, Holland DM, Gerber EP, and Yoo C (2013) Impacts of the north and tropical Atlantic Ocean on the Antarctic Peninsula and sea ice, Nature, 505, 538-542, doi:10.1038/nature12945

Liberato MLR, Pinto JG, Trigo IF, and Trigo RM (2011) Klaus - an exceptional winter storm over northern Iberia and southern France, Weather, 66, 330 - 334.

López-Parages J, and Rodríguez-Fonseca B (2012) Multidecadal modulation of El Niño influence on the Euro-Mediterranean rainfall, Geophys. Res. Lett., 39, L02704, doi:10.1029/2011GL050049

López-Parages J, Rodríguez-Fonseca B, and Terray L (2014) A mechanism for the multidecadal modulation of ENSO teleconnection with Europe, Clim. Dyn., 45 (3-4), pp 867-880. 10.1007/s00382-014-2319-x

Lorenz EN (1956) Empirical orthogonal functions and statistical weather prediction. Science Report 1, Statistical Forecasting Project, Department of Meteorology, MIT (NTIS AD 110268), 49 pp.

Lorenz D, and Hartmann D (2001) Eddy-zonal flow feedback in the Southern Hemisphere, J. Atmos. Sci., 58, 3312-3327.

Losada T, Rodríguez-Fonseca B, Mechoso CR, and Ma HY (2007) Impacts of SST anomalies on the North Atlantic atmospheric circulation: a case study for the northern winter 1995/1996, Clim. Dyn., 29, 7-8, 807-819.

Losada T, Rodríguez-Fonseca B, Mohino E, Bader J, Janicot S, and Mechoso CR (2012) Tropical SST and Sahel rainfall: A non-stationary relationship, Geophys. Res. Lett., 39, L12705, doi: 10.1029/2012GL052423.

Lu J, and Greatbatch RJ (2002) The changing relationship between the NAO and northern hemisphere climate variability, Geophys. Res. Lett., 29, 7, doi: 10.1029/2001GL014052.

Ludwig P, Pinto JG, Reyers M, and Gray SL (2014) The role of anomalous SST and surface fluxes over the southeastern North Atlantic in the explosive development of windstorm Xynthia, Q.J.R. Meteorol. Soc., 140, 1729–1741, doi: 10.1002/qj.2253.

Luksch U, Raible CC, Blender R, and Fraedrich K (2005) Decadal Cyclone Track Variability in the North Atlantic, Metorol. Z., special issue 14, 747-753.

Mahlstein I, Martius O, Chevalier C, and Ginsbourger D (2012) Changes in the odds of extreme events in the Atlantic basin depending on the position of the extratropical jet, Geophys. Res. Lett., 39, L22805.

Mailier PJ, Stephenson DB, Ferro CAT, and Hodges KI (2006) Serial clustering of extratropical cyclones, Mon. Weather Rev., 134, 2224-2240.

Manobianco J (1989) Explosive east coast cyclogenesis over the west-central North Atlantic Ocean: A composite study derived from ECMWF operational analyses, Mon. Weather Rev., 117, 2365 - 2383.

Mariotti A, Zeng N, and Lau KM (2002) Euro-Mediterranean rainfall and ENSO-a seasonally varying relationship, Geophys. Res. Lett., 29(12), doi:10.1029/2001GL014248

Marshall J, and co-authors (2001) North Atlantic climate variability: Phenomena, impacts and mechanisms, Int. J. Climatol., 21, 1863-1898.

Masato G, Hoskins BJ, and Woollings TJ (2012) Wave-breaking characteristics of midlatitude atmospheric blocking, Q. J. R. Meteorol. Soc., 138, 1285 - 1296.

Masato G, BJ Hoskins, and Woollings T (2013a) Wave-breaking characteristics of Northern Hemisphere winter blocking: a two-dimensional approach, J. Climate, 26, 4535–4549.

Masato G, Hoskins BJ, and Woollings T (2013b) Winter and Summer Northern Hemisphere Blocking in CMIP5 Models, J. Climate, 26, 7044–7059.

Matulla C, Schöner W, Alexandersson H, von Storch H, and Wang XL (2007) European storminess: late nineteenth century to present, Clim. Dyn., DOI 10.1007/s00382-007-0333-y.

McCallum E, and Norris WJT (1990) The storms of January and February 1990, Meteorol. Mag., 119, 201–210.

McIntyre ME, and Palmer TM (1983) Breaking planetary waves in the stratosphere, Nature, 305, 593 - 600.

Michel C, and Rivière G (2011) The link between Rossby wave breakings and weather regime transitions, J. Atmos. Sci., 68, 1730 - 1748.

Michel C, Rivière G, Terray L, and Joly B (2012) The dynamical link between surface cyclones, upper-tropospheric Rossby wave breaking and the life cycle of the Scandinavian blocking, Geophys. Res. Lett., 39, L10806, doi:10.1029/2012GL051682.

Minobe S, Kuwano-Yoshida A, Komori N, Xie SP, and Small RJ (2008) Influence of the Gulf Stream on the troposphere, Nature, 452 (7184), 206–209.

Mo KC, and Livezey RE (1986) Tropical-extratropical geopotential height teleconnections during the Northern Hemisphere winter, Mon. Weather Rev., 114(12), 2488-2515.

Mohino E, Janicot S, and Bader J (2011) Sahel rainfall and decadal to multi-decadal sea surface temperature variability, Clim. Dyn., 37(3), 419-440. DOI:10.1007/s00382-010-0867-2.

Moore GWK, Renfrew IA, and Pickart RS (2013) Multidecadal mobility of the North Atlantic Oscillation, J. Climate, 26, 2453–2466.

Müller WA, Frankignoul C, and Chouaib N (2008) Observed decadal tropical Pacific–North Atlantic teleconnections, Geophys. Res. Lett., 35, L24810, doi:10.1029/2008GL035901

Mumby PJ, Vitolo R, and Stephenson DB (2011) Temporal clustering of tropical cyclones and its ecosystem impacts, Proc. Natl. Acad. Sci. U. S. A., 108, 17,626–17,630

MunichRe (2010) Significant European winter storms 1980−June 2010. Overall losses. Available at www.munichre.com (in German).

Murray RJ, and Simmonds I (1991) A numerical scheme for tracking cyclone centers from digital data. Part I: development and operation of the scheme, Austr. Meteorol. Mag., 39, 155-166.

Nakamura H, and Wallace JM (1993) Synoptic Behavior of Baroclinic Eddies during the Blocking Onset, Mon. Weather Rev., 121, 1892 - 1903.

Nakamura H, Sampe T, Tanimoto Y, and Shimpo A (2004) Observed associations among storm tracks, jet streams and midlatitude oceanic fronts, in Earth's Climate: The Ocean-Atmosphere Interaction, Geophys. Monogr. Ser. 147. Edited by C. Wang, S.-P. Xie, and J. A. Carton, pp 329-345, AGU, Washington, D. C.

Nakamura H, Sampe T, Goto A, Ohfuchi W, and Xie SP (2008) On the importance of mid-latitude oceanic frontal zones for the mean state and dominant variability in the tropospheric circulation, Geophys. Res. Lett.,35, doi: 10.1029/2008GL034010

Neu U, and co-authors (2013) IMILAST: A Community Effort to Intercompare Extratropical Cyclone Detection and Tracking Algorithms, Bull. Amer. Meteor. Soc., 94, 529 – 547, doi: 10.1175/BAMS-D-11-00154.1

Nissen KM, Ulbrich U, Leckebusch GC, and Kuhnel I (2013) Decadal windstorm activity in the North Atlantic-European sector and its relationship to the meridional overturning circulation in an ensemble of simulations with a coupled climate model, Clim. Dyn., doi:10.1007/s00382-013-1975-6

North GR, Bell TL, Cahalan RF, and Moeng FJ (1982) Sampling errors in the estimation of empirical orthogonal functions, Mon. Weather Rev., 110, 699–706, doi:10.1175/1520-0493(1982)110<0699:SEITEO> 2.0.CO;2.

Orlanski I (2003) Bifurcation in eddy life cycles: Implications for storm track variability, J. Atmos. Sci., 60, 993 - 1023.

Osborn TJ, Briffa KR, Tett SFB, Jones PD, and Trigo RM (1999) Evaluation of the North Atlantic oscillation as simulated by a coupled climate model, Clim. Dyn., 15, 685-702.

Parker DJ (1998) Secondary frontal waves in the North Atlantic region: A dynamical perspective of current ideas, Q. J. R. Meteorol. Soc., 124, 829–856.

Peixoto JP, and Oort AH (1991) Physics of Climate, American Institut of Physics, 335 East 45" Street, New York 10017. ISBN 0-88318-712-4.

Pelly JL, and Hoskins BJ (2003) A New Perspective on Blocking, J. Atmos. Sci., 60, 743 - 755.

Petterssen S, and Smebye SJ (1971) On the development of extratropical cyclones, Q. J. R. Meteorol. Soc., 97, 457-482, doi: 10.1002/qj.49709741407

Pfahl S, and Wernli H (2012) Quantifying the Relevance of Cyclones for Precipitation Extremes, J. Climate, 25, 6770-6780.

Pinto JG, Spangehl T, Ulbrich U, and Speth P (2005) Sensitivities of a cyclone detection and tracking algorithm: individual tracks and climatology, Meteorol. Z., 14, 823-838. doi:10.1127/0941-2948/2005/0068

Pinto JG, Ulbrich U, Leckebusch GC, Spangehl T, Reyers M, and Zacharias S (2007) Changes in storm track and cyclone activity in three SRES ensemble experiments with the ECHAM5/MPI-OM1 GCM, Clim. Dyn., 29, 195 - 210.

Pinto JG, Zacharias S, Fink AH, Leckebusch GC, and Ulbrich U (2009) Factors contributing to the development of extreme North Atlantic cyclones and their relationship with the NAO, Clim. Dyn. 32, 711 - 737.

Pinto JG., Reyers M, and Ulbrich U (2011) The variable link between PNA and NAO in observations and in multi-century CGCM simulations, Clim. Dyn., 36 (1-2), 337-354, doi: 10.1007/s00382-010-0770-x

Pinto JG, and Raible CC (2012) Past and recent changes in the North Atlantic oscillation, Wiley Interdisciplinary Reviews, Climate Change, 3, 79 – 90, doi:10.1002/wcc.150

Pinto JG, Karremann MK, Born K, Della-Marta PM, and Klawa M (2012) Loss potentials associated with European windstorms under future climate conditions, Clim. Res., 54, 1 - 20.

Pinto JG, Bellenbaum N, Karremann MK, and Della-Marta PM (2013) Serial clustering of extratropical cyclones over the North Atlantic and Europe under recent and future climate conditions, J. Geophys. Res. Atmos., 118, 12,476–12,485.

Pinto JG, Gómara I, Masato G, Dacre HF, Woollings T, and Caballero R (2014) Large-scale dynamics associated with clustering of extratropical cyclones affecting Western Europe, J. Geophys. Res. Atmos., 119, 13,704–13,719, doi:10.1002/2014JD022305.

Plant RS, Craig GC, and Gray SL (2003) On a threefold classification of extratropical cyclogenesis, Q. J. R. Meteorol. Soc., 129, 2989-3012.

Pozo-Vázquez D, Esteban-Parra MJ, Rodrigo FS, and Castro-Diez Y (2001) The association between ENSO and winter atmospheric circulation and temperature in the North Atlantic region, J. Climate, 14, 3408–3420.

Rahmstorf S (2006) Thermohaline Ocean Circulation. In: Encyclopedia of Quaternary Sciences, Edited by S. A. Elias. Elsevier, Amsterdam 2006.

Raible CC, Luksch U, Fraedrich K, and Voss R (2001) North Atlantic decadal regimes in a coupled GCM simulation, Clim. Dyn., 18, 321-330.

Raible CC, Luksch U, and Fraedrich K (2004) Precipitation and Northern Hemisphere regimes, Atmos. Sci. Lett., 5, 43–55.

Raible CC, Stocker TF, Yoshimori M, Renold M, Beyerle U, Casty C, and Luterbacher J (2005) Northern Hemispheric trends of pressure indices and atmospheric circulation patterns in observations, reconstructions, and coupled GCM simulations, J. Climate, 18, 3968-3982.

Raible CC (2007) On the relation between extremes of midlatitude cyclones and the atmospheric circulation using ERA40, Geophys. Res. Lett., 34, L07703, doi:10.1029/2006GL029084

Raible CC, Yoshimori M, Stocker TF, and Casty C (2007) Extreme midlatitude cyclones and their implications to precipitation and wind speed extremes in simulations of the Maunder Minimum versus present day conditions, Clim. Dyn., 28, 409 - 423.

Raible CC, Della-Marta P, Schwierz C, Wernli H, and Blender R (2008) Northern Hemisphere extratropical cyclones: A comparison of detection and tracking methods and different reanalyses, Mon. Weather Rev., 136, 880-897.

Raible CC, Lehner F, Gonzalez-Rouco JF, and Fernandez-Donado L (2014) Changing correlation structures of the Northern Hemisphere atmospheric circulation from 1000 to 2100 AD, Climate of the Past, 10, 537-550, doi:10.5194/cp-10-537-2014.

Randel WJ, and Held IM (1991) Phase speed spectra of transient eddy fluxes and critical layer absorption, J. Atmos. Sci., 48, 688 - 697.

Randel WJ (2004) Climate: Wider connections for El Niño, Nature, 431, 920–921.

Rayner, and co-authors (2003) Global analyses of sea surface temperature, sea ice, and night marine air temperature since the late nineteenth century, J. Geophys. Res., 108-14, doi: 10.1029/2002JD002670

Reader MC, and Moore GWK (1995) Stratosphere-troposphere interactions associated with a case of explosive cyclogenesis in the Labrador Sea, Tellus A., 47, 849 - 863.

Reed RJ, and Albright MD (1986) A case study of explosive cyclogenesis in the eastern Pacific, Mon. Weather Rev., 114, 2297 - 2319.

Reed RJ, Georg AG, and Kuo YH (1993) The ERICA IOP 5 Storm. Part I: Analysis and Simulation. Mon. Weather Rev., 121, 1577–1594.

doi: http://dx.doi.org/10.1175/1520-0493(1993)121<1577:TEISPI>2.0.CO;2

Reichler T, Kim J, Manzini E, and Kröger J (2012) A stratospheric connection to Atlantic climate variability, Nature Geoscience, 5, 783-787, doi:10.1038/ngeo1586.

Renfrew IA, Thorpe AJ, and Bishop CH (1997) The role of the environmental flow in the development of secondary frontal cyclones, Q. J. R. Meteorol. Soc., 123, 1653-1675.

Riemer M, Jones SC, and Davis CS (2008) The impact of extratropical transition on the downstream flow: An idealized modelling study with a straight jet, Q. J. R. Meteorol. Soc., 134, 69–91.

Rienecker MM, and co-authors (2011) MERRA: NASA's Modern-Era Retrospective Analysis for Research and Applications, J. Climate, 24, 3624-3648, doi:10.1175/JCLI-D-11-00015.1.

Rivals H, Cammas JP, and Renfrew IA (1998) Secondary cyclogenesis: The initiation phase of a frontal wave observed over the eastern Atlantic, Q. J. R. Meteorol. Soc., 124, 243–267.

Rivière G, and Joly A (2006a) Role of the low-frequency deformation field on the explosive growth of extratropical cyclones at the jet exit. Part I: barotropic critical region., J. Atmos. Sci., 63, 1965 - 1981.

Rivière G, and Joly A (2006b) Role of the low-frequency deformation field on the explosive growth of extratropical cyclones at the jet exit. Part II : baroclinic critical region., J. Atmos. Sci., 63, 1982 - 1995.

Rivière G, and Orlanski I (2007) Characteristics of the Atlantic Storm-Track Eddy activity and Its Relation with the North Atlantic Oscillation, J. Atmos. Sci., 64, 241 - 266.

Rivière G, Arbogast P, Maynard K, and Joly A (2010) The essential ingredients leading to the explosive `growth stage of the European wind storm Lothar of Christmas 1999, Q. J. R. Meteorol. Soc., DOI:10.1002/qj.585

Rivière G, Arbogast P, Lapeyre G, and Maynard K (2012) A potential vorticity perspective on the motion of a mid-latitude winter storm, Geophys. Res. Lett., 39, L12808. doi:10.1029/2012GL052440.

Rodríguez-Fonseca B (2001) Relación entre el régimen anómalo de precipitación en la Península Ibérica y la variabilidad de baja frecuencia del sistema climático en el Atlántico Norte, Memoria de Tesis Doctoral (Universidad Complutense de Madrid).

Rodríguez-Fonseca B, Polo I, Serrano E, and Castro M (2006) Evaluation of the North Atlantic SST forcing on the European and North African Winter climate, Int. J. Climatol., 25, DOI 10.1002/7joc.1234

Rodríguez-Fonseca B, Polo I, García-Serrano J, Losada T, Mohino E, Mechoso CR, and Kucharski F (2009) Are Atlantic Niños enhancing Pacific ENSO events in recent decades? Geophys. Res. Lett., 36, L20705, doi:10.1029/2009GL040048.

Rodríguez-Puebla C, Encinas AH, and Sáenz J. (2001) Winter precipitation over the Iberian Peninsula and its relationship to circulation indices, Hydrol. Earth Syst. Sci., 5, 233-244, doi:10.5194/hess-5-233-2001.

Roebber PJ (2009) Planetary Waves, Cyclogenesis, and the Irregular Breakdown of Zonal Motion over the North Atlantic, Mon. Weather Rev., 137, 3907 - 3917.

Roebber PJ, and Schumann MR (2011) Physical Processes Governing the Rapid Deepening Tail of Maritime Cyclogenesis, Mon. Weather Rev., 139, 2776 - 2789.

Roeckner E, and co-authors (2003) The atmospheric general circulation model ECHAM 5. PART I: model description, MPI Report 349.

Rogers JC (1997) North Atlantic Storm Track Variability and Its Association to the North Atlantic Oscillation and Climate Variability of Northern Europe, J. Climate, 10, 1635-1647, doi: 10.1175/1520-0442(1997)010<1635:NASTVA>2.0.CO;2

Rudeva I, and Gulev SK (2007) Climatology of Cyclone Size Characteristics and Their Changes during the Cyclone Life Cycle, Mon. Weather Rev., 135, 2568–2587.

Ruiz-Barradas A, Carton JA, and Nigam S (2003) Role of the atmosphere in climate variability of the tropical Atlantic, J. Climate, 16, 2052–2065.

Sanders F, and Gyakum JR (1980) Synoptic-Dynamic climatology of the bomb, Mon. Weather Rev., 108, 1589-1606.

Sanders F (1986) Explosive cyclogenesis in the west-central North Atlantic Ocean. Part I: Composite structure and mean behaviour, Mon. Weather Rev., 114, 1781 - 1794.

Santos JA, Pinto JG, and Ulbrich U (2009) On the development of strong ridge episodes over the eastern North Atlantic, Geophys. Res. Lett., 36, L17804, doi:10.1029/2009GL039086.

Santos JA, Woollings T, and Pinto JG (2013) Are the Winters 2010 and 2012 Archetypes Exhibiting Extreme Opposite Behavior of the North Atlantic Jet Stream? Mon. Weather Rev., 141, 3626–3640, doi: http://dx.doi.org/10.1175/MWR-D-13-00024.1.

Scaife AA, and co-authors (2014) Skillful long-range prediction of European and North American winters, Geophys. Res. Lett., 41, 2514–2519, doi:10.1002/2014GL059637.

Schär C, and Davies HC (1990) An instability of mature cold fronts, J. Atmos. Sci., 47, 929-950.

Schneider EK, Bengtsson L, and Hu ZZ (2003) Forcing of Northern Hemisphere climate trends, J. Atmos. Sci., 60, 1504-1521.

Schultz DM, Keyser D, and Bosart LF (1998) The effect of large-scale flow on low-level frontal structure and evolution in midlatitude cyclones, Mon. Weather Rev., 126, 1767-1791.

Schwierz C, Köllner-Heck P, Zenklusen Mutter E, Bresch DN, Vidale PL, Wild M, and Schär C (2010) Modelling European winter wind storm losses in current and future climate, Climatic Change, 101, 3-4, 485 – 514, doi:10.1007/s10584-009-9712-1.

Seiler C, and Zwiers FW (2015) How well do CMIP5 climate models reproduce explosive cyclones in the extratropics of the Northern Hemisphere? Clim. Dyn., doi: 10.1007/s00382-015-2642-x

Shaffrey LC, and co-authors (2009) UK-HiGEM: The new UK High Resolution Global Environment Model. Model description and Basic Evaluation, J. Climate, 22, 1861-1896.

Shapiro MA, and Keyser D (1990) Extratropical Cyclones: The Erik Palmen memorial volume, chapter 10. Amer. Meteorol. Soc.

Shindell DT, Schmidt GA, Mann ME, Rind D, and Waple A (2001) Solar forcing of regional climate change during the Maunder Minimum, Science, 294, 2149-2152, doi:10.1126/science.1064363.

Shutts GJ (1983) The propagation of eddies in diffluent jet streams: Eddy vorticity forcing of 'blocking' flow fields, Q. J. R. Meteorol. Soc., 109, 737 – 761, doi: 10.1002/qj.49710946204

Simmonds I, Murray RJ, and Leighton RM (1999) A refinement of cyclone tracking methods with data from FROST, Aust. Met. Mag. Spec. Ed., 35 - 49.

Simmonds I (2000) Size changes over the life of sea level cyclones in the NCEP reanalysis, Mon. Weather Rev., 128, 4118–4125.

Simmonds I, and Keay K (2000) Mean Southern Hemisphere extratropical cyclone behavior in the 40-year NCEP–NCAR reanalysis, J. Climate, 13, 873–885.

Simmons AJ, and Hoskins BJ (1979) The downstream and upstream development of unstable baroclinic waves, J. Atmos. Sci., 36, 1239-1254.

Simmons AJ, and co-authors (1989) The ECMWF medium-range prediction model: Development of the numerical formulations and the impact of increased resolution, Meteorol. Atmos. Phys., 40, 28–60.

Stephenson DB, Pavan V, and Bojariu R (2000) Is the North Atlantic Oscillation a random walk? Int. J. Climatol., 20, 1–18.

Stewart R (2008) Introduction to Physical Oceanography, Department of Oceanography, Texas A&M University.

Strong C, and Magnusdottir G (2008a) How Rossby wave breaking over the Pacific forces the North Atlantic Oscillation, Geophys. Res. Lett., 35, L10706. doi: 10.1029/2008GL033578.

Strong C, and Magnusdottir G (2008b) Tropospheric Rossby wave breaking and the NAO/NAM, J. Atmos. Sci., 65, 2861 - 2876.

Sung MK, Ham YG, Kug JS, and An SI (2013) An alterative effect by the tropical North Atlantic SST in intraseasonally varying El Nino teleconnection over the North Atlantic, Tellus A., 65.

Thorncroft CD, Hoskins BJ, and McIntyre ME (1993) Two paradigms of baroclinic wave life-cycle behaviour, Q. J. R. Meteorol. Soc., 119, 17 - 55.

Tomikawa Y, Sato K, and Shepherd TG (2006) A Diagnostic Study of Waves on the Tropopause, J. Atmos. Sci., 63, 3315 - 3332.

Toniazzo T, and Scaife AA (2006) The influence of ENSO on winter North Atlantic climate, Geophys. Res. Lett., 33, L24704, doi:10.1029/2006GL027881.

Trenberth KE (1986) An assessment of the impact of transient eddies on the zonal flow during a blocking episode using localized Eliassen–Palm flux diagnostics, J. Atmos. Sci., 43, 2070–2087.

Trenberth KE (1997) The Definition of El Niño, Bull. the Am. Meteorol. Soc., 78, 2771-2777.

Trenberth KE, Branstator GW, Karoly D, Kumar A, Lau NC, and Ropelewski C (1998) Progress during TOGA in understanding and modeling global teleconnections associated with tropical sea surface temperatures, J. Geophys. Res., 103(C7), 14,291–14,324, doi:10.1029/ 97JC01444.

Trenberth KE, and Shea DJ (2006) Atlantic hurricanes and natural variability in 2005, Geophys. Res. Lett., 33, L12704, doi:10.1029/2006GL026894.

Trigo IF (2006) Climatology and interannual variability of storm tracks in the Euro-Atlantic sector: A comparison between ERA-40 and NCEP/NCAR reanalyses, Clim. Dyn., 26, 127 – 143.

Uccellini LW, and Johnson DR (1979) The coupling of upper and lower tropospheric jet streaks and implications for the development of severe convective storms, Mon. Weather Rev., 107, 682-6703.

Uccellini LW, and Kocin PJ (1987) The interaction of jet streak circulations during heavy snow events along the east coast of the United States, Wea. Forecasting, 2, 289-308.

Uccellini LW (1990) Processes contributing to the rapid development of extratropical cyclones. Extratropical Cyclones: The Erik Palmen Memorial Volume, C. Newton and E. O. Holopainen, Eds., Amer. Meteor. Soc., 81 - 105.

Ulbrich U, and Christoph M (1999) A shift of the NAO and increasing storm track activity over Europe due to anthropogenic greenhouse gas forcing, Clim. Dyn., 15, 551–559.

Ulbrich U, Fink AH, Klawa M, and Pinto JG (2001) Three extreme storms over Europe in December 1999, Weather, 56,70–80.

Ulbrich U, Leckebusch GC, and Pinto JG (2009) Extra-tropical cyclones in the present and future climate: a review, Theor. Appl. Climatol., 96, 117-131, doi:10.1007/s00704-008-0083-8

Uppala, and co-authors (2005) The ERA-40 re-analysis. Q.J.R. Meteorol. Soc., 131, 2961-3012, doi:10.1256/qj.04.176

Vallis GK (2006) Atmospheric and Oceanic Fluid Dynamics, Cambridge University Press, 745 pp.

van Loon H, and Rogers JC (1978) The Seesaw in Winter Temperatures between Greenland and Northern Europe, Part I: General Description, Mon. Weather Rev., 106, 296 - 310.

van Oldenborgh GJ, and co-authors (2015) Nature Clim. Change, 5, 490–491.

Vautard R (1990) Multiple Weather Regimes over the North Atlantic: Analysis of Precursors and Successors, Mon. Weather Rev., 118, 2056-2081.

Vicente-Serrano SM, and López-Moreno JI (2008) Differences in the non-stationary influence of the North Atlantic Oscillation on European precipitation under different scenarios of greenhouse gas concentrations, Geophys. Res. Lett., 35, L18710, doi:10.1029/2008GL034832

Visbeck M, Chassignet E, Curry R, Delworth T, Dickson B, and Krahmann G (2003) The Ocean's response to North Atlantic oscillation variability. In: Hurrell, J.W., Kushnir, Y., Ottersen, G., Visbeck, M. (Eds.), The North Atlantic Oscillation. AGU, pp. 113–146.

Vitolo R, Stephenson DB, Cook IM, and Mitchell-Wallace K (2009) Serial clustering of intense European storms, Meteorol. Z., 18, 411-424.

von Storch H, and Zwiers F (1999) Statistical analysis in Climate research Cambridge University press, Cambridge.

Walker GT (1924) Correlations in seasonal variations of weather. IX. Mem. India Meteorol. Dept. 24, 275 - 332.

Wallace JM, and Gutzler DS (1981) Teleconnections in the geopotential height field during the Northern Hemisphere winter, Mon. Weather Rev., 109, 784 - 812.

Wallace JM, and Thompson DWJ (2002) The Pacific Center of Action of the Northern Hemisphere Annular Mode: Real or Artifact? J. Climate, 15, 1987-1991.

Wang C, and Rogers JC (2001) A Composite Study of Explosive Cyclogenesis in Different Sectors of the North Atlantic. Part I: Cyclone Structure and Evolution, Mon. Weather Rev., 129, 1481 - 1499.

Wang C (2002) Atlantic Climate Variability and Its Associated Atmospheric Circulation Cells, J. Climate, 15, 1516-1536. doi: 10.1175/1520-0442(2002)015<1516:ACVAIA>2.0.CO;2

Wang C (2004) ENSO, climate variability and the Walker and Hadley circulations, in The Hadley Circulation: Present, Past and Future, Adv. Global Change Res., vol. 21, edited by H. F. Diaz, and R. S. Bradley, pp. 173–202, Springer, New York.

Wang C, and Zhang L (2013) Multidecadal Ocean Temperature and Salinity Variability in the Tropical North Atlantic: Linking with the AMO, AMOC, and Subtropical Cell, J. Climate, 26, 6137-6162, doi: http://dx.doi.org/10.1175/JCLI-D-12-00721.1

Wang YH, Magnusdottir G, Stern H, Tian X, and Yu Y (2012) Decadal variability of the NAO: Introducing an augmented NAO index, Geophys. Res. Lett., 39, L21702, doi:10.1029/2012GL053413.

Wanner H, Bronnimann S, Casty C, Gyalistras D, Luterbacher J, Schmutz C, Stephenson DB, and Xoplaki E (2001) North Atlantic Oscillation-concepts and studies, Surv. Geophys., 22, 321 - 382.

Watanabe M (2004) Asian jet waveguide and a down-stream extension of the North Atlantic Oscillation, J. Climate, 17, 4674–4691.

Wernli H, Dirren S, Liniger MA, and Zillig M (2002) Dynamical aspects of the life-cycle of the winter storm "Lothar" (24–26 December 1999), Q. J. R. Meteorol. Soc., 128, 405 - 429.

Wilks DS (2006) Statistical methods in the Atmospheric Sciences, Second Edition, Elsevier Inc., ISBN 13: 978-0-12-751966-1

Woollings T, Hoskins B, Blackburn M, and Berrisford P (2008) A New Rossby Wave-breaking Interpretation of the North Atlantic Oscillation, J. Atmos. Sci., 65, 609 - 626.

Woollings T, Hannachi A, and Hoskins BJ (2010) Variability of the North Atlantic eddy-driven jet stream, Q. J. R. Meteorol. Soc., 136, 856–868.

Woollings T, Pinto JG, and Santos JA (2011) Dynamical evolution of North Atlantic ridges and poleward jet stream displacements, J. Atmos. Sci., 68, 954 - 963.

Woollings T, Gregory JM, Pinto JG, Reyers M, and Brayshaw DJ (2012) Response of the North Atlantic storm track to climate change shaped by ocean-atmosphere coupling, Nature Geoscience, 5, 313–317. doi:10.1038/ngeo1438

Woollings T, Franzke C, Hodson DLR, Dong B, Barnes EA, Raible CC, and Pinto JG (2015) Contrasting interannual and multi-decadal NAO variability, Clim. Dyn., 45, 539-556. doi:10.1007/s00382-014-2237-y

Wunsch C (1999) The interpretation of short climate records, with comments on the North Atlantic and Southern Oscillations, Bull. Amer. Meteor. Soc., 80, 245–255.

Zappa G, Masato G, Shaffrey L, Woollings T, and Hodges K (2014) Linking Northern Hemisphere blocking and storm track biases in the CMIP5 climate models, Geophys. Res. Lett., 41, 135-139. doi:10.1002/2013GL058480.

Zhang W, Wang L, Xiang B, Qi L, and He J (2015) Impacts of two types of La Niña on the NAO during boreal winter, Clim. Dyn., 44, 1351-1366.

List of Acronyms

AMO: Atlantic Multi-decadal Oscillation

AO: Arctic Oscillation

ASCII: American Standard Code for Information Interchange

CERA: Center for Environmental Risk Assessment

COADS: Comprehensive Ocean-Atmosphere Data Set

DB: Direction of Breaking

DKRZ: *Deutsches Klimarechenzentrum*

E: East

EC: Explosive Cyclones

ECHAM5: European Centre Hamburg Model 5

ECMWF: European Centre for Medium-Range Weather Forecasts

ECN: Explosive cyclones followed by negative NAO variations

ECP: Explosive cyclones followed by positive NAO variations

EMF: Eddy Momentum Fluxes

ENSO: El Niño-Southern Oscillation

EOF: Empirical Orthogonal Function

EP: Eliassen-Palm

ERA: European Reanalysis

ERSST: Extended Reconstructed SST

FU: *Freie Universität Berlin*

GCM: General Circulation Model

GRIB: Gridded Binary or General Regularly-distributed Information in Binary form

GTS: Global Telecommunications System

HadISST: Met Office Hadley Centre's sea ice and Sea Surface Temperature

IPCC: Intergovernmental Panel on Climate Change

ITCZ: Inter-Tropical Convergence Zone

JMA: Japan Meteorological Agency

JRA-55: Japanese 55-yr. Reanalysis

LC: Life-Cycle

MARS: Meteorological Archival and Retrieval System

MDB: Met Office Marine Data Bank

MERRA: Modern-Era Retrospective Analysis for Research and Applications

MOC: Meridional Overturning Circulation

MOM: Modular Ocean Model

MPI-M: Max Planck Institute for Meteorology

MPIOM1: Max Planck Institute Ocean Model 1

MSLP: Mean Sea Level Pressure

N: North

NA: North Atlantic

NAO: North Atlantic Oscillation

NASA: National Aeronautics and Space Administration

NCAR: National Centers for Atmospheric Research

NCEP: National Centers for Environmental Prediction

NDR: Normalized Deepening Rate

NetCDF: Network Common Data Form

NOAA: National Oceanic and Atmospheric Administration

NoEC: Non-Explosive Cyclones

OHC: Ocean Heat Content

PC: Principal Component

PCA: Principal Components Analysis

PNA: Pacific North American pattern

PV: Potential Vorticity

P95: 95th Percentile

P98: 98th Percentile

RE: Random Explosive

RNE: Random Non-Explosive

RWB: Rossby Wave-Breaking

S: South

SLP: Sea Level Pressure

SODA: Simple Ocean Data Reanalysis

SST: Sea Surface Temperature

THC: Thermohaline Ocean Circulation

UK: United Kingdom

US: United States

W: West

WMO: World Meteorological Organization

WT: Water Temperature

20CR: 20th century Reanalysis

List of Publications

Within the context of this thesis:

Gómara I, Pinto JG, Woollings T, Masato G, Zurita-Gotor P, and Rodríguez-Fonseca B (2014a) Rossby wave-breaking analysis of explosive cyclones in the Euro-Atlantic sector, Q.J.R. Meteorol. Soc., 140, 738–753, doi: 10.1002/qj.2190

Gómara I, Rodríguez-Fonseca B, Zurita-Gotor P, and Pinto JG (2014b) On the relation between explosive cyclones affecting Europe and the North Atlantic Oscillation, Geophys. Res. Lett., 41, 2182-2190, doi: 10.1002/2014GL059647

Pinto JG, **Gómara** I, Masato G, Dacre HF, Woollings T, and Caballero R (2014) Large-scale dynamics associated with clustering of extratropical cyclones affecting Western Europe, J. Geophys. Res. Atmos., 119, 13704–13719, doi:10.1002/2014JD022305

Gómara I, Rodríguez-Fonseca B, Zurita-Gotor P, Ulbrich S, and Pinto JG (2015) Abrupt transitions in the variability of explosive cyclones over the North Atlantic, Clim. Dyn. (under review, CLDY-D-15-00358)

Other publications during the PhD period:

López-Parages J, Villamayor J, **Gómara** I, Losada T, Martín-Rey M, Mohíno E, Polo I, Rodríguez-Fonseca B, and Suárez R (2013) Nonstationary interannual teleconnections modulated by multidecadal variability, Física de la Tierra, 25, 11-39. ISSN 0214-4557

Román-Cascón C, Yagüe C, Viana S, Sastre M, Maqueda G, Lothon M, and **Gómara** I (2015) Near-monochromatic ducted gravity waves associated with a convective system close to the Pyrenees, Q. J. R. Meteorol. Soc., 141, 1320–1332. doi: 10.1002/qj.2441